CT Imaging of the Thoracic Aorta: Size assessment and follow-up after surgical and endovascular intervention

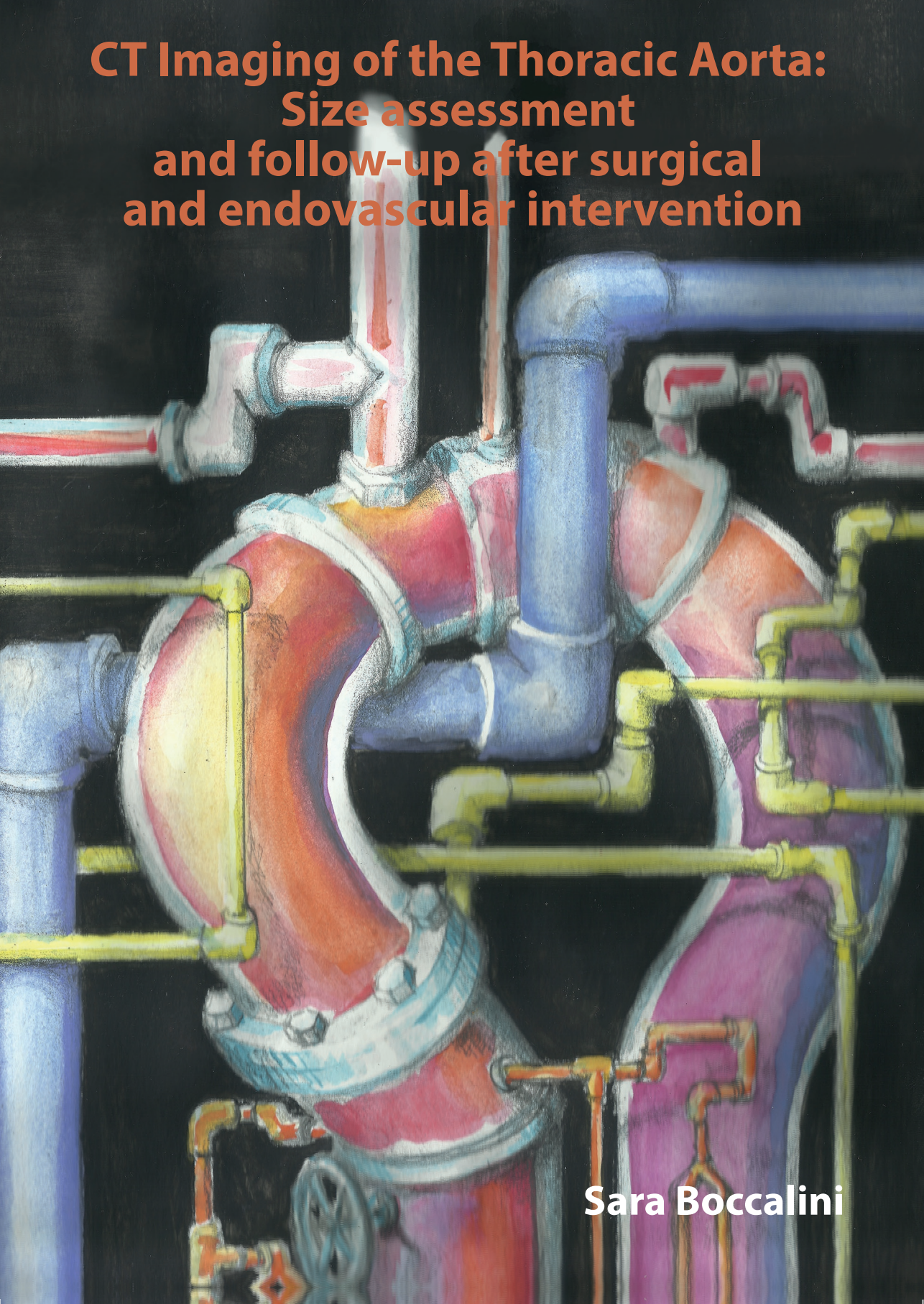

Sara Boccalini

CT Imaging of the Thoracic Aorta:

Size assessment and follow-up after surgical and endovascular intervention

Sara Boccalini

Financial support by the Department of Radiology of EMC for the publication of this thesis is gratefully acknowledged

ISBN: 978-94-6380-526-1
Cover and inside art work by: Anna Maria Traverso
Inside layout by: Bregje Jaspers | ProefschriftOntwerp.nl
Printed by: ProefschriftMaken | www.proefschriftmaken.nl

CT Imaging of the Thoracic Aorta:
Size assessment and follow-up after surgical and endovascular intervention

CT Beeldvorming van de Thoracale Aorta:
Beoordeling van de grootte en follow-up na chirurgie en endovasculaire interventie

Proefschrift

ter verkrijging van de graad van doctor aan de
Erasmus Universiteit Rotterdam
op gezag van de
rector magnificus
Prof. dr. R.C.M.E. Engels

en volgens besluit van het College voor Promoties.
De openbare verdediging zal plaatsvinden op
woensdag 6 november 2019 om 13:30 uur

door

Sara Boccalini
geboren te Genova, Italie

Erasmus University Rotterdam

Promotoren:	prof. dr. G.P. Krestin
	prof. dr. J.W. Roos - Hesselink
Overige leden:	J.J. Wentzel, PhD
	prof. dr. J.H.C. Reiber
	prof. dr. A.J.J.C. Bogers
Copromotor:	dr. R.P.J. Budde

Contents

Chapter 1	General introduction and outline of the thesis	9
Part 1	**CT assessment of aortic diameters**	25
Chapter 2	How to measure the diameter of the aorta on CT: systematic review of available techniques. *Submitted*	27
Chapter 3	A novel software tool for semi-automatic quantification of thoracic aorta dilatation on baseline and follow-up computed tomography angiography. *Int J Cardiovasc Imaging. 2019 Apr;35(4):711-723*	63
Chapter 4	Intermodality variation of aortic dimensions: How, where and when to measure the ascending aorta. *Int J Cardiol. 2019 Feb 1;276:230-235*	85
Chapter 5	Quantification of aortic annulus in computed tomography angiography: validation of a fully automatic methodology *Eur J Radiol. 2017 Aug;93:1-8*	115
Chapter 6	Bicuspid aortic valve annulus: standardized method to define the annular plane and assessment of geometry changes during the cardiac cycle. Implications for TAVI planning. *Submitted*	135
Part 2	**CT assessment of the thoracic aorta after surgery and endovascular intervention**	159
Chapter 7	CT Angiography for depiction of complications after the Bentall procedure *Br J Radiol. 2018 Aug 13:20180226*	161
Chapter 8	Peri-aortic fluid after surgery of the ascending aorta: worrisome indicator of complications or innocent postoperative finding? *Eur J Radiol. 2017 Oct;95:332-341*	189

Chapter 9 Complications after stent placement for aortic coarctation. A pictorial essay of Computed Tomography Angiography 213
J Thorac Imaging. 2017 Nov;32(6):W69-W80

Chapter 10 Computed tomography image quality of great vessel stents in patients with aortic coarctation: a multicentre evaluation 237
Eur Radiol Exp. 2018 Dec; 2: 17

Part 3 **Epilogue** 259

Chapter 11 Discussion and general conclusion 263
Summary in Dutch (Nederlandse samenvetting) 277
List of publications 281
PhD portfolio 285
About the autho 287
Acknowledgments (Dankwoord) 289

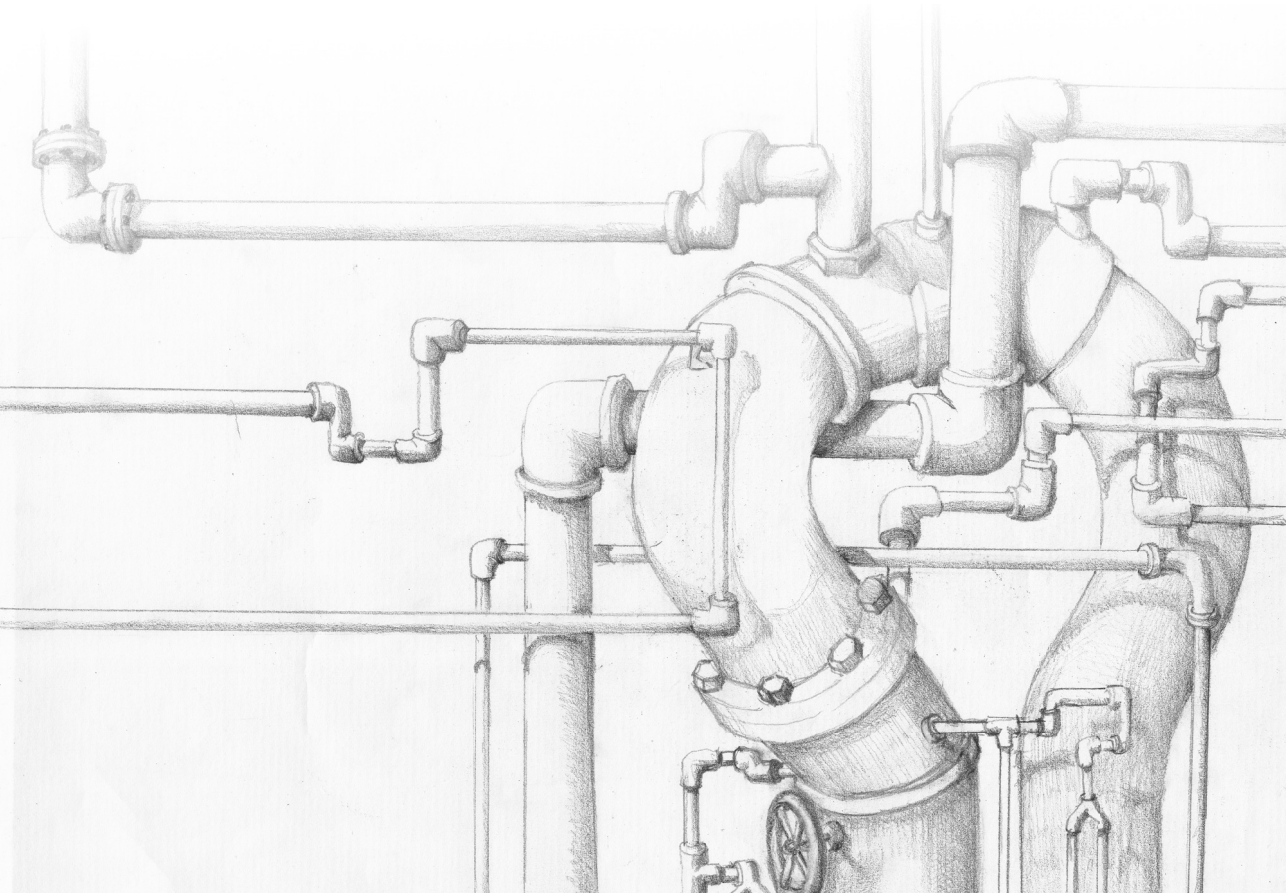

CHAPTER 1

General introduction and thesis outline

Introduction

Technological developments including fast acquisitions, reduced contrast and radiation dose, electrocardiographic (ECG) synchronization, submillimeter spatial resolution, the possibility to perform reconstructions in any desired plane and to visualize the aortic wall as well as the broad availability of the method have contributed to establish the central role of computed tomography (CT) in aortic imaging. Very far seems the year 2004, when it was still debated by some whether physical examination was more accurate than CT and ultrasound for the measurement of abdominal aneurysms[1]. In fact, nowadays CT is often the imaging modality of choice for diagnosis and follow-up of all patients with aortic pathology, both treated conservatively, for pre-procedural assessment of aortic anatomy and diameters, during post-procedural follow-up and for evaluation of complications[2, 3]. Although magnetic resonance imaging (MRI) can be considered as another option to image the aorta, especially for young patients that will require lifelong imaging surveillance, CT is generally preferred for several reasons, including faster acquisitions, better spatial resolution and easier access.

This is true not only for the abdominal aorta but also for the thoracic aorta that yields additional challenges for imaging techniques such as the proximity to the heart and consequent transmitted movements and the more complex anatomy. Furthermore, the thoracic aorta is often involved in genetic diseases such as connective tissue diseases and in patients with bicuspid aortic valves.

The aim of this thesis was to review current knowledge regarding the role of CT for thoracic aorta pathology assessment as well as to further investigate several aspects of this field. Due to the vastness of the topic, we focused our attention on specific aspects of aortic diameter measurements and CT imaging after two interventions, namely the Bentall procedure and stent placement for the treatment of aortic coarctation.

CT assessment of aortic diameters

CT imaging is employed for diagnosis and pre-interventional planning of aortic pathology as it allows not only precise definition of anatomy, of the aorta and of all other thoracic structures (as shown in Figure 1), but also aortic diameter assessment.

A correct measurement of aortic diameters is fundamental in almost all stages of the management of aortic pathology. Important clinical decisions, namely if and when to intervene and the best procedural approach, are based almost entirely on the absolute value of aortic diameters and/or their change over time[2, 3]. Therefore, precise, reliable and reproducible aortic diameter measurements based on imaging techniques are a fundamental prerequisite for a correct management of aortic pathologies.

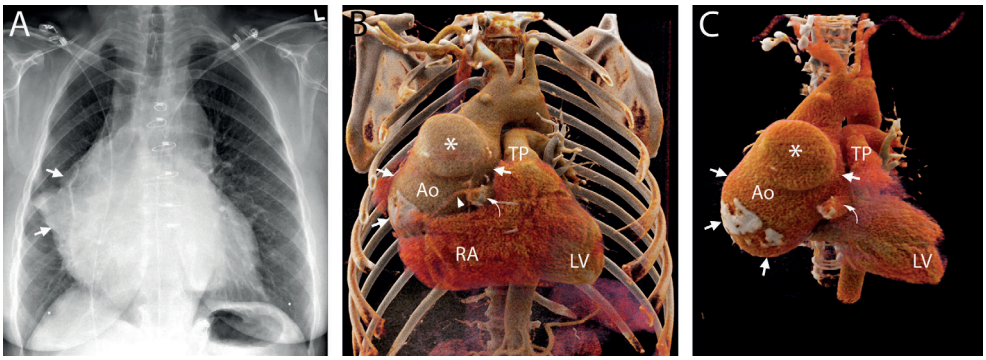

Figure 1

A –The X-Ray of the thorax in the PA projection highlighted the enlargement of the left profile of the heart (**arrows**).
B and **C** – 3D reconstructions of the CTA scan demonstrated that the enlargement seen on the X-Ray of the thorax was due to the presence of a very large aneurysm of the ascending aorta (**arrows**). The anterior wall of the ascending presented an additional focal enlargement (**asterisk**), at the level where the aorta was previously incised, that was defined as pseudoaneurysm. An anomalously enlarged origin of the right coronary artery (**curved arrow**), remnant of the corrected fistula, could be seen adjacent to the wall of the aneurysm. More distally, after an abrupt change in diameters, the coronary showed normal dimensions (**arrowhead**). *Ao* – aorta; *LV* – left ventricle; *RA* – right atrium; *TP* – truncus pulmonalis.
Figure 1 is extracted from: A Ten-centimetre wide Aneurysm of the Ascending Aorta in a 57-year old Female with a Previously Surgically Corrected Congenital Fistula from the Right Coronary Artery to the Right Atrium. Daniel J.F.M. Thuijs, Maurits Zegel, Sara Boccalini, Jos. A. Bekkers. Submitted.

The way aortic measurements are derived from CT images has dramatically changed over the past decades. Once estimated one by one with callipers on printed axial images[1, 4], they can now be automatically calculated by software on any plane perpendicular to the vessel in a few minutes[5].

Technological advancement in CT scanner hardware and image reconstruction, such as the employment of ECG-gating and the increment in number of detectors resulting in acquisitions with high temporal resolution and isotropic voxels, are now broadly diffused in clinical routine. These improvements allow the manipulation of motion-free images of the entire aorta in any plane desired after the acquisition has been completed. Due to the complex 3D anatomy of the aorta, it has been postulated that axial measurements of aortic diameters are not representative of real dimensions of the vessel, especially in the thoracic and more tortuous tracts where the angle between the longitudinal axis of the aorta and the axial CT plane is more acute. Therefore, it is currently recommended to measure diameters on planes perpendicular to the longitudinal axis of the vessel that can be achieved either manually or by employing software[2, 6]. With the manual method, the axes are rotated by an operator until the desired plane is obtained. Although different

approaches have been introduced, many software programs rely on the same basic principle: the identification of all the points having the same distance from the aortic wall that, combined, define the so-called "centerline"[7]. However, there are conspicuous differences in relation to operator interaction and on the definition of the boundaries of the aorta and subsequent diameter calculations. Nevertheless, the variety of different possible methods to measure aortic diameters hasn't been completely addressed in guidelines and there is still no precise consensus on which technique should be employed.

Since the aorta is a single organ that can be affected by pathology at multiple locations along all its length, the entire vessel should be imaged and measured. An exception is represented by patients with bicuspid aortic valve (BAV) that typically show dilation limited to the aortic root or ascending aorta[8]. All patients with aortic pathology (with the possible exclusion of atherosclerosis) will undergo lifelong imaging surveillance to assess changes in aortic size. Thus, diameters should be calculated for all examinations at several and standardized landmarks with the same measurement method[2]. To the best of our knowledge there is no automatic software that is able to compare multiple scans of the thoracic and entire aorta of the same patient. Hence at the moment the only feasible method to evaluate diameters progression is by manually defining planes perpendicular to the longitudinal axis of the vessel at multiple locations. The result is a very time-consuming post-processing evaluation, almost incompatible with a busy clinical schedule. Furthermore, although guidelines specifically state that consecutive measurements should be performed in the same manner, often imaging techniques different from CT are employed in clinical practise to assess aortic diameters[9]. These include echocardiography and MRI. Therefore, agreement between techniques and methods is a fundamental parameter to take in consideration when comparing subsequent aortic diameters of the same patient calculated in a different way.

Moreover, as measurements of the aortic root and ascending aorta have to be performed on ECG synchronized images, the best cardiac phase has to be chosen. Although diastole is generally preferred because of better reproducibility and image quality, there is still no general consensus about which one should be employed [6].This is particularly relevant for the proximal portions of the aorta where, due to transmitted pulsation movements, aortic diameters change significantly during the cardiac cycle. Another unsolved issue is whether the aortic wall thickness should be included in aortic diameter measurements. At present, in clinical practise there is often a difference between imaging techniques considering that measurements are performed leading-edge to leading-edge on echocardiographic images (2DE) and inner-edge to inner-edge on CT and MRI images[6].

An additional source of variability in thoracic aorta diameter assessment is its complex anatomy (Figure 2). In particular the aortic root at the level of the sinus of Valsalva does

not present the same circular or slightly oval cross-section of the other aortic portions. Therefore different methods are commonly employed to report diameters at this level without general consensus regarding which one should be used.

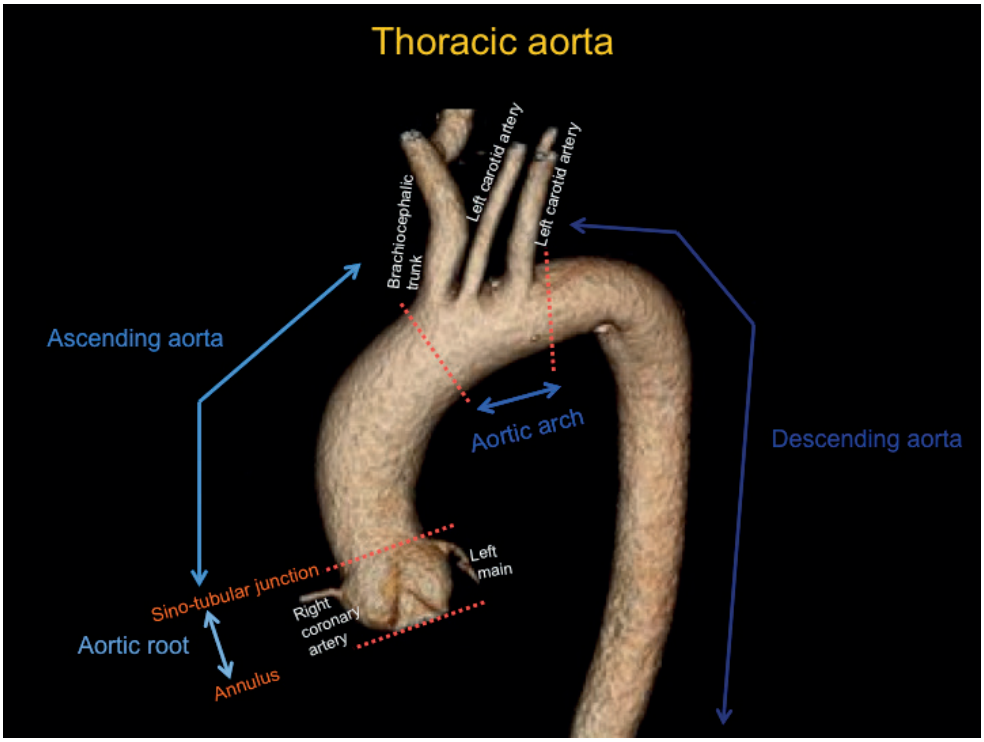

Figure 2

Figures 2 is extracted and adapted from: "CT assessment of aortic diameters: what radiologists should know". Boccalini S, Nieman K, Seitun S, Ferro C, Krestin GP, Budde RPJ
Educational poster at RSNA 2016

Furthermore, an aortic location that presents peculiar function and anatomy and is therefore different from all others is the aortic annulus. This term does not correspond to a specific physical anatomical structure but it indicates the level with the smallest diameter along the flow of the blood out of the left ventricle[10], corresponding to the location where aortic valve prostheses are placed. The need for a precise definition of this structure arose with the increasing number of transcatheter aortic valve replacements (TAVI). Since the size of the prosthesis has to be chosen before the procedure, measurements of the landing zone are performed on pre-implantation images. Precise measurements of the annulus are fundamental to avoid under or oversizing of the valve which might lead to potentially fatal complications, namely paravalvular leakage and rupture of the

left ventricular outflow tract[11, 12]. For assessment on CT images, the annulus has been defined as the ring of aortic wall identified by a plane passing through the hinge points of the three aortic cusps[13].

Measurements of the annulus have to be performed according to this definition both manually and automatically. Since manual definition of the annulus is time-consuming and requires expertise as well as experience, precise and reliable automatic software could improve the workflow. However, since at this level software cannot rely (only) on the definition of the centerline as for the other aortic locations, new solutions for the identification of the annulus plane have to be created and validated[14, 15]. In addition, anatomical variations/malformations of the aortic cusps and/or aortic root, such as those found in patients with bicuspid aortic valves (BAV), can result in the impossibility to rely on the generally accepted definition of the annulus plane on CT images.

Moreover, the annulus of patients with tricuspid aortic valves has an elliptic shape and undergoes conformational changes during the cardiac cycle [16]. These dynamic features have important consequences on the choice of the most appropriate parameter on which to base prosthesis sizing and of the cardiac phase when to measure the diameters [13, 17]. Therefore, assessing the annular shape and its changes throughout the cardiac cycle in patients with other types of valves, such as BAV, is fundamental particularly in light of the broader diffusion of the TAVI procedure in these patients.

CT assessment of the thoracic aorta after surgery and endovascular intervention

Therapeutic options for the treatment of aortic pathology include surgical and endovascular interventions. The first ones generally consist of the replacement of specific segments of the aorta with a prosthesis and, nowadays, are generally limited to the ascending aorta. Another specific type of surgery is the resection of the diseased aorta as performed for aortic coarctation. Endovascular interventions allow the deployment of endoprostheses or stents via a percutaneous approach and are the preferred option for the descending aorta. Depending on the extent of the disease, surgical and endovascular procedures can also be associated in a single operation time or at different time points. Also the aortic valve can be replaced with a surgical or endovascular approach although the second approach is generally reserved for patients with a general physical condition not allowing open surgery.

CT generally is the modality of choice for follow-up and to assess the occurrence of any complications after surgical or percutaneous procedures of the aorta.

We focused our research on CT findings after the Bentall procedure and after stent placement for the correction of aortic coarctation.

The Bentall procedure consists of the replacement of the aortic valve and ascending aorta during a single operation and it represents one of the most commonly practised treatments for type A dissections or aneurysms of the ascending aorta associated with valvular insufficiency or stenosis[18].
Stent placement is the treatment of choice for adolescents and adults with coarctation. Furthermore, this procedure is increasingly more practised also in children[19, 20].

Due to the generic and late symptomatology (if any at all) of many important complications, including infection of aortic prosthesis and pseudo-aneurysms of suture lines, most guidelines suggest periodic check-up with imaging even after uncomplicated procedures and in asymptomatic patients[9, 21, 22]. In this scenario diagnoses rely mainly on imaging findings. However, after operations or interventions, the anatomy of the aorta and surrounding structures will be altered. Therefore, radiologists should be familiar with the techniques employed and know how the normal anatomy was altered. As patients with aortic pathology may undergo more than one operation during their lives, the entire medical history is relevant.

Moreover, due to the manipulation of tissues during these complex and delicate interventions, changes in the surrounding structures can also be expected, especially in the early period after surgery. For instance, the presence of fluid or blood in the adipose tissue surrounding the aorta can be considered a normal physiological response to the operation. However, complications such as infections might have a similar appearance on CT images. The distinction can be arduous but is fundamental as infection of prosthetic material is potentially lethal and needs to be promptly treated. Therefore, our aim was to describe CT characteristics of normal post-Bentall scans as opposed to those suggesting the occurrence of complications.

After the procedure surgical material employed during the procedure as replacement for affected structures (grafts, stents, valve prosthesis) and as support for the operation (for instance to reinforce sutures and cannulation sites) and thereafter left in place can be visible on CT images. The presence of these exogenous structures can influence the assessment of the scan in several ways. The material can have an appearance similar to that of complications (as in the case of hyperdense material and extravasated contrast). Valvular prostheses cannot be assessed in their dynamic function unless a specific protocol with specific ECG-gating is employed. In addition, surgical material can determine artefacts so relevant that images are not interpretable or that they might be misinterpreted for complications.
With the introduction of new surgical products that differ in material and architecture that add up to the variations in terms of scanners and protocols of CT examinations, it

is fundamental to assess if diagnostic image quality can be achieved to avoid additional unnecessary exams and misdiagnosis.

Thesis outline

Part 1:
In the first part of this thesis we investigated the literature regarding the methods to measure aortic diameters on CT scans and we aimed to contribute to more effective aortic diameter assessment by means of new software and more insight in the definition of the annulus plane and its mechanics in BAV patients.

Chapter 2 of this thesis provides a review of the articles comparing different methods to measure aortic diameters on CT scans.

In **Chapter 3** we present the first software able to automatically calculate multiple diameters of the thoracic aorta, as well as their change over time, in two consecutive scans of the same patient. The software was validated against manual measurements.

In **Chapter 4** we investigate differences between measurement methods (2DE, CT and MR), and technique to assess ascending aorta diameters including measurements at the sinus, sinotubular junction and ascending aorta.

In **Chapter 5** we present a new automatic software for the definition of annular sizing parameters based on the identification of the three hinge points, which was validated against manual definition of the annulus plane and annular measurements.

In **Chapter 6** we present a new standardized method for the definition of the annulus plane in patients with BAV based on the specific anatomy of valve types. Furthermore, we investigated the shape of the annulus in BAV patients and its changes during the cardiac cycle.

Part 2:
In the second part of this thesis we focused on CT imaging after two specific aortic procedures: the Bentall procedure and the implantation of stents for the treatment of aortic coarctation. A pictorial review of normal findings and complications is presented for both procedures.

In **Chapter 7** the appearance of normal findings, complications and confounders on CT scans performed after the Bentall procedure is described.

In **Chapter 8** we investigate the CT characteristics and amount of peri-aortic fluid detectable on examinations performed within three months after a Bentall procedure to establish a reference standard to differentiate normal findings from complications.

In **Chapter 9** the appearance of normal findings, complications and confounders on CT scans performed after stent implantation for the treatment of artic coarctation is described.

In **Chapter 10** we compare the image quality of different types of stent employed for the treatment of aortic coarctation on post-procedural CT scans. The effect of technical parameters of the scan on image quality was investigated as well.

Chapter 11 provides a general discussion on the results of the studies presented in this thesis.

Bibliography:

1. Lal BK, Cerveira JJ, Seidman C, Haser PB, Kubicka R, Jamil Z, Padberg FT, Hobson RW, Pappas PJ (2004) Observer variability of iliac artery measurements in endovascular repair of abdominal aortic aneurysms. Ann Vasc Surg 18:644–652
2. Erbel R, Aboyans V, Boileau C, et al (2014) 2014 ESC Guidelines on the diagnosis and treatment of aortic diseases: Document covering acute and chronic aortic diseases of the thoracic and abdominal aorta of the adult. The Task Force for the Diagnosis and Treatment of Aortic Diseases of the European . Eur Heart J 35:2873–2926
3. Hiratzka LF, Bakris GL, Beckman J a., et al (2010) 2010 ACCF/AHA/AATS/ACR/ASA/SCA/SCAI/SIR/STS/SVM Guidelines for the Diagnosis and Management of Patients With Thoracic Aortic Disease: A Report of the American College of Cardiology Foundation/American Heart Association Task Force on Practice Guidelines, A. Circulation 121:e266–e369
4. Sprouse LR, Meier GH, Parent FN, Demasi RJ, Stokes GK, Lesar CJ, Marcinczyk MJ, Mendoza B (2004) Is three-dimensional computed tomography reconstruction justified before endovascular aortic aneurysm repair? J Vasc Surg 40:443–447
5. Delgado V, Ng ACT, Schuijf JD, et al (2011) Automated Assessment of the Aortic Root Dimensions With Multidetector Row Computed Tomography. Ann Thorac Surg 91:716–723
6. Goldstein SA, Evangelista A, Abbara S, et al (2015) Multimodality Imaging of Diseases of the Thoracic Aorta in Adults: From the American Society of Echocardiography and the European Association of Cardiovascular Imaging. J Am Soc Echocardiogr 28:119–182
7. Kirbas C, Quek F (2004) A review of vessel extraction techniques and algorithms. ACM Comput Surv 36:81–121
8. Fazel SS, Mallidi HR, Lee RS, Sheehan MP, Liang D, Fleischman D, Herfkens R, Mitchell RS, Miller DC (2008) The aortopathy of bicuspid aortic valve disease has distinctive patterns and usually involves the transverse aortic arch. J Thorac Cardiovasc Surg. doi: 10.1016/j.jtcvs.2008.01.022
9. Erbel R, Aboyans V, Boileau C, et al (2014) 2014 ESC Guidelines on the diagnosis and treatment of aortic diseases. Eur Heart J 35:2873–2926
10. Piazza N, de Jaegere P, Schultz C, Becker AE, Serruys PW, Anderson RH (2008) Anatomy of the aortic valvar complex and its implications for transcatheter implantation of the aortic valve. Circ Cardiovasc Interv 1:74–81
11. Blanke P, Reinöhl J, Schlensak C, et al (2012) Prosthesis oversizing in balloon-expandable transcatheter aortic valve implantation is associated with contained rupture of the aortic root. Circ Cardiovasc Interv 5:540–548
12. Willson AB, Webb JG, Labounty TM, et al (2012) 3-dimensional aortic annular assessment by multidetector computed tomography predicts moderate or severe paravalvular regurgitation after transcatheter aortic valve replacement: A multicenter retrospective analysis. J Am Coll Cardiol 59:1287–1294
13. Achenbach S, Delgado V, Hausleiter J, Schoenhagen P, Min JK, Leipsic J a. (2012) SCCT expert consensus document on computed tomography imaging before transcatheter aortic valve

implantation (TAVI)/transcatheter aortic valve replacement (TAVR). J Cardiovasc Comput Tomogr 6:366–380

14. Queirós S, Dubois C, Morais P, Adriaenssens T, Fonseca JC, Vilaça JL, D'hooge J (2016) Automatic 3D aortic annulus sizing by computed tomography in the planning of transcatheter aortic valve implantation. J Cardiovasc Comput Tomogr. doi: 10.1016/j.jcct.2016.12.004
15. Samim M, Stella PR, Agostoni P, et al (2013) Automated 3D analysis of pre-procedural MDCT to predict annulus plane angulation and C-arm positioning: Benefit on procedural outcome in patients referred for TAVR. JACC Cardiovasc Imaging 6:238–248
16. Suchá D, Tuncay V, Prakken NHJ, Leiner T, Van Ooijen PM a., Oudkerk M, Budde RPJ (2015) Does the aortic annulus undergo conformational change throughout the cardiac cycle? A systematic review. Eur Heart J Cardiovasc Imaging 16:1307–1317
17. Jurencak T, Turek J, Kietselaer BLJH, Mihl C, Kok M, van Ommen VGV a, van Garsse L a FM, Nijssen EC, Wildberger JE, Das M (2015) MDCT evaluation of aortic root and aortic valve prior to TAVI. What is the optimal imaging time point in the cardiac cycle? Eur Radiol 25:1975–1983
18. Bentall H, De Bono A (1968) A technique for complete replacement of the ascending aorta. Thorax 23:338–339
19. Forbes TJ, Kim DW, Du W, et al (2011) Comparison of surgical, stent, and balloon angioplasty treatment of native coarctation of the aorta: An observational study by the CCISC (Congenital cardiovascular interventional study consortium). J Am Coll Cardiol 58:2664–2674
20. Moore JW, Vincent RN, Beekman RH, et al (2014) Procedural results and safety of common interventional procedures in congenital heart disease: Initial report from the national cardiovascular data registry. J Am Coll Cardiol 64:2439–2451
21. Svensson LG, Adams DH, Bonow RO, et al (2013) Aortic valve and ascending aorta guidelines for management and quality measures: executive summary. Ann Thorac Surg 95:1491–505
22. Hiratzka LF, Bakris GL, Beckman JA, et al (2010) 2010 ACCF/AHA/AATS/ACR/ASA/SCA/SCAI/SIR/STS/SVM Guidelines for the Diagnosis and Management of Patients With Thoracic Aortic Disease. Circulation 121:e266–e369
23. Rengier F, Weber TF, Partovi S, Müller-Eschner M, Böckler D, Kauczor H-U, von Tengg-Kobligk H (2011) Reliability of Semiautomatic Centerline Analysis versus Manual Aortic Measurement Techniques for TEVAR among Non-experts. Eur J Vasc Endovasc Surg 42:324–331
24. Müller-Eschner M, Rengier F, Partovi S, Weber TF, Kopp-Schneider a., Geisbüsch P, Kauczor HU, Von Tengg-Kobligk H (2013) Accuracy and variability of semiautomatic centerline analysis versus manual aortic measurement techniques for TEVAR. Eur J Vasc Endovasc Surg 45:241–247
25. Diehm N, Kickuth R, Gahl B, Do D-D, Schmidli J, Rattunde H, Baumgartner I, Dick F (2007) Intraobserver and interobserver variability of 64-row computed tomography abdominal aortic aneurysm neck measurements. J Vasc Surg 45:263–268
26. Kauffmann C, Tang A, Therasse É, Giroux MF, Elkouri S, Melanson P, Melanson B, Oliva VL, Soulez G (2012) Measurements and detection of abdominal aortic aneurysm growth: Accuracy and reproducibility of a segmentation software. Eur J Radiol 81:1688–1694

27. Lu T-LC, Rizzo E, Marques-Vidal PM, Segesser LK Von, Dehmeshki J, Qanadli SD (2010) Variability of ascending aorta diameter measurements as assessed with electrocardiography-gated multidetector computerized tomography and computer assisted diagnosis software. Interact Cardiovasc Thorac Surg 10:217–221
28. Entezari P, Kino A, Honarmand AR, Galizia MS, Yang Y, Collins J, Yaghmai V, Carr JC (2013) Analysis of the thoracic aorta using a semi-automated post processing tool. Eur J Radiol 82:1558–1564
29. Biesdorf A, Rohr K, Feng D, von Tengg-Kobligk H, Rengier F, Böckler D, Kauczor HU, Wörz S (2012) Segmentation and quantification of the aortic arch using joint 3D model-based segmentation and elastic image registration. Med Image Anal 16:1187–1201
30. Kauffmann C, Tang A, Dugas A, Therasse É, Oliva V, Soulez G (2011) Clinical validation of a software for quantitative follow-up of abdominal aortic aneurysm maximal diameter and growth by CT angiography. Eur J Radiol 77:502–508
31. Quint LE, Liu PS, Booher AM, Watcharotone K, Myles JD (2013) Proximal thoracic aortic diameter measurements at CT: repeatability and reproducibility according to measurement method. Int J Cardiovasc Imaging 29:479–488
32. Anderson RH (2000) Clinical anatomy of the aortic root. Heart 84:670–673
33. Gurvitch R, Wood D a., Leipsic J, Tay E, Johnson M, Ye J, Nietlispach F, Wijesinghe N, Cheung A, Webb JG (2010) Multislice computed tomography for prediction of optimal angiographic deployment projections during transcatheter aortic valve implantation. JACC Cardiovasc Interv 3:1157–1165
34. Lou J, Obuchowski N a., Krishnaswamy A, et al (2015) Manual, semiautomated, and fully automated measurement of the aortic annulus for planning of transcatheter aortic valve replacement (TAVR/TAVI): Analysis of interchangeability. J Cardiovasc Comput Tomogr 9:42–49
35. Ionasec RI, Voigt I, Georgescu B, Wang Y, Houle H, Vega-Higuera F, Navab N, Comaniciu D (2010) Patient-specific modeling and quantification of the aortic and mitral valves from 4-D cardiac CT and TEE. IEEE Trans Med Imaging 29:1636–1651
36. Elattar M, Wiegerinck E, van Kesteren F, Dubois L, Planken N, Vanbavel E, Baan J, Marquering H (2016) Automatic aortic root landmark detection in CTA images for preprocedural planning of transcatheter aortic valve implantation. Int J Cardiovasc Imaging 32:501–511
37. Zegdi R, Ciobotaru V, Noghin M, Sleilaty G, Lafont A, Latrémouille C, Deloche A, Fabiani JN (2008) Is It Reasonable to Treat All Calcified Stenotic Aortic Valves With a Valved Stent?. Results From a Human Anatomic Study in Adults. J Am Coll Cardiol 51:579–584
38. Smith CR, Leon MB, Mack MJ, et al (2011) Transcatheter versus Surgical Aortic-Valve Replacement in High-Risk Patients. N Engl J Med 364:2187–2198
39. Wijesinghe N, Ye J, Rodés-Cabau J, et al (2010) Transcatheter aortic valve implantation in patients with bicuspid aortic valve stenosis. JACC Cardiovasc Interv 3:1122–1125
40. Hayashida K, Bouvier E, Lefèvre T, et al (2013) Transcatheter aortic valve implantation for patients with severe bicuspid aortic valve stenosis. Circ Cardiovasc Interv 6:284–291

41. Phan K, Wong S, Phan S, Ha H, Qian P, Yan TD (2015) Transcatheter Aortic Valve Implantation (TAVI) in Patients With Bicuspid Aortic Valve Stenosis - Systematic Review and Meta-Analysis. Hear Lung Circ 24:649–659
42. Mylotte D, Lefevre T, Søndergaard L, et al (2014) Transcatheter aortic valve replacement in bicuspid aortic valve disease. J Am Coll Cardiol 64:2330–2339
43. Xie X, Shi X, Xun X, Rao L (2016) Efficacy and safety of transcatheter aortic valve implantation for bicuspid aortic valves: A systematic review and meta-analysis. Ann Thorac Cardiovasc Surg 22:203–215
44. Sievers HH, Schmidtke C (2007) A classification system for the bicuspid aortic valve from 304 surgical specimens. J Thorac Cardiovasc Surg 133:1226–1233
45. Clouse WD, Hallett JW, Schaff H V., Gayari MM, Ilstrup DM, Melton LJ (1998) Improved prognosis of thoracic aortic aneurysms. A population-based study. J Am Med Assoc 280:1926–1929
46. Sampson UK a., Norman PE, Fowkes FGR, et al (2014) Global and regional burden of aortic dissection and aneurysms: Mortality trends in 21 world regions, 1990 to 2010. Glob Heart 9:171–180
47. Habib G, Lancellotti P, Antunes MJ, et al (2015) 2015 ESC Guidelines for the management of infective endocarditis. Eur Heart J. doi: 10.1093/eurheartj/ehv319
48. Hoang JK, Martinez S, Hurwitz LM (2009) Imaging of the Postoperative Thoracic Aorta: The Spectrum of Normal and Abnormal Findings. Semin Roentgenol 44:52–62
49. Fagman E, Bech-Hanssen O, Flinck A, Lamm C, Svensson G (2016) Increased aortic wall thickness on CT as a sign of prosthetic valve endocarditis. Acta Radiol 0:1–7
50. Sundaram B, Quint LE, Patel HJ, Deeb GM (2007) CT findings following thoracic aortic surgery. Radiographics 27:1583–1594
51. Sundaram B, Quint LE, Patel S, Patel HJ, Deeb GM (2007) CT appearance of thoracic aortic graft complications. Am J Roentgenol 188:1273–1277
52. Krasemann T, Bano M, Rosenthal E, Qureshi S a. (2011) Results of stent implantation for native and recurrent coarctation of the aorta-follow-up of up to 13 years. Catheter Cardiovasc Interv 45:405–412
53. Vergales JE, Gangemi JJ, Rhueban KS, Lim DS (2013) Coarctation of the aorta - the current state of surgical and transcatheter therapies. Curr Cardiol Rev 9:211–9
54. Forbes TJ, Gowda ST (2014) Intravascular stent therapy for coarctation of the aorta. Methodist Debakey Cardiovasc J 10:82–87
55. Zuckerman B (2016) FDA approval Cheatham Platinum stent.
56. Meadows J, Minahan M, McElhinney DB, McEnaney K, Ringel R (2015) Intermediate outcomes in the prospective, multicenter coarctation of the aorta stent trial (COAST). Circulation 131:1656–1664

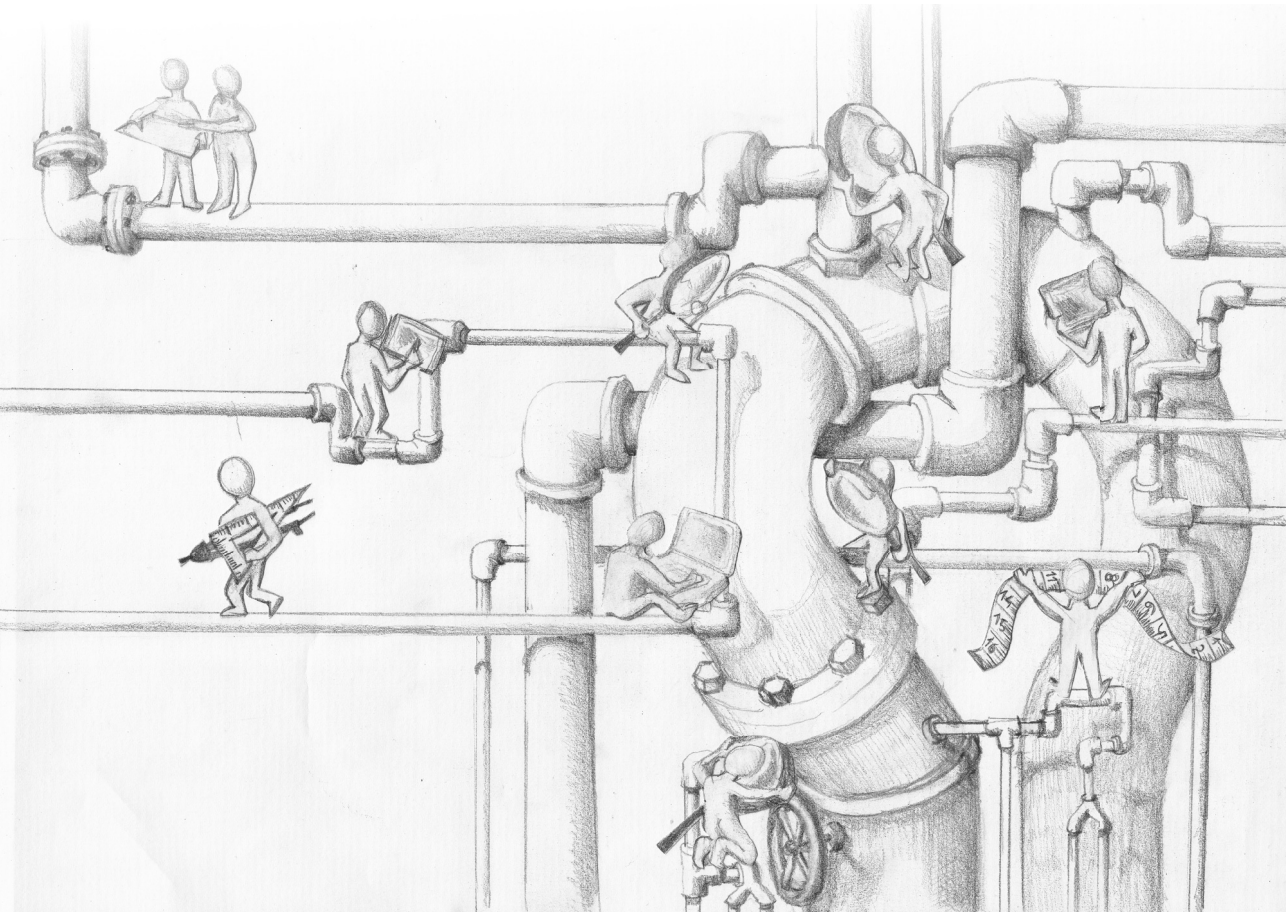

PART 1

CT assessment of aortic diameters

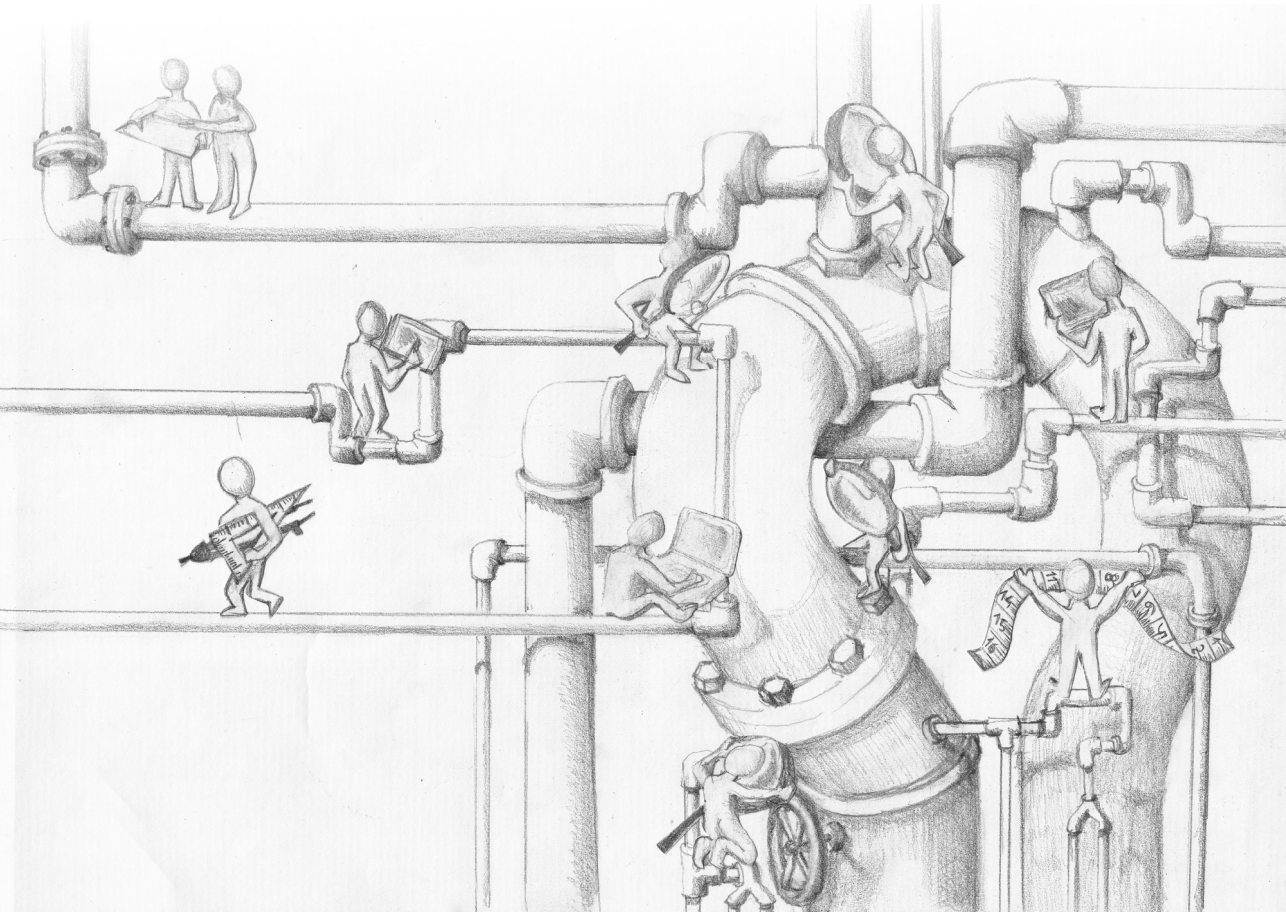

CHAPTER 2

How to measure aortic diameters on CT scans: systematic review of available techniques

Sara Boccalini, Jolien W. Roos-Hesselink, Gabriel P. Krestin, Ricardo P.J. Budde

Submitted

Abstract

Accurate aortic diameter assessment is fundamental for the management of most aortic pathologies. Although computed tomography (CT) is often the modality of choice to calculate aortic diameters, there is still no universal consensus regarding the best technique. Our aim was to assess which CT techniques have the lowest variability by investigating the average and maximum absolute difference. We performed a systematic search in PubMed and reviewed all available literature regarding the comparison of different methods to measure aortic diameters on CT scans. In total 23 articles, published from 1996 to 2014, were included in the analysis. Articles were divided based on the main techniques assessed, although, due also to the variability of additional options, this resulted in few studies being comparable. The maximum mean difference between diameters calculated on axial planes and planes obtained with the double-oblique technique was 3.3mm (limits of agreement (LAO) -3.6-10,4mm). Between the double-oblique method and automatic measurements the maximum difference was 2±1,2mm (LAO: -4.8 to 0.5mm). The lowest interobserver variability was found for automatic calculations and the highest for manual measurements on axial planes. Collected data indicate that minimum axial diameters do not show significant differences compared to corresponding ones obtained with the double-oblique technique. Further studies systematically comparing different but standardized techniques are needed to establish the most reliable one and to indicate the clinically significant threshold of aortic diameter increase.

Introduction

In the management of many aortic pathologies the single most important parameter is aortic dimensions [1–3]. The decision whether or not to perform an intervention is often based solely on aortic diameters and/or their change over time.

In a clinical context where guidelines suggest surgical intervention when aortic diameters exceed specific thresholds (e.g. >50 mm for the ascending aorta in Marfan patients) [1] or increase faster than reported thresholds [2], even a few millimeters measurement difference implicates a substantial impact on patient management. However, it is fundamental to realize there is still a wide overlap between growth thresholds indicated by guidelines published a few years ago [2] and inter-, intra-observer, intermodality and intertechnique variability, as acknowledged by recent guidelines [1]. Also, guidelines specify the theoretical principles of how to perform aortic measurements, but provide no indication on the way they should be performed in clinical practice[1, 2]. Therefore, what might seem a merely technical debate over the optimal way to measure aortic diameters is a very actual and practical issue.

Traditionally, measurements were performed on axial plane CT images but these represent true aortic dimensions only if the vessel course is perpendicular to the image plane, which often is not the case. With the possibility to perform multi-planar CT image reconstructions a plane perpendicular to the direction of the vessel can be manually defined by rotating the imaging planes in two directions (double-oblique). This method provides a true diameter, but is believed to be operator-dependent, require specific training and be time consuming. In clinical practice where follow-up studies are rarely performed by the same and/or specialized radiologists, these limitations can lead to unacceptable measurement variability. Combining a busy clinical day and the compliance with guidelines stating that a diseased aorta should be measured at multiple levels [1], is therefore a challenge. To overcome these limitations semiautomated and automated software have been introduced. However due to their specific features that differ from vendor to vendor, to their inherent way of functioning based on a centerline and the need of an expert operator interaction, they do not represent a perfect measurement tool either.

We systematically reviewed the literature regarding the comparison of different methods of aortic diameter measurements based on CT imaging and assessed the average and maximum difference obtained with the different techniques.

Methods

Literature search

We performed a Pubmed search as specified in appendix 1, which was updated last on August 10th 2015. The abstracts of the 1549 hits were screened by one author to select articles that met the following criteria: aortic diameters were evaluated based on CT imaging; two or more CT-based modalities to assess aortic diameter were compared. Ninety-eight articles were selected for further analysis. All studies regarding dynamic diameters changes during the cardiac cycle and segmentation algorithms/software prototypes that didn't provide any data about diameter measurements were excluded. Upon settlement of uncertainties by a second reviewer 52 articles were included for further analysis.

Upon completion of integral reading of the full text by one author and doubts settlement by a second reviewer, 29 studies were excluded due to one of the following reasons: a single slice or cone-beam CT scanner was employed; measurements were obtained with outdated techniques; data extraction was not feasible; reviews or educational content; measurements performed on hand held devices. All papers describing only aortic annulus measurements were excluded as well, due to its distinct features. Two relevant papers from references were included. Ultimately, 23 papers were included (**Figure 1**).

Data extraction

From the 23 included articles predefined data were systematically extracted. Collected data regarded study design, patient selection and demographics, CT scan protocol, methods and sites of measurements. All data about annulus measurements were disregarded for the reasons mentioned above. Only data about diameter measurements were investigated. Inter and intra-observer variability were investigated only in regard to agreement and no data about correlations were collected.

Results

In total 23 articles, published from 1996 to 2014, were included in the analysis. General details about the studies are summarized in **Table 1**.

One paper didn't specify if the study population had aortic disease [4] and another [5] included patients with CT scans performed prior to TAVI implantation in otherwise unknown aortic conditions. All other human studies, except three [6–8], were performed in patients with known or suspected aortic pathology, most commonly aneurysms.

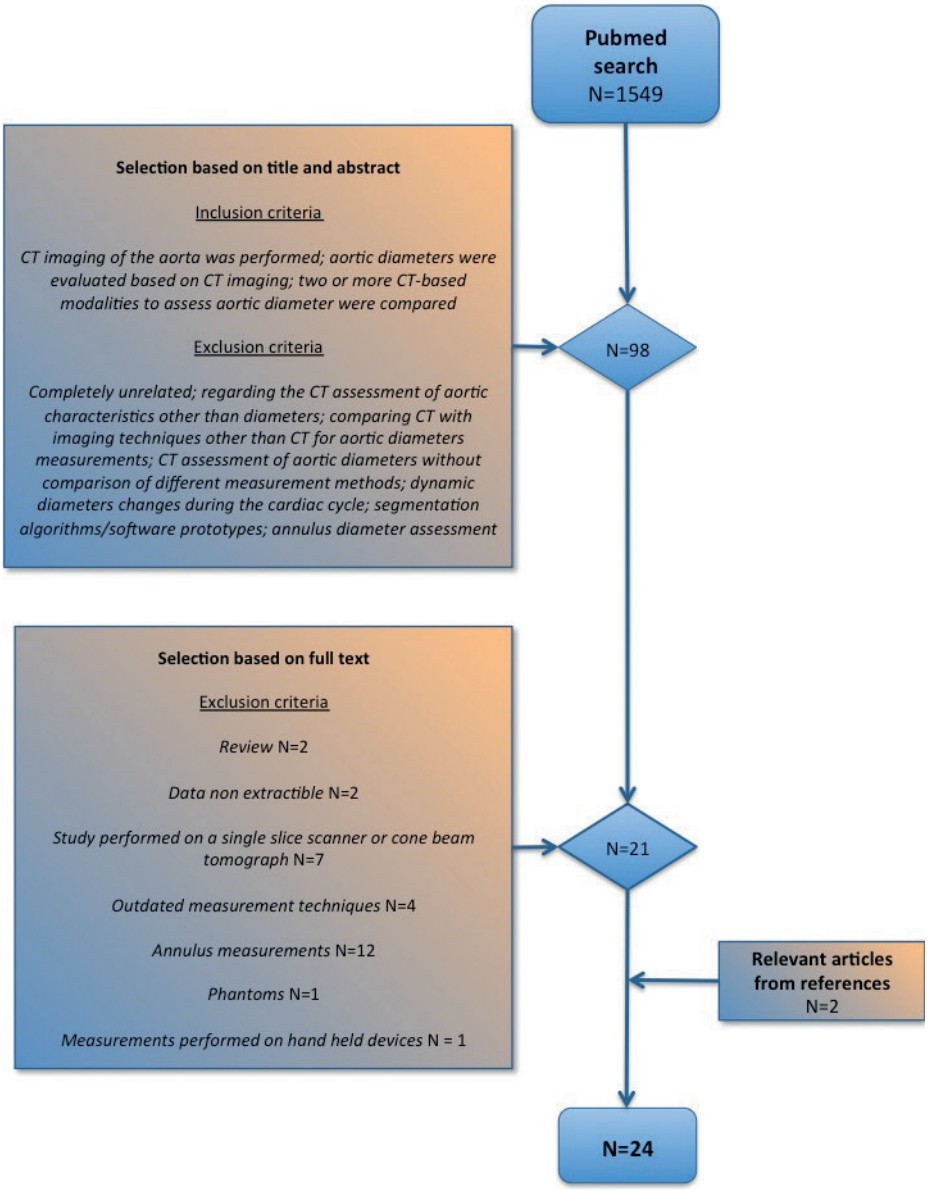

Figure 1

Flowchart illustrating the process of articles selection

Table 1. General details about included studies and study population

	Publication year	Population	Subjects number	Main protocol
Ahmed et al[15]	2014	Suspected or known aneurysm	30	Axial, sagittal and coronal vs SA
Banno et al[13]	2013	AAA	268	Unknown vs SA
Sobocinski et al[26]	2013	AAA	149 and 146	Axial and SA vs clinical outcome
Entezari et al[9]	2013	Suspected or known aneurysm	50	DO vs SA
Quint et al[12]	2013	TAA and known aortic valve disease	25	DO vs SA
Müller-Eschner et al[20]	2012	TAA or PAU	30	Axial vs DO vs SA
Ihara et al[22]	2012	Aneurysm	156	Axial vs SA
Duquette et al[7]	2011	AAA + healthy	24 (21 AAA)	Unknown vs SA
Dugas et al[18]	2011	Aneurysm	40+follow up	Axial, sagittal and coronal vs axial and DO
Mendoza et al[14]	2011	Aortic dilations and syndromic conditions involving the aorta	50	Axial vs DO
Rengier et al[16]	2011	Aneurysm or PAU	30	Axial vs DO vs SA
Delgado et al[5]	2011	Aortic valve pathology (no mention of aortic status)	90	DO vs SA
Kauffmann et al[11]	2011	AAA	40+fu	DO vs SA
Kaladji et al[10]	2010	Aneurysm	32	Unknown vs SA
Han et al[23]	2010	Aneurysm	87	Axial vs SA
Lu et al[4]	2010	NA	30	SA vs FA
Manning et al[17]	2009	AAA	109	Axial vs axial and SA
Lin et al[8]	2008	Healthy	103 (36 for comparison)	Axial vs SA
Diehm et al[19]	2007	AAA	25	Axial vs axial
Diehm et al[24]	2005	AAA	30	SA (manual mesurements) vs SA
Parker et al[25]	2005	AAA	20	Unknown vs SA
Sprouse et al[21]	2004	AAA	38	Axial vs SA
Cayne et al[27]	2004	AAA	25	Unknown vs SA
Jaakkola et al[6]	1996	Aneurysm +healthy	33 (19 aneurysms)	Axial vs axial

AAA: abdominal aortic aneurysm; DO: double-oblique technique; FA: fully-automatic software; SA: semi-automatic software.

Several methods were employed to measure aortic diameters. Moreover, each method implies several other sequential alternatives and choices along the measurement process, thus determining a multitude of possible combinations. We defined three main categories summarizing different methods: axial, double-oblique and semi-automated software

measurements (**Figure 2-4**). Only one study [4] evaluating the performance of a fully automated software was included. For each of these categories a summary of subsequent measurements options with the authors' choices is reported in (**Table 2**). A visual synopsis of the combinations of compared methods is provided in **Table 3**.

In five articles [9–13] measurements assessed with different modalities were not only performed with a different technique but also by different observers.

The anatomic locations where measurements were performed are summarized in **Table 4**. In one paper [14] out of those where the plane to derive the diameters was redefined for the different measurements methods, the authors specify how they ensured that measurements were obtained exactly in the same anatomic location.

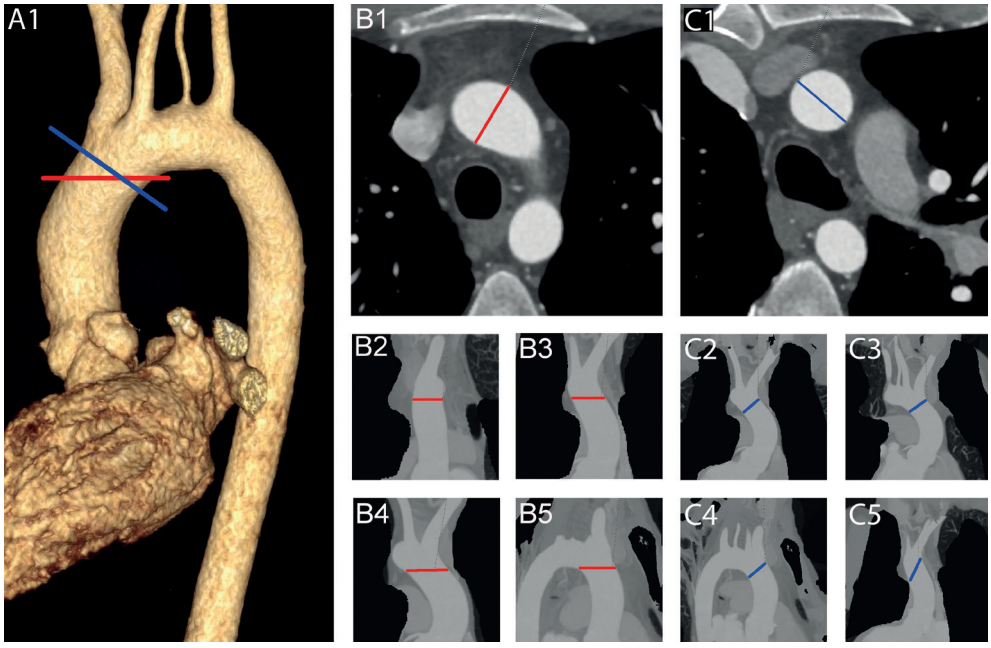

Figure 2

3D reconstructions of the thoracic aorta showing measurements of the diameter of the aorta at the level of the proximal arch performed on an axial plane (**A1; red line**) and on a plane perpendicular to the long axis of the vessel (**A1; blue line**). The difference in the angulation of the two planes is demonstrated by representing the measurements on maximum intensity projection (**red line** for the axial measurement in **B2-B5**; **blue line** for the measurement perpendicular to the axis of the vessel in **C2-C5**).

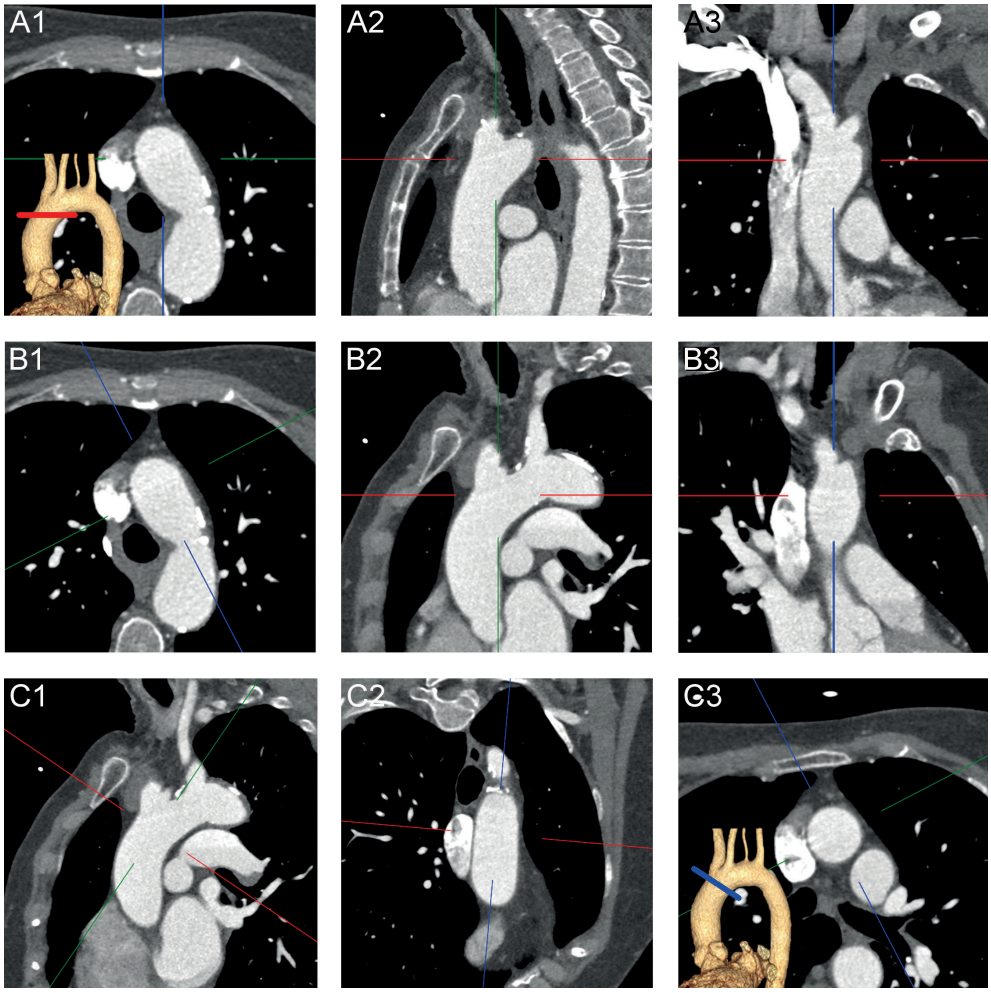

Figure 3

Double-oblique measurements. The first step for double-oblique measurement is to identify an axial plane (**A**; corresponding to the plane identified by the red line in the 3D reconstruction in **A1**) at the level of the aorta where the diameter has to be measured as shown by the crosshair on the sagittal (**A2**) and coronal (**A3**) planes. Then, the axes have to be rotated one first time. In this example the blue axis was rotated on the axial image (**B1**) until it was parallel to the aorta thus obtaining the corresponding images on modified sagittal (**B2**) and modified coronal (**B3**) planes. Then, the other axis has to be rotated. Therefore, the green axis was rotated on the modified parasagittal image until it was parallel to the aorta (**B1**). Finally it has to be verified that the blue axis is still parallel to the aorta (**B2**). The result is a cross section of the aorta at the desired level (**B3**) perpendicular to the centreline of the aorta (as shown by the blue line in the 3D reconstruction in **B3).**

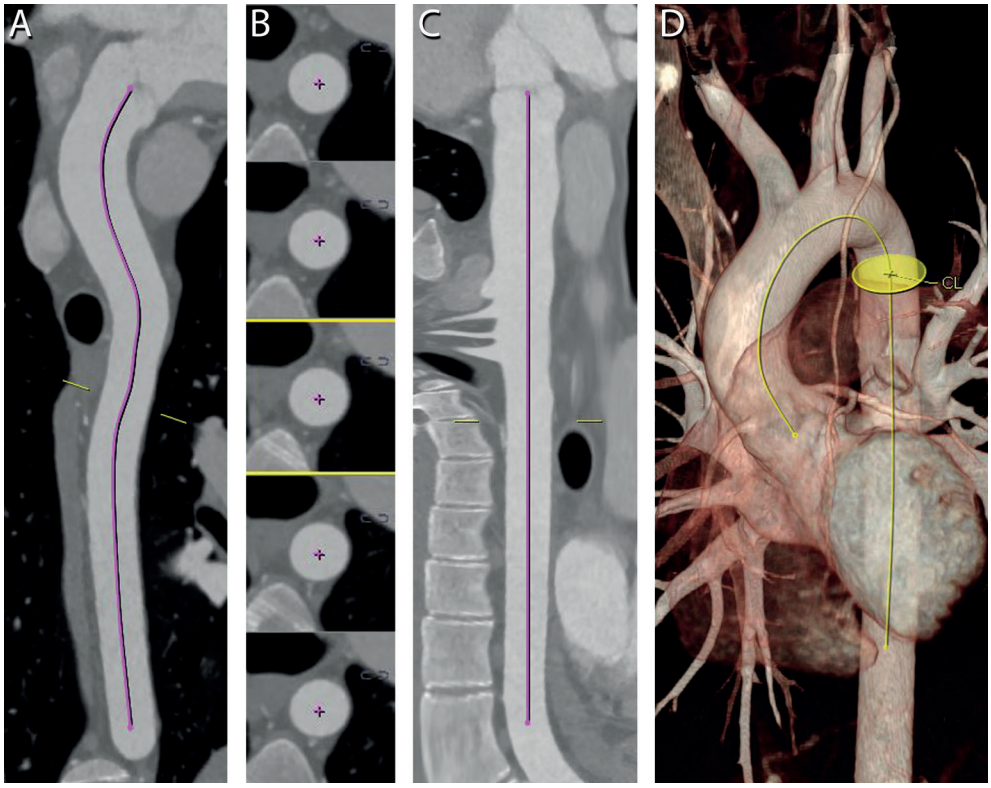

Figure 4

Semi-automatic software. The software defines a centerline that can be shown on a curved planar reconstruction (CPR) (**pink line** in **A**) for users's approval. Multiple planes perpendicular to the centerline (**B;** the point where the centerline crosses the section is indicated by **pink crosses**) can be used to check and modify the course of the centerline and to calculate diameters. The centerline can be shown also on different reconstructions such as stretched multiplanar reconstructions (**C**, **pink line**) and 3D (**D**, **yellow line**)

Table 2. Details of the measurement methods

	Software	Definition of diameters	Diameter				Edges used as boundary for measurements
			max	min	to max	others	
Axial							
Ahmed et al[15]	EVMS advanced visualization+multi modality workstation		max				outer
Sobocinski et al[26]	NA	NA	NA	NA	NA	NA	NA
Müller-Eschner et al[20]	Terarecon		max	min at angulated sections			inner (including thrombus; excluding calcifications)
Ihara et al[22]	NA		max	min			NA
Dugas et al[18]	Impax 5.2 agfa		max		to max diam	AP; LL	outer
Mendoza et al[14]	Advantage 4.2		max		to max diam	mean; area based on mean diam or max diam at angulated sections	inner
Rengier et al[16]	Terarecon		max	min at angulated sections			- inner (including thrombus; excluding calcifications) - outer at maximum aneurysm diameter
Delgado et al[5]	Vitrea2		max				NA
Han et al[23]	Synapse fujifilm		max	min			outer
Manning et al[17]	Aquarius		max		to max diam		outer
Lin et al[8]	AW 4.3 Advantage Workstation					AP; LL	inner
Diehm et al[19]	Syngo CT 2006 AUB 20B	manual	max	min			outer

Parker et al[25]	NA	NA	NA	NA	NA	NA	NA
Sprouse et al[21]	Medical media system preview		max	min			outer
Jaakkola et al[6]	NA					AP; LL	NA
Double-oblique							
Entezari et al[9]	NA		max				outer
Müller-Eschner et al[20]	Terarecon		max				inner (including thrombus and excluding calcium)
Dugas et al[18]	Impax 5.2 agfa		max				outer
Quint et al[12]	Vital images workstation		max				outer
Mendoza et al[14]	Advantage 4.2		max		to max diam	mean perimeter; area (calculated based on average or one diam depending on location)	inner
Rengier et al[16]	Terarecon		max				- inner (including thrombus; excluding calcification) - outer at maximum aneurysm diameter
Delgado et al[5]	Vitrea2		max				NA
Kauffmann et al[11]	Impax 5.2 agfa		max				outer
Lin et al[8]	AW 4.3 Advantage Workstation/ Vitrea Workstation					AP; LL; area	inner
Cayne et al[27]	NA		max				outer
Semi-automated							

Table 2 - continued

Banno et al[13]	Terarecon	NA	NA	NA		NA
Sobocinski et al[26]	Terarecon	NA	max			NA
Entezari et al[9]	Vitrea 6.0.0.1	automatic	max			outer
Quint et al[12]	Advantage windows workstation 4.5	NA	max			outer
Müller-Eschner et al[20]	Terarecon	Automatic (If calcium or a thrombus interfered, manual)	max			inner (including thrombus and excluding calcium)
Ihara et al[22]	Terarecon	NA	max	min		NA
Duquette et al[7]	Own software		max			outer
Rengier et al[16]	Terarecon	- automatic (If calcium or a thrombus interfered, manual) - manual at maximum aneurysm diam				- inner (including thrombus; excluding calcification) - outer at maximum aneurysm diameter
Delgado et al[5]	3mensio valves	NA	max			NA
Kaladji et al[10]	Endosize	NA	max	min		inner
Han et al[23]	M2S preview software	manual	max	min	AP; LL	outer
Lu et al[4]	Advantage window workstation 4.3	manual	max	min		inner
Kauffmann et al[11]	NA	automatic	max			outer
Manning et al[17]	Aquarius	NA	max			outer

Diehm et al[24]	Advantage adw workstation (AVA software)	Manual vs automatic	max		inner
Parker et al[25]	Preview medical metrx solution	NA	max		NA
Sprouse et al[21]	Medical media system	NA	max	min	outer
Fully-automated					
Lu et al[4]	Advantage window workstation 4.3	automatic	max		inner

AP: anteroposterior; LL: latero-lateral; diam: diameter

Table 3. Visual synopsis of measurement methods comparisons

	CT protocol				Clinical outcome
CT protocol	**Axial**	**Double oblique**	**Semiautomated software**	**Fully automated software**	**Endoleak; reintervention**
Unknown		Cayne et al[27]	Banno et al[13] Duquette et al[7] Kaladij et al [10] Parker et al[25]		
Axial	Manning et al[17] Diehm et al[19] Jaakkola et al[6]	Muller Eschner et al[20] Mendoza et al[14] Rengier et al[16] Lin et al[8]	Muller Eschner et al[20] Ihara et al[22] Rengier et al[16] Han et al[23] Manning et al[17] Sprouse et al[21]		Sobocinsky et al[26]
Axial, sagittal, coronal	Dugas et al[18]	Dugas et al[18]	Ahmed et al[15]		
Double oblique			Entezari et al[9] Quint et al[12] Muller Eschner et al[20] Rengier et al[16] Delgado et al[5] Kauffmann et al[11]		
Semiautomated software					Sobocinsky et al[26]
Semiautomated software with manual measurements			Diehm et al[24]	Lu et al[4]	

Table 4. Anatomic locations where measurements were performed

	N	Locations of measurements												
		Sinus	STJ	AA	PROX/mid arch	DIST arch/ isthmus	DA	Aneurysm		Below lower RA	Infrarenal	Iliac arteries		Other
								neck	max			right	left	
Ahmed et al[15]	1			yes										
Banno et al[13]	6						yes				yes			CT, SMA, RRA, LRA
Sobocinski et al[26]	5								AAA	yes	15 mm below lower RA	yes	yes	
Entezari et al[9]	6	yes	yes	yes	prox to BC	yes	yes							
Müller-Eschner et al[20]	3				distal to LCCA	yes	prox to celiac trunk							
Ihara et al[22]	1								TAA/ AAA					
Quint et al[12]	3	- cusp to cusp - cusps to commissures (only in research setting)	yes	yes										
Duquette et al[7]	1	NA	NA	NA	NA	NA	NA	NA	NA	NA	NA	NA	NA	NA
Dugas et al[18]	1								AAA					
Mendoza et al[14]	8	yes	yes	yes	- origin BC - distal to LCCA	yes	- pulm art - diaphragm							
Rengier et al[16]	4				distal to LCCA	yes	prox to celiac trunk		TAA/ PAU					
Delgado et al[5]	2	cusps to commissure	yes											

Table 4 - continued

Kauffmann et al[11]	1					AAA					
Kaladji et al[10]	6				yes	AAA	yes	15mm below lower RA	yes	yes	
Han et al[23]	1					AAA					
Lu et al[4]	1	yes									
Manning et al[17]	1					AAA					
Lin et al[8]	2	yes	yes								
Diehm et al[19]	2						yes	10mm below lower RA			
Diehm et al[24]	4					AAA	yes		yes	yes	
Parker et al[25]	4					AAA	yes		yes	yes	
Sprouse et al[21]	1					AAA					
Cayne et al[27]	1					AAA					
Jaakkola et al[6]	4					AAA					suprarenal; level of RA; 2 and 5 cm above aortic bifurcation

STJ: sino-tubular junction; AA: ascending aorta; PROX arch: proximal arch; DIST arch: distal arch; DA: descending aorta; BC: brachiocephalic artery; prox: proximal; LCCA: left common carotid artery; RA: renal artery; CT: celiac trunk; SMA: superior mesenteric artery; RRA: right renal artery; LRA: left renal artery; AAA: abdominal aortic aneurysm; TAA: thoracic aortic aneurysm; PAU: penetrating atherosclerotic ulcer

CT scans technical parameters with potential impact on aortic diameter measurements

In the included studies the CT examinations were performed in different centers, at different times and with different scanners and scan protocols (**Table 5**).

Out of 11 papers investigating only or also the ascending aorta, ECG gating was employed in 6 studies for all patients [4, 5, 8, 9, 12, 15] and in one for an unknown percentage of them [14]. Reconstructions for aortic measurements were obtained in diastolic phases in 5 papers ([4, 9, 12, 15] and systolic phase in one [5].

In three studies [4, 8, 12] scans of low quality (due to motion artifacts [4, 12] and streak artifacts from contrast in the superior vena cava [4]) were excluded from the analysis.

Although in all the other studies no scans were excluded for these reasons, data about image quality is provided only in five [5, 11, 14–16].

Images were reconstructed with a wide range of slice thicknesses (0.63 to 10 mm). In only five studies [4, 5, 9, 14, 15] all scans had a slice thickness ≤ 1mm. The one study [6] with a slice thickness of 10 mm (increment 15mm) was not excluded because only measurements performed on axial slices were compared.

Comparison between different CT techniques for aortic diameter measurements

Axial

Diameters of abdominal aneurysms in the antero-posterior (AP) plane on axial images were compared with other measures performed on axial images: transverse plane [6]; the maximum diameter, perpendicular to the maximum diameter [17]; axial maximum, right to left lateral wall and perpendicular to axial max (shortaxis) [18]. The maximum diameter was on average 5 mm longer than the AP [17].

With data from three observers [6], interobserver variability on the AP plane was statistically significant for only one pair of measurements on normal aortas; for aneurysmatic aortas for two pairs of AP diameters as well as all three pairs of transverse ones, reaching an absolute difference of ^{3}10 mm in 5% of cases. With all measurement methods at least one case had an interobserver difference ^{3}10 mm and shortaxis measurements showed the highest percentage (11.25%) of interobserver difference values between 5 and 10 mm [18].

It has been postulated that whenever the aorta is enlarged and/or its major axis is angulated the aortic minor diameter derived on an axial plane is more representative of the real lumen dimensions than the major one.

Table 5. CT scans protocols

	CT scan protocol								
	Number of scans	**Scanner**	**Slices**	**kv**	**mAs**	**Slice thickness (mm)**	**Increment (mm)**	**ECG gating**	**Employed cardiac phase**
Ahmed et al[15]	30	Flash	128	120	320(caredose4d)	0.75	0.5	retrospective	best diastole
Banno et al[13]	268	NA	NA	NA	NA	1 to 5	NA	NA	
Sobocinski et al[26]	149+146	Brilliance	64	NA	NA	NA	NA	NA	
Entezari et al[9]	50	Definition	64	100	170(caredose)	0.75	0.4	prospective	70%
Müller-Eschner et al[20]									
Protocol 1	17	Aquilion	16	120	120	1	0.8	NA	
Protocol 2	13	Volume zoom	4	120	120	3	3	NA	
Ihara et al[22]	156	Aquilion	64	120	NA	NA	NA	0	
Quint et al[12]	25	Discovery ct750hd	64	100-120	438-700	1.25	0.625	retrospective	75%
Duquette et al[7]	24	Lightspeed ultra	8	NA	NA	1 to 8	NA	NA	
Dugas et al[18]									
Protocol 1	NA	Sensation	4	NA	NA	1 to 2	NA	0	
Protocol 2	NA	Sensation 16	16	NA	NA	NA	NA	0	
Protocol 3	NA	Sensation 64	64	NA	NA	1 to 2	NA	0	
Protocol 4	NA	Lightspeed 16	16	NA	NA	1 to 2	NA	0	
Mendoza et al[14]	50	multiple	NA	120	500	0.6	NA	Some/NA protocol	NA
Rengier et al[16]									
Protocol 1	17	Aquilion	16	120	120	1	8	NA	
Protocol 2	13	Volume zoom	4	120	120	3	3	NA	

Delgado et al[5]									
Protocol 1	NA	Aquilion	64	120, 135	300 to 400	0.5	NA	retrospective	30-35%
Protocol 2	NA	Aquilion one	320	100, 120, 135	400 to580	0.5	NA	prospective	30-35%
Kauffmann et al[11]									
Protocol 1	NA	Sensation	4	NA	NA	1 to 4	NA	0	
Protocol 2	NA	Sensation	16	NA	NA	1 to 4	NA	0	
Protocol 3	NA	Sensation	64	NA	NA	1 to 4	NA	0	
Protocol 4	NA	Lightspeed	16	NA	NA	1 to 4	NA	0	
Kaladji et al[10]	32	Lightspeed	16	120	215 to 360	1.25	NA	0	
Han et al[23]	87	Lightspeed pro16	16	NA	NA	1 to 2	NA	0	
Lu et al[4]	30	VCT	64	NA	NA	0.63	0	retrospective	75%
Manning et al[17]	NA	Siemens	NA	NA	NA	<5	NA	NA	
Lin et al[8]	103	Lightspeed VCT	64	120	350-750	2.5	NA	retrospective	end diastole
Diehm et al[19]	25	Sensation	64	100	320	1.2	1.5	0	
Diehm et al[24]	30	Asteion ms (toshiba)	4	120	200	2	2	0	
Parker et al[25]	20	GE	NA	120	≥ 280	≥ 5	2.5	0	
Sprouse et al[21]	38	Light speed plus	4	NA	NA	2 to 5	NA	0	
Cayne et al[27]									
Protocol 1	22	GE	NA	NA	NA	≥ 5	5	0	
Protocol 2	3	GE	NA	NA	NA	≥ 5	5	0	
Jaakkola et al[6]	33	Somatom plus	4	NA	NA	10	15	0	

The cardiac phase employed for measurements is expressed as % of the R-R interval unless stated otherwise.

Diehm et al. [19] demonstrated statistically significant interobserver variability for most pairs of measurements both for minor and major diameter (minimum mean difference of -0.17mm±2.48 and maximum mean difference of 3.31mm±3.89).

Axial vs double-oblique

Comparing alternately maximum diameter or minimum diameter in case of "oblique projections" on axial images and maximum diameter on double-oblique, two studies [16, 20] did not demonstrate any significant difference in these measurements in the thoracic and abdominal aorta. On the contrary, Mendoza et al. [14] found a statistically significant difference at all sites with the average between the maximum diameter and the diameter perpendicular to the maximum diameter on the axial plane being bigger than the corresponding double-oblique at all locations, except at the arch and proximal descending aorta, where only maximum diameter was measured, and mid descending. The minimum and maximum absolute mean differences were off 1±2mm at mid ascending, mid arch, mid descending and thoracoabdominal aorta and 8±7mm at STJ level, respectively. The magnitude of difference between the measurements obtained with the two methods, as well as the difference between the two diameters in the axial plane, correlated with the aorta angular displacement. Dugas et al. [18] also found that maximum axial diameter, at the largest point of abdominal aneurysms, was significantly larger than double-oblique maximum diameter. Double oblique diameters were significantly larger than the other types of axial measurements assessed except for the anteroposterior. Therefore the axial maximum diameter overestimated the true aneurysms diameter while all other axial measurements (except for the anteroposterior) underestimated it.

In another study, AP and transverse end systolic axial measurements were higher than corresponding double oblique by 0.52mm (95% CI 0.14-0.9) and 0.12mm (95% CI -0.13 to 0.37), respectively for the ascending aorta and 0.24 mm (95% CI -0.08 to 0.58) and 0.14 mm (95% CI -0.15 to 0.43) respectively for the descending thoracic aorta [8].

Two papers found that intra [14] and inter [16] observer difference was not statistically significant for both methods. Dugas et al. [18] found an interobserver difference greater than 10 mm only for axial measurements in 1.9% of all measurements performed on an axial plane (AP, LL and maximum) and also the percentage of interobserver differences between 5 and 10 mm was higher for axial measurements (7.2% against 3.8%). According to Muller-Eschner et al. [20] 90% of expected values of interobserver variability would be lower for axial measurements at all locations by at least one millimeter.

In summary, the maximal diameter measured on axial images was generally larger than the actual double oblique measurement.

Axial vs centerline

Measurements performed on the axial plane were compared with measurements obtained with semi-automated software on planes orthogonal to the aortic major axis. In two cases the maximum diameters obtained with the two techniques were compared [17, 21]. In two papers [16, 20], the authors evaluated the maximum axial diameter only for segments of the aorta parallel to the z-axis, otherwise they calculated the minimum axial diameter. Other authors compared also the minor diameter [21, 22], the antero-posterior diameter and the diameter perpendicular to the maximal one [17] derived in the axial plane, with the major (and minor [22]) diameter obtained with the software. Han et al [23] provide data only about axial minor and centerline major diameters. Only in two papers [16, 20] the authors enlisted the manual interactions that were performed to obtain a representative centerline, including deployment of "seed points" and correction of the centreline and automatically defined borders. The same authors are the only ones who specify that once the appropriate plane based on the centerline was defined, the diameters were automatically calculated, except if thrombus or calcification interfered and always at the point of maximum aneurysm diameter [16].

The mean diameters calculated as specified above, were found to have a statistically significant difference in two studies assessing abdominal aneurysms [17, 21]. Only two papers [17, 21] reported maximum axial diameters higher than those obtained with the centerline. Values obtained with the two modalities, demonstrated poor agreement as calculated with Bland-Altman plots [17, 21, 23], with the lowest mean difference of 1.2 ± 1.2mm for axial maximum diameter compared with centerline maximum diameter for an angulation of the abdominal aneurysm <25° [21] and the highest (-5.9±6 mm) between the diameter perpendicular to the maximum measured on the axial plane and the centerline of abdominal aneurysms [17] (**Table 6**).

Only one paper investigated intraobserver variability reported as number of measurement pairs for all methods with a variation of <2mm (78%) and >5mm (9.5%) [17]. The interobserver variability in the above-mentioned study is reported in the same manner (variation <2mm in 65% and >5mm in 9.5% of pairs). Rengier et al.[16] found that both interobserver reliability and variability by not-expert readers were significantly lower for centerline measurements compared to axial ones and significantly higher at the level of the maximum diameter of the aneurysm in comparison to the other locations of measurement.

Sprouse et al. [21] compared the difference between axial major diameters and major centerline diameters in relation to the angle of the abdominal aneurysm. For angles lower than 25 degrees no statistically significant difference could be demonstrated, while for angles of more than 25 degrees the average of axial maximum diameters was statistically

Table 6. Mean difference (mm) between measurements performed on the axial plane and with a semi-automated software

Study	Mean difference ±SD (Limits of agreement)			
Ihara et al[22]	**Axial min vs centerline min (degree of aortic angulation =0°)**			
	0.5±3.29			
	(-2.79 to 3.79)			
Han et al[23]	**Axial min vs centerline max**			
	4.25±4.37			
	3.30-5.19 (P=.05)[a]			
Manning et al[17]	**Axial AP vs centerline**	**Axial ME vs centerline**	**Axial PME vs centerline**	
	-3.0±6.6	2.4±5.0	-5.9±6.0	
Parker et al[25]	**Lower renal artery**	**Maximal aneurysm diameter**	**Right iliac artery**	**Left iliac artery**
	0.51±2.6	-4.5±13	0.29±2.4	1.0±6.0
Sprouse et al[21]	**Axial max vs centerline max**	**Axial max vs centerline max (Angle aortic angulation <25°)**	**Axial min vs centerline max (Angle aortic angulation >25°)**	
	3.3 (± NA)	1.2±1.2	5.0 (± NA)	
	(- 3.6 to 10.4)	(-1.2 to 3.6)	(-2.4 to 12.4)	
	Axial min vs centerline max	**Axial min vs centerline max (Angle aortic angulation <25°)**	**Axial min vs centerline max (Angle aortic angulation >25°)**	
	2.6 (± NA)	2.9 (± NA)	2.4 (± NA)	
	(- 5.4 to 10.6)	(-5.3 to 11.4)	(-5.0 to 11.8)	

[a] : 95% CI of difference; AP: anteroposterior; ME: maximum ellipse; PME: diameter perpendicular to the maximum ellipse

higher (mean of 5mm with limits of agreement of -2.4 to 12.4mm). The overall mean difference between methods, regardless of aortic angulation, was higher for axial maximum vs centerline maximum diameters (=3.3mm) as compared to axial minimum vs centerline maximum (=2.6mm), however for angles lower than 25 degree it was higher for axial minor and for angles higher than 25 degrees it was higher for axial maximum. Ihara et al. [22] didn't find any correlation between the difference of the axial minor and centerline minor diameters and the aortic angulation for both abdominal and thoracic aneurysms.

In summary, the maximal diameter measured on axial images was generally larger than the diameter measured using centreline based approaches and may be related to the aortic angulation.

Double-oblique vs centerline

Six studies compared maximum diameters obtained with double-oblique and centerline measurements [5, 9, 11, 12, 16, 20]. Double oblique measurements were performed by orientating the axes in two planes in order to obtain a plane perpendicular to the longitudinal axis of the aorta. Subsequently aortic diameters were manually measured. In all cases of semi-automatic measurements an operator manually interacted with the software in order to obtain an appropriate centerline. Thereafter diameters were automatically calculated, except by Muller-Eschner et al. [20] who resorted to manual measurements if calcium or thrombus interfered.

No statistically significant difference was found between measurements performed with the two techniques in two different studies at the level of the arch, celiac trunk and maximum dilatation of abdominal aneurysm [16, 20]. However other studies found statistically significant differences: at all locations (sinuses, sinotubular junction (STJ), ascending aorta), with semiautomatic centerline diameters consistently larger (absolute value of the maximum difference: 4.8mm) [12]; between the software and one of the observers at the level of abdominal aneurysms maximum dilatation [11]. Three studies [5, 9, 12] provide data about the mean difference between the two modalities at multiple locations (**Table 7**). The maximum mean difference was found at the STJ (2.0 ± 1.2mm) [12] and the smallest by Delgado et al. [5] at the level of the sinuses (right coronary cusp-commissure=0.01±0.7mm; left coronary cusp-commissure= 0.01±0.8mm).

Quint et al. [12] reported a higher intraobserver difference for the semiautomated (range of mean differences at different locations= 0.2-2.3mm; maximum absolute difference values of 9mm) compared to the double oblique measurements (range of mean difference for two radiologists of −0.3-0.6mm and 1.0-0.2mm with maximum absolute difference values of 9 and 11mm respectively); for manual measurements the difference was statistically

Table 7. Mean difference (mm) between double oblique and semi-automated measurements

Study		Mean difference (95% CI)								
		NCS-C	**RCS-C**	**LCS-C**	**C-C**	**STJ**	**MAA**	**PROX**	**DIST**	**DESC**
Entezari et al[9]	Manual vs semi-automated reader 1				0.07	1.26	0.38	1.05	0.29	−0.14
					−0.46–0.62	0.71–1.85	−0.14–0.9	0.44–1.68	−1.14–0.58	−0.44–0.72
	Manual vs semi-automated reader 2				0.44	0.86	0.52	1.2	0.9	−0.24
					−0.04–0.92	0.1–1.6	0.04–1	0.53–1.9	−0.27–02.1	−0.82–0.34
		Mean difference ± SD (Limits of agreement)								
		NCS-C	**RCS-C**	**LCS-C**	**C-C**	**STJ**	**MAA**	**PROX**	**DIST**	**DESC**
Quint et al[12]		−1.3±1.3	−1.5±1.0	−1.8±1.4	−0.9±0.9	−2.0±1.2	−0.5±1.4			
		(−4.5, 0.8)	(−3.5, 0.3)	(−4.3, 2.0)	(−2.3, 0.8)	(−4.8, 0.5)	(−3.8, 3.8)			
Delgado et al[5]		0.05 ± 0.5	0.01 ± 0.7	0.01 ±0.8		−0.05±0.5				

NCS-C: non coronary sinus cusp to commissure; RCS-C: right coronary sinus cusp to commissure; LCS-C: left coronary sinus cusp to commissure; C-C cusp to cusp; STJ: sino-tubular junction; PROX: proximal arch (immediately proximal to innominate artery), DIST: distal arch (distal to left subclavian artery), DESC: descending aorta

significant ($p<0.05$) at one and two locations for the two radiologists, respectively, whereas it was significant at all but one locations for the software.

When comparing double-oblique measurements obtained by two radiologists a significant difference between the two means (maximum mean difference of 1.3 ± 2.0mm with a maximum absolute difference value of 6 mm) was reached at all locations except when measuring the sinus cusp-to-cusp [12]. In the same study, for repeated measurements obtained with the software by different observers the maximum mean difference was 0.7±1.2mm, the maximum absolute value 5mm and the difference was statistically significant at mid-ascending aorta.

In summary different studies yielded opposite results regarding whether or not the difference between diameters obtained manually with the double oblique technique and with automatic software was significant. According to one study [12] automatic measurements present higher intraobserver variability but lower interobserver differences.

Centerline with manual vs automatic definition of borders

Diehm et al. [24] compared measurements performed with the automatic detection of centerline and lumen borders, after the identification by the reader of appropriate landmarks, with reader-assisted freehand diameter assessment (apparently, although not clearly stated, on a plane defined by the software). However, while the software derived the diameters only of the aortic lumen, the reader also included the aortic wall in the measurements resulting in a systematic diameter underestimation with the first method (**Table 8**). Overall intraobserver differences were not significant at any aortic location. However, with reader-assisted freehand assessment the less experienced radiology resident showed higher mean differences (range of absolute values of means: 1 to 1.7mm) compared to the expert reader (range of absolute values of means: 0.1 to 0.4mm). This was less evident with the employment of the software (range of absolute values of means: 0 to 0.3mm and 0 to 0.9mm). On the contrary, interobserver differences were significant and with higher values for the semi-automated assessment (range of absolute values of means: 0.5 to 3.1mm vs 0 to 1.2mm for the freehand).

Other methods vs semi-automatic software

Several studies compared measurements obtained with a semi-automated software with those derived with poorly or not defined manual methods and are therefore not expanded upon here.

Parker et al. [25] didn't demonstrate any statistically significant difference between the software and the unspecified modality at any location with a mean difference ranging from 0.29±2.4 mm to -4.8±13mm at the level of the maximum aneurysm diameter (**Table**

Table 8. Mean difference (mm) between measurements performed on a plane defined by a software with manual vs automatic diameters calculation

Study	**Mean difference ± SD**							
Lu et al[4]	**Obs 1.1 vs SAS 1**	**Obs 1.1 vs SAS 2**	**Obs 1.2 vs SAS 1**	**Obs 1.2 vs SAS 2**	**Obs 2.1 vs SAS 1**	**Obs 2.1 vs SAS 2**	**Obs 2.2 vs SAS 1**	**Obs 2.2 vs SAS 2**
	-0.5±0.7	-0.6±0.7	-0.4±0.6	-0.5±0.7	-0.1±0.6	-0.2±0.8	-0.1±0.5	-0.2±0.6
Diehm et al[24]	**Observer 1**				**Observer 2**			
	Lower renal artery	**Maximal aneurysm diameter**	**Right iliac artery**	**Left iliac artery**	**Lower renal artery**	**Maximal aneurysm diameter**	**Right iliac artery**	**Left iliac artery**
	-1.4±NA	-14.1±NA	0±NA	-0.4±NA	-3.1±NA	-17.2±NA	-0.8±NA	-1.5±NA

Obs: observer; SAS: semi-automated software

6). Duquette et al. [7] found that the mean difference between the software and the other observers, removing 10% of the outlying patients, was 2.86±1.77mm for aneurysmatic aortas and 1.96±1.54mm for healthy aortas. Kaladji et al.[10] found a minimum mean difference between methods of 0.57mm (LAO -0.32-0.48) and maximum of 2.09mm (LAO -0.46-3.67).

In one study inter and intraobserver mean differences with the software were less than one millimeter with 95% of absolute difference values <2 mm and 100% <5mm [10]. Ahmed et al. [15] found opposite results for intraobserver agreement of the two observers in regard to the different methods but with all biases below 1 mm. In another paper when comparing each operator (including the software) with all the other observers and the software the mean fractional error ranged from 2.04±1.76mm to 2.96±2.35mm for diseased aortas and from 1.35±1.12mm to 3.05±1.24mm for normal aorta [7]. Interobserver variability was significantly positive for manual measurements (bias 2.5 mm; 95% CI, 1.2-3.8 mm) but not for centerline measurements (bias 0.3 mm; 95% CI, -0.5 to 1.1 mm).

Semiautomated vs fully automated software

One study [4] aimed at comparing mid ascending aorta measurements obtained with fully and semi-automated software differing solely in the diameter measurements step. With mean differences ranging from -0.1±0.6mm to -0.6±0.7mm (**Table 8**), the mean diameters were significantly lower only for one observer compared to the software.

Others

Sobocinsky et al. [26] compared complication rates in two patient groups within two years after a procedure that had been planned based on axial or semi-automated measurements. The rate of complications was higher in the axial measurements group although the difference was statistically significant only for endoleaks ($p = .004$) and related secondary interventions ($p < .001$) but not for the overall freedom from secondary interventions at two years ($p = .617$).

Cayne et al. [27] compared measurements performed by the same observers at first with an unknown method and subsequently with a standardized protocol based on several criteria including multiplanar measurements. The mean difference between observers was significantly decreased with the standardized method compared to the unstandardized (2.8±4.4mm and 4.0±5.1mm respectively; p=0.05mm). It was noted that with both research methods the highest values of standard deviation were found in the largest vessels. These measurements were compared with what had previously been annotated in the clinical report based on an unknown method of measurement. These results are difficult to interpret, and therefore are not reported, considering that at least one of the measurements method was unknown.

In addition to the findings discussed above, Dugas et al. [18] found that abdominal aortic aneurysm maximum diameters measured on sagittal and coronal planes were smaller than the maximum diameters on axial planes and on the manually defined orthogonal planes.

Time consumption

Data on time consumption was very limited and contradictory. The authors not retaining these results significant, they were disregarded.

Discussion

This systematic review highlighted the numerous available methods to measure aortic diameters on CT images and the resulting limited number of comparable studies. Moreover, the few comparable studies presented heterogeneous results. Intermethod variability was similar for all methods. Inter and intra-observer variabilities were higher for axial measurements. It is commonly believed that measurements performed on planes perpendicular to the true axis of the aorta are the most representative of the real aortic dimensions. However, data supporting this theory is scarce. Measuring the minimum axial diameter yielded results similar to measurements perpendicular to the long axis of the aorta.

The importance of a precise and reproducible assessment of aortic diameters cannot be overstated. CT is often the imaging modality of choice to provide these measurements. However, even the most recent guidelines [1] still lack precise indication about the most reliable method to calculate aortic diameters.

One of the few clear indications provided in the guidelines is that measurements should be performed on a plane orthogonal to the vessel long axis. Therefore, we need to distinguish between axial plane measurements and those performed on planes perpendicular to the centerline of the vessel. The axial planes define aortic sections with a shape progressively more different from the orthogonal cross-section as the angle between the aortic major axis and the z-axis increases. Accordingly, various studies demonstrated that all axial measurements (except the minimum diameter) overestimated diameters obtained with the manual double technique [8, 14, 18] or semi automatic software [16, 17] with a maximum mean difference of 3.3mm (LAO -3.6-10,4mm).

However, in one study [14], axial maximum diameters were lower than corresponding double-oblique ones at the arch and proximal descending aorta and the difference was correlated with the angular displacement of the two planes [14]. This was confirmed by

Sprouse et al. [21] who found a significant difference between axial and semi-automatic maximum diameters only for 3D aortic angulations ≥25 degrees. The two studies that compared minimum axial aortic arch diameters with double-oblique as well as semi-automatic measurements [16, 20] and at the level of the maximum aneurysmatic dilatation [16] did not find any statistically significant difference. Therefore, evidence seems to confirm that the minimum axial aortic diameter could be a reliable estimation of aortic dimensions. Thus, clinical measurements could be routinely performed this way without multiplanar reconstructions.

Unexpectedly, with mean differences as high as 2±1.2mm (LAO: -4.8 to 0.5mm) [12] at the STJ, intermethod variability between double-oblique and semi-automatic measurements did not seem to provide better results, although both techniques rely on measurements performed on a plane perpendicular to the longitudinal axis of the vessel. On the contrary, the only study relating manual and automatic measurements performed on a semi-automatically defined plane showed excellent results with the highest mean of differences of -0.6±0.7mm.

Diagnostic, follow up and pre-interventional diameters have to be calculated based on imaging modalities in the absence of a true gold standard to assess their reliability. Ex-vivo measurements are performed in a non–physiological condition without blood circulating, which might greatly influence results [28]. During surgery some aortic diameters can be assessed directly, but the procedure has significant limitations (i.e. cardioplegic heart and with metric sizers of different dimensions) [29, 30].

For these reasons and given the importance of diameter change over time, intra and interobserver variability constitute a fundamental parameter for the applicability of any method in daily clinical practise.

The scarce data on intraobsever agreement showed comparable means between double-oblique and semi-automated methods with all values ≤1mm [4, 10, 12, 14, 16]. However, for single pairs of measurements, differences >5mm were found for all methods [12, 17] in up to 9.5% of cases [17].

Interobserver variability varied between a mean of <1mm for semi-automated software [4, 10, 12, 15] to 3.31±3.89mm [19] for axial measurements (up to >10mm in single cases [6, 18]). Interobserver differences for double-oblique measurements proved to be lower than for axial [18, 20] and higher than for semi-automatic [12, 15]. Standardized measurements reduced interobserver variability [27] and, for non-expert readers, the employment of a semi-automated software reduced interobserver reliability and variability compared to axial measurements [16].

The 2010 ACCF/AHA/AATS/ACR/ASA/SCA/SCAI/SIR/STS/SVM guidelines [2] propose aortic aneurysms to be treated before reaching absolute threshold sizes, when a higher growth rate than expected is seen (e.g ≥0.5 cm/year for aneurysms without genetic aortic pathology). The rate of aortic enlargement over time is estimated to be 0.7 mm/year for the ascending aorta and 1.9 mm/year for the descending aorta in the general population [31]. The 2014 ESC guidelines [1] doubted such a difference can be reliably detected, removed growth thresholds and proposed to consider only increases of ≥5 mm as clinically relevant. Our analysis of inter-method, intra- and inter-observer variability points in the same direction and confirms that a cautious approach to diameter change over time is warranted.

Several methodological differences between studies pose further limitations to effectively compare studies and assess the reliability of the results.

First, CT scans performed with ECG-gating were employed in a limited number of studies [4, 5, 8, 9, 12, 14, 15].

Second, in order to compare measurements performed with different CT methods involving manipulation of images in space, the definition and identification of the same location is of utmost importance. When comparing axial with double oblique or centerline measurements, the planes, where the diameters have been derived, were not the same by definition. Moreover, the prescribed landmarks refer to segments of the aorta identified along the longitudinal axis of the vessel; therefore, each location extends along the z-axis for more than one axial slice (**Figure 1**). This is likely to have had an impact also on the intra and inter-observer variability of axial measurements. However, only one group took into account this aspect and provided a possible solution [14].

Third, in five articles [9–13] measurements were performed not only with different modalities but also by different observers in this way restraining the significance of the findings. Only one paper [16] specified if the diameters were derived manually or automatically once the cross-sectional plane was located. Three papers changed not only the measurement methods but also the definition of the diameter (i.e. outer-edge versus inner-edge definition) [16, 20, 24].

Conclusions

The large number of different methods and variations employed to measure aortic diameters results in the scarcity of comparable studies. Dividing the methods in three categories (axial, DO and automatic), the collected data suggest that: inter-method

variability is high for all methods; axial measurements present the highest interobserver variability; measurements performed with automatic software are the most reproducible, especially for not expert readers; measurements of minor diameters on axial planes showed results similar to DO and semi-automatic assessment and, therefore, cannot be ruled out as a fast alternative measurement option. Thus, more studies with similar and comparable parameters are necessary to define both the clinical meaning of a single measurement and, particularly, the threshold to consider diameter changes over time as clinically relevant.

References

1. Erbel R, Aboyans V, Boileau C, et al (2014) 2014 ESC Guidelines on the diagnosis and treatment of aortic diseases: Document covering acute and chronic aortic diseases of the thoracic and abdominal aorta of the adult. The Task Force for the Diagnosis and Treatment of Aortic Diseases of the European . Eur Heart J 35:2873–2926
2. Hiratzka LF, Bakris GL, Beckman J a., et al (2010) 2010 ACCF/AHA/AATS/ACR/ASA/SCA/SCAI/SIR/STS/SVM Guidelines for the Diagnosis and Management of Patients With Thoracic Aortic Disease: A Report of the American College of Cardiology Foundation/American Heart Association Task Force on Practice Guidelines, A. Circulation 121:e266–e369
3. Goldstein SA, Evangelista A, Abbara S, et al (2015) Multimodality Imaging of Diseases of the Thoracic Aorta in Adults: From the American Society of Echocardiography and the European Association of Cardiovascular Imaging. J Am Soc Echocardiogr 28:119–182
4. Lu T-LC, Rizzo E, Marques-Vidal PM, Segesser LK Von, Dehmeshki J, Qanadli SD (2010) Variability of ascending aorta diameter measurements as assessed with electrocardiography-gated multidetector computerized tomography and computer assisted diagnosis software. Interact Cardiovasc Thorac Surg 10:217–221
5. Delgado V, Ng ACT, Schuijf JD, et al (2011) Automated Assessment of the Aortic Root Dimensions With Multidetector Row Computed Tomography. Ann Thorac Surg 91:716–723
6. Jaakkola P, Hippeläinen M, Farin P, Rytkönen H, Kainulainen S, Partanen K (1996) Interobserver variability in measuring the dimensions of the abdominal aorta: comparison of ultrasound and computed tomography. Eur J Vasc Endovasc Surg 12:230–237
7. Duquette AA, Jodoin PM, Bouchot O, Lalande A (2012) 3D segmentation of abdominal aorta from CT-scan and MR images. Comput Med Imaging Graph 36:294–303
8. Lin FY, Devereux RB, Roman MJ, et al (2008) Assessment of the thoracic aorta by multidetector computed tomography: Age- and sex-specific reference values in adults without evident cardiovascular disease. J Cardiovasc Comput Tomogr 2:298–308
9. Entezari P, Kino A, Honarmand AR, Galizia MS, Yang Y, Collins J, Yaghmai V, Carr JC (2013) Analysis of the thoracic aorta using a semi-automated post processing tool. Eur J Radiol 82:1558–1564
10. Kaladji A, Lucas A, Kervio G, Haigron P, Cardon A (2010) Sizing for Endovascular Aneurysm Repair: Clinical Evaluation of a New Automated Three-Dimensional Software. Ann Vasc Surg 24:912–920
11. Kauffmann C, Tang A, Dugas A, Therasse É, Oliva V, Soulez G (2011) Clinical validation of a software for quantitative follow-up of abdominal aortic aneurysm maximal diameter and growth by CT angiography. Eur J Radiol 77:502–508
12. Quint LE, Liu PS, Booher AM, Watcharotone K, Myles JD (2013) Proximal thoracic aortic diameter measurements at CT: repeatability and reproducibility according to measurement method. Int J Cardiovasc Imaging 29:479–488

13. Banno H, Kobeiter H, Brossier J, Marzelle J, Presles E, Becquemin JP (2014) Inter-observer variability in sizing fenestrated and/or branched aortic stent-grafts. Eur J Vasc Endovasc Surg 47:45–52
14. Mendoza DD, Kochar M, Devereux RB, et al (2011) Impact of image analysis methodology on diagnostic and surgical classification of patients with thoracic aortic aneurysms. Ann Thorac Surg 92:904–913
15. Ahmed S, Zimmerman SL, Johnson PT, Lai H, Kawamoto S, Horton KM, Fishman EK (2014) MDCT interpretation of the ascending aorta with semiautomated measurement software: Improved reproducibility compared with manual techniques. J Cardiovasc Comput Tomogr 8:108–114
16. Rengier F, Weber TF, Partovi S, Müller-Eschner M, Böckler D, Kauczor H-U, von Tengg-Kobligk H (2011) Reliability of Semiautomatic Centerline Analysis versus Manual Aortic Measurement Techniques for TEVAR among Non-experts. Eur J Vasc Endovasc Surg 42:324–331
17. Manning BJ, Kristmundsson T, Sonesson B, Resch T (2009) Abdominal aortic aneurysm diameter: A comparison of ultrasound measurements with those from standard and three-dimensional computed tomography reconstruction. J Vasc Surg 50:263–268
18. Dugas A, Therasse É, Kauffmann C, Tang A, Elkouri S, Nozza A, Giroux MF, Oliva VL, Soulez G (2012) Reproducibility of abdominal aortic aneurysm diameter measurement and growth evaluation on axial and multiplanar computed tomography reformations. Cardiovasc Intervent Radiol 35:779–787
19. Diehm N, Kickuth R, Gahl B, Do D-D, Schmidli J, Rattunde H, Baumgartner I, Dick F (2007) Intraobserver and interobserver variability of 64-row computed tomography abdominal aortic aneurysm neck measurements. J Vasc Surg 45:263–268
20. Müller-Eschner M, Rengier F, Partovi S, Weber TF, Kopp-Schneider a., Geisbüsch P, Kauczor HU, Von Tengg-Kobligk H (2013) Accuracy and variability of semiautomatic centerline analysis versus manual aortic measurement techniques for TEVAR. Eur J Vasc Endovasc Surg 45:241–247
21. Sprouse LR, Meier GH, Parent FN, DeMasi RJ, Glickman MH, Barber G a. (2004) Is ultrasound more accurate than axial computed tomography for determination of maximal abdominal aortic aneurysm diameter? Eur J Vasc Endovasc Surg 28:28–35
22. Ihara T, Komori K, Yamamoto K, Kobayashi M, Banno H, Kodama A (2013) Three-dimensional workstation is useful for measuring the correct size of abdominal aortic aneurysm diameters. Ann Vasc Surg 27:154–161
23. Han SM, Patel K, Rowe VL, Perese S, Bond A, Weaver F a. (2010) Ultrasound-determined diameter measurements are more accurate than axial computed tomography after endovascular aortic aneurysm repair. J Vasc Surg 51:1381–1389
24. Diehm, Baumgartner, Silvestro, Herrmann, Triller, Schmidli, Do, Dinkel (2005) Automated software supported versus manual aorto-iliac diameter measurements in CT angiography of patients with abdominal aortic aneurysms: Assessment of inter- and intraobserver variation. Vasa 34:255–261
25. Parker M V., O'Donnell SD, Chang AS, Johnson C a., Gillespie DL, Goff JM, Rasmussen TE, Rich NM (2005) What imaging studies are necessary for abdominal aortic endograft sizing? A prospective

blinded study using conventional computed tomography, aortography, and three-dimensional computed tomography. J Vasc Surg 41:199–205

26. Sobocinski J, Chenorhokian H, Maurel B, Midulla M, Hertault a., Le Roux M, Azzaoui R, Haulon S (2013) The benefits of EVAR planning using a 3D workstation. Eur J Vasc Endovasc Surg 46:418–423
27. Cayne NS, Veith FJ, Lipsitz EC, Ohki T, Mehta M, Gargiulo N, Suggs WD, Rozenblit A, Ricci Z, Timaran CH (2004) Variability of maximal aortic aneurysm diameter measurements on CT scan: Significance and methods to minimize. J Vasc Surg 39:811–815
28. Da Silva ES, Rodrigues A.J. J, Magalhaes E, De Tolosa C, Periera PRB, Zanoto a., Martins J (1999) Variation of infrarenal aortic diameter: A necropsy study. J Vasc Surg 29:920–927
29. Kempfert J, Van Linden A, Lehmkuhl L, Rastan AJ, Holzhey D, Blumenstein J, Mohr FW, Walther T (2012) Aortic annulus sizing: Echocardiographic versus computed tomography derived measurements in comparison with direct surgical sizing. Eur J Cardio-thoracic Surg 42:627–633
30. Wang H, Hanna JM, Ganapathi A, Keenan JE, Hurwitz LM, Vavalle JP, Kiefer TL, Wang A, Harrison JK, Hughes GC (2015) Comparison of Aortic Annulus Size by Transesophageal Echocardiography and Computed Tomography Angiography With Direct Surgical Measurement. Am J Cardiol 115:1568–1573
31. Davies RR, Goldstein LJ, Coady M a., Tittle SL, Rizzo J a., Kopf GS, Elefteriades J a. (2002) Yearly rupture or dissection rates for thoracic aortic aneurysms: Simple prediction based on size. Ann Thorac Surg 73:17–28

Appendix 1

Pubmed search strategy 10th August 2015	
#1	CT OR CTs OR "computer tomography" OR "computed tomography" OR "computerized tomography" OR "CAT scan" OR "CAT scans" OR MDCT OR MSCT OR CTA OR "computer assisted tomography" OR "computed assisted tomography"
#2	aorta OR aortic OR "aortic annulus" OR "aortic annular" OR "aortic root" OR "aortic bulb" OR "aortic sinuses" OR "Valsalva sinuses" OR "sinuses of Valsalva" OR "sinus Valsalva" OR "Valsalva sinus" OR "sinotubular junction" OR "aortic arch" OR "arch of aorta" OR "aortic isthmus" OR "thoracic aorta" OR "abdominal aorta" OR "thoracoabdominal aorta" OR "ascending aorta" OR "descending aorta" OR "descending thoracic aorta"
#3	size OR sizing OR diameter OR diameters OR measurement OR measure OR measures OR value OR values OR reference value OR reproducibility of results OR dimensional measurement accuracy OR post-processing OR image reconstruction OR "image reconstructions" OR "3D reconstruction" OR "three-dimensional reconstruction" OR "three-dimensional reconstructions" OR centerline OR segmentation OR "inner wall" OR "inner edge" OR "outer wall" OR "leading edge" OR "wall thickness" OR "ECG-gated" OR "ECG-gating" OR ECG-triggered OR ECG-triggering
#4	compare OR compared
#5	#1 AND #2 AND #3 AND #4

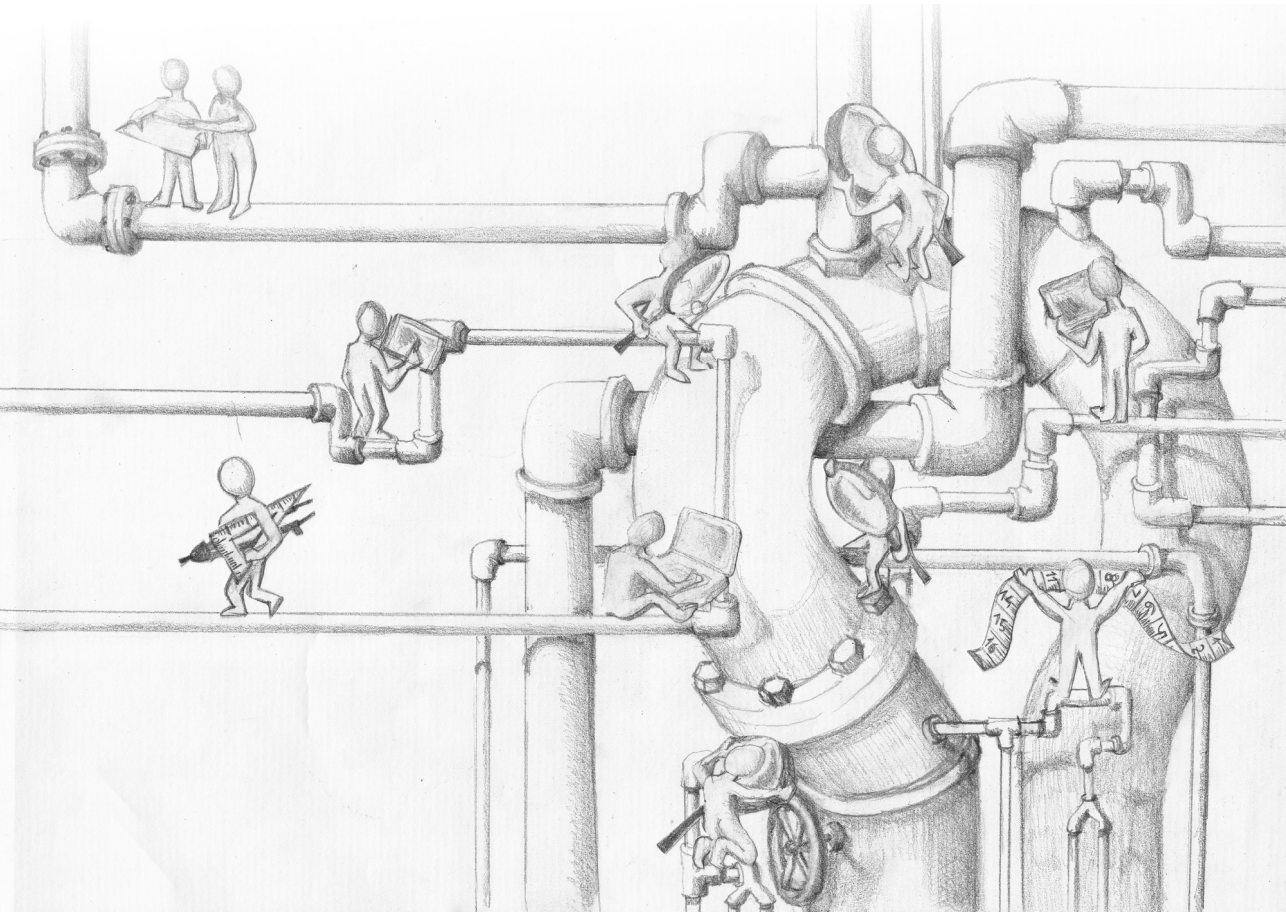

CHAPTER 3

A novel software tool for semi-automatic quantification of thoracic aorta dilatation on baseline and follow-up computed tomography angiography

Sara Boccalini*, Xinpei Gao*, Pieter H. Kitslaar, Ricardo P.J. Budde, Shengxian Tu, Boudewijn P.F. Lelievedlt, Jouke Dijkstra, Johan H.C. Reiber

Int J Cardiovasc Imaging. 2019 Apr;35(4):711-723

Abstract

Objectives: A dedicated software package that could semi-automatically assess differences in aortic maximal cross-sectional diameters from consecutive CT scans would most likely reduce the post-processing time and effort by the physicians. The aim of this study was to present and assess the quality of a new tool for the semi-automatic quantification of thoracic aorta dilation dimensions.

Methods: Twenty-nine patients with two CTA scans of the thoracic aorta for which the official clinical report indicated an increase in aortic diameters were included in the study. Aortic maximal cross-sectional diameters of baseline and follow-up studies generated semi-automatically by the software were compared with corresponding manual measurements. The semi-automatic measurements were performed at seven landmarks defined on the baseline scan by two operators. Bias, Bland-Altman plots and intraclass correlation coefficients were calculated between the two methods and, for the semi-automatic software, also between two observers.

Results: The average time difference between the two scans of a single patient was 1188 ±622 days. For the semi-automatic software, in 2 out of 29 patients, manual interaction was necessary; in the remaining 27 patients (93.1%), semi-automatic results were generated, demonstrating excellent intraclass correlation coefficients (all values ≥0.91) and small differences, especially for the proximal aortic arch (baseline: 0.19±1.30 mm; follow-up: 0.44±2.21mm), the mid descending aorta (0.37±1.64mm; 0.37±2.06mm), and the diaphragm (0.30±1.14mm; 0.37±1.80mm). The inter-observer variability was low with all errors in diameters ≤1mm, and intraclass correlation coefficients all ≥0.95. The semi-automatic tool decreased the processing time by 40% (13 vs 22 minutes).

Conclusions: In this work, a semi-automatic software package that allows the assessment of thoracic aorta diameters from baseline and follow-up CTs (and their differences), was presented, and demonstrated high accuracy and low inter-observer variability.

Introduction

Aortic aneurysms are the second most frequent disease of the aorta after atherosclerosis. The estimated risk of rupture or dissection depends on the maximal cross-sectional diameter of the aneurysm, which is also the most important parameter to decide if and when to undergo surgery or percutaneous intervention [1, 2]. For patients with aortic dilatation who do not meet the criteria for intervention, imaging follow-up is recommended to monitor diameters at intervals that vary depending also on the underlying aortic pathology. Aortic dilatations/aneurysms are a manifestation of a diffuse aortic pathology and therefore the entire aorta, not only the enlarged segment, should be assessed both at baseline and at follow-up. To reduce variability between institutions and/or operators, measurements of the aorta should be performed at several specific predefined landmarks and reported accordingly [1-3].

CT is the imaging modality of choice to measure aortic diameters. Measurements have to be performed in a plane perpendicular to the long axis of the vessel that can be identified manually or by semi-automatic/automatic software [1, 3]. The manual technique requires a workstation for multiplanar reconstructions, knowledge and experience on how to obtain the correct planes, about the aortic anatomy as well as the positions of specific landmarks. Moreover, for each exam and at all locations, the operator must repeat the process to define the planes perpendicular to the long axis of the aorta ensuing a very time consuming post-processing procedure, especially when the baseline scans have to be reassessed as well. Several commercially available semi-automatic and automatic software packages are available and able to detect the aortic centerline and aortic diameters, reducing the reporting time and measurement variability especially among non-expert readers [4-8].

A single software package that would be able to semi-automatically/automatically calculate the differences in aortic diameters from multiple scans of the same patient, would reduce reporting time further and likely decrease the inter-observer variability. Kauffmann et al. [4, 5] developed a semi-automatic tool to compare volumes and diameters of the abdominal aorta of two successive scans. However, to the best of our knowledge there is no such tool currently available for the thoracic aorta.

Therefore, the aim of this study was to analyze the accuracy and inter-observer variability of our newly developed tool for the semi-automatic assessment of thoracic aorta diameters changes over time by comparison with manual measurements.

Methods

Study population and CT protocol

In this this single-center retrospective study, for which a waiver for informed consent was received from the local Medical Ethics Committee, two CT scans of patients who had shown an increase of thoracic aorta diameters over time were included. To identify these patients, the PACS of the Erasmus Medical Center was searched for radiological reports of CT scans performed between 2006 and March 2016 including the following predefined terms: "more dilated", "increase in diameter", "increased dilatation", "wider dilatation", "wider aneurysm", and "change in diameter". The 111 patients with reports containing any of these search phrases, were eligible for inclusion regardless of the amount of diameter increase. Next, the quality of the corresponding CT scan and of the one used as a comparison for clinical purposes, was subjectively assessed by a radiologist with four years of experience in cardiovascular radiology regarding the presence of motion artifacts and contrast opacification of the aorta. A 4-point scale was employed with the following image quality grades: 1) not acceptable, being non-diagnostic images with not assessable diameters; 2) acceptable, having limited diagnostic value with possible estimation of diameters, but with doubtful reliability at the level of artefacts; 3) good, diagnostic images with limited artefacts allowing a reliable estimation of diameters; and 4) perfect, diagnostic images without artefacts. Only patients who had two contrast enhanced CT scans with qualities judged acceptable to perfect (scale 2-4) were included. Whenever the two so identified scans did not have sufficient quality but the patient had undergone prior and/or later scans that met this criterion, the latter were included. In case multiple exams with adequate qualities were available, the two with the longest time period in-between were selected. The amount and distribution of calcifications and thrombosis were not considered as one of the criteria to classify image quality. All scans that did not have thin slice reconstructions (<2mm) with medium-soft convolution kernel of the entire thoracic aorta were excluded. All patients with congenital anatomical variations of the aorta (except for mild aortic coarctation) or who had been operated upon with replacement of any part of the ascending aorta and/or aortic arch prior to the CT scans (except for end-to-end anastomosis for aortic coarctation), were excluded. In total 29 patients whose scans met all the above mentioned parameters were identified.

Patient demographics were retrieved from the electronic patient files. Technical parameters of the CT scans including date, scanner, ECG gating, kV, mAs, reconstruction slice thickness and kernel were collected. The phase of the cardiac cycle at the level of the aortic valve (approximated at 5% intervals) of the reconstruction employed for manual and semi-automatic measurements was noted and, whenever possible, the same phase was chosen to assess the two scans of a single patient.

Assessment of semi-automatic aorta dilatation quantification software package

The quality of the new software package was assessed by comparing semi-automatically obtained maximal cross-sectional diameter measurements against a manual reference standard. The comparison of semi-automatic and manual diameter values was performed for both baseline and follow-up scans.

Reference standard

Manual measurements were performed by a radiologist with four years of experience in cardiovascular imaging (observer 1) in the use of a multimodality workstation (Syngo.via, Siemens). Measurements were performed on planes perpendicular to the centerline of the aorta that were manually identified with the double-oblique method. Inner-edge to inner-edge maximal cross-sectional diameters were manually defined.

All older scans were assessed first. The more recent scans were assessed at least two weeks after the first ones, by the same radiologist blinded to the results of the first datasets. The time needed to perform all the measurements on one dataset was recorded.

Measurements locations

To assess changes of aortic dimensions over time, diameters were measured at seven prescribed and standardized anatomical locations in accordance with the 2014 guidelines of the European Society of Cardiology [1] being : sinotubular junction (STJ), mid ascending aorta (MAA), proximal aortic arch (PROX), mid aortic arch, proximal descending thoracic aorta (DIST), mid descending aorta (DESC) and diaphragm. The specifics for each location are described in Figure 1.

The same landmarks and locations were employed for both manual and semi-automatic measurements.

Semi-automatic aorta dilatation quantification software

Software package overview

The entire software procedure was constituted of multiple steps, as summarized in Figure 2 (A). The inputs were represented by baseline dataset, follow-up dataset and landmarks identified on the baseline dataset. At first, the thoracic aorta was semi-automatically segmented from the baseline CTA images; next, the two datasets (baseline and follow-up) were aligned using the intensity-based registration algorithm. Subsequently, the aorta in the follow-up dataset was segmented. With the segmented contour of the baseline CTA scan as the initial contour, the contour of the thoracic aorta in the follow-up dataset was extracted by deforming the initial contour. Finally, based on the manually defined landmarks on the baseline dataset, the maximal cross-sectional diameters of different locations in baseline and follow-up images were calculated.

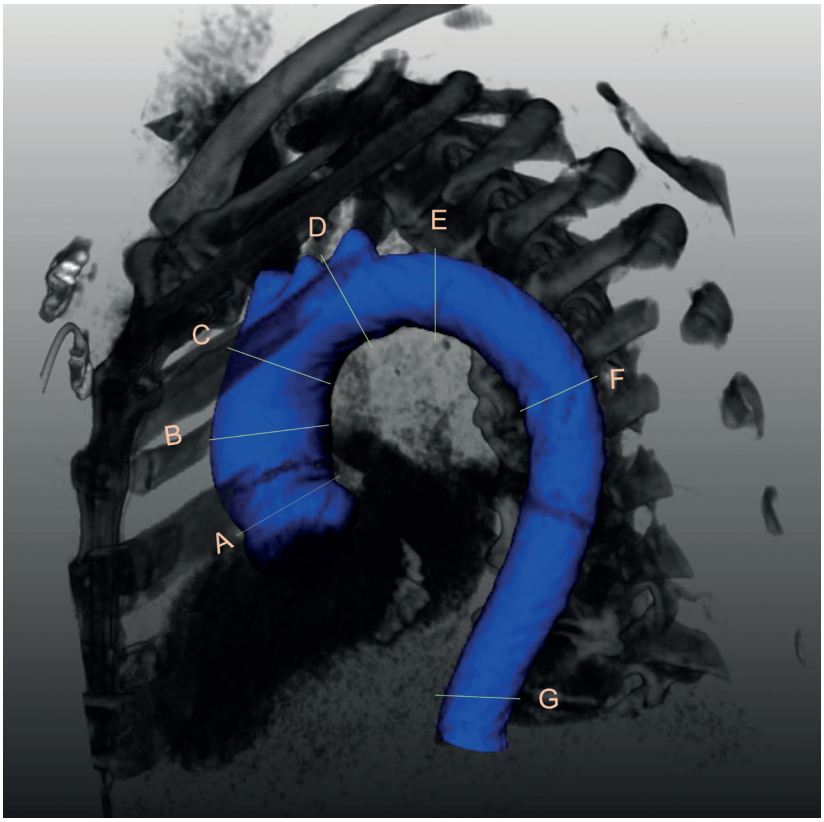

Figure 1

3D reconstruction of the thoracic aorta showing the level of the 7 locations where measurements were performed. **A**= sinotubular junction (at the connection of the aortic root and the ascending aorta); **B**= mid ascending aorta (at the level of the pulmonary trunk); **C**= proximal aortic arch (at the origin of the brachiocephalic trunk); **D**= mid aortic arch (between the left carotid artery and the left subclavian artery; after the left vertebral artery if it had a separate origin from the aorta); **E**= proximal descending thoracic aorta (at approximately 2 cm distal to the left subclavian artery; however if at this level there was either a dilatation or a steep bending of the aorta, the plane was moved closer to the left subclavian artery); **F**= mid descending aorta (at the same level as the MAA); **G**= diaphragm.

The semi-automatic software was implemented in the MeVisLab platform (version 2.7.1, MeVis Medical Solutions AG, Bremen, Germany) using C++ and Python code, and integrated in an in-house tool.

Preprocessing

If the length of a scan was longer than the region of the thoracic aorta, for instance extended into the femoral arteries, or if the baseline and follow-up scans had a different length of the aorta that was imaged, the datasets were manually adjusted by removing unnecessary images along the z-axis to obtain two matching datasets of the sole thoracic aorta.

Automatic segmentation of baseline CTA

The automatic thoracic aorta segmentation scheme was based on the centerline extraction and subsequent contour detection methods. The centerline extraction method was similar to the algorithm that we developed and described previously [9], based on the wave-propagation algorithm, Gaussian probabilistic distribution model and Dijkstra shortest path algorithm. The previous automatic landmark detection algorithm was modified from the previous algorithm which allows the detection of two femoral end points to the aortic root end point. The contour detection method was implemented as a deformable subdivision surface model fitting algorithm [10]. The result on one particular image is shown in Figure 2 (B, C).

Automatic alignment of baseline and follow-up CTA

The automatic alignment was implemented by an intensity-based registration (voxel-based registration) algorithm. First, the follow-up image was coarsely aligned to the baseline image by rigid registration. Next, affine registration was implemented for further refinement. By means of this registration, the follow-up image (the moving image) is deformed to fit the baseline image (the fixed image) to find an optimal coordinate transformation. The optimal transformation is obtained when the bias of the baseline and follow-up images reaches minimum value. The bias was evaluated by mutual information, which is the relation between the probability distributions of the intensities. To maximize the mutual information, a stochastic gradient descent algorithm was used to converge to the optimal value. To avoid the influence of structures such as the rib cage, a mask including the aorta was generated by minimum bounding box of the segmented thoracic aorta in the baseline CTA. The mask was used as the region of interest for the fixed image during registration.

In our study, the Elastix open source toolbox [14] was used for the intensity-based registration.

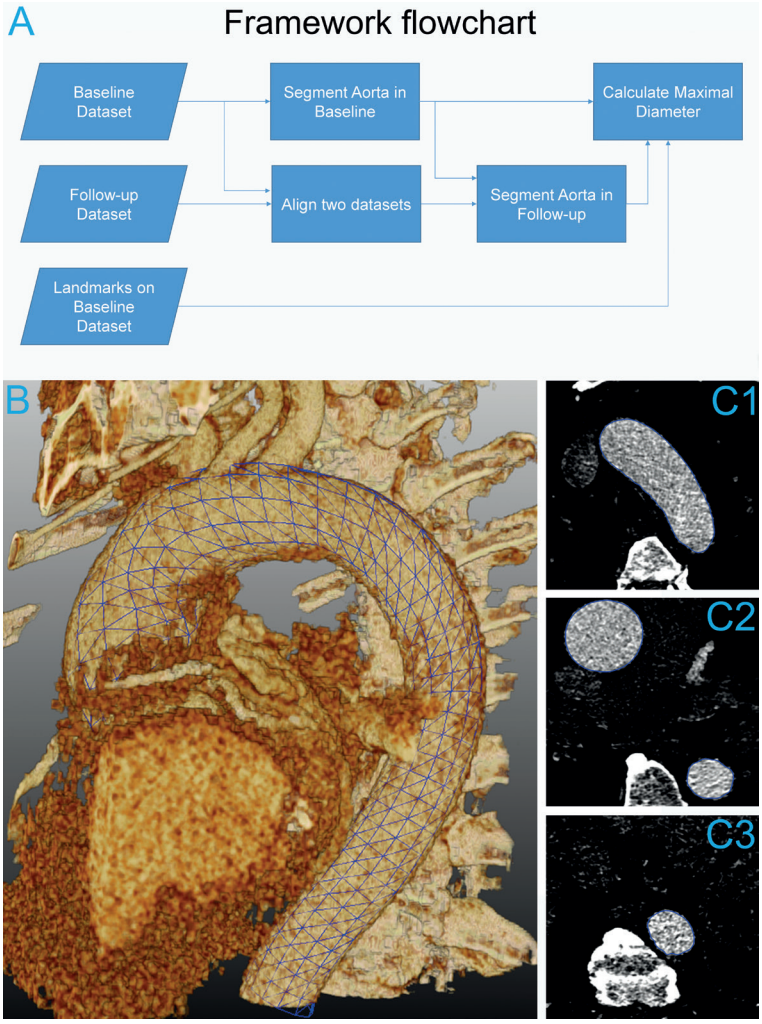

Figure 2

In **A** flowchart representing the main steps that were automated in the software to obtain the measurements from both baseline and follow-up datasets. 3D grid (**B,** blue grid) and 2D axial (**C1-C3,** red contours) views showing the result of semi-automatic segmentation.

Automatic segmentation of follow-up CTA

The aligned follow-up CTA image was processed by the centerline-based adaptive threshold method [11] to reduce the influence of the surrounding tissues in the background, such as high intensity tissue like bone, and low intensity tissue like muscle.

With the alignment of the baseline and follow-up images as described in the previous step, the position and shape of the aorta in the two images became the same with the exception of differences due to the dilatation. By using the aligned follow-up CTA image as the cost

function image and the baseline aorta contour as the initial contour, the subdivision surface fitting algorithm will deform the initial contour to detect the edge with the highest gradient in the cost function image [11]. Following the segmentation of the aorta by subdivision fitting, a region-growing algorithm was used to detect in detail the aortic arch and its branches.

Manual definition of landmarks for diameter assessment

With the in-house tool, the user could manually annotate the positions of the seven locations where measurements should be performed in multiplanar reconstructions of the baseline scan of each patient. Thereafter, the cross-sectional contours of the aorta could be detected by intersecting the landmark plane with the 3D contour, and the maximum cross-sectional diameter was calculated automatically. The software automatically identified the same locations and derived the aortic diameters at those levels, as well as the differences in diameter compared to baseline, on the follow-up scan.

Visualization of diameter progression

To improve the visualization of the size changes in the aorta, several graphic presentations were implemented in the software and are illustrated in Figures 3-4.

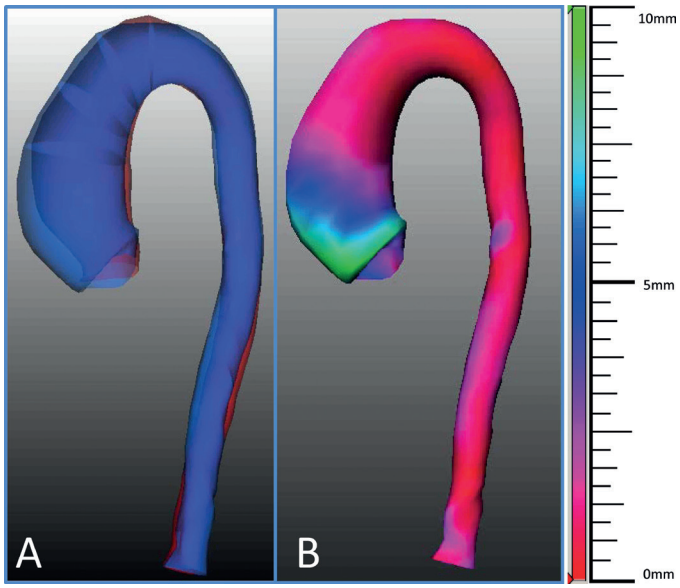

Figure 3

Tools for the visualization of the size changes in the aorta. In **A** superimposed 3 dimensional views of the surfaces of the thoracic aorta based on the semi-automatically segmented contour of both baseline (in red) and follow-up (in blue) CTA images. In **B** the semi-automatically calculated changes in diameters between the baseline and follow-up scans are represented with colors (red, blue and green indicate 0, 5 and 10 mm differences in diameters, respectively) for an immediate and comprehensive overview of the results.

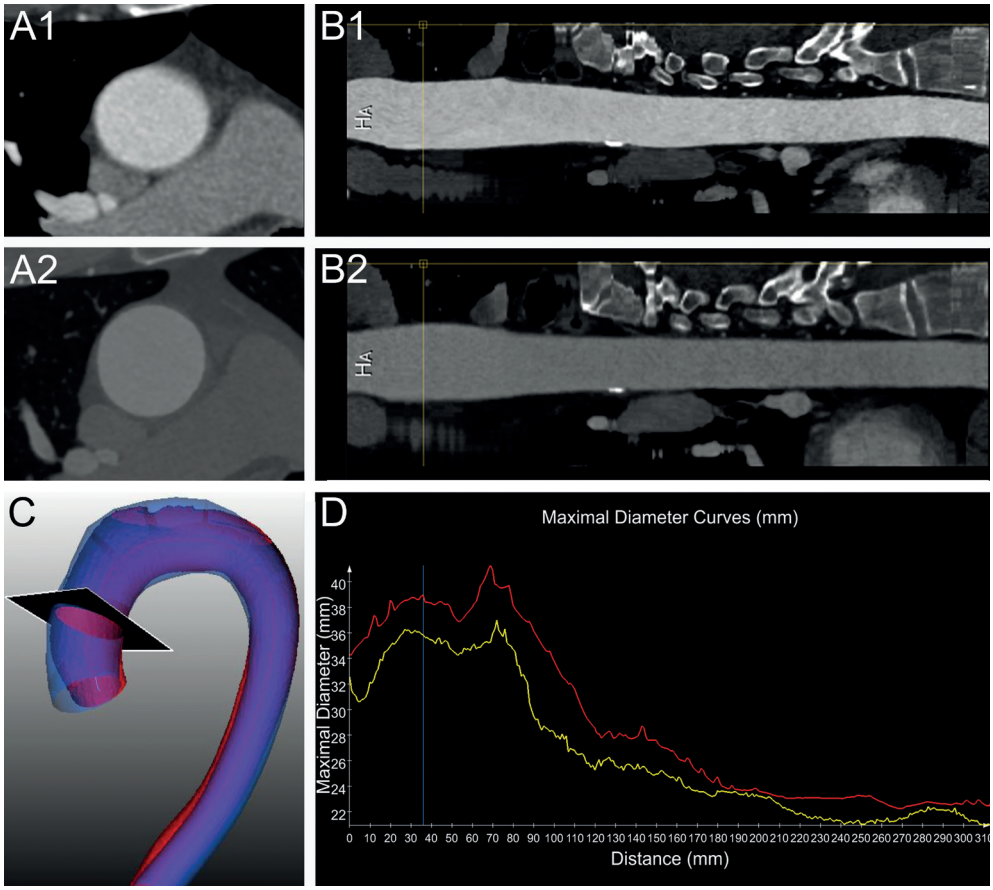

Figure 4

Tools for the visualization of the size change of the aorta. Cross-sectional views of the aorta (A1 and A2) and straightened MPR reconstructions (B1 and B2) of the aligned baseline (A1 and B1) and follow-up (A2 and B2) images. In C superimposed 3-dimensional views of the surfaces of the thoracic aorta based on the semi-automatically segmented contours of both baseline (in red) and follow-up (in blue) CTA images. In D the two diameters curves (baseline in yellow and follow-up in red), starting from the sinotubular junction, drawn together on the same graph. The black plane in C shows the level where the cross-sectional diameter indicated by the yellow lines in B1 and B2 and by the blue line in D was calculated.

Inter-observer variability

To analyze the inter-observer variability of the in-house tool, two observers (observer 1 and 2) independently used the in-house tool to annotate the seven aortic landmarks manually on the baseline scan of each patient. Observer 2 had 4 years of experience in cardiovascular imaging.

Statistical analysis

Statistical analyses were performed using SPSS (version 20.0, SPSS Inc., Chicago, IL, USA) and MedCalc (version 15.6, Ostend, Belgium). Quantitative data was described by the mean, standard deviation, and intraclass correlation coefficient (ICC). To visualize the bias between the semi-automatic results and the reference standard, Bland-Altman plots were created.

Results

Patient population

Twenty-nine patients who had two contrast enhanced CT scans with reasonable to perfect quality of the thoracic aorta were included (23 males; average age: 55.5±14.3 years). The patient characteristics are summarized in Table 1.

Table 1. Patient population characteristics

	Total (n=29)
Male	23(79%)
Age (mean, SD, range) in years	55.5±14.3(25-82)
Height (mean, SD, range) in m	1.75±0.1(1.5-1.9)
Weight (mean, SD, range) in Kg	82.6±18(50-117)
BMI (mean, SD, range)	27.2±6.9(16.9-52.7)
Congenital aortic valve/aortic diseases	
- Ehlers-Danlos type 4	2
- Bicuspid aortic valve	5
- Coarctation	2
Risk factors for cardiovascular diseases	
- Smoking	6 (3 past smokers)
- Hypertension	12
- Diabetes	4
- Hypercholesterolemia	8
Previous related surgical procedures	
- Aortic Valve Replacement	6
- Coarctation repair	1
- Ross procedure	1

CT scan technical parameters

In total 58 scans were included, 29 baseline and 29 follow-up examinations. The technical parameters are summarized in Table 2. All but one scans were acquired with scanners with more than 64 detectors. ECG gating or triggering was employed in most of the cases (52 scans; =90%). The slice thickness of the reconstructions was on average 1±0.2 mm and only in two baseline exams the thickness was bigger than 1mm.

Accuracy of the tool

From the total of 29 patients included in the study, in only two patients, the automated extraction was not successful. In 1 patient, the extracted centerline was found outside of the vessel; in another patient, the contour was at least 2mm biased from the boundary of the aorta. These two patients were excluded for further statistical analysis. In the remaining 27 patients (93.1%), no manual interaction was needed for possible modification of the centerline or contours; all the results were compared with the manual measurements.

Table 2. CT scans technical parameters

	Baseline CT scans (n=29)	**Follow-up CT scans** (n=29)	**Total CT scans** (n=58)
Patient age at CT (average ±SD; range) [years]	50.1 ±13.7; 22-71	53.4 ±14; 24-78	51.7 ±13.8
Time difference between CT scans (average ±SD; range) [days]		1187.9 ±622.4; 344-2558	
Scanner			
- Sensation 16	1	0	1
- Definition	3	0	3
- Definition AS+	8	2	10
- Definition Flash	12	10	22
- Definition Edge	1	1	2
- Sensation 64	2	1	3
- Somatom Force	2	15	17
kV			
- 70 kV	1	1	2
- 80 kV	2	6	8
- 90 kV	1	5	6
- 100 kV	12	12	24
- 110 kV	0	2	2
- 120 kV	13	3	16
Slice thickness (average ±SD; range) [mm]	1±0.2; 0.75-2	0.97 ±0.1; 0.75-1	1 ±0.2
- 0.75 mm	2	3	5
- 1 mm	25	26	51
- 1.5 mm	1	0	1
- 2 mm	1	0	1
Kernel			
- B20f	9	2	11
- B25f	1	0	1
- B26f	10	1	11
- Bv40	2	15	17
- I26f	6	11	17
ECG-gating			
- not gated	6	0	6
- unknown protocol	1	2	3
- retrospective	2	1	3
- prospective	7	5	12
- prospective high-pitch	12	21	33
Phase of the cardiac cycle			
- 0%-20%	2	4	6
- 25%-40%	5	12	17
- 45%-60%	5	9	14
- 65%-80%	11	3	14

Table 3 presents the mean and standard deviation of the maximal cross-sectional diameters at different locations obtained by the manual measurement and the semi-automatic assessments by the two observers.

Table 3. Average diameter in different locations along the aorta

Maximal diameter (mm)	Baseline			Follow-up		
	Manual	Automatic 1	Automatic 2	Manual	Automatic 1	Automatic 2
Sinotubular junction	37 ± 5	40 ± 5	39 ± 5	39 ± 5	42 ± 5	42 ± 4
Mid ascending aorta	44 ± 5	43 ± 6	44 ± 6	47 ± 6	45 ± 6	46 ± 6
Proximal aortic arch	37 ± 5	37 ± 4	38 ± 5	39 ± 4	39 ± 4	39 ± 4
Mid aortic arch	29 ± 3	30 ± 5	30 ± 5	30 ± 4	33 ± 5	32 ± 5
Proximal descending aorta	27 ± 5	27 ± 5	27 ± 5	29 ± 7	30 ± 6	29 ± 6
Mid descending aorta	26 ± 4	26 ± 4	26 ± 4	27 ± 4	28 ± 5	27 ± 5
Diaphragm	24 ± 4	24 ± 5	24 ± 4	25 ± 4	25 ± 5	25 ± 5

Manual = measurements performed manually with the double oblique method by observer 1. Automatic 1 and Automatic 2 = automatically calculated diameters based on the locations identified on the baseline scan by observer 1 and 2 respectively. Data as mean ±SD

For observer 1 the mean differences between the manual measurement and the semi-automatic measurement at different landmarks were all less than 1mm, except at the mid aortic arch, the MAA and the STJ (Table 4). In the baseline and the follow-up scans, the ICC between manual and semi-automatic measurements with landmarks defined by observer 1 were all higher than 0.90.

Inter-observer variability

The semi-automatic software demonstrated a low inter-observer variability (Table 5). The mean differences were around 1mm at all the locations; the ICC values all higher than 0.90

Also for observer 2 the mean differences at different landmarks were all lower than 1mm, except at the mid aortic arch and STJ (Table 4). The ICC coefficients for baseline diameters were all higher than 0.90.

Bland-Altman plots for the differences between the two observers and the semi-automatic results combining data from the baseline and follow-up scans for each of the seven locations are presented in Figures 5-6.

Table 4. Assessment of automatic framework compared with manual results. The automatic results were generated based on landmarks defined by observer 1 (Automatic 1) and observer 2 (Automatic 2)

Maximal diameter Automatic 1 vs Manual		Sinotubular junction	Mid ascending aorta	Proximal aortic arch	Mid aortic arch	Proximal descending aorta	Mid descending aorta	Diaphragm
Baseline	**Mean difference ±SD** [mm]	2.2 ± 2.2	1.1 ± 2.2	0.2 ± 1.3	1.1 ± 2.3	0.2 ± 1.0	0.4 ± 1.6	0.3 ± 1.1
	ICC	0.95	0.96	0.98	0.91	0.99	0.95	0.98
Follow-up	**Mean difference ±SD** [mm]	3 ± 2.6	1.3 ± 2.5	0.44 ± 2.2	2.4 ± 2.6	0.9 ± 2.8	0.4 ± 2.1	0.4 ± 1.8
	ICC	0.92	0.96	0.93	0.90	0.95	0.94	0.96
Maximal diameter Automatic 2 vs Manual								
Baseline	**Mean difference ±SD** [mm]	2.0 ± 1.8	0.4 ± 1.7	0.6 ± 1.2	1.2 ± 1.9	0.0 ± 1.4	0.4 ± 2.0	0.4 ± 1.1
	ICC	0.97	0.97	0.98	0.94	0.98	0.93	0.98
Follow-up	**Mean difference ±SD** [mm]	3.2 ± 2.6	0.3 ± 2.0	0.9 ± 2.1	2.3 ± 2.6	0.6 ± 2.6	0 ± 2.3	0.3 ± 1.6
	ICC	0.92	0.97	0.94	0.91	0.96	0.93	0.97

Table 5. Inter-observer variability for the automatic framework.

Maximal diameter Automatic 1 vs Automatic 2		Sinotubular junction	Mid ascending aorta	Proximal aortic arch	Mid aortic arch	Proximal descending aorta	Mid descending aorta	Diaphragm
Baseline	**Mean difference ±SD** [mm]	0.3 ± 1.4	0.6 ± 2.4	0.4 ± 1.2	0.0 ± 2.0	0.2 ± 1.3	0.0 ± 1.6	0.1 ± 0.8
	ICC	0.98	0.96	0.98	0.95	0.99	0.96	0.99
Follow-up	**Mean difference ±SD** [mm]	0.2 ± 1.6	1.0 ± 1.9	0.4 ± 1.2	0.1 ± 1.2	0.3 ± 1.4	0.3 ± 1.5	0.1 ± 0.9
	ICC	0.97	0.98	0.98	0.98	0.99	0.97	0.99

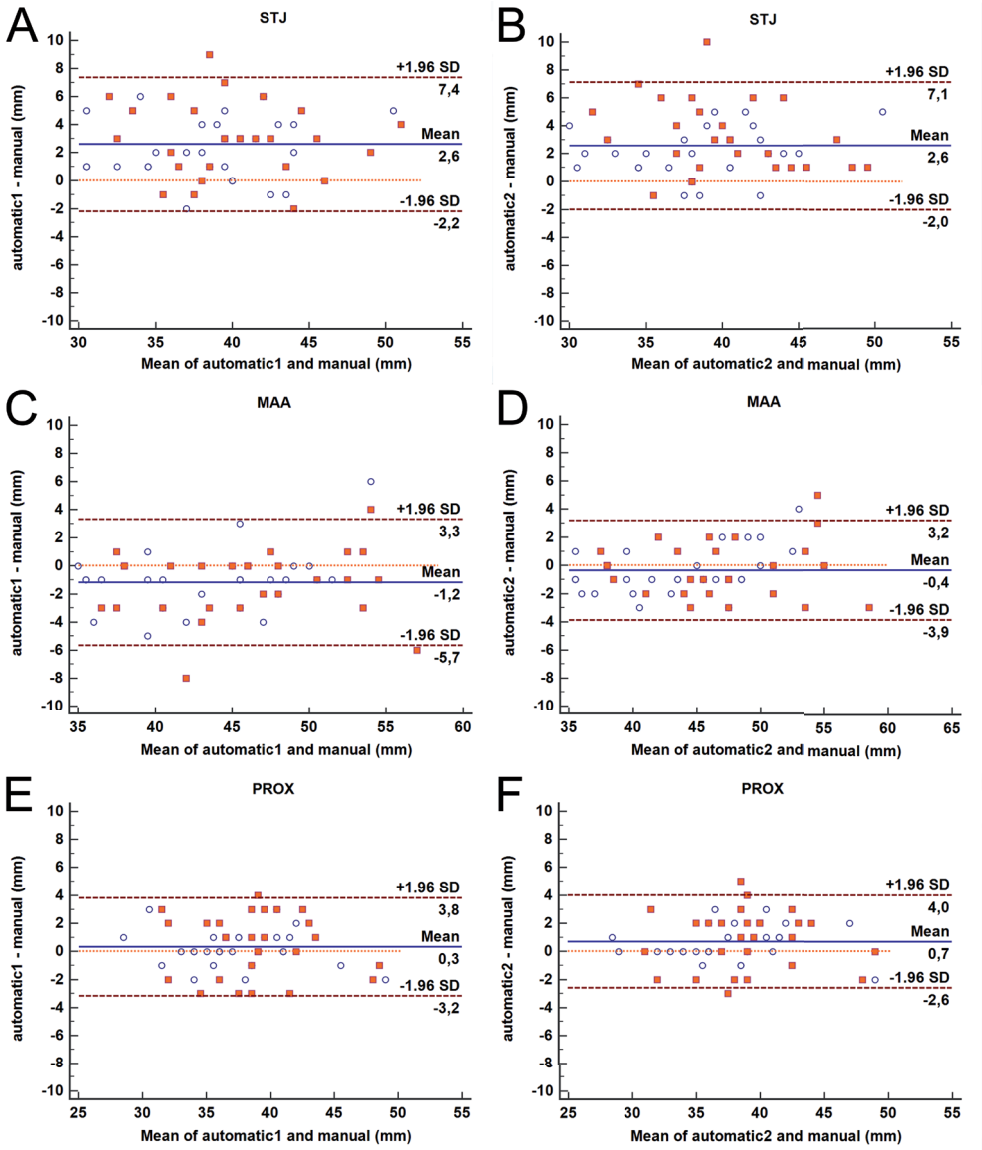

Figure 5

Bland-Altman plots representing the difference between semi-automatic and manual measurements at the sinotubular junction (**A-B**), MAA (**C-D**) and PROX (**E-F**). Blue circles: baseline diameters. Red squares: follow-up diameters. Semi-automatic 1 and Semi-automatic 2 = semi-automatically calculated diameters by observers 1 and 2, respectively.

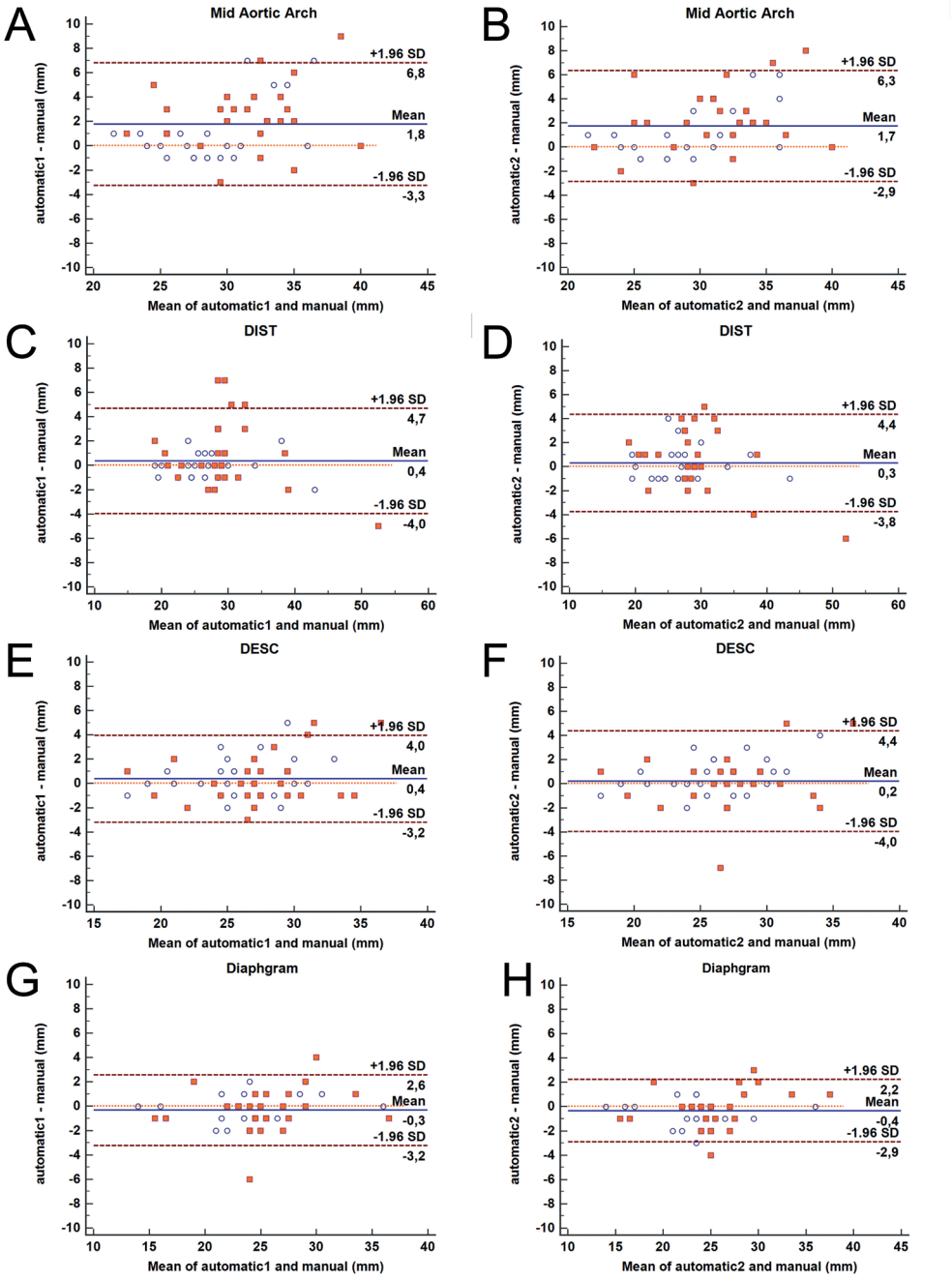

Figure 6

Bland-Altman plots representing the difference between the semi-automatic and manual measurements at mid aortic arch (**A-B**), DIST (**C-D**), DESC (**E-F**) and diaphragm (**G-H**). Blue circles: baseline diameters. Red squares: follow-up diameters. Semi-automatic 1 and Semi-automatic 2 = semi-automatically calculated diameters by observers 1 and 2, respectively.

Analysis time

The overall mean time needed to manually measure all the diameters on both datasets was 22 minutes (11 minutes for baseline; 11 minutes for follow-up). The average time for semi-automatic measurement of both baseline and follow-up diameters was 13 minutes (1 min for manual image preprocessing, 4min for manual landmark annotation, 2min for the processing of the baseline images, 6min for the processing (registration and segmentation) and the automatic measurement of the follow-up images and the comparison with baseline).

Discussion

Although the double-oblique technique has been regarded and used as the reference standard for aortic measurements, it is very time consuming and it has been associated with significant intra- and inter-observer variabilities (defined as mean difference ±SD) of -0.8±1.3mm and 1.3±2mm, respectively and absolute difference values of up to 11mm [12]. It has also been demonstrated, that the experience of the observers plays an important role in reducing the variability [13]. Therefore, notwithstanding standardization of the measurements, previous growth thresholds for intervention [2] have been removed and it is now suggested that only differences over time of more than 5mm should be considered relevant [1].

Although several studies exist regarding the detection of the aorta on single time point CT scans using analytical software solutions [6-8, 15-17] only one previous study was published presenting a framework for semi-automatic/automatic comparison of baseline and follow-up abdominal aneurysms volume and diameters [4].

For single time point CT scans, several semi-automatic/automatic software packages for the thoracic aorta measurements have been validated and showed lower intra and inter-observer variability and reduced measurement time compared to manual measurements [6-8, 15-17].

The method developed by Martínez-Mera et al. [15] can segment the thoracic aorta completely automatically; the mean correlation coefficient of the aorta's segmented volume of the 10 patients analyzed was 0.976. Vitanovski et al. [16] proposed a method that is able to detect the thoracic aorta and main branches automatically. The error was represented by the mean point-model Euclidean distance, which was found to be 2.29 ± 1.74 mm for the aorta. For Kovács et al. [17], the overall average bias of the patients was 1.1 ± 0.17 mm comparing the mean distance of the automatic and manual segmented aortic dissection meshes. In the study by Biesdorf et al. [6] the aortic arch was segmented by

three different approaches: a model-based approach, a 2D joint approach and a 3D joint approach. The errors in the maximal diameters in the ten 3D CTA with mild pathologies of the aorta were 2.24±0.72mm, 1.51±0.66mm, and 1.52±0.69mm, respectively for the three methods. In the seven 3D CTA with severe pathologies, the errors were 5.45±2.98mm, 3.34±2.23mm, 2.04±0.83mm respectively. In Lu et al. 's study [7] the ascending aorta was semi-automatically measured by two observers. The inter-observer variability was 1.1mm during the first session of measurements, and 1.2mm during the second session. However, no comparison against manual reference standard was performed. The tool by Entezari et al. [8] which can segment the thoracic aorta semi-automatically, has the most similar features to our study; however, it only segmented and measured diameters without automatic comparison between two consecutive exams. The maximum diameters were measured manually and semi-automatically in multiple locations and the mean difference was calculated: all the differences were less than 1mm, except at STJ and PROX locations.

In our study with the new tool differences with baseline manual measurements were <1mm except at the STJ, MAA (only for one observer) and at the mid aortic arch, all ICC values >0.90 and low inter-observer variability (<1mm differences with ICC values >0.95 at all locations). Therefore, the contour detection algorithm for the baseline thoracic aorta has at least similar, or even better, accuracy and reproducibility compared to the published tools listed above.

The software [4] described by Kauffmann et al. relies on the semi-automatic segmentation of both datasets requiring the operators' intervention at multiple steps, such as the user definition of the aortic lumen location and the correction of aortic contours. In Kauffmann 's study, the mean difference of the measured maximum cross-sectional diameters carried out by a senior radiologist and one of three medical students, was 0.07mm and the ICC values for baseline and follow-up examinations were in the range from 0.989 to 0.998. In this study, the performance of the software was not compared to a reference standard, although in their previous study [5], they reported a mean error compared to manual measurement of 1.1±0.9mm.

To the best of our knowledge, no other software solutions have been described that can semi-automatically align the baseline and follow-up CT datasets of the thoracic aorta of the same patient, and allow the measurement of the diameters of both scans at the same time. In our study, the semi-automatic detection of changes in the follow-up thoracic aorta diameters showed differences <1mm compared to manual measurements, except at the STJ, mid aortic arch and MAA positions (for one observer). The inter-observer variability was <1mm at all locations, except at the MAA (1.04mm), while the ICC were all higher than 0.95. The accuracy and inter-observer variability of the measurements on the follow-up scans of the thoracic aorta proved to be comparable to the results on baseline datasets.

The measurement time was reduced compared to the manual measurements with the possibility of further improvements in the future.

Compared to the published studies, our software package presents the following new features: 1) the landmark locations can be identified automatically on the follow-up scan based on the baseline locations; 2) the contours of both the baseline and follow-up images can be compared automatically; and 3) the dilatation of the aorta (difference in diameters) between the baseline and the follow-up, can be visualized in color coding on a 3D reconstruction which gives an instantaneous overview of all relevant information.
There are some limitations in this study. First, the number of patients in this study is relatively small due to the strict inclusion criteria (patients with clinical reports presenting changes in aortic diameters; no congenital aortic anomalies or previous surgery; both baseline and follow-up scans with reasonable to high quality and thin slices reconstructions). Especially the choice to include only scans with reasonable to high quality does not reflect real world variability and further studies are needed to assess the quality of the software with a broader spectrum of qualities of the scans. In our study, only CT scans with not-acceptable image quality were excluded, which correspond to studies that are not diagnostic and that would therefore require further or repeated examinations for correct assessment of aortic diameters in clinical practise. Secondly, measurements were not compared to a true gold standard. However, this is a general issue for studies regarding aortic diameters assessment with imaging techniques. Even if the patients would undergo surgery at which time aortic dimensions could be derived, measurements performed in this setting cannot be considered the gold standard considering the limitations and.difficulties of intraoperative measurements.

In conclusion, a novel semi-automatic tool which is able to align baseline and the follow-up images to allow the accurate measurement of the thoracic aorta at several landmarks, was developed and evaluated. This study has demonstrated that the tool has high accuracy and inter-observer variability, especially at PROX, DESC, and diaphragm locations. The processing time turned out to be decreased by 40% of manual measurements.

References

1. Erbel R, Aboyans V, Boileau C, et al (2014) ESC Guidelines on the diagnosis and treatment of aortic diseases: Document covering acute and chronic aortic diseases of the thoracic and abdominal aorta of the adult. The Task Force for the Diagnosis and Treatment of Aortic Diseases of the European. *Eur Heart J* 35(41):2873-2926. doi:10.1093/eurheartj/ehu281.
2. Hiratzka LF, Bakris GL, Beckman J a., et al (2010) ACCF/AHA/AATS/ACR/ASA/SCA/SCAI/SIR/STS/SVM Guidelines for the Diagnosis and Management of Patients With Thoracic Aortic Disease: A Report of the American College of Cardiology Foundation/American Heart Association Task Force on Practice Guidelines. *Circulation* 121(13):e266-e369. doi:10.1161/CIR.0b013e3181d4739e.
3. Goldstein S a, D AEM, Abbara S, et al (2015) Multimodality Imaging of Diseases of the Thoracic Aorta in Adults: From the American Society of Echocardiography and the European Association of Cardiovascular Imaging. *J Am Soc Echocardiogr* 28(2):119-182. doi:10.1016/j.echo.2014.11.015.
4. Kauffmann C, Tang A, Therasse É, et al (2012) Measurements and detection of abdominal aortic aneurysm growth: Accuracy and reproducibility of a segmentation software. *Eur J Radiol* 81(8):1688-1694. doi:10.1016/j.ejrad.2011.04.044.
5. Kauffmann C, Tang A, Dugas A, Therasse É, Oliva V, Soulez G (2011) Clinical validation of a software for quantitative follow-up of abdominal aortic aneurysm maximal diameter and growth by CT angiography. *Eur J Radiol* 77(3):502-508. doi:10.1016/j.ejrad.2009.07.027.
6. Biesdorf A, Rohr K, Feng D, et al (2012) Segmentation and quantification of the aortic arch using joint 3D model-based segmentation and elastic image registration. *Med Image Anal* 16(6):1187-1201. doi:10.1016/j.media.2012.05.010.
7. Lu T-LC, Rizzo E, Marques-Vidal PM, Segesser LK v., Dehmeshki J, Qanadli SD (2010) Variability of ascending aorta diameter measurements as assessed with electrocardiography-gated multidetector computerized tomography and computer assisted diagnosis software. *Interact Cardiovasc Thorac Surg* 10(2):217-221. doi:10.1510/icvts.2009.216275.
8. Entezari P, Kino A, Honarmand AR, et al (2013) Analysis of the thoracic aorta using a semi-automated post processing tool. *Eur J Radiol* 82(9):1558-1564. doi:10.1016/j.ejrad.2013.03.024.
9. Gao X, Tu S, de Graaf MA, et al (2014) Automatic extraction of arterial centerline from whole-body computed tomography angiographic datasets. In: *Computing in Cardiology* IEEE; 2014:697-700.
10. Kitslaar PH, van't Klooster R, Staring M, Lelieveldt BPF, van der Geest RJ (2015) Segmentation of branching vascular structures using adaptive subdivision surface fitting. In: *Medical Imaging 2015: Image Processing* Vol 9413.; 2015:94133Z. doi:10.1117/12.2082222.
11. Gao X, Kitslaar PH, Budde RPJ, et al (2016) Automatic detection of aorto-femoral vessel trajectory from whole-body computed tomography angiography data sets. *Int J Cardiovasc Imaging* 32(8):1311-1322.
12. Quint LE, Liu PS, Booher AM, Watcharotone K, Myles JD (2013) Proximal thoracic aortic diameter measurements at CT: repeatability and reproducibility according to measurement method. *Int J Cardiovasc Imaging* 29(2):479-488. doi:10.1007/s10554-012-0102-9.

13. Rengier F, Weber TF, Partovi S, et al (2011) Reliability of Semiautomatic Centerline Analysis versus Manual Aortic Measurement Techniques for TEVAR among Non-experts. *Eur J Vasc Endovasc Surg* 42(3):324-331. doi:10.1016/j.jvs.2011.07.042.
14. Klein, S., Staring, M., Murphy, K., et al, "Elastix: a toolbox for intensity-based medical image registration," IEEE Transactions on Medical Imaging 29(1), 196-205 (2010).
15. Martínez-Mera, J. A., Tahoces, P. G., Carreira, J. M., Suárez-Cuenca, J. J., & Souto, M. (2013). A hybrid method based on level set and 3D region growing for segmentation of the thoracic aorta. Computer Aided Surgery, 18(5-6), 109-117.
16. Vitanovski D, Ralovich K, Ionasec R, et al. Personalized learning-based segmentation of thoracic aorta and main branches for diagnosis and treatment planning[C]//Biomedical Imaging (ISBI), 2012 9th IEEE International Symposium on. IEEE, 2012: 836-839.
17. Kovács, T., Cattin, P., Alkadhi, H., Wildermuth, S., & Székely, G. (2006). Automatic segmentation of the vessel lumen from 3D CTA images of aortic dissection. In Bildverarbeitung für die Medizin 2006 (pp. 161-165). Springer, Berlin, Heidelberg.

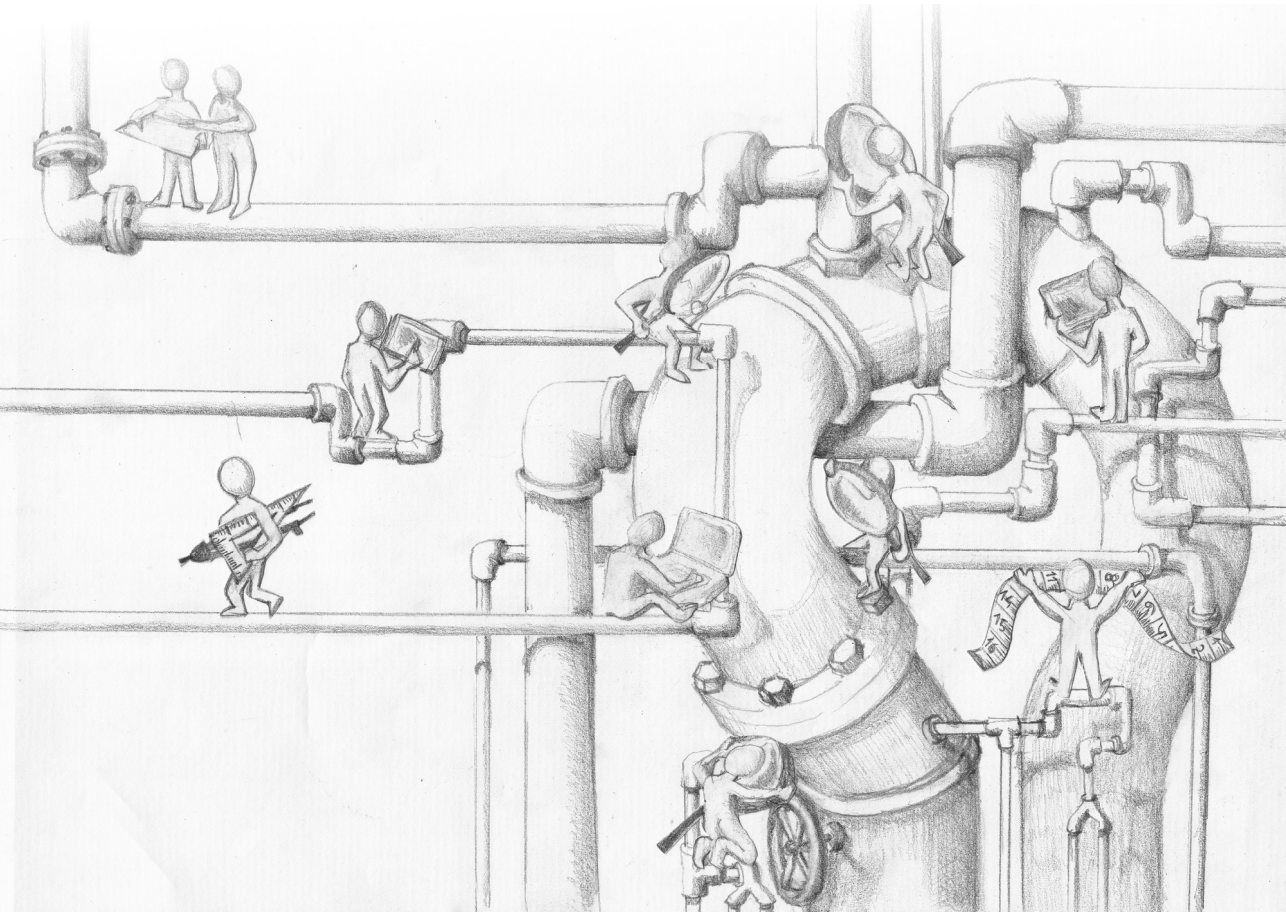

CHAPTER 4

Intermodality variation of aortic dimensions: How, where and when to measure the ascending aorta

Lidia R. Bons, Anthonie L. Duijnhouwer, Sara Boccalini, Allard T. Van Den Hoven, Maureen J. Van Der Vlugt, Raluca G. Chelu, Jackie S. McGhie, Isabella Kardys, Annemien E. Van Den Bosch, Hans-Marc J. Siebelink, Koen Nieman, Alexander Hirsch, Craig S. Broberg, Ricardo PJ. Budde, Jolien W. Roos-Hesselink

Int J Cardiol. 2019 Feb 1;276:230-235

Abstract

Background: No established reference-standard technique is available for ascending aortic diameter measurements. The aim of this study was to determine agreement between modalities and techniques.

Methods: In patients with aortic pathology transthoracic echocardiography, computed tomography angiography (CTA) and magnetic resonance angiography (MRA) were performed. Aortic diameters were measured at the sinus of Valsalva (SoV), sinotubular junction (STJ) and tubular ascending aorta (TAA) during mid-systole and end-diastole. In echocardiography both the inner edge-to-inner edge (I-I edge) and leading edge-to-leading edge (L-L edge) methods were applied, and the length of the aortic annulus to the most cranial visible part of the ascending aorta was measured. In CTA and MRA the I-I method was used.

Results: Fifty patients with bicuspid aortic valve (36 ± 13 years, 26% female) and 50 Turner patients (35 ± 13 years) were included. Comparison of all aortic measurements showed a mean difference of 5.4 ± 2.7 mm for the SoV, 5.1 ± 2.0 mm for the STJ and 4.8 ± 2.1 mm for the TAA. The maximum difference was 18 mm. The best agreement was found between echocardiography L-L edge and CTA during mid-systole. CTA and MRA showed good agreement. A mean difference of 1.5 ± 1.3 mm and 1.8 ± 1.5 mm was demonstrated at the level of the STJ and TAA comparing mid-systolic with end-diastolic diameters. The visible length of the aorta increased on average 5.3 ± 5.1 mm during mid-systole.

Conclusions: MRA and CTA showed best agreement with L-L edge method by echocardiography. In individual patients large differences in ascending aortic diameter were demonstrated, warranting measurement standardization. The use of CTA or MRA is advised at least once.

Introduction

Progressive dilation of the ascending aorta is an important risk factor for aortic dissection and rupture [1], which is associated with significant morbidity and mortality. The estimated incidence of thoracic aortic enlargement (including ascending aortic aneurysm) is 10.4 cases per 100.000 person-years [2, 3]. This figure varies in part by non-standardized definitions of how the aorta should be measured or what constitutes an abnormal diameter. The more widespread application of multiple imaging modalities in a given patient adds to the variations seen in clinical practice. Three imaging modalities are currently in use for measuring the ascending aorta: transthoracic two-dimensional echocardiography (2DE), computed tomography (CT) and magnetic resonance imaging (MRI) [4]. Each modality has its strengths and weaknesses [5]. Recently, guidelines specifically focused on the ascending aorta have been published. The American College of Cardiology Foundation (ACCF)/American Heart Association (AHA) guidelines [6] recommend measuring the outer edge-to-outer edge (O-O) edge of the vessel wall for CT or MRI derived diameters, but the inner edge-to-inner edge (I-I) for 2DE. In contrast, the American Society of Echocardiography (ASE) and the European Association of Cardiovascular Imaging (EACVI) guidelines for 2DE suggest that the leading edge-to-leading edge (L-L edge) convention at end-diastole should be used [7, 8]. Finally, the 2010 ASE pediatric guidelines [9] pose that by 2DE the I-I measurement, during systole is preferred. Just as guidelines are inconsistent [10, 11] so is clinical practice. By CT, the I-I method is most frequently used when contrast is given since the wall itself is hardly visible [12, 13], while the O-O method is used in non-contrast enhanced scans [14, 15]. In contrast, most physicians using 2DE prefer the L-L edge method [16, 17]. Also in the general population, age, gender and BSA have impact on aortic diameters as discussed by Vriz et al. [18]. Furthermore, since the aortic root is not circular, there is debate of whether to report cusp-to-commissure or cusp-to-cusp measurements for sinus of Valsalva measurements. Despite attempts at congruency, the ASE/EACVI concluded that there was insufficient data to favor one standard [7]. Some studies have compared reported measurements, though currently there are no studies comparing all three imaging modalities performed in the same patient on the same day. The aim of this study was to determine agreement between modalities and techniques and provide guidance on the optimal approach to measure the ascending aorta. The following measurements were compared: (1) ascending aortic measurements on echocardiography, CTA and MRA, (2) cusp-to-cusp and cusp-to-commissure diameter at the level of the sinus of Valsalva on CTA and (3) aortic measurement during diastole and systole.

Methods

Study population

The study population consisted of adult patients with a bicuspid aortic valve (BAV) and/or Turner syndrome who had been included in a prospective cohort study to elucidate the etiologies and pathogenic mechanisms leading to BAV/aneurysm formation and unravel risk factors for disease progression [19]. For research purposes the patients were scheduled for 2DE, CTA and magnetic resonance angiography (MRA) on the same day. Therefore, the data of this cohort made it possible to directly compare 2DE, CTA and MRA measurements of the ascending aortic diameter. Patients visited our tertiary center between October 2014 and March 2016. The inclusion criteria for BAV patients were age ≥18 year and one of the following: (1) aortic stenosis (gradient >2.5 m/sec), (2) aortic regurgitation (at least moderate) or (3) ascending aortic dilation ≥40 mm and/or aortic size index >2.1 cm/m2. All three types of a bicuspid aortic valve according to the Sievers classification were included. This classification is based on the number of raphes, which is a fused area between two cusps. Bicuspid aortic valves with no raphe are called type 0, valves with one raphe type 1 and valves with two raphes type 2. Turner patients needed to have a genetically confirmed 45,X or 45,X/46,XX mosaic karyotype. Patients with contra-indication to CTA, MRA or contrast agents were excluded. Renal function was checked in all patients. Patients with no MRA due to claustrophobia or technical problems remained in the study, but patients who did not receive either 2DE or CTA were excluded. Patients without MRA were included, because some of our research questions do not require information about MRA measurements. Patients also underwent physical examination. Hypertension was defined as current use of antihypertensive medication. The study complied with the Declaration of Helsinki and was approved by the medical ethical committee of the Erasmus Medical Center (MEC14-225). Written informed consent was provided by all patients.

Transthoracic two-dimensional echocardiography (2DE)

Standard 2DE was performed by one of two experienced sonographers. All studies were acquired using harmonic imaging on an iE33 or EPIQ7 ultrasound system (Philips Medical Systems, Best, the Netherlands) equipped with an x5–1 matrix-array transducer (composed of 3040 elements operating at 1-5 MHz). The aorta was measured from either the standard parasternal long axis view or from a more cranial intercostal window to improve visualization of the ascending aorta [6]. Aortic stenosis was defined based on peak aortic velocity and aortic regurgitation was evaluated according to the EAE/ASE guidelines [20].

Computed tomography angiography (CTA)

A retrospectively ECG-gated spiral CTA was performed using a dual-source CT system (Somatom Force or Somatom Definition Flash, Siemens Healthineers, Forchheim,

Germany). In order to image the ventricles, aortic valve and aorta, the scan range was set from the aortic arch to the inferior border of the heart. Dose modulated ECG-pulsing was employed with nominal tube current during the 0 to 40% window of the R-R interval, and tube current reduced to 20% of the nominal output for the remainder to reduce the radiation dose. In total 20 different reconstructions with a 1.5-mm slice thickness and 1.0-mm overlap were made in each patient at each 5% of the R-R interval. Reference tube current was set at 150 mAs per rotation. Automatic kV selection was used. The table speed was adapted to the heart rate. No beta blockers were administered prior to the scan. A 65 ml bolus of iodinated contrast material (Iodixanol 320, Visipaque, GE. Health Care, Cork, Ireland) was administered through an antecubital vein followed by a 40 ml 70/30% saline/contrast medium bolus, both at 5 ml/s. Image acquisition was started using bolus tracking in the ascending aorta.

Magnetic resonance angiography (MRA)

Image acquisition was performed using a 1.5 T scanner (Discovery MR450, GE Medical Systems, Milwaukee, WI, USA) using a 32-channel phased-array cardiac surface coil. For aortic imaging an angiography sequence was used. First a test bolus of 1 ml gadobutrol (Gadovist, Bayer Schering Pharma, Leverkusen, Germany) followed by 20 ml of saline flush, was injected to identify the individual scan delay time to the maximum enhancement of contrast in the descending aorta. Second, non-ECG-gated MRA images were acquired in coronal orientation after injection of a double dose of 7 ml gadobutrol (0.05-0.18 mmol/kg) followed by 20 ml of saline flush, both with an injection rate of 2.5 ml/s. Typical scan parameters were: FOV 460 mm (phase 90%), matrix size 320 x 192, slice thickness 2.0 mm, flip angle 17°, NEX 0.75, bandwidth 83.3 kHz, TR 3.1 ms, TE 1.09 ms.

Measurements of the ascending aorta

Analyses of the 2DE, CTA and MRA images were performed by experienced investigators blinded to the results of the other imaging modalities. Images were analyzed offline with the use of dedicated software: Xcelera (version R4.1, Philips Medical Systems, the Netherlands) for 2DE and Syngo.Via (Version VB10B, Siemens, Germany) for CTA and MRA. For CTA and MRA maximal aortic diameters were measured from reconstructed short-axis images generated with double-oblique multiplanar reformation [21].

To compare the diameter between the three modalities the aorta was measured at three predefined levels for all three imaging techniques: sinus of Valsalva (SoV), sinotubular junction (STJ) and tubular ascending aorta (TAA, 1 cm cranial of the sinotubular junction), as indicated in figure 1A. When referring to the widest diameter at any level of the ascending aorta, we used 'ascending aorta'. Both the L-L edge and I-I edge methods were applied in 2DE (figure 1B). For CTA and MRA only the I-I edge method was applied, because the vessel wall is difficult to distinguish on contrast-enhanced images in the absence

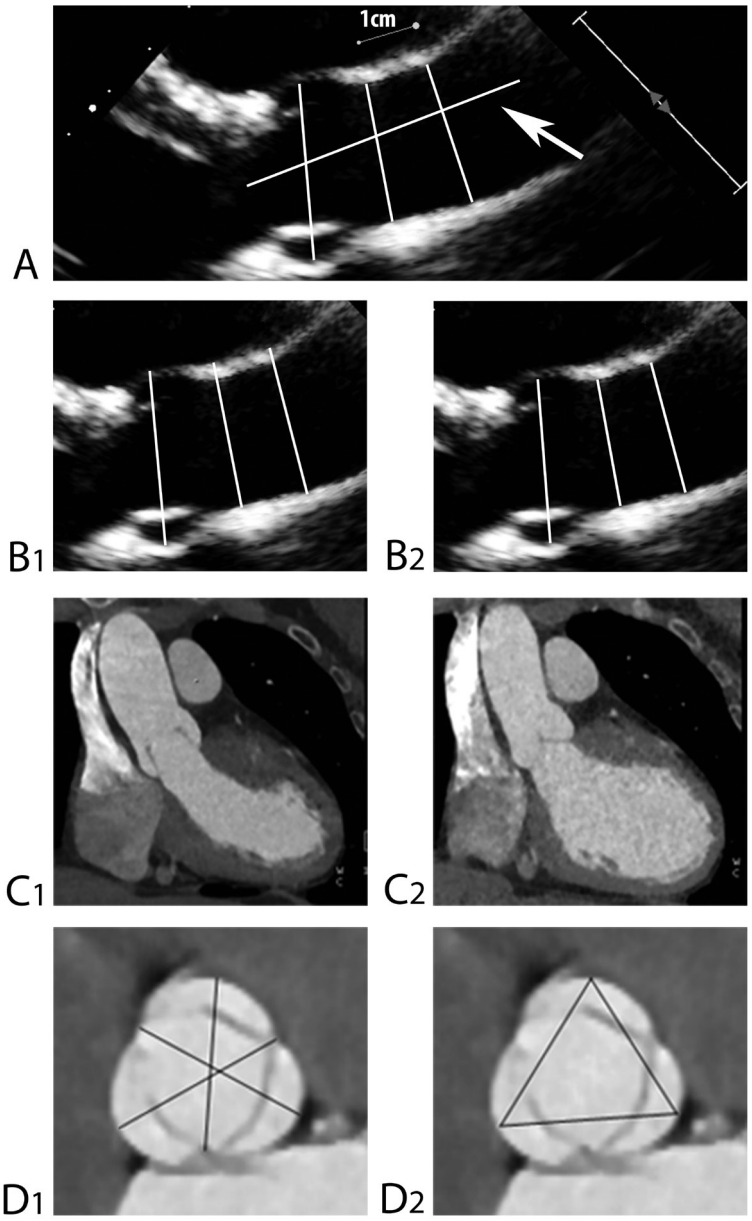

Figure 1. Measurements of the aortic root and ascending aorta

Aortic diameters are measured at three predefined levels: the Sinus of Valsalva, the sinotubular junction and the ascending aorta (A), with use of the leading edge-to-leading edge (B1) and inner edge-to-inner edge (B2) methods in echocardiography and during mid-systole (C1) and end-diastole (C2) in both echocardiography and CTA. Also the length of the aorta (arrow in A) was measured by 2DE. At the level of the sinus of Valsalva both the cusp-to-commissure diameter (D1) and the cusp-to-cusp diameter (D2) were measured by CTA.

of atherosclerotic disease. For this reason, measurements with the O-O edge method were not possible for CTA and MRA. Calcified plaques were included in the diameter measurement. Measurements were made at both end-diastole and mid-systole for 2DE and CTA according to the guidelines(7,8) (figure 1C). The MRA was acquired without ECG-synchronization. The measurements on MRA were compared with both the end-diastolic and mid-systolic measurement on CTA. End-diastole was defined as the moment before opening of the aortic valve and ranged between 75% and 100% of the R-R interval on CTA. Mid-systole was defined as the phase exactly halfway between opening and successive closure of the aortic valve and ranged between 15% and 35% of the R-R interval on CTA. The maximal length of the aorta that was visualized with 2DE (defined as the length from the aortic annulus to the most cranial part of the ascending aorta which was visible) was measured during mid-systole and end-diastole (figure 1A).

For CTA and MRA three cusp-to-commissure distances were measured at the level of the SoV (widest plane) when patients had a tricuspid aortic valve or bicuspid aortic valve type 1 or 2 according to the Sievers classification [22]. In CTA the diameter was also measured with the cusp-to-cusp method according to Goldstein et al. [7] (figure 1D). For bicuspid aortic valves type 0 this was measured in two directions (maximum diameter and diameter perpendicular to the maximum diameter). At the level of the sinus of Valsalva the largest measurements on CTA and MRA was compared to echocardiography. Detailed information about separate analysis of the three cusp-to-cusp measurements (tricuspid or bicuspid type 1 or 2 valves) and measurements in two directions (bicuspid type 0 valves) can be found in the supplemental material. Using this protocol, the aorta was measured with seven different methods across all modalities at each of three levels (supplemental table 1). The absolute value of the maximum difference between these seven measurements at each level (maximum difference) was calculated for each patient. Inter- and intra-observer agreement was assessed by repeated analyses of a randomly selected sample of 25 subjects.

Table 1. Baseline characteristics

	All (n=100)	Bicuspid aortic valve without Turner syndrome (n=50)	Turner syndrome (n=50)		p-value BAV and TS vs BAV without TS	p-value TS and BAV vs TS without BAV
			Tricuspid aortic valve (n=38)	Bicuspid aortic valve (n=12)		
Age (y)	35 ± 13	35 ± 13	35 ± 13	36 ± 13	0.882	0.892
Gender, female	63 (63%)	13 (26%)	38 (100%)	12 (100%)	<0.001†	-
Height (cm)	169 ± 16	181 ± 12	157 ± 9	154 ± 7	<0.001	0.330
Weight (kg)	72 ± 17	78 ± 15	69 ± 18	61 ± 11	<0.001	0.131
Systolic blood pressure (mmHg)	124 ± 16	124 ± 15	124 ± 18	126 ± 16	0.685	0.719
Diastolic blood pressure (mmHg)	80 ± 11	80 ± 10	80 ± 12	83 ± 14	0.319	0.449
Hypertension	16 (16%)	8 (16%)	7 (18%)	1 (8%)	0.675†	0.661†
Coarctation	13 (13%)	9 (18%)	0 (0%)	4 (33%)	0.256†	0.002†
Aortic dilatation (>40mm and/or ASI>2.1 cm/cm^2)	47 (47%)	33 (66%)	7 (18%)	7 (58%)	0.618	0.023†
Aortic stenosis (echo V_{max} >2.5 m/s)	29 (29%)	28 (56%)	0 (0%)	1 (8%)	0.003†	0.240†
Aortic regurgitation (moderate or severe)	17 (17%)	16 (32%)	0 (0%)	1 (8%)	0.153†	0.240†
Echocardiography	100 (100%)	50 (100%)	38 (100%)	12 (100%)	-	
Computed tomography angiography*	100 (100%)	50 (100%)	38 (100%)	12 (100%)	-	
Diameter sinus of Valsalva (mm)	35 ± 6	39 ± 6	31 ± 3	34 ± 5	0.005	0.140
Diameter sinotubular junction (mm)	31 ± 6	34 ± 6	27 ± 3	29 ± 6	0.016	0.233
Diameter ascending aorta (mm)	33 ± 7	37 ± 7	29 ± 4	31 ± 6	0.004	0.244
Magnetic resonance angiography	88 (88%)	44 (88%)	33 (87%)	11 (92%)	1.000†	1.000†

Data are expressed as mean ± SD or number (percentage). ASI=aortic size index (aortic diameter divided by BSA), TS = Turner syndrome, Vmax=maximum velocity. *Aortic measurements during systole and with the inner-to-inner edge method. † Fisher's exact test.

Statistical analysis

Categorical variables are presented as frequencies with percentages. Comparison of categorical variables was done using the Chi-square test and in case of an expected count <5 in one of the cells of the crosstable the Fisher's exact test was used. All continuous variables are presented as mean with standard deviation when normally distributed, and in case of non-normal distribution, medians with interquartile ranges are provided. Data distribution was checked using histograms. Comparison of normally distributed continuous variables was done using the Student's t-test or, in case of a skewed distribution, the Mann-Whitney test. Comparison of normally distributed continuous variables between two imaging modalities or techniques in one patient was done using the paired student's t-test or, in case of a skewed distribution, the Wilcoxon one-sample test. Pearson correlation coefficient and linear regression analysis was applied for associations. Mean differences between imaging modalities or techniques were determined by Bland-Altman plots, and the limits of agreement calculated using the mean and standard deviation of the difference. To assess intra- and inter observer variability the intraclass correlation coefficient (ICC) was calculated. The IBM SPSS® statistics 21.0 software was used for data analysis. Two-sided p values of <0.05 were considered statistically significant.

Results

Study population

In total 100 subjects were included: 50 subjects with BAV (age 36±13 years; 26% female) and 50 subjects with Turner syndrome (age 35±13 years, 100% female, 24% BAV). Nineteen patients had BAV type 0, 36 patients BAV type 1 and 7 patients BAV type 2. Renal function was normal in all. MRA was not performed in 12 subjects due to claustrophobia (n = 4), technical problems (n = 4), contra-indications (n = 2) and logistic reasons (n = 2). In 26 subjects (26%) the investigations were not performed on the same day. In these subjects the median time between investigations was 7 (IQR 6.5-22.8) days, mostly due to technical or practical issues. The mean total dose length product was 362.2 ± 196.4 mGy * cm. Table 1 shows the baseline patient characteristics of the total study population and separately for the three groups: BAV subjects, Turner subjects without BAV and Turner subjects with BAV.

Comparison of aortic diameters among different imaging modalities

All absolute measurements of the aorta with 2DE, CTA and MRA are shown in supplemental table 2 and 3. Comparison between MRA and CTA showed a Pearson correlation coefficient of 0.84 -0.95 at the level of the SoV and >0.96 at the levels of the STJ and TAA (table 2 and supplemental table 4).

Table 2. Agreement between echocardiography, CTA and MRA

			Lower limit-upper limit of agreement (mm)						
Mean difference ± standard deviation (mm)			**Echo L-L Diastole**	**Echo L-L Systole**	**Echo I-I Diastole**	**Echo I-I Systole**	**CTA I-I Diastole**	**CTA I-I Systole**	**MRA I-I**
	Echo L-L Diastole	SoV		-3.4 - 1.4	1.1 - 4.2	-0.6 - 4.1	-6.6 - 5.9	-7.6 - 4.6	-7.1 - 5.3
		STJ		-4.5 - 1.8	1.1 - 4.7	-2.0 - 4.9	-3.2 - 3.8	-5.0 - 2.6	-5.3 - 3.5
		AA		-4.6 - 2.3	1.2 - 4.1	2.6 - 5.3	-3.1 - 4.8	-5.7 - 3.5	-4.9 - 4.9
	Echo L-L Systole	SoV	-1.0 ± 1.2		0.9 - 6.3	1.1 - 4.3	-5.8 - 7.0	-6.7 - 5.8	-6.2 - 6.4
		STJ	-1.3 ± 1.6		0.9 - 7.6	1.1 - 4.5	-2.1 - 5.3	-3.4 - 3.7	-3.9 - 4.6
		AA	-1.2 ± 1.8		0.1 - 7.5	1.2 - 3.9	-2.3 - 6.2	-3.8 - 4.0	-3.4 - 5.7
	Echo I-I Diastole	SoV	2.7 ± 0.8	3.6 ± 1.4		-3.3 - 1.4	-9.3 - 3.2	-10.4 - 2.1	-9.7 - 2.6
		STJ	2.9 ± 0.9	4.3 ± 1.7		-4.6 - 1.7	-6.3 - 1.2	-8.3 - 0.0	-8.4 - 7.0
		AA	2.7 ± 0.7	3.8 ± 1.9		-5.3 - 2.7	-5.8 - 2.2	-8.5 - 1.0	-7.9 - 2.5
	Echo I-I Systole	SoV	1.8 ± 1.2	2.7 ± 0.8	-0.9 ± 1.2		-8.4 - 4.1	-9.5 - 3.0	-8.9 - 3.5
		STJ	1.5 ± 1.8	2.8 ± 0.9	-1.4 ± 1.6		-5.1 - 2.7	-6.5 - 1.1	-7.0 - 2.1
		AA	1.4 ± 2.0	2.5 ± 0.7	-1.3 ± 2.0		-5.0 - 3.9	-6.6 - 1.7	-6.2 - 3.4
	CTA I-I Diastole	SoV	-0.3 ± 3.2	0.6 ± 3.2	-3.0 ± 3.2	-2.1 ± 3.2		-4.0 - 1.8	-4.2 - 3.0
		STJ	0.3 ± 1.8	1.6 ± 1.9	-2.6 ± 1.9	-1.2 ± 2.0		-4.0 - 1.1	-4.8 - 2.3
		AA	0.9 ± 2.0	2.0 ± 2.2	-1.8 ± 2.0	-0.6 ± 2.3		-4.6 - 1.1	-4.3 - 2.7
	CTA I-I Systole	SoV	-1.5 ± 3.1	-0.5 ± 3.2	-4.1 ± 3.2	-3.2 ± 3.2	-1.1 ± 1.5		-3.0 - 4.1
		STJ	-1.2 ± 2.0	0.1 ± 1.8	-4.1 ± 2.1	-2.7 ± 1.9	-1.5 ± 1.3		-3.0 - 3.7
		AA	-1.1 ± 2.3	0.1 ± 2.0	-3.8 ± 2.4	-2.4 ± 2.1	-1.8 ± 1.5		-2.2 - 4.4
	MRA I-I	SoV	-0.9 ± 3.2	0.8 ± 3.2	-3.6 ± 3.1	-2.7 ± 3.2	-0.6 ± 1.8	0.6 ± 1.8	
		STJ	-0.9 ± 2.3	0.3 ± 2.2	-3.8 ± 2.3	-2.5 ± 2.3	-1.3 ± 1.8	0.3 ± 1.7	
		AA	-0.0 ± 2.5	1.1 ± 2.3	-2.8 ± 2.7	-1.4 ± 2.4	-0.8 ± 1.8	1.1 ± 1.7	

Mean difference ± standard deviation (colored boxes) and lower limit-upper limit of agreement (non-colored boxes) for comparison between different measurements at the level of the sinus of Valsalva (SoV) sinotubular junction (STJ) and the ascending aorta (AA). Green: mean difference < 1.0 mm. Orange: mean difference 1.0 - 2.0 mm. Red: mean difference ≥ 2.0 mm.

When comparing 2DE with CTA, the L-L edge method showed best agreement with CTA compared to the I-I edge method at the level of the STJ and TAA in both end-diastole and mid-systole (table 2 and supplemental figure 1). The smallest difference between 2DE and CTA was found at the STJ in mid-systole with the L-L edge method (r = 0.96, mean difference 0.1 ± 1.8 mm). At the level of the SoV the I-I edge method underestimated the diameter compared to the cusp-to-commissure method in CTA (supplemental figures 2 and 3 and supplemental table 5). In the majority of cases, lower Pearson correlation coefficients and higher mean differences were found at the level of the SoV.

Comparison between cusp-to-commissure and cusp-to-cusp diameter

Between the cusp-to-commissure and the cusp-to-cusp diameter measured on CTA no significant difference was found (mean difference 0.0 ± 1.5 mm, p = 1.00). The maximum difference between these two methods in one patient was 4 mm.

Comparison between end-diastole and mid-systole

Mid-systolic aortic diameters were significantly larger than end-diastolic diameters at nearly all levels (supplemental table 6). Comparison of mid-systolic and end-diastolic aortic diameters demonstrated mean differences from 0.7 ± 2.3 mm up to 1.8 ± 1.5 mm. The standard deviations of mid-systole and end-diastole did not differ significantly at all levels by both 2DE and CTA (Levene's test p>0.05). The aortic length by 2DE was significantly longer during mid-systole (51.1 ± 13.8 mm) compared to end-diastole (45.8 ± 13.2 mm) with a mean difference of 5.3 ± 5.1 mm (p<0.001).

Maximum single-subject difference between all aortic measurements

Distribution of differences by aortic level are displayed in figure 2. The maximum difference was 5.4 ± 2.7 mm for the SoV (maximum 18 mm), 5.1 ± 2.0 mm for the STJ (maximum 11 mm) and 4.8 ± 2.1 mm for the TAA (maximum 11 mm). The maximum difference is a result from both inter-modality differences as from differences between modalities, but was most often explained by the differences between measurements on 2DE (29%) or between 2DE and CTA (38%, supplemental figure 4). Maximum difference showed a moderate positive correlation with the absolute diameter at each level (supplemental figure 5), specifically SoV (r = 0.42, p ≤ 0.001), STJ (r = 0.41, p ≤ 0.001) and TAA (r = 0.45, p ≤ 0.001). Patients with BAV showed a larger maximum difference (SoV p = 0.001, STJ p < 0.001, TAA p < 0.001). After adjustment for aortic diameter, this correlation remained significant for the STJ (β = 0.87, p = 0.042) and TAA (β = 0.95, p = 0.027). Patients in which investigations were performed on different days (n = 26), did not show a larger maximum difference compared to the patients who received all investigations on the same day.

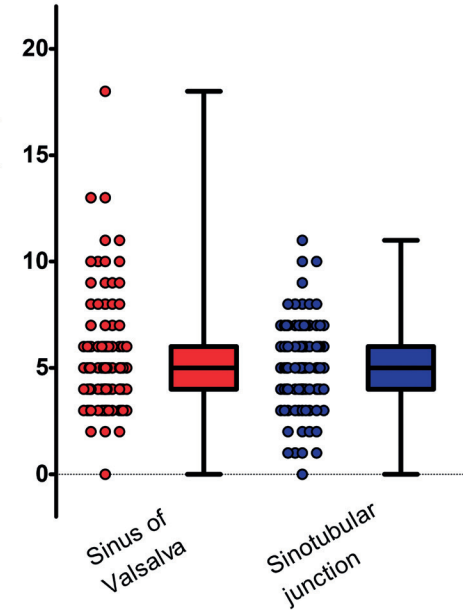

Figure 2. Distribution of maximum differences found between the seven measurements

The maximum difference are plotted for the three different levels: sinus of Valsalva, the sinotubular junction and the ascending aorta.

Intra- and interobserver variability

Intra- and interobserver variability for 2DE, CTA and MRA are shown in supplemental tables 7 and 8. There was good agreement with most comparisons. Agreement was least optimal at the SoV.

Discussion

Our study compared measurements of three aortic levels using three imaging modalities (CTA, MRA and 2DE), different edge detections and different cardiac phases. Our goals were to determine agreement and provide guidance on the optimal approach to measure the ascending aorta. We included two groups of patients giving a wide spectrum of aortic dimensions and leaflet configurations. The findings are important for all patients with confirmed or suspected aortic pathology.

Although overall agreement was very good, the maximum difference between two measurements in any given subject was high. Despite measurements performed by experienced investigators, we showed differences up to 18 mm at the SoV, 11 mm

at the STJ and 11 mm at the TAA. Given the guideline thresholds for the definition of aortic dilation (>40 mm) and indications for preventive surgery (>55 mm) [6, 23], measured differences of this range are too large to be of use in clinical practice. Intra- and interobserver variability were good to excellent, so these differences are probably related to the differences in technique and not to differences in individual measurements. Larger maximum differences were found in larger aortas, and most often between the different measurements on 2DE or between 2DE and CTA. Also patients with BAV show larger maximum differences. Since the root is generally well-imaged on all standard 2DE, one would assume that there would be better agreement at this level. Yet lower Pearson correlation coefficients and higher mean differences were observed at the SoV relative to higher up the aorta, suggesting that for patients with dilation at this level CTA or MRA may be preferable for accurate follow-up.

Our data also showed that the L-L edge method by 2DE corresponds best with the I-I edge method by CTA and MRA. Although it seems logical to use the same method for comparison between modalities, it appears that the L-L edge method is preferable for 2DE. This supports current clinical practice, since most physicians who use 2DE already apply the L-L edge method and current reference values are based on this method [16, 17]. An advantage of the current study is that in most subjects imaging with all three modalities was performed on the same day, meaning any variation due to loading conditions should be controlled. In addition, the twenty-six patients who received the investigations on different days, did not show larger maximum differences. Although our data does not contain information about physiological conditions, such as heart rate or blood pressure, we assume this will probably not have affected our results. However, we have to admit that our MRA protocol was not completely optimal. Despite this limited MRA sequences, we found excellent agreement between CTA and MRA, as others have similarly reported(24,29). Also intermodality comparisons between echocardiography and CTA/MRA are previously published using studies in varying aortic patient groups, with some findings that are congruent with our own. By 2DE for example, better agreement with CTA has been shown using L-L techniques rather than I-I [24-30]. Several studies show echo dimensions to be smaller than either MRI or CTA [31, 32] including our previous study [28]. Consistency with other publications adds credibility to the findings overall.

Based on these results, several recommendations can be made to maximize intermodality agreement. Our findings support the necessity of using the same imaging modality and technique in an individual patient to accurately compare serial measurements. CTA or MRA should be performed at least once in addition to 2DE for optimal imaging of the aorta. In patients with good agreement 2DE may be used for serial follow-up. We found no difference between the cusp-to-commissure and cusp-to-cusp methods in CTA. Although another study [26] found a slightly larger diameter of 1.3 mm when using the cusp-to-

cusp method, there is currently not enough evidence for the use of one technique over another. Preferably the same technique should be used every time.

Our study is the first to assess the length of aorta visible during 2DE. Echocardiographic images showed on average a 5.3 mm longer segment of the aorta during mid-systole compared to end-diastole. This could be an additional reason to measure the aorta during systole. Guidelines generally advise end-diastolic measures because of the greater reproducibility (blood pressure is most stable and distension is more plateaued), but this is not confirmed in our and other studies [25, 33]. In addition, physicians prefer to use the largest diameter of the aorta in their decision making. For this reason, the higher values found during mid-systole shown in our together with one other study [34], could be an additional reason to choose systole. Yet since natural history studies have largely been based on 2DE measurements in diastole, some have argued that changing conventions would adversely impact clinical management.

A limitation of our study was the inclusion of both bicuspid and tricuspid valve subjects. Because in some bicuspid aortic valves it was not possible to measure three cusp-to-commissure distances, we also analyzed this group separately at the level of the SoV. This resulted in a small number of subjects for analysis. We did not include healthy participant, which could have made the results even more generalizable. Because we used the protocols of a previous developed cohort study, the imaging modalities showed some limitations, such as the reduced tube current during the last 60% of the R-R interval. Also, the slice thickness of CTA was 1.5 mm, which is slightly thicker than recommended by guidelines [7]. Our MRA protocol was non-ECG-gated, which caused some blurring and limited comparisons to averaged diastole/systole measurements from CTA. Others have shown sharper edge detection and favorable variation for steady-state free precession imaging without contrast [35, 36] than the methods we were able to use here. Despite these potential limitations there was good agreement between CTA and MRA. Also the large maximum single-subject difference was not caused by the limited MRA sequences.

In conclusion, our study supports the L-L edge method by 2DE to provide the best agreement with the I-I edge method by CTA or MRA. This is also recommended by the ASE/EACVI guidelines [7, 8]. CTA or MRA should be performed at least once and follow-up measurements of the aorta should be done at the same level, during the same cardiac phase and using the same technique and modality.

References

1. Davies RR, Goldstein LJ, Coady MA, Tittle SL, Rizzo JA, Kopf GS, et al. Yearly rupture or dissection rates for thoracic aortic aneurysms: simple prediction based on size. Ann Thorac Surg 2002;73(1):17-27; discussion 27-8.
2. Clouse WD, Hallett JW, Jr., Schaff HV, Gayari MM, Ilstrup DM, Melton LJ, 3rd. Improved prognosis of thoracic aortic aneurysms: a population-based study. Jama 1998;280(22):1926-9.
3. Olsson C, Thelin S, Stahle E, Ekbom A, Granath F. Thoracic aortic aneurysm and dissection: increasing prevalence and improved outcomes reported in a nationwide population-based study of more than 14,000 cases from 1987 to 2002. Circulation 2006;114(24):2611-8.
4. Cantinotti M, Giordano R, Clemente A, Assanta N, Murzi M, Murzi B, et al. Strengths and Limitations of Current Adult Nomograms for the Aorta Obtained by Noninvasive Cardiovascular Imaging. Echocardiography 2016;33(7):1046-68.
5. Mongeon FP, Marcotte F, Terrone DG. Multimodality Noninvasive Imaging of Thoracic Aortic Aneurysms: Time to Standardize? Can J Cardiol 2016;32(1):48-59.
6. Hiratzka LF, Bakris GL, Beckman JA, Bersin RM, Carr VF, Casey DE, Jr., et al. 2010 ACCF/AHA/AATS/ACR/ASA/SCA/SCAI/SIR/STS/SVM guidelines for the diagnosis and management of patients with Thoracic Aortic Disease: a report of the American College of Cardiology Foundation/American Heart Association Task Force on Practice Guidelines, American Association for Thoracic Surgery, American College of Radiology, American Stroke Association, Society of Cardiovascular Anesthesiologists, Society for Cardiovascular Angiography and Interventions, Society of Interventional Radiology, Society of Thoracic Surgeons, and Society for Vascular Medicine. Circulation 2010;121(13):e266-369.
7. Goldstein SA, Evangelista A, Abbara S, Arai A, Asch FM, Badano LP, et al. Multimodality imaging of diseases of the thoracic aorta in adults: from the American Society of Echocardiography and the European Association of Cardiovascular Imaging: endorsed by the Society of Cardiovascular Computed Tomography and Society for Cardiovascular Magnetic Resonance. J Am Soc Echocardiogr 2015;28(2):119-82.
8. Lang RM, Badano LP, Mor-Avi V, Afilalo J, Armstrong A, Ernande L, et al. Recommendations for cardiac chamber quantification by echocardiography in adults: an update from the American Society of Echocardiography and the European Association of Cardiovascular Imaging. J Am Soc Echocardiogr 2015;28(1):1-39 e14.
9. Lopez L, Colan SD, Frommelt PC, Ensing GJ, Kendall K, Younoszai AK, et al. Recommendations for quantification methods during the performance of a pediatric echocardiogram: a report from the Pediatric Measurements Writing Group of the American Society of Echocardiography Pediatric and Congenital Heart Disease Council. J Am Soc Echocardiogr 2010;23(5):465-95; quiz 576-7.
10. Son MK, Chang SA, Kwak JH, Lim HJ, Park SJ, Choi JO, et al. Comparative measurement of aortic root by transthoracic echocardiography in normal Korean population based on two different guidelines. Cardiovasc Ultrasound 2013;11:28.

11. Bossone E, Yuriditsky E, Desale S, Ferrara F, Vriz O, Asch FM. Normal Values and Differences in Ascending Aortic Diameter in a Healthy Population of Adults as Measured by the Pediatric versus Adult American Society of Echocardiography Guidelines. J Am Soc Echocardiogr 2016;29(2):166-72.
12. Hager A, Kaemmerer H, Rapp-Bernhardt U, Blucher S, Rapp K, Bernhardt TM, et al. Diameters of the thoracic aorta throughout life as measured with helical computed tomography. J Thorac Cardiovasc Surg 2002;123(6):1060-6.
13. Mao SS, Ahmadi N, Shah B, Beckmann D, Chen A, Ngo L, et al. Normal thoracic aorta diameter on cardiac computed tomography in healthy asymptomatic adults: impact of age and gender. Acad Radiol 2008;15(7):827-34.
14. Kalsch H, Lehmann N, Mohlenkamp S, Becker A, Moebus S, Schmermund A, et al. Body-surface adjusted aortic reference diameters for improved identification of patients with thoracic aortic aneurysms: results from the population-based Heinz Nixdorf Recall study. Int J Cardiol 2013;163(1):72-8.
15. Wolak A, Gransar H, Thomson LE, Friedman JD, Hachamovitch R, Gutstein A, et al. Aortic size assessment by noncontrast cardiac computed tomography: normal limits by age, gender, and body surface area. JACC Cardiovasc Imaging 2008;1(2):200-9.
16. Biaggi P, Matthews F, Braun J, Rousson V, Kaufmann PA, Jenni R. Gender, age, and body surface area are the major determinants of ascending aorta dimensions in subjects with apparently normal echocardiograms. J Am Soc Echocardiogr 2009;22(6):720-5.
17. Devereux RB, de Simone G, Arnett DK, Best LG, Boerwinkle E, Howard BV, et al. Normal limits in relation to age, body size and gender of two-dimensional echocardiographic aortic root dimensions in persons >/=15 years of age. Am J Cardiol 2012;110(8):1189-94.
18. Vriz O, Aboyans V, D'Andrea A, Ferrara F, Acri E, Limongelli G, et al. Normal values of aortic root dimensions in healthy adults. Am J Cardiol 2014;114(6):921-7.
19. van den Hoven AT, Mc-Ghie JS, Chelu RG, Duijnhouwer AL, Baggen VJM, Coenen A, et al. Transthoracic 3D echocardiographic left heart chamber quantification in patients with bicuspid aortic valve disease. Int J Cardiovasc Imaging 2017;33(12):1895-1903.
20. Lancellotti P, Tribouilloy C, Hagendorff A, Popescu BA, Edvardsen T, Pierard LA, et al. Recommendations for the echocardiographic assessment of native valvular regurgitation: an executive summary from the European Association of Cardiovascular Imaging. Eur Heart J Cardiovasc Imaging 2013;14(7):611-44.
21. Rudarakanchana N, Bicknell CD, Cheshire NJ, Burfitt N, Chapman A, Hamady M, et al. Variation in maximum diameter measurements of descending thoracic aortic aneurysms using unformatted planes versus images corrected to aortic centerline. Eur J Vasc Endovasc Surg 2014;47(1):19-26.
22. Sievers HH, Schmidtke C. A classification system for the bicuspid aortic valve from 304 surgical specimens. J Thorac Cardiovasc Surg 2007;133(5):1226-33.
23. Erbel R, Aboyans V, Boileau C, Bossone E, Bartolomeo RD, Eggebrecht H, et al. 2014 ESC Guidelines on the diagnosis and treatment of aortic diseases: Document covering acute and chronic aortic diseases of the thoracic and abdominal aorta of the adult. The Task Force for

the Diagnosis and Treatment of Aortic Diseases of the European Society of Cardiology (ESC). Eur Heart J 2014;35(41):2873-926.

24. Paelinck BP, Van Herck PL, Rodrigus I, Claeys MJ, Laborde JC, Parizel PM, et al. Comparison of magnetic resonance imaging of aortic valve stenosis and aortic root to multimodality imaging for selection of transcatheter aortic valve implantation candidates. Am J Cardiol 2011;108(1):92-8.
25. Park JY, Foley TA, Bonnichsen CR, Maurer MJ, Goergen KM, Nkomo VT, et al. Transthoracic Echocardiography versus Computed Tomography for Ascending Aortic Measurements in Patients with Bicuspid Aortic Valve. J Am Soc Echocardiogr 2017.
26. Rodriguez-Palomares JF, Teixido-Tura G, Galuppo V, Cuellar H, Laynez A, Gutierrez L, et al. Multimodality Assessment of Ascending Aortic Diameters: Comparison of Different Measurement Methods. J Am Soc Echocardiogr 2016;29(9):819-826 e4.
27. Tsang JF, Lytwyn M, Farag A, Zeglinski M, Wallace K, daSilva M, et al. Multimodality imaging of aortic dimensions: comparison of transthoracic echocardiography with multidetector row computed tomography. Echocardiography 2012;29(6):735-41.
28. van der Linde D, Rossi A, Yap SC, McGhie JS, van den Bosch AE, Kirschbaum SW, et al. Ascending aortic diameters in congenital aortic stenosis: cardiac magnetic resonance versus transthoracic echocardiography. Echocardiography 2013;30(5):497-504.
29. Leone D, Tosello F, Faletti R, Schivazappa G, Bruno G, Avenatti E, et al. Accuracy of transthoracic echocardiography in the assessment of proximal aortic diameter in hypertensive patients: comparison with cardiac magnetic resonance. J Hypertens 2017;35(8):1626-1634.
30. Tamborini G, Galli CA, Maltagliati A, Andreini D, Pontone G, Quaglia C, et al. Comparison of feasibility and accuracy of transthoracic echocardiography versus computed tomography in patients with known ascending aortic aneurysm. Am J Cardiol 2006;98(7):966-9.
31. Nejatian A, Yu J, Geva T, White MT, Prakash A. Aortic Measurements in Patients with Aortopathy are Larger and More Reproducible by Cardiac Magnetic Resonance Compared with Echocardiography. Pediatr Cardiol 2015;36(8):1761-73.
32. Tsai SF, Trivedi M, Daniels CJ. Comparing imaging modalities for screening aortic complications in patients with bicuspid aortic valve. Congenit Heart Dis 2012;7(4):372-7.
33. de Heer LM, Budde RP, Mali WP, de Vos AM, van Herwerden LA, Kluin J. Aortic root dimension changes during systole and diastole: evaluation with ECG-gated multidetector row computed tomography. Int J Cardiovasc Imaging 2011;27(8):1195-204.
34. Muraru D, Maffessanti F, Kocabay G, Peluso D, Dal Bianco L, Piasentini E, et al. Ascending aorta diameters measured by echocardiography using both leading edge-to-leading edge and inner edge-to-inner edge conventions in healthy volunteers. Eur Heart J Cardiovasc Imaging 2014;15(4):415-22.

35. Veldhoen S, Behzadi C, Derlin T, Rybczinsky M, von Kodolitsch Y, Sheikhzadeh S, et al. Exact monitoring of aortic diameters in Marfan patients without gadolinium contrast: intraindividual comparison of 2D SSFP imaging with 3D CE-MRA and echocardiography. Eur Radiol 2015;25(3):872-82.
36. von Knobelsdorff-Brenkenhoff F, Gruettner H, Trauzeddel RF, Greiser A, Schulz-Menger J. Comparison of native high-resolution 3D and contrast-enhanced MR angiography for assessing the thoracic aorta. Eur Heart J Cardiovasc Imaging 2014;15(6):651-8.

Supplemental material

Supplemental table 1. Seven different methods for aortic measurement used and compared

Echocardiography	Inner edge-to-inner edge during mid-systole(1)
	Inner edge-to-inner edge during end-diastole(2)
	Leading edge-to-leading edge during mid-systole(3)
	Leading edge-to-leading edge during end-diastole(4)
CTA*	Inner edge-to-inner edge during mid-systole(5)
	Inner edge-to-inner edge during end-diastole(6)
MRA*	Inner edge-to-inner edge(7)

*At the level of the sinus of Valsalva the highest value of the three cusp-to-commissure measurements was used

Supplemental table 2. Aortic measurements with 2DE

	End-diastole			Mid-systole		
	n	Inner edge-to-inner edge	Leading edge-to-leading edge	n	Inner edge-to-inner edge	Leading edge-to-leading edge
Sinus of Valsalva	99	31.3 ± 5.6	34.0 ± 5.8	99	32.3 ± 5.7	35.0 ± 6.0
Sinotubular junction	92	27.2 ± 5.6	30.1 ± 5.7	92	28.6 ± 5.5	31.4 ± 5.8
Ascending aorta	86	30.2 ± 6.7	32.9 ± 7.0	88	31.4 ± 6.8	33.9 ± 6.9

Data are expressed as mean ± SD (mm).

Supplemental table 3. Aortic measurements with computed tomography angiography and magnetic resonance angiography

	Computed tomography angiography				Magnetic resonance angiography	
	n	End-diastole	n	Mid-systole	n	
Sinus of Valsalva						
Tricuspid or BAV Sievers type 1						
RCC-commissure	78	30.0 ± 5.0	81	31.7 ± 4.7	68	31.1 ± 5.2
LCC-commissure	78	32.4 ± 5.2	81	34.0 ± 5.3	68	33.2 ± 5.2
NCC-commissure	78	32.7 ± 5.9	81	33.9 ± 6.1	68	33.8 ± 6.1
BAV valve Sievers type 0						
Maximum diameter	18	36.8 ± 6.6	19	37.7 ± 6.6	16	37.5 ± 6.9
Perpendicular diameter	18	30.2 ± 4.8	19	31.3 ± 5.3	16	30.1 ± 4.9
Sinotubular junction (STJ)	97	29.5 ± 6.2	100	31.0 ± 6.2	88	30.7 ± 6.4
Ascending aorta	97	31.7 ± 7.0	100	33.4 ± 6.8	88	32.5 ± 7.4

RCC-commissure = right coronary cusp to commissure, LCC-commissure= left coronary cusp to commissure, NCC-commissure = non-coronary cusp to commissure. Data are expressed as mean ± SD (mm).

Supplemental table 4. Magnetic resonance angiography vs computed tomography angiography

	n*	Max absolute difference (mm)	Mean difference ± SD (mm)	Pearson coefficient †	Lower limit/Upper limit (mm)	
CTA end-diastole vs MRA						
Sinus of Valsalva						
Tricuspid or BAV Sievers type 1						
RCC-commissure	65	8.0	-0.9 ± 2.3	0.90	-5.4	3.6
LCC-commissure	65	7.0	-0.3 ± 2.2	0.91	-4.6	4.0
NCC-commissure	65	7.0	-0.7 ± 2.0	0.95	-4.6	3.2
BAV Sievers type 0						
Maximum diameter	15	6.0	-0.9 ± 2.2	0.95	-5.2	3.4
Perpendicular diameter	15	8.0	0.0 ± 2.8	0.84	-5.5	5.5
Sinotubular junction	85	8.0	-1.3 ± 1.8	0.96	-4.8	2.2
Ascending aorta	85	7.0	-0.8 ± 1.8	0.97	-4.3	2.7
CTA mid-systole vs MRA						
Sinus of Valsalva						
Tricuspid or BAV Sievers type 1						
RCC-commissure	68	7.0	0.9 ± 2.3	0.90	-3.6	5.4
LCC-commissure	68	5.0	1.2 ± 1.9	0.93	-2.5	4.9
NCC-commissure	68	7.0	0.4 ± 2.0	0.95	-3.5	4.3
BAV Sievers type 0						
Maximum diameter	16	5.0	-0.1 ± 2.2	0.95	-4.4	4.2
Perpendicular diameter	16	7.0	1.2 ± 2.8	0.87	-4.3	6.7
Sinotubular junction	88	8.0	0.3 ± 1.7	0.96	-3.0	3.6
Ascending aorta	88	5.0	1.1 ± 1.7	0.97	-2.2	4.4

RCC-commissure = right coronary cusp to commissure, LCC-commissure= left coronary cusp to commissure, NCC-commissure = non-coronary cusp to commissure.
* Not possible to measure the sinus of Valsalva with CTA during end-diastole in 1 subject (artefact) and with MRA in 4 subjects (bad quality). In 12 patients MRA was missing and in 3 patients the CT could not be performed during end-diastole.
† All $p < 0.0001$

Supplemental table 5. Echocardiography versus computed tomography angiography in mid-systole

	n	Max difference (mm)	Mean difference ± SD (mm)	Pearson coefficient*	p-value	Lower limit/ Upper limit (mm)
Echo leading edge-to-leading edge vs CTA						
Sinus of Valsalva						
Tricuspid or BAV Sievers type 1						
RCC-commissure	81	10	3.1±2.5	0.921	0.000	-1.8/8.0
LCC-commissure	81	10	0.8±3.1	0.861	0.000	-5.3/6.9
NCC-commissure	81	6	1.0±2.3	0.926	0.000	-3.5/5.5
BAV valve Sievers type 0						
Maximum diameter	18	13	-2.2±4.7	0.684	0.002	-11.4/7.0
Perpendicular diameter	18	10	3.8±4.1	0.754	0.000	-4.2/11.8
Sinotubular junction	92	8	0.1±1.8	0.959	0.000	-3.4/3.7
Ascending aorta	88	6	0.1±2.0	0.960	0.000	-3.8/4.0
Echo inner edge-to-inner edge vs CTA						
Sinus of Valsalva						
Tricuspid or BAV Sievers type 1						
RCC-commissure	81	6	0.4±2.2	0.930	0.000	-3.9/4.7
LCC-commissure	81	13	-1.8±3.0	0.857	0.000	-7.7/4.1
NCC-commissure	81	9	-1.7±2.4	0.918	0.000	-6.4/3.0
BAV valve Sievers type 0						
Maximum diameter	18	16	-5.2±4.6	0.691	0.002	-14.2/3.8
Perpendicular diameter	18	6	0.9±3.7	0.794	0.000	-6.4/8.2
Sinotubular junction	92	11	-2.7±1.9	0.954	0.000	-6.5/1.1
Ascending aorta	88	9	-2.4±2.1	0.953	0.000	-6.6/1.7

RCC-commissure=right coronary cusp to commissure, LCC-commissure=left coronary cusp to commissure, NCC-commissure=non-coronary cusp to commissure. *All p<0.001.

Supplemental table 6. Difference between end-diastole and mid-systole by echocardiography and CTA

	n	Max difference (mm)	Mean difference ± SD (mm)	p value paired T-test	Mid-systole ≥ end-diastole (%)	Pearson coefficient*	Limits of agreement (mm)	
							Lower limit	Upper limit
Echocardiography								
Leading edge-to-leading edge								
Sinus of Valsalva	99	5	1.0 ± 1.2	<0.001	90	0.98	-1.4	3.4
Sinotubular junction	92	5	1.3 ± 1.6	<0.001	88	0.96	-1.8	4.5
Ascending aorta	86	5	1.2 ± 1.8	<0.001	87	0.97	-2.3	4.6
Inner edge-to-inner edge								
Sinus of Valsalva	99	5	0.9 ± 1.2	<0.001	89	0.98	-1.4	3.3
Sinotubular junction	92	5	1.4 ± 1.6	<0.001	90	0.96	-1.7	4.6
Ascending aorta	86	6	1.3 ± 2.0	<0.001	86	0.95	-2.7	5.3
Computed tomography angiography								
Sinus of Valsalva								
Tricuspid or BAV Sievers type 1								
RCC-commissure	78	7	1.6 ± 1.7	<0.001	95	0.94	-1.7	4.9
LCC-commissure	78	5	1.5 ± 1.7	<0.001	92	0.95	-1.8	4.8
NCC-commissure	78	4	1.1 ± 1.6	<0.001	89	0.97	-2.0	4.2
BAV valve Sievers type 0								
Maximum diameter	18	7	0.7 ± 2.3	0.200	78	0.94	-3.8	5.2
Perpendicular diameter	18	10	1.1 ± 3.8	0.260	78	0.75	-6.3	8.5
Sinotubular junction	97	5	1.5 ± 1.3	<0.001	96	0.98	-1.1	4.0
Ascending aorta	97	6	1.8 ± 1.5	<0.001	96	0.98	-1.1	4.6

RCC-commissure = right coronary cusp to commissure, LCC-commissure= left coronary cusp to commissure, NCC-commissure = non-coronary cusp to commissure.

Supplemental table 7. Intra- and interobserver variability in echocardiography

		Inner edge-to-inner edge				Leading edge-to-leading edge			
		End-diastole		Mid-systole		End-diastole		Mid-systole	
	n*	Mean difference ± SD (mm)	ICC	Mean difference ± SD (mm)	ICC	Mean difference ± SD (mm)	ICC	Mean difference | ± SD (mm)	ICC
Intraobserver variability									
Sinus of Valsalva	25	-0.3 ± 0.9	0.98	-0.3 ± 0.7	0.99	-0.6 ± 0.9	0.98	-0.5 ± 0.7	0.99
Sinotubular junction	25	0.1 ± 0.9	0.99	0.3 ± 1.0	0.98	-0.0 ± 0.9	0.99	0.1 ± 1.0	0.99
Ascending aorta	25	0.1 ± 1.1	0.99	0.7 ± 1.1	0.98	0.2 ± 0.9	0.99	0.3 ± 1.3	0.98
Interobserver variablity*									
Sinus of Valsalva	25	-0.3 ± 2.0	0.94	0.1 ± 1.4	0.97	-0.2 ± 1.8	0.95	0.3 ± 1.5	0.97
Sinotubular junction	25	-0.4 ± 1.6	0.97	0.6 ± 1.5	0.96	0.1 ± 1.7	0.96	1.1 ± 1.5	0.96
Ascending aorta	25	-0.5 ± 2.0	0.97	0.3 ± 1.5	0.98	0.3 ± 2.0	0.96	1.2 ± 1.7	0.97

* Number of measurements missing by the second observer during mid-systole due to insufficient quality of images: 4x Sinus of Valsalva, 2x sinotubular junction, 6x ascending aorta.

Supplemental table 8. Intra- and interobserver variability in computed tomography angiography and magnetic resonance angiography

		Computed tomograhpy angiography				Magnetic resonance angiography	
		End-diastole		Mid-systole			
	n	Mean difference ± SD (mm)	ICC	Mean difference ± SD (mm)	ICC	Mean difference ± SD (mm)	ICC
Intraobserver variability							
Sinus of Valsalva							
Tricuspid or BAV Sievers type 1							
RCC-commissure	20	-0.1 ± 0.8	0.99	-0.5 ± 0.9	0.98	0.4 ± 1.8	0.92
LCC-commissure	20	-0.1 ± 1.1	0.97	-0.3 ± 0.8	0.99	-0.1 ± 1.4	0.96
NCC-commissure	20	-0.2 ± 1.0	0.99	-0.2 ± 0.6	1.00	0.7 ± 1.6	0.96
BAV valve Sievers type 0							
Maximum diameter	5	0.0 ± 0.0	1.00	0.2 ± 1.1	0.98	0.6 ± 0.9	0.99
Perpendicular diameter	5	-0.6 ± 1.1	0.98	0.8 ± 0.8	0.99	0.8 ± 1.1	0.97
Sinotubular junction	25	0.0 ± 0.7	1.00	0.2 ± 0.8	0.99	0.4 ± 1.4	0.98
Ascending aorta	25	-0.1 ± 0.4	1.00	-0.2 ± 0.8	0.99	0.1 ± 1.2	0.99
Interobserver variability							
Sinus of Valsalva							
Tricuspid or BAV Sievers type 1							
RCC-commissure	20	0.6 ± 1.1	0.97	0.1 ± 1.1	0.97	0.2 ± 2.6	0.85
LCC-commissure	20	1.0 ± 1.3	0.94	0.5 ± 1.2	0.96	0.2 ± 1.7	0.93
NCC-commissure	20	0.5 ± 1.4	0.97	0.6 ± 1.0	0.98	0.6 ± 1.6	0.97
BAV valve Sievers type 0							
Maximum diameter	5	0.8 ± 0.8	0.98	0.8 ± 1.5	0.96	0.2 ± 1.6	0.97
Perpendicular diameter	5	1.2 ± 1.9	0.92	2.6 ± 2.4	0.85	4.0 ± 2.3	0.63
Sinotubular junction	25	0.4 ± 0.8	0.99	0.7 ± 1.0	0.99	0.6 ± 1.6	0.97
Ascending aorta	25	0.4 ± 0.9	0.99	0.2 ± 1.1	0.99	0.3 ± 1.4	0.98

RCC-commissure = right coronary cusp to commissure, LCC-commissure= left coronary cusp to commissure, NCC-commissure = non-coronary cusp to commissure.

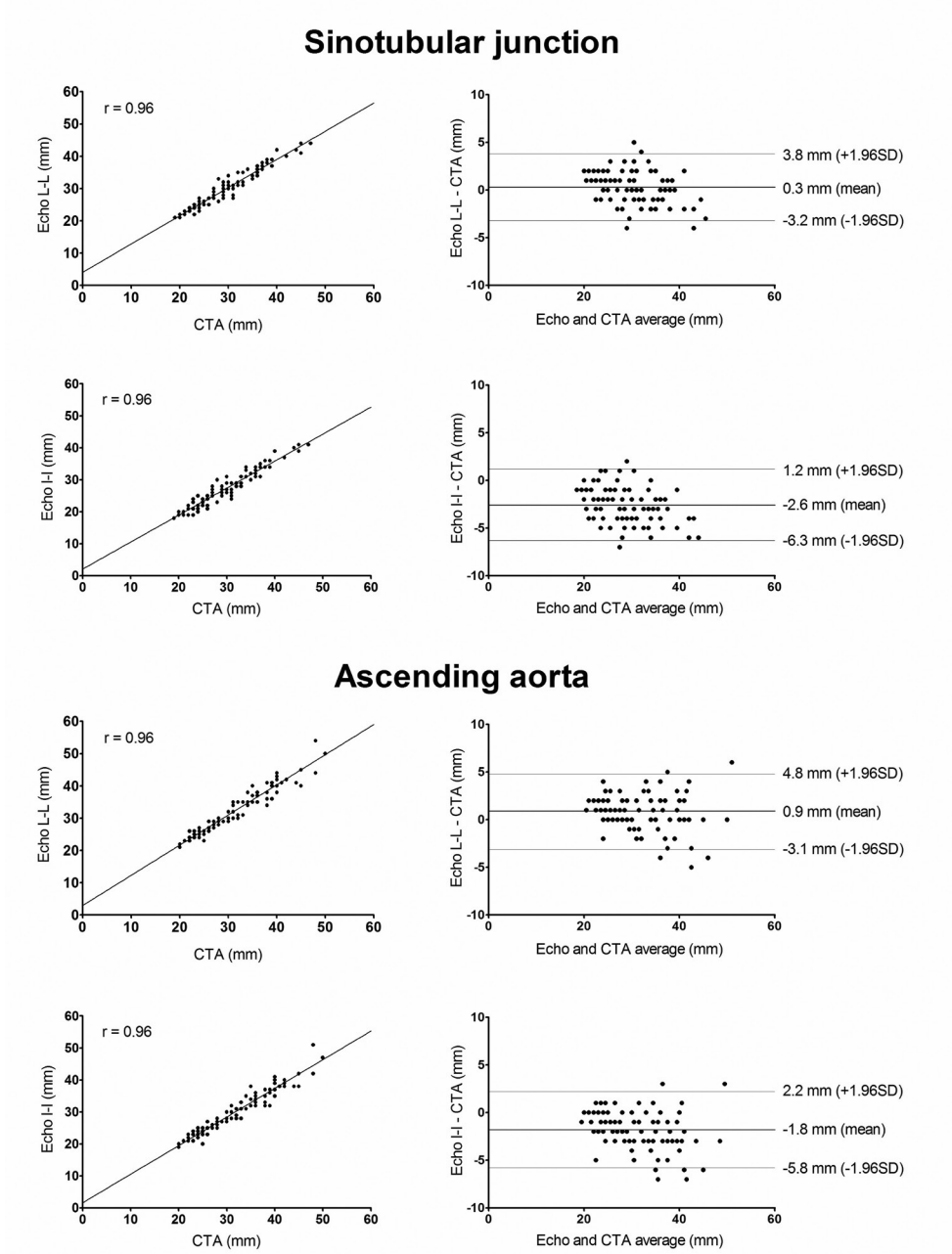

Supplemental figure 1. Agreement between echocardiography and CTA (STJ and ascending aorta)

Linear regression lines and Bland-Altman plots for echocardiography and computed tomography angiography at the level of the sinotubular junction and the ascending aorta using the I-I edge method and L-L edge method during end-diastole.

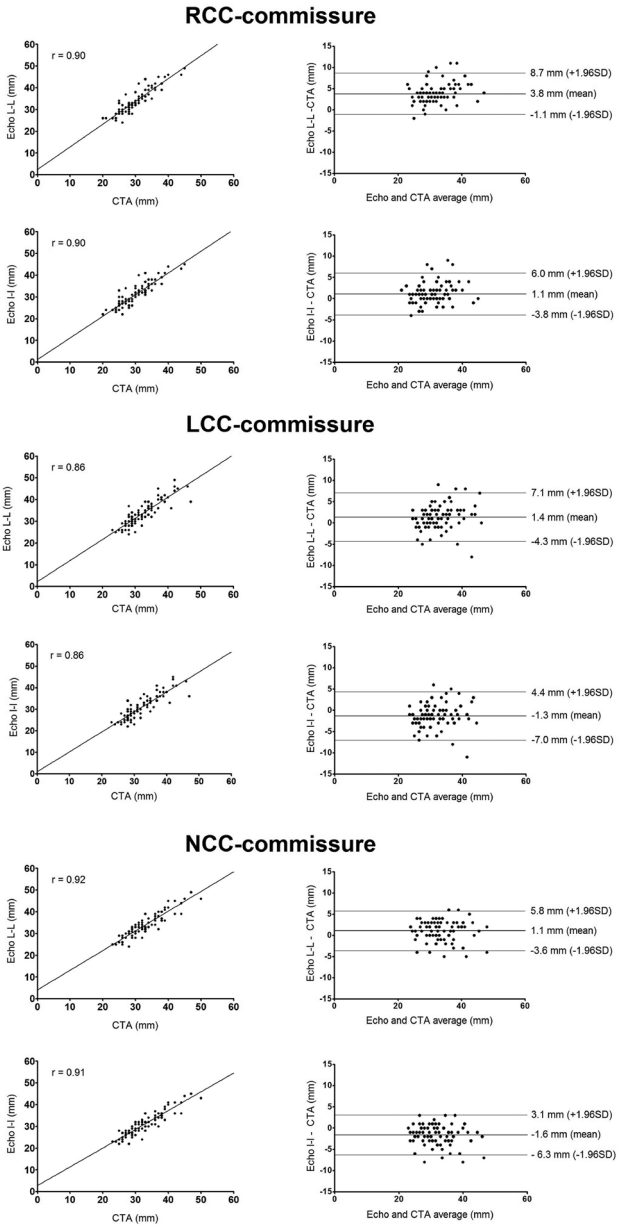

Supplemental figure 2. Agreement between echocardiography and CTA for tricuspid or bicuspid type 1 aortic valves (sinus of Valsalva)

Linear regression and Bland-Altman plots for echocardiography and computed tomography angiography at the level the sinus of Valsalva for tricuspid or bicuspid type 1 aortic valves using the L-L edge method and I-I edge method during end-diastole. RCC-commissure = right coronary cusp to commissure, LCC-commissure= left coronary cusp to commissure, NCC-commissure = non-coronary cusp to commissure.

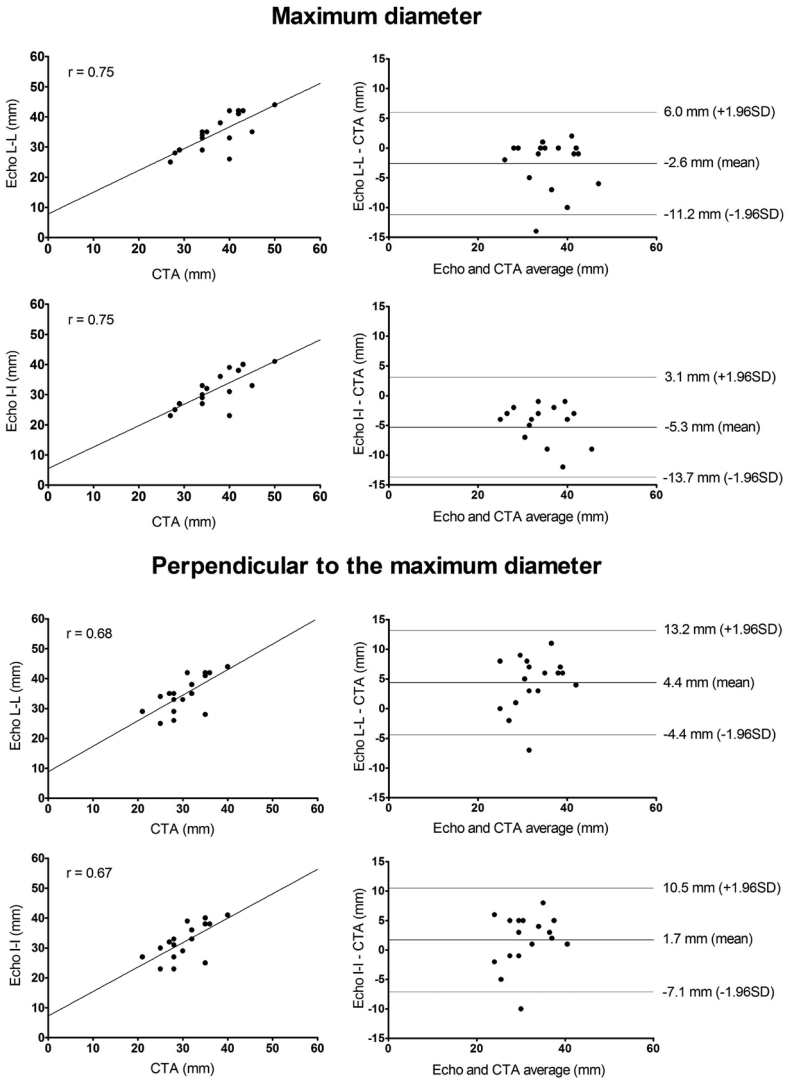

Supplemental figure 3. Agreement between echocardiography and CTA for bicuspid type 0 aortic valves (sinus of Valsalva)

Linear regression and Bland-Altman plots for echocardiography and computed tomography angiography at the level of the sinus of Valsalva for bicuspid type 0 aortic valves using the I-I edge method and L-L edge method during end-diastole. One data point is outside the axis limits in the Bland-Altman figure of the perpendicular to the maximum diameter with use of the I-I edge (X = 31.50, Y = -17.00).

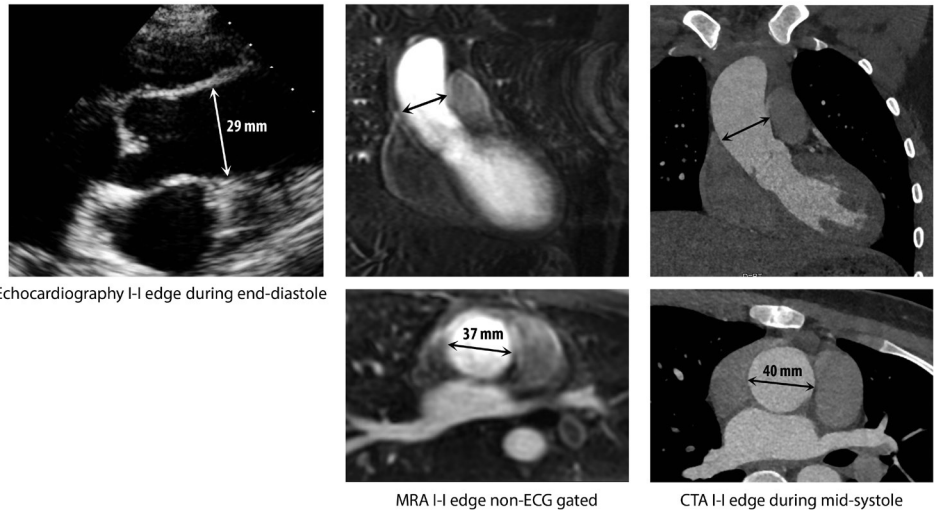

Supplemental figure 4. Maximum differences in the diameter of the ascending aorta (1cm above the STJ) in one patient (difference 11mm)

Aortic diameter measured with CTA during mid-systole was 40mm and measured with MRA 37mm. The aortic diameter measured with echocardiography during end-diastole and with the inner edge-to-inner edge method was 29mm.

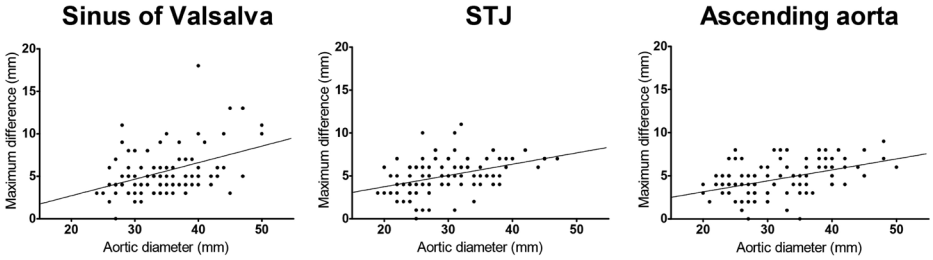

Supplemental figure 5. Scatter plot of maximum differences (found between the seven different measurements) and the absolute diameter measured with end-diastolic diameter of CTA

The regression line is plotted for the three different levels: sinus of Valsalva, the sinotubular junction and the ascending aorta.

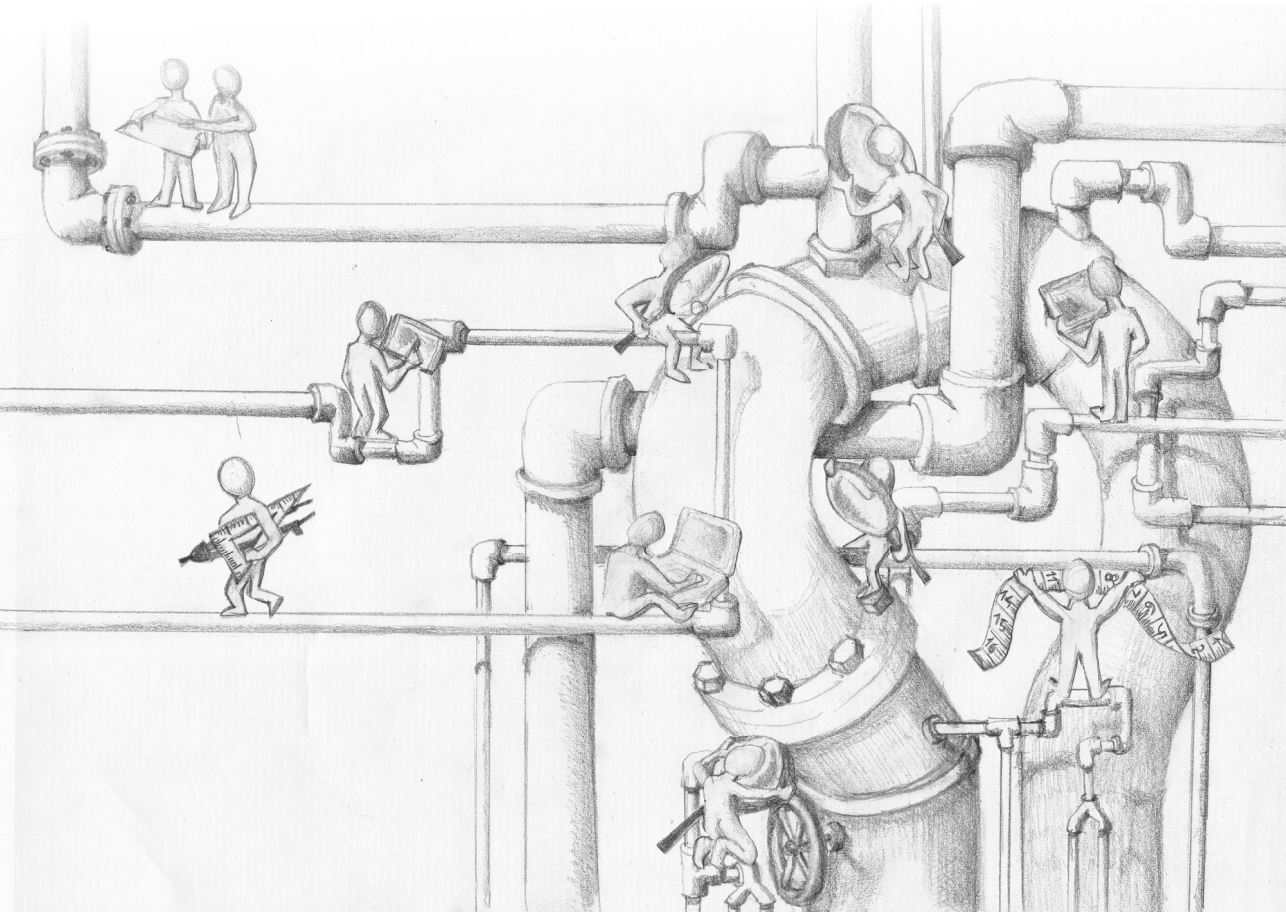

CHAPTER 5

Quantification of aortic annulus in computed tomography angiography: validation of a fully automatic methodology

Xinpei Gao, Sara Boccalini, Pieter H. Kitslaar, Ricardo P.J. Budde, Mohamed Attrach, Shengxian Tu, Michiel A. de Graaf, Tomas Ondrus, Martin Penicka, Arthur J.H.A. Scholte, Boudewijn P.F. Lelieveldt, Jouke Dijkstra, Johan H.C. Reiber

Eur J Radiol. 2017 Aug;93:1-8

Abstract

Background: Automatic accurate measuring of the aortic annulus and determination of the optimal angulation of X-ray projection are important for the trans-catheter aortic valve replacement (TAVR) procedure. The objective of this study was to present a novel fully automatic methodology for the quantification of the aortic annulus in computed tomography angiography (CTA) images.

Methods: CTA datasets of 26 patients were analyzed retrospectively with the proposed methodology, which consists of a knowledge-based segmentation of the aortic root and detection of the orientation and size of the aortic annulus. The accuracy of the methodology was determined by comparing the automatically derived results with the reference standard obtained by semi-automatic delineation of the aortic root and manual definition of the annulus plane.

Results: The difference between the automatic annulus diameter and the reference standard by observer 1 was 0.2 ± 1.0 mm, with an inter-observer variability of 1.2 ± 0.6 mm. The Pearson correlation coefficient for the diameter was good (0.92 for observer 1). For the first time, a fully automatic tool to assess the optimal projection curves was presented andvalidated. The mean difference between the optimal projection curves calculated based on the automatically defined annulus plane and the reference standard was 6.4º in the cranial/caudal (CRA/CAU) direction. The mean computation time was short with around 60 seconds per dataset.

Conclusion: The new fully automatic and fast methodology described in this manuscript not only provided precise measurements about the aortic annulus size with results comparable to experienced observers, but also predicted optimal X-ray projection curves from CTA images.

Introduction

During the trans-catheter aortic valve replacement (TAVR) procedure, the aortic root is not directly visible for physicians, thus pre-operative imaging is necessary to determine the size and orientation of the aortic annulus. These measurements are essential to select and deliver the appropriate prosthesis in the aortic valve. Bias in the selection and placement of the prosthesis, may result in complications e.g. aortic annulus rupture, prosthesis shift or paravalvular regurgitation.

As a noninvasive, high-resolution 3D imaging modality, multi-detector computed tomography (MDCT) enables the accurate imaging of the anatomical structures of the aortic root [1]. The orientation or the aortic root can be determined manually from the CTA dataset in order to predict the optimal X-ray projection angle during prosthesis implantation in the Cath lab. An optimal X-ray projection curve with multiple available angles can be useful for physicians to choose their familiar angles [2]. This reduces procedure time, the amount of contrast material used and radiation dose. However, in order to avoid the potential reproducibility issues of a manual measurement and to achieve faster reporting time, a fully automatic aortic root measurement methodology based on CTA images would be promising.

In this paper, we presented a novel fully automatic methodology which is able to size the aortic annulus, and predict the optimal projection curve based on CTA image. The results were validated in datasets from two clinical centers to investigate its accuracy and robustness.

Material and Methods

Study population and CT protocol

26 patients from two hospitals were candidates for TAVR and underwent an ECG-gated CTA scan as the routine clinical investigation. The patients' identifiable information was completely anonymized before this study started. Table 1 describes the scan protocols for the CTA scans used in this study. Diastolic phases from the reconstructed images were used.

Table 1. CTA protocols of the two clinical centers

	Hospital A	Hospital B
Number of patients	19	7
CT scanner	320-row detector	128 x2 detector
	Single source	Dual source
	Aquilion ONE	Somatom Definition Flash
	Toshiba Medical System, Otawara, Japan	Siemens Healthcare, Forchheim, Germany
Acquisition	R-R full dose, in most cases no ECG modulation.	Prospective ECG-gating
Scan parameter‡	100, 120kV or 135kV, 400-580mA	100,120kV, 350–400mA
Injection protocol	Bi-phasic injection	Bi-phasic injection
	Intravenous in ante-cubital vein	Intravenous in ante-cubital vein
	70ml contrast (5ml/sec) and 50ml saline (5ml/sec)	90ml contrast (4ml/sec) and 100ml saline (4ml/sec)
Reconstruction parameters	Slice thickness 0.5mm, interval 0.25mm	Slice thickness 0.75mm, 0.4mm increment

‡ Tube voltage and current were adapted for each patient on the basis of body mass index (BMI) and thoracic anatomy.

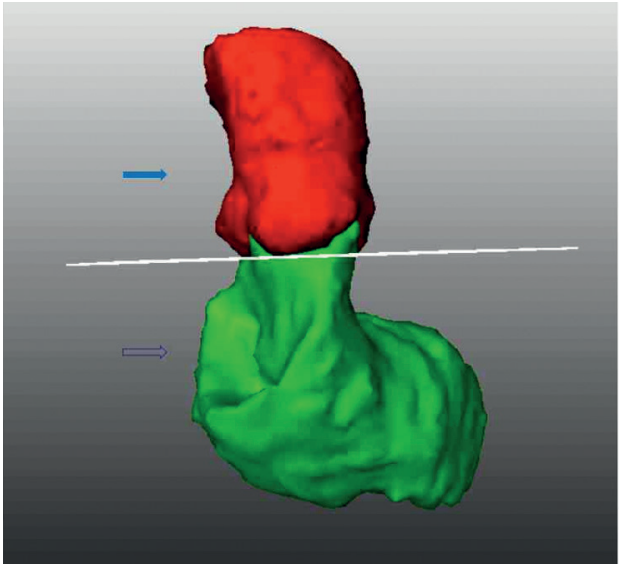

Figure 1

Annular plane detection: the red top part represents the segmentations of the aortic root(solid arrow) and green low part LVOT(hollow arrow), the white plane corresponds to the plane of the aortic annulus.

Fully automatic aortic annulus detection framework

In a previously published study [3], we described a fully automatic segmentation method for pre-TAVR whole-body CTA datasets with a high mean dice similarity coefficient (0.965 ± 0.024) between the contours of the automatic methodology and the ground truth. In this study, an adapted framework based on the previous method was used for segmentation of the aortic root in the cardiac CTA images.

The procedure for automatic annulus detection works as follows: first, the data sets were resampled and the heart region was masked out automatically by a deformable subdivision surface fitting algorithm [3]. Then, the three-dimensional contours of the aortic root and left ventricle outflow tract (LVOT) were detected with an atlas-based segmentation algorithm. Eight cardiac CTA images with manual annotations were used as the atlas images. Each patient's image was registered to the atlas images by an affine registration algorithm. The most similar atlas image was selected based on the similarity measure (Mutual information) between the atlas image and the patient image for a subsequent B-Spline deformation registration algorithm [4]. After registration, the manual segmentation of the selected atlas image was deformed by the transformation parameters from previous steps, therewith the patient's image was initially segmented. Finally, we refined the segmentation by a deformable subdivision surface model fitting method based on gradient information [5].

The automatic extraction of the aortic annulus is based on the anatomy of the aortic root. The aortic root is a complex 3-dimensional structure that starts at the left ventricle outflow tract (LVOT). It consists of the sinotubular junction, aortic sinuses of Valsalva, valve leaflets, and aortic annulus [6]. The aortic annulus plane is a virtual plane defined at the lowest point of the aortic leaflets beyond the LVOT. It can also be called 'basal ring' [7]. The prosthesis is settled on the location of the aortic annulus during the TAVR procedure.

After the extraction of the aortic root and the LVOT by the atlas-based segmentation, we calculated the connecting region between the aortic root and the LVOT. By applying the principal component analysis (PCA) algorithm [8], the orientation of the connecting region between the aortic root and the LVOT can be found, which defines the orientation of the annulus plane.

Prediction of optimal projection curve for X-ray

The identification of X-ray projections orthogonal to the aortic annular plane is important for the correct valve deployment during the TAVR procedure. With the orientation of the aortic annulus plane computed in the previous step, an infinite number of projections can be calculated which allows the 3 hinge points of the valves to appear on the same line in the X-ray projection view [9]. An optimal projection curve with left/right anterior oblique

(LAO/RAO) angles as the x-axis, and cranial/caudal (CRA/CAU) angles as the y-axis, was calculated. Following the diagram style employed in the study by Binder et al [10], LAO/RAO angles ranging from 45° RAO to 45° LAO were represented with 5° steps. Based on these LAO/RAO angles, each patient's CRA/CAU angles were computed (Figure 2).

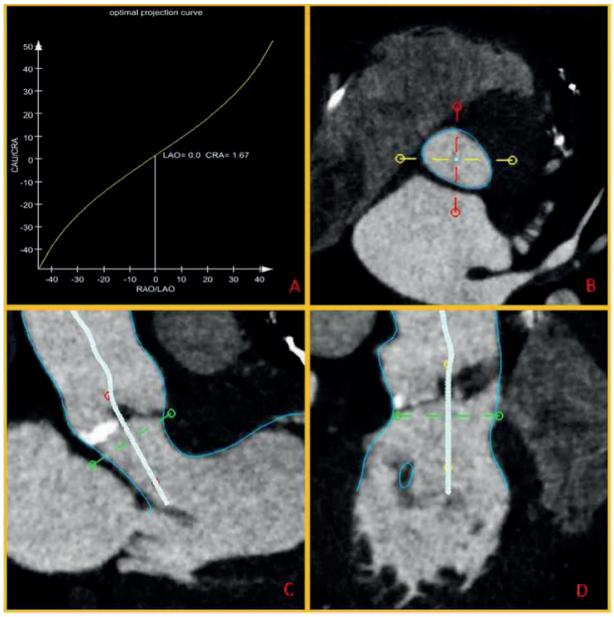

Figure 2

The optimal projection curve and related images: A - the optimal projection curve; B – multi-planar image of the annulus plane; C – oblique image corresponding to the optimal X-ray projection D – oblique image perpendicular to image B & C.

Evaluation of aortic annulus detection

The automatic methodology was integrated into a dedicated in-house tool (AortaValveViewer 1.2, LKEB, Leiden, Netherlands), with functions for manual interactions. The tool was implemented in the MeVisLab environment (version 2.7.1, MeVis Medical Solutions AG, Bremen, Germany) with C++ and Python code.

Two observers performed the measurements for the evaluation of the performance of our automatic methodology (observer 1: a radiologist with 5-year experience in cardiovascular imaging and about 90 - 100 annulus diameters assessments; observer 2: a radiologist with 4-year experience and about 140 -150 pre-TAVI cases). The two observers used the in-house tool independently to create a reference standard for statistical analysis. The observer adjusted double oblique multiplanar reconstruction (MPR) images manually to find the plane in which the three aortic valve hinge points appear in the same slice. Three landmarks were annotated manually on the hinge points, which defined the

annulus plane. Then the observer corrected the automatically segmented surface from the sinotubular junction to the LVOT (5mm under the aortic annulus) by drawing contours in cross-sectional and oblique view images (Figure 2 B, C & D).

The annular cross-sectional contour was extracted from the aortic root segmentation where it intersected with the annulus plane. The size of the aortic annulus was measured using the area, radius, diameter, long-axis diameter (LAD), short-axis diameter (SAD), and perimeter. The radius (R) of the aortic annulus was calculated based on the area (A): $R = \sqrt{(A/\pi)}$; the diameter was obtained based on the radius (D): $D = 2R$ [1].

The center of the annulus was defined as the center of its contour and automatically calculated. Next, the angle between automatic and manual plane orientations, the 3D Euclidean distance between the centers of the annulus contours obtained from the automatic and manual planes were measured [11]. In addition, the optimal X-ray projection curve was calculated for each patient from the automatic and manual plane orientations by observer 1. The mean optimal X-ray projection curve of all the patients was obtained. Automatic and manual curves were compared with each other in the CRA/CAU axis.

A four points scale quality score (4 = perfect, 3 = good, 2 = reasonable, 1 = poor) based on motion artifacts and contrast in the aortic root was used to evaluate the image quality by observer 1. The extent of the calcification in the aortic root at the level of the annulus or immediately nearby (caudal part of the cusps and cranial LVOT) was graded into 4 levels: 1 = none, 2 = light, 3 = medium, 4 = heavy.

Evaluation of prosthesis size selection

The sizes of the prosthesis which had been implanted during the TAVR procedure into the patients from hospital A were retrieved. The selection of the prosthesis performed in clinical practice was retrospectively compared with a theoretical choice of the valve based on the automatic and semi-automatic annulus measurements of our tool. The annulus area measurements of the in-house tool were categorized based on the commercially available valve sizes: 23, 26, 29 mm for the Edwards SAPIEN XT valves and 23, 26, 29, 31 mm for the CoreValve [12, 13]. Prosthesis selection based on area measurements is summarized in Table 5 and 6 [12, 13]. If the measurement fell into the gray zone, both prostheses with smaller or bigger size were considered as suitable.

Statistical analysis

In this study, SPSS (version 20.0, SPSS Inc., Chicago, IL) and MedCalc (version 15.6, Ostend, Belgium) were used for the statistical analyses. Normally distributed continuous variables were analyzed by the mean, standard deviation, and the Pearson correlation coefficient. The normality was evaluated by the Shapiro-Wilk test [14]. Bland-Altman plots were drawn to visualize the bias. P value < 0.05 indicated significant result.

Results

This study population consists of 26 patients, and the baseline characteristics are described in Table 2. The patients differ in age, gender, as well as the presence of previous percutaneous coronary intervention (PCI), previous coronary artery bypass grafting (CABG) and previous myocardial infarction (MI), in other words, a population with pathological diversity.

Table 2. Baseline characteristics of the patients included in the study

Patient number	Total (26)
Age (years)	79 ± 13
Gender (% male)	15 (58%)
Diabetes	4 (15%)
Hypertension	17 (65%)
Hypercholesterolemia	16 (62%)
Family history of CAD	3 (12%)
Smoking	2 (8%)
Obesity	5 (19%)
Previous PCI	13 (50%)
Previous CABG	12 (46%)
Previous MI	5 (19%)

In the data, age is described by mean ± SD, other items are outlined by percentages of the population.

Image quality score and calcification level

The average image quality score was 2.4. The percentage of scans with poor image quality was 15%, reasonable 42%, good 31%, and perfect 12%. The average score of images from hospital A was 2.6, the mean score of hospital B was 1.9. Only 1 patient had no calcification (4%). The amount of calcification in the remaining patients was light in 12 cases (46%), medium in 10 cases (39%) and heavy in 3 patients (12%). The mean calcification amount of all the patients was light to medium (2.6) with a lower average value for patients scanned at hospital A (2.4) compared to hospital B (3.1).

Accuracy of the orientation of the aortic annulus

The difference between the annulus plane orientations was 9.4 ± 4.6 degrees for observer 1, and 7.6 ± 3.7 degrees for observer 2, with 4.2 ± 3.3 degrees for the inter-observer variability. The mean and standard deviation of the distance between the automatic and manual annulus center locations was found to be 1.7 ± 1.0 mm for observer 1, 1.6 ± 1.0 mm for observer 2, and the inter-observer variability was 1.2 ± 0.7 mm. The individual errors are presented in Figure 3, where the patients are represented by numbers. For patients 13 and 19 with an associated error higher than 15 mm, the image quality was

poor. For patients 10 and 26, who presented an error for the location of the center higher than 3mm, the image quality was reasonable.

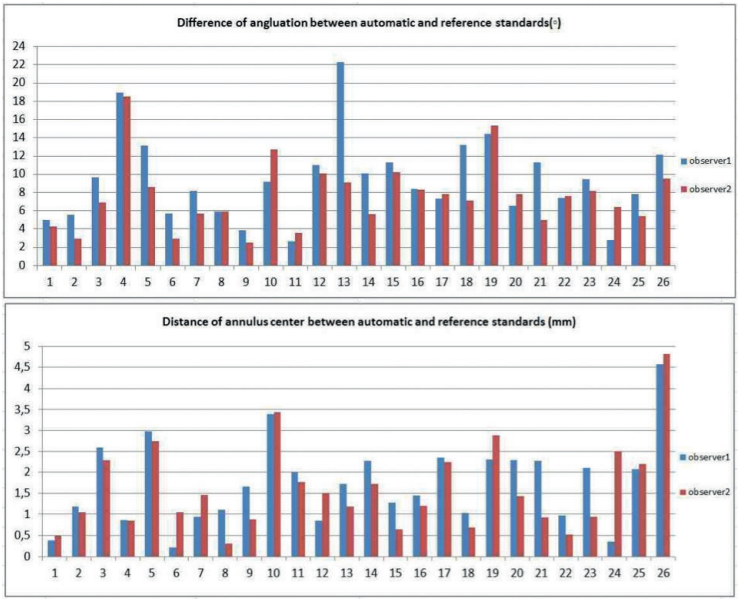

Figure 3

The difference in the degree of the aortic annulus orientation between automatic and the observers.

For the patients from hospital A, the average error of the plane orientation was 9.0 degrees for observer 1 and 7.2 degrees for observer 2; for patients from hospital B, the mean error of the orientation was 10.4 degrees for observer 1 and 8.2 degrees for observer 2.

Assessment of the optimal projection curve

In Figure 4, the mean optimal projection curves of the patients from the automatic methodology and observer 1 are presented together with their standard deviations. The mean difference in CAU/CRA for all the patients was 6.4 degree. The standard deviations of the two curves were similar to each other, representing the range of the CAU/CRA angle in all the patients.

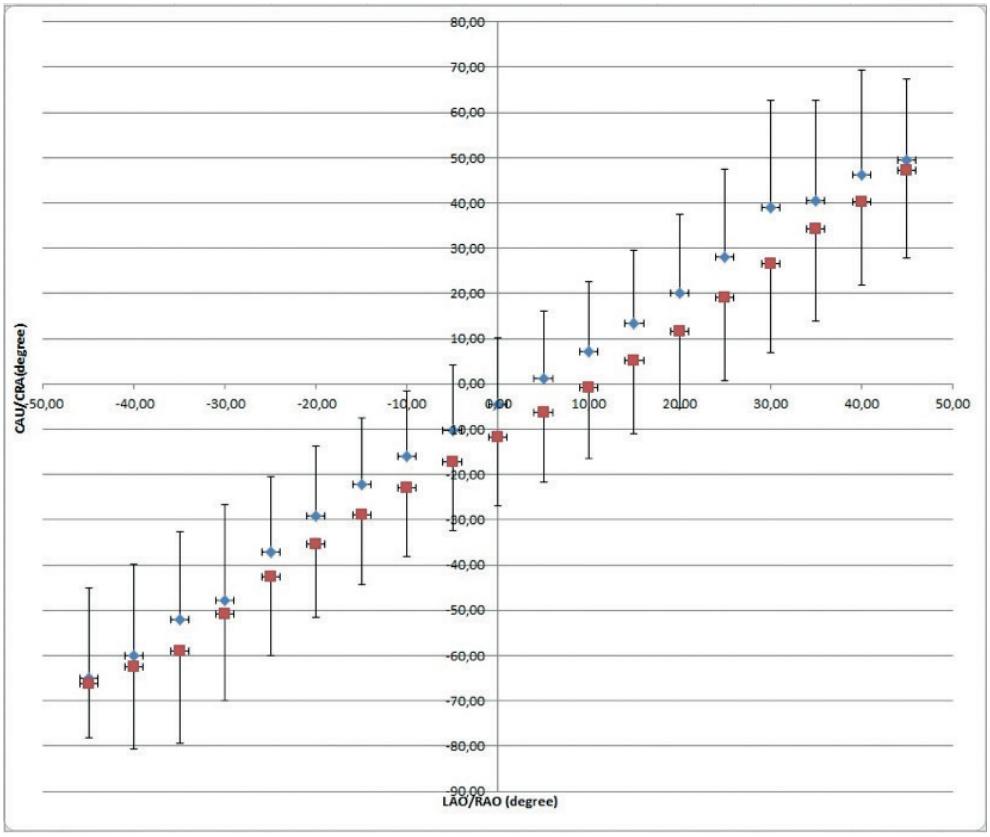

Figure 4

Optimal projection curve: the mean optimal projection curve of the CAU/CRA angulation of automatic measurement (blue) and observer's measurement (red). The horizontal bars above the blue dots show the SDs of automatically extracted CAU/CRA of all the patients. The bars beneath the red dots represent the SDs of the observer's measurement.

Evaluation of the size of the aortic annulus

Area, radius, diameter, LAD, SAD, and perimeter were calculated for the evaluation of the aortic annulus size measurement. Table 3 shows the mean, standard deviation and 95% CI of these parameters of the automatic measurement and the two observers. Table 4 shows the Pearson correlation coefficient and mean difference of the parameters between the automatic measurement and the reference standards. Figure 5 shows the Bland-Altman plots for all the annulus size measurements (automatic VS observer 1).

Table 3. Results of the detection of aortic annulus size from automatic measurement and reference standard

Aortic annulus		Automatic measurement			Observer 1			Observer 2		
	Unit	**mean**	**SD**	**95% CI**	**mean**	**SD**	**95% CI**	**mean**	**SD**	**95% CI**
Area	cm2	4.8	1.0	4.4 to 5.2	4.7	1.0	4.3 to 5.1	5.1	1.0	4.7 to 5.6
Radius	mm	12.3	1.3	11.7 to 12.8	12.1	1.3	11.6 to 12.7	12.8	1.3	12.2 to 13.2
Diameter	mm	24.5	2.6	23.5 to 25.6	24.3	2.6	23.2 to 25.3	25.5	2.6	24.4 to 26.5
Long-axis diameter	mm	30.5	4.4	28.8 to 32.3	29.9	3.5	28.5 to 31.3	31.1	3.3	29.8 to 32.5
Short-axis diameter	mm	21.4	2.6	20.4 to 22.4	21.1	2.5	20.1 to 22.1	22.2	2.5	21.2 to 23.1
perimeter	mm	80.3	9.5	76.4 to 84.1	78.5	8.2	75.2 to 81.8	82.1	8.0	78.9 to 85.3

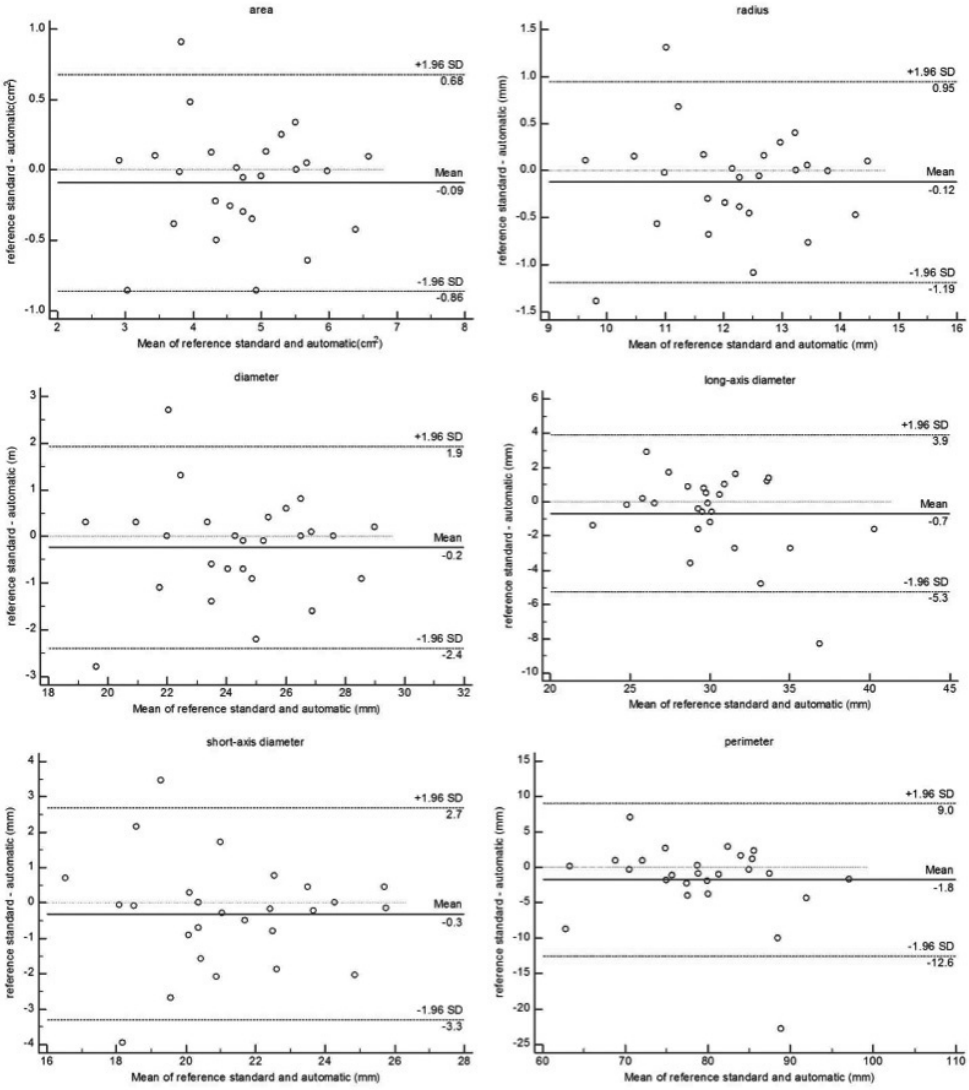

Figure 5

Bland-Altman plots of aortic annulus parameters

Evaluation of prosthesis size selection

Based on our fully-automatic measurement, in 78.9% (15 out of 19) of cases the choice of the prosthesis size would have been the same as in clinical practice. When observer 1 applied corrections to the fully-automatic measurement, the agreement rate increased to 89.5% (17 out of 19).

Computation time of the method

Our automatic methodology takes around 60 seconds to detect the contour of the aortic root and measure the aortic annulus in one dataset on a workstation. Observers needed on average 12 minutes to generate the reference standard.

Discussion

In recent years, many studies have been published on aortic annulus size quantification based on CTA images, for the evaluation and validation of both semi-automatic [15-18] and fully-automatic [12, 19-21] tools. Fully automatic tools require less user interaction for the physicians. In our study, the main goal was to evaluate our tool for fully automatic annulus size quantification. Ionasec et al.[19] developed a system for patient-specific modeling and quantification of the left heart valves. In their study the precision of the annular circumference was 8.46 ± 3.0 mm. Elattar et al. [20] introduced an automated detection method which enabled automated sizing based on Normalized cut, and Gaussian curvature map.The automatically generated aortic annulus radius average difference was 0.2 ± 0.7 mm with observer 1, and 0.4 ± 0.8 mm with observer 2. Lou et al. [12] evaluated the results of fully automatic aortic annulus sizing from a commercial tool, and reported an area measurement calculated by observer 1 with the automated method without manual correction of 5.4 ± 0.96 cm^2, and of 4.8 ± 0.87 cm^2 with manual correction; with the same methods, observer 2 obtained area values of 5.4 ± 0.95 cm^2 versus 5.0 ± 0.91 cm^2. Wachter et al. [21] used a model-based algorithm to detect the aortic valve anatomy, obtaining errors for the short and long diameters of the annulus of 0.8 and 1.0 mm, respectively. Our framework can detect the aortic root in all the patients, the correlation of the diameter was good, and the errors of the aortic annulus size parameters were smaller than in previous studies [12, 19-21] and comparable to the human observer difference (Table 4).

Just a few studies about optimal X-ray projection curve prediction were published [22, 23]. In Faquir et al.'s study [22], the optimal projection curves of the automated software were calculated based on the aortogram, not on CTA images. In Samim et al.'s study [23], the calculation was based on CTA images, however, the prediction of optimal projection curves was not performed fully automatically. The novelty of the present study consists in the fact that for the first time a fully automatic tool is presented which can perform the optimal projection curve prediction on CTA images.

Table 4. Results of aortic annulus size measurement comparing the automatic measurement to reference standard

Aortic annulus		Automatic vs Observer 1		Automatic vs Observer 2		Observer 1 vs Observer 2	
	Unit	Correlation	Difference	Correlation	Difference	Correlation	Difference
Area	cm2	0.92	0.1 ± 0.4	0.89	0.4 ± 0.5	0.97	0.5 ± 0.2
Radius	mm	0.91	0.1 ± 0.5	0.88	0.5 ± 0.6	0.97	0.6 ± 0.3
Diameter	mm	0.91	0.2 ± 1.0	0.88	1.0 ± 1.2	0.97	1.2 ± 0.6
Long-axis diameter	mm	0.85	0.7 ± 2.3	0.78	0.6 ± 2.8	0.94	1.2 ± 1.2
Short-axis diameter	mm	0.82	0.3 ± 1.5	0.78	0.8 ± 1.7	0.96	1.0 ± 0.7
Perimeter	mm	0.82	1.8 ± 5.5	0.81	1.8 ± 5.5	0.97	3.6 ± 2.0

In the study by Lou et al. [12], the influence of the measurement on the prosthesis size selection was also evaluated. For the first observer, the fully automated and the manual measurements agreed on the prosthesis selection in 51.8% of the patients, while the agreement of the semi-automated and the manual measurements was 87.6%. For the second observer, the fully-automated and the manual measurement agreed in 52.8% of the cases, while the agreement of the semi-automated and the manual measurement was 82.4%. In our study, the agreement rate between our fully automatic measurement and clinical practice was 78.9%, and between our semi-automatic measurement and clinical practice 89.5%.

Due to the broader employment of the TAVR procedure and the subsequent increase in the number of pre-procedural CT scans, the images processing time is becoming crucial. According to Elattar et al.'s description [24], their automatic contour detection of the aortic root took 90 seconds without the detection of the aortic annulus and the calculation of the clinical parameters in the aortic root. In our study, the average computation time including aortic root segmentation, automatic detection, and calculation of the clinical parameters of the aortic annulus was shorter (around 60 seconds) and can be further improved,.

Only diastolic images were used in this study. There have been studies which investigated the impact of using diastolic and systolic images on prosthesis sizing [25-27]. Bertaso et al.[25] measured the difference of aortic annulus size between diastole and systole, and found that the difference was not significant enough to change prosthesis size selection; while in de Heer et al.'s study [26], the opposite conclusion was reached. In Blanke et al.'s study [27], the annulus was measured throughout the full cardiac cycle, and it turned out that the phase in which the annulus has the biggest size would be the most suitable phase for prosthesis selection. However, this ideal phase can be diastolic or systolic depending on the patient. The method presented in this study can be used for automatic annulus measurement in patients whose ideal phase is in diastole.

In our study, two kinds of CT scanners (Aquilion ONE scanner and Somatom Definition Flash scanner) with different acquisition protocols were used from two hospitals. The patients who were scanned in hospital A had a higher image quality and a lower amount of calcium. Image quality had an impact on our automatic tool. The angulation results were better in the patients from hospital A, where an Aquilion ONE scanner was used. However, the 3 patients with the heavy calcifications didn't show higher error, which indicates that our framework is not influenced by calcification.

The current study has a number of limitations. Firstly, given the limited number of data sets, the robustness of the method cannot be adequately assessed. We plan to investigate

this in a more extensive study with more data. Secondly, the automatic measurement of the sinotubular junction, sinus of Valsalva and LVOT have been developed in our methodology, but not validated in this study. Finally, the optimal projection curve hasn't been compared with the actual projection during the TAVR procedure in the Cath lab.

Table 5. Selection table for Edwards SAPIEN XT valve

Edwards SAPIEN Valve (mm)	23	gray zone	26	gray zone	29
Area (mm2)	300 - 380	380 - 415	415 - 490	490 - 530	530 - 620

Table 6. Selection table for CoreValve

CoreValve (mm)	23	26	29	31
Area (mm2)	254.5 - 314.2	314.2 – 415.5	415.5 – 572.6	530.9 – 660.5

Conclusion

Our newly developed methodology of automatic aortic annulus quantification on CTA images has been demonstrated to be accurate compared to the semi-automatic results. A fully automatic optimal X-ray projection curve prediction algorithm based on CT image was described. Our methodology provides physicians with detailed information about the size and orientation of the aortic annulus, which can help with the prosthesis selection in the pre-operative planning of TAVR.

References

1. Achenbach, S., et al., SCCT observer consensus document on computed tomography imaging before transcatheter aortic valve implantation (TAVI)/transcatheter aortic valve replacement (TAVR). J Cardiovasc Comput Tomogr, 2012. 6(6): p. 366-80.
2. Gurvitch, R., et al., Multislice computed tomography for prediction of optimal angiographic deployment projections during transcatheter aortic valve implantation. JACC Cardiovasc Interv, 2010. 3(11): p. 1157-65.
3. Gao, X., et al. Automatic aortic root segmentation in CTA whole-body dataset. 2016.
4. Klein, S., et al., elastix: a toolbox for intensity-based medical image registration. IEEE Trans Med Imaging, 2010. 29(1): p. 196-205.
5. Kitslaar, P.H., et al. Segmentation of branching vascular structures using adaptive subdivision surface fitting. 2015.
6. Underwood, M.J., et al., The aortic root: structure, function, and surgical reconstruction. Heart, 2000. 83(4): p. 376-80.
7. Schoenhagen, P., et al., Computed tomography in the evaluation for transcatheter aortic valve implantation (TAVI). Cardiovasc Diagn Ther, 2011. 1(1): p. 44-56.
8. Shlens, J., A tutorial on principal component analysis. arXiv preprint arXiv:1404.1100, 2014.
9. Kurra, V., et al., Pre-procedural imaging of aortic root orientation and dimensions. JACC: Cardiovascular Interventions, 2010. 3(1): p. 105-113.
10. Binder, R.K., et al., Prediction of Optimal Deployment Projection for Transcatheter Aortic Valve Replacement. Circulation: Cardiovascular Interventions, 2012. 5(2): p. 247-252.
11. Deza, M.M. and E. Deza, Encyclopedia of distances, in Encyclopedia of Distances. 2009, Springer. p. 1-583.
12. Lou, J., et al., Manual, semiautomated, and fully automated measurement of the aortic annulus for planning of transcatheter aortic valve replacement (TAVR/TAVI): analysis of interchangeability. Journal of cardiovascular computed tomography, 2015. 9(1): p. 42-49.
13. Kasel, A.M., et al., Standardized Imaging for Aortic Annular Sizing. Implications for Transcatheter Valve Selection, 2013. 6(2): p. 249-262.
14. Shapiro, S.S. and M.B. Wilk, An analysis of variance test for normality (complete samples). Biometrika, 1965. 52(3-4): p. 591-611.
15. Delgado, V., et al., Automated assessment of the aortic root dimensions with multidetector row computed tomography. The Annals of thoracic surgery, 2011. 91(3): p. 716-723.
16. Watanabe, Y., et al., Automated 3-dimensional aortic annular assessment by multidetector computed tomography in transcatheter aortic valve implantation. JACC: Cardiovascular Interventions, 2013. 6(9): p. 955-964.
17. Stortecky, S., et al., Accuracy and reproducibility of aortic annulus sizing using a dedicated three-dimensional computed tomography reconstruction tool in patients evaluated for transcatheter aortic valve replacement. EuroIntervention, 2014. 10(3): p. 339-346.

18. Foldyna, B., et al., CT evaluation prior to transapical aortic valve replacement: semi-automatic versus manual image segmentation. The international journal of cardiovascular imaging, 2015. 31(6): p. 1233-1242.
19. Ionasec, R.I., et al., Patient-specific modeling and quantification of the aortic and mitral valves from 4-D cardiac CT and TEE. IEEE transactions on medical imaging, 2010. 29(9): p. 1636-1651.
20. Elattar, M., et al., Automatic aortic root landmark detection in CTA images for preprocedural planning of transcatheter aortic valve implantation. The international journal of cardiovascular imaging, 2016. 32(3): p. 501-511.
21. Wächter, I., et al. Patient specific models for planning and guidance of minimally invasive aortic valve implantation. in International Conference on Medical Image Computing and Computer-Assisted Intervention. 2010. Springer.
22. El Faquir, N., et al., Definition of the aortic valve plane by means of a novel dedicated software program: Proof of concept and validation with multi slice computed tomography. International Journal of Diagnostic Imaging, 2016. 3(1): p. p63.
23. Samim, M., et al., Automated 3D analysis of pre-procedural MDCT to predict annulus plane angulation and C-arm positioning: benefit on procedural outcome in patients referred for TAVR. JACC: Cardiovascular Imaging, 2013. 6(2): p. 238-248.
24. Elattar, M.A., et al., Automatic segmentation of the aortic root in CT angiography of candidate patients for transcatheter aortic valve implantation. Medical & biological engineering & computing, 2014. 52(7): p. 611-618.
25. Bertaso, A.G., et al., Aortic annulus dimension assessment by computed tomography for transcatheter aortic valve implantation: differences between systole and diastole. The international journal of cardiovascular imaging, 2012. 28(8): p. 2091-2098.
26. de Heer, L.M., et al., Aortic root dimension changes during systole and diastole: evaluation with ECG-gated multidetector row computed tomography. The international journal of cardiovascular imaging, 2011. 27(8): p. 1195-1204.
27. Blanke, P., et al., Conformational pulsatile changes of the aortic annulus: impact on prosthesis sizing by computed tomography for transcatheter aortic valve replacement. JACC: Cardiovascular Interventions, 2012. 5(9): p. 984-994.

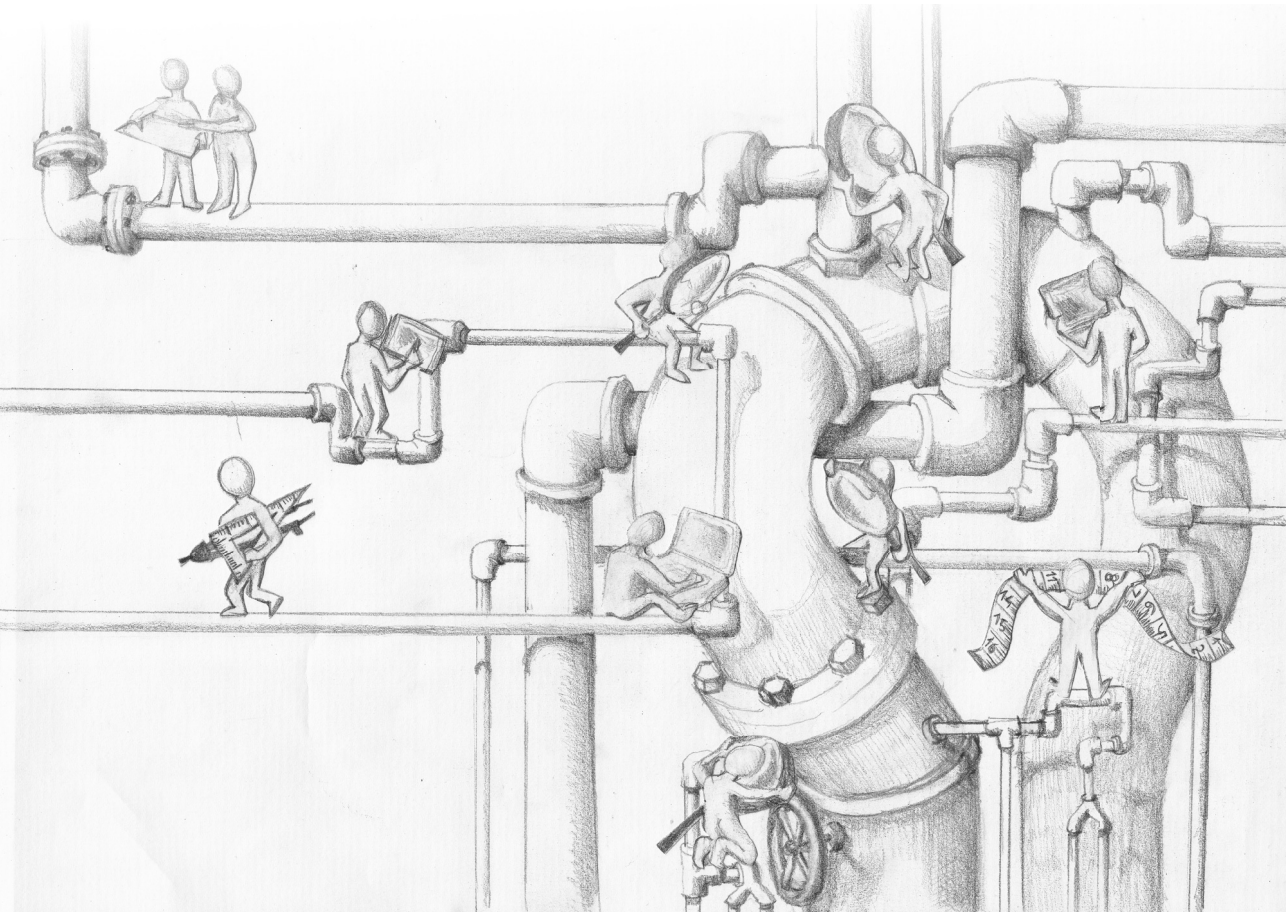

CHAPTER 6

Bicuspid aortic valve annulus: standardized method to define the annular plane and assessment of geometry changes during the cardiac cycle. Implications for TAVI planning

Sara Boccalini, Lidia R. Bons, Allard T. van den Hoven, Annemien E. van den Bosch, Gabriel P. Krestin MD, Jolien Roos-Hesselink, Ricardo P.J. Budde

Submitted

Abstract

Background: Transcatheter aortic valve implantation (TAVI) is increasingly practised also in bicuspid aortic valve (BAV) patients. Determining the BAV annular plane is more challenging than for tricuspid aortic valves (TAV). Furthermore, it is unknown if the BAV annulus has a physiology similar to TAV. Our aim was to present a standardized methodology to determine BAV annulus and investigate its changes in shape and dimensions during the cardiac cycle.

Methods: BAV patients were prospectively included and underwent an ECG-gated cardiac CTA. The annulus plane was manually identified on reconstructions at 5% intervals of the cardiac cycle with a new standardized method for different BAV types. Based on semi-automatically defined contours, maximum and minimum diameter, area, area-derived diameter, perimeter, asymmetry ratio and relative area were calculated. Differences of dynamic annular parameters were assessed also per BAV type.

Results: Of the 55 patients included (age: 38.4±13.3 years; 58% males) 38 had BAV Sievers type 1, 10 type 0 and 7 type 2. The minimum diameter, perimeter, area and area-derived diameter were significantly higher in systole than in diastole with a relative change of 13.7%, 4.8%, 13.7% and 7.2% respectively (all $p<0.001$). The AR was ≥1.1 in all phases, indicating an elliptic shape, with more pronounced flattening in diastole ($p<0.001$). Different BAV types showed comparable dynamic changes.

Conclusions: The aortic annulus of BAV patients undergoes significant changes in shape during the cardiac cycle with a wider area in systole and a more elliptic conformation in diastole. Therefore, it is recommended that pre-TAVI measurements be performed in early systole.

Aknowledgments: we thank Sara Baart, Msc, for her support in statistical analysis

Introduction

With an estimated incidence of 0.9-2% in the general population, bicuspid aortic valve (BAV) is the most common congenital cardiac anomaly [1]. BAV are prone to precocious stenosis and regurgitation, often requiring an intervention early in life [2]. Transcatheter aortic valve insertion (TAVI) is an established alternative to traditional open surgery for stenotic tricuspid aortic valves (TAV). BAV has been regarded as an absolute contra-indication for TAVI due to concerns related to the morphological anomalies of the aortic valve [3]. Yet, in the last few years the procedure has been performed with an increasing frequency in BAV patients demonstrating the feasibility and safety of the technique in this population [4] with short term results comparable to those obtained in patients with TAV [5].

Precise pre-procedural assessment of the annulus and aortic root dimensions and anatomy are fundamental to avoid under- or over-estimation of the valve size and subsequent complications after TAVI [6]. The broad variability in cusp morphology of BAV results in the cumbersome and, more importantly, sometimes impossible identification of the annulus plane as defined based on the standard anatomy of TAV. Therefore, a specific method for the definition of the annulus plane in BAV patients is lacking.

The annulus has been shown to have an elliptical shape that undergoes conformational changes during the cardiac cycle in normal as well as stenotic TAV using ECG-gated CT imaging [7, 8]. Furthermore, most sizing parameters for the TAV aortic annulus show significant changes between diastole and systole [9]. If, and to what extent, such dynamic geometry changes also occur in the BAV annulus is unknown, but of paramount importance to establish the cardiac phase in which to perform the pre-procedural measurements and one of the prerequisites for increased use of TAVI in BAV. Furthermore, these measurements require a standardized and reproducible method to determine the BAV annulus plane.

We describe a method to determine the BAV annulus plane and assessed the presence and magnitude of geometrical and dimensional changes of the annulus during the cardiac cycle using ECG-gated CT as well as investigated if different BAV subtypes present different patterns.

Materials and Methods

Study population and BAV classification

Sixty consecutive patients with a BAV were prospectively included as part of a clinical study at Erasmus Medical Centre between November 2014 and March 2016 [10]. The local medical ethics committee approved the study and all patients provided written informed consent. As part of the study an ECG-gated contrast enhanced CT of the heart was performed.

The morphology of the aortic valve was classified as previously described by Sievers et al. [1] based on images obtained with echo, CT and MR.

CT scans

Contrast enhanced CT scans were acquired with a third generation dual-source CT scanner (Somatom Force, Siemens, Forchheim, Germany). All scans were performed with retrospective ECG-gating, 192x0.6mm collimation and 250ms rotation time. Reconstructions of 1.5mm thickness were performed throughout the entire cardiac cycle at 5% intervals resulting in 20 image datasets per patient. The heart rate of the patient during the scan was recorded.

Annulus analysis

A radiologist with >5 years of experience in cardiovascular radiology defined the annulus plane and semi-automatically measured the annulus dimensions on the CT scans for each of the 20 reconstructed phases.

Annulus plane definition

Images were exported to a commercially available workstation (IntelliSpace Portal, Philips, Best, The Netherlands) to allow for manual multiplanar reconstructions (MPR). The annulus plane was identified with a different methodology depending on the morphology of the bicuspid valve. In bicuspid valves with three equally/similarly sized cusps (Sievers type 1 and 2) the annulus plane was identified as the plane passing through the three hinge points (defined as the lowest insertion point of the valve leaflet on the aortic wall) as indicated by guidelines for TAV [11]. In case the fused cusps had different dimensions (Sievers type 1) or there were only two cusps (Sievers type 0) the annulus plane was identified with a newly developed approach consisting of multiple steps based on a combination of previously published definitions of the annulus: first, one of the planes passing through the hinge point of the non-fused cusp and the hinge point of the bigger one of the two fused cusps (or through the two hinge points in valves type 0) was identified; then, this plane was tilted until the minimum annulus area at that level was identified [12, 13]; if this plane was considered to be too steeply angled in respect to the LVOT and the sinuses, a

compromise between the plane with the smallest diameter and a plane perpendicular to the centerline at this level was reached [14, 15] (**Figure 1 and 2**). The plane was checked and adapted when necessary for each of the analysed phases to account for displacement of the annulus due to the contraction of the heart.

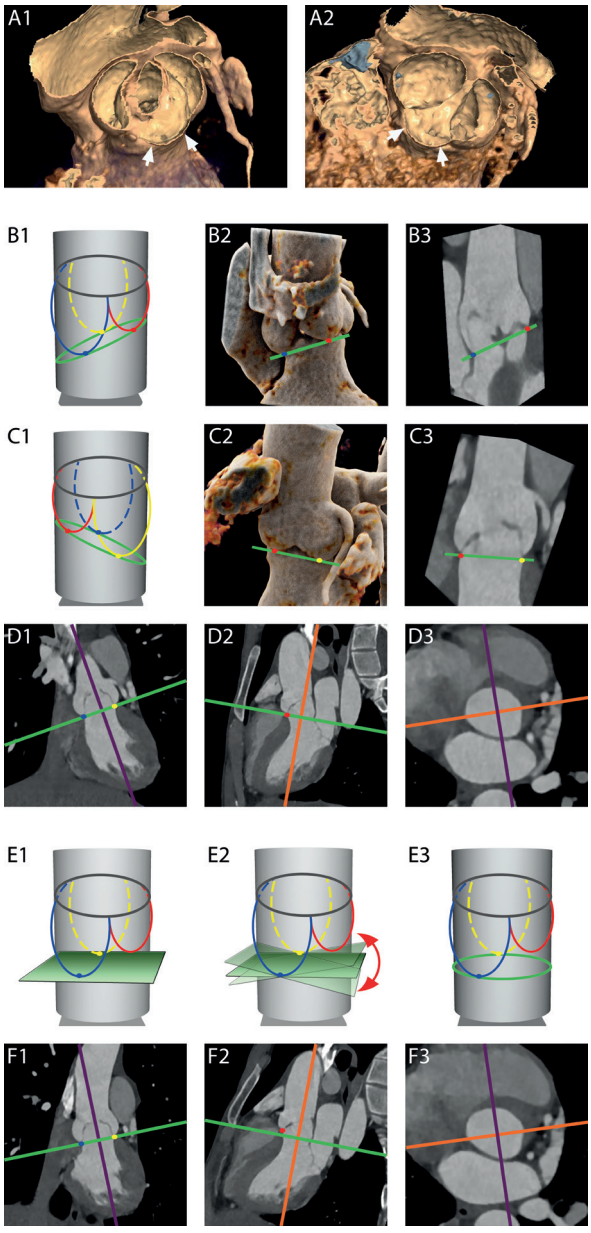

Figure 1. Determination of the annulus in patients with BAV type 1 with asymmetric cusps

A – Volume rendered (VR) reconstructions in systole (**A1**) and diastole (**A2**) demonstrating the

asymmetry of the sinuses due to the smaller dimensions of the right coronary cusp (RCC) (**arrows**).
B-D – Wrong annulus plane definition based on the three hinge points. In **B1** and **C1** schematic representations of the LVOT, sinuses of Valsalva (**red, yellow, blue lines**) and sinotubular junction (**grey line**) where the annulus plane (**green line**) was identified as the plane passing through the three hingepoints (hinge point of the RCC in **red**; hinge point of the non-coronary cusp (NCC) in **blue;** hinge point of the left coronary cusp (LCC) in **yellow**). In **B2**-**B3** and **C2**-**C3** VR reconstructions showing the angulation between the centerline passing through the LVOT/aortic root and the line (**B2-B3** and **C2-C3**; **green lines**) passing through the hinge points of the LCC and the NCC (**B**) and RCC (**C**), respectively. In **D1** and **D2** MPR showing the position of the axis in the longitudinal planes when identifying the plane passing through the three hinge points (**D3**).
E-F – Correct annulus plane definition. At first one plane passing through the two hinge points of the two biggest cusps is idenfied (**E1**); then this plane is tilted along the only still undetermined direction (**E2**) until the minimum cross-sectional area and/or a plane perpendicular to the centerline is obtained (**E3**). In **F1** and **F2** MPR showing the position of the axis in the longitudinal planes when determining the plane passing through the two hinge points and then make adjustements by tilting the violet and orange axis to identify the smallest possible area and a plane perpendicular to the centerline (**E3**).

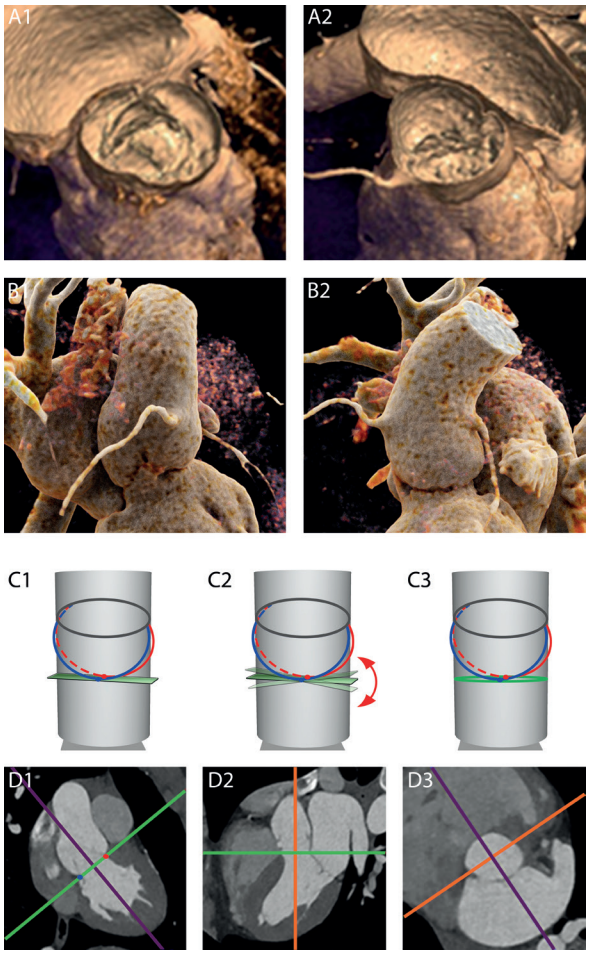

Figure 2. Determination of the annulus plane in patients with BAV type 0

A – VR reconstructions in systole (**A1**) and diastole (**A2**) showing the presence of only two cusps.
B – 3D anatomy of the aortic root.
C-**D** – One plane passing through the two hinge points of the two cusps is defined (**C1**); then this plane is tilted along the only still undetermined direction (**C2**) until the minimum cross-sectional area and/or a plane perpendicular to the centerline is obtained (**C3**). In **D1** and **D2** MPR showing the position of the axis in the longitudinal planes when determining the annulus plane (**D3**) as detailed above.

Annulus measurements

The annulus measurements were performed semi-automatically with the "edge finder" tool available in the reconstruction software (IntelliSpace Portal). With this tool, two seed points are placed somewhere inside the annulus and in the tissues surrounding the aortic root, respectively. Thereafter, the software automatically defines the contour of the annulus where there is a sharp transition of Hounsfield Unit values between the contrast enhanced lumen and surrounding tissues. For each phase, the automatically traced contour was checked and adjusted when deemed necessary. The contour was modified to encircle the inner edge of small calcifications and to extend over big calcifications in continuity with the adjacent outline. The maximum diameter, the diameter perpendicular to the maximum (referred to as "the minimum diameter"), the area and the perimeter were recorded (**Figure 3**). The average diameter was calculated as the average of the maximum and minimum. The effective diameter was derived from the area [11]. The asymmetry ratio (AR) and relative area (RA) were calculated as previously defined [7]. The AR was defined as the ratio between the maximum and the minimum diameter. The RA was calculated as the ratio between the area at each individual phase and the average area of all phases throughout the cycle.

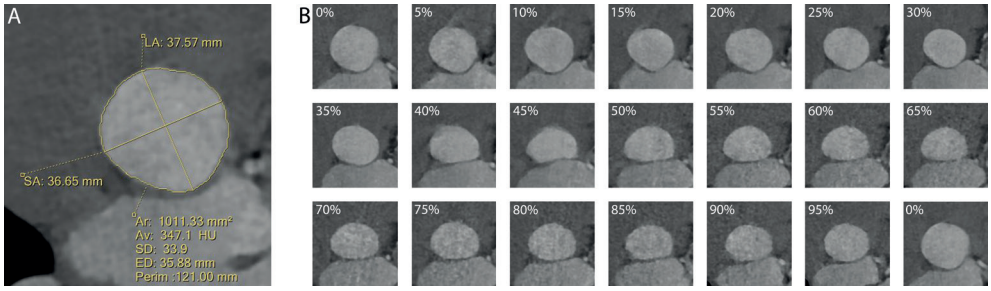

Figure 3. Annulus measurements

A – Measurement of the annulus parameters (maximum and minimum diameters, perimeter, area and area-derived diameter) based on the semi-automatically defined contour.
B – A case example showing all the 20 phases analyzed in a patient with BAV type 1 LR. The annulus shows a more circular shape in systole and a more elliptic shape during diastole.

Image quality assessment

The image quality of each phase at the level of the annulus was subjectively assessed based on a 2-point scale (insufficient quality; acceptable to perfect quality) based on the following criteria: the definition of the cusps and hinge points and subsequent reliability in the identification of these landmarks; the presence of motion artefacts; the adequate opacification of the LVOT and aortic root. The phases with insufficient quality were excluded from further analysis.

Intra and inter-observer variability

The same observer re-measured all phases of one third of the patients (n=18) at least one month after the first measurement. A second observer blinded to previous results, analysed 20 phases of 6 patients.

Statistical analysis

Continuous data are presented as mean ±standard deviation (SD). Student's t-test for paired samples and Wilcoxon signed-ranks tests were employed to assess differences during the cardiac cycle for all annular parameters. Data were examined with the Kolmogorov-Smirnov test to ensure normal distribution. A one-way ANOVA model with Bonferroni correction and Welch's test was used to investigate differences between valve types. A p value of <0.05 was considered as statistically significant.

Results

Patients and valve characteristics

Of the 60 eligible patients, 5 were excluded because of overall insufficient image quality (n=1), not all reconstruction phases available (n=3) and the presence of a large septal aneurysm (n=1).

In total 55 patients were included (mean age: 38.4±13.3(21-66); males: 32(58%)) of whom 10 had a Sievers type 0 BAV, 38 a type 1 BAV and 7 a type 2 valve. Patients' characteristics are summarized in **Table 1**.

In 9 patients with Sievers type 1, the new method for the definition of the annulus plane based on two hinge points was used. Ten patients had calcifications of the annulus that were of considerable amount in only one case.

Table 1. Patient characteristics

	Total (n=55)	Sievers type 0 (n=10)		Sievers type 1 (n=38)		Sievers type 2 (n=7)
		ap (n=6)	lat (n=4)	LR (n=30)	RN (n=8)	
Male*	32(58%)	4(67%)	3(75%)	17(57%)	4(50%)	4(57%)
Age (mean, SD, range) in years*	38.4±13.3(21-66)	41.7±18(24-62)	35±7.8(24-41)	39.8±14.2(21-66)	36.7±12.7(22-54)	33.8±8.5(22-43)
Height (mean, SD, range) in m*	1.7±0.2(1.3-2)	1.8±0.1(1.6-1.9)	1.8±0.1(1.6-1.9)	1.7±0.2(1.3-2)	1.7±0.2(1.4-2)	1.8±0.2(1.5-2)
Weight (mean, SD, range) in kg*	75±16(48-132)	76.7±15.9(55-95)	77.7±10(69-92)	75.5±16.5(48-132)	67.7±16.1(48-90)	77.7±18.4(52-106)
BMI (mean, SD, range) *	24.3±3.2(17.9-34)	24.1±1.1(22.3-25.8)	24.5±2.6(20.9-26.6)	24.9±3.8(17.9)	23.1±2.5(18.3-26.8)	23.2±2.6(20-27)
Blood pressure (the day of the CT scan)*						
- Max	124±16(94-170)	130±22(102-170)	138±27(107-161)	124±15(94-156)	119±8(109-130)	117±14(99-134)
- Min	81±11(64-117)	81±10(69-94)	94±24(66-117)	83±9.8(65-104)	76±7(67-91)	75±8(64-89)
Aortic valve dysfunction*						
- Insufficiency (at least mild)	9(16%)	1(17%)	0	3(10%)	2(25%)	3(42%)
- Stenosis (peak velocity>2.5cm/sec)	24(44%)	2(33%)	1(25%)	8(27%)	7(87%)	6(86%)
- Severe stenosis (peak velocity >4cm/sec)	6(11%)	1(17%)	0	1(3%)	3(4%)	1(14%)
Additional valve related events						
- Previous endocarditis	1(2%)	0	0	0	0	1(14%)
- Previous balloon-dilation	5(9%)	0	0	3(1%)	2(25%)	0
Congenital aortic valve or aortic diseases						
- Subvalvular stenosis	1(2%)	0	0	1(3%)	0	0
- Turner syndrome	9(6%)	0	1(25%)	6(20%)	1(12%)	1(14%)
- Coarctation	5(9%)	0	2(50%)	3(1%)	0	0
- Turner syndrome and coarctation	2(4%)	1(17%)	0	1(3%)	0	0

Percentages were rounded to the nearest integer. ap = BAV Sievers type 0 with the maximum diameter of the valve opening oriented along an anter-oposterior axis. lat = BAV Sievers type 0 with the maximum diameter of the valve opening oriented along a latero-lateral axis. LR = BAV Sievers type 1 with fusion of the left coronary cusp (LCC) and the right coronary cusp (RCC). RN = BAV Sievers type 1 with fusion of the RCC and the non coronary cusp (NCC). * No statistically significant differences in age, sex, height, weight, BMI, blood pressure or aortic valve pathology were found between patients with valve types 0, 1 and 2.

Variation of annulus parameters during the cardiac cycle

Out of a total of 1100 phase datasets (55 patients with 20 reconstructed phases each), 71 (6.4%) were excluded due to insufficient quality. The excluded datasets were randomly distributed over the cardiac cycle (p=0.6).

All of the measured annulus parameters presented statistically significant differences during the cardiac cycle (**Table 2** and **Figure 4**). The minimum diameter, the average diameter, the area, the perimeter and the area-derived perimeter demonstrated the highest values during early systole (5-10% of the cardiac cycle) with a significant reduction in diastole of 13.7%, 6.7%, 13.7%, 4.8% and 7.2%, respectively (all p values <0.001). The RA was >1 during systole (0-30%) and in late diastole (90-100%) (p<0.001). The maximum diameter showed the highest value in diastole (p<0.001). The AR was ≥1.1 in all phases indicating an elliptic shape of the annulus throughout the entire cardiac cycle. The annulus demonstrated significant deformation with increased elliptic morphology during diastole (relative change of 13.9%; p<0.001).

Table 2. Changes of the annulus parameters values during the cardiac cycle

	Max value*	Min value*	Relative Difference[%]†‡ (±SD of the difference)	p Value‡ Min vs Max
Maximum diameter [mm]	30.2±4.5	28.4±4.2	3.6% (±3.9%)	<0.001
Minimum diameter [mm]	22.4±4.1	26.0±4.1	13.8% (±8.4%)	<0.001
Average diameter [mm]	27.8±4.1	25.4±4	6.7% (±3.5%)	<0.001
Perimeter [mm]	92.9±13.7	86.9±14	4.8% (±4.3%)	<0.001
Area [mm^2]	586.7±169.1	486.5±144.3	13.7% (±6.8%)	<0.001
Diameter based on area [mm]	27.1±4.0	24.6±3.7	7.2% (±3.7%)	<0.001
Relative area	1.1±0.1	0.9±0.1	13.8% (±8.3%)	<0.001
Asymmetry ratio	1.3±0.2	1.1±0.1	12.8% (±10.8%)	<0.001

*Values calculated based on all data available for each phase; †relative difference compared to the maximum value; ‡ values calculated based on the number of cases available per comparison of the means; values for relative area and asymmetry ratio were calculated with Wilcoxon signed-ranked test.

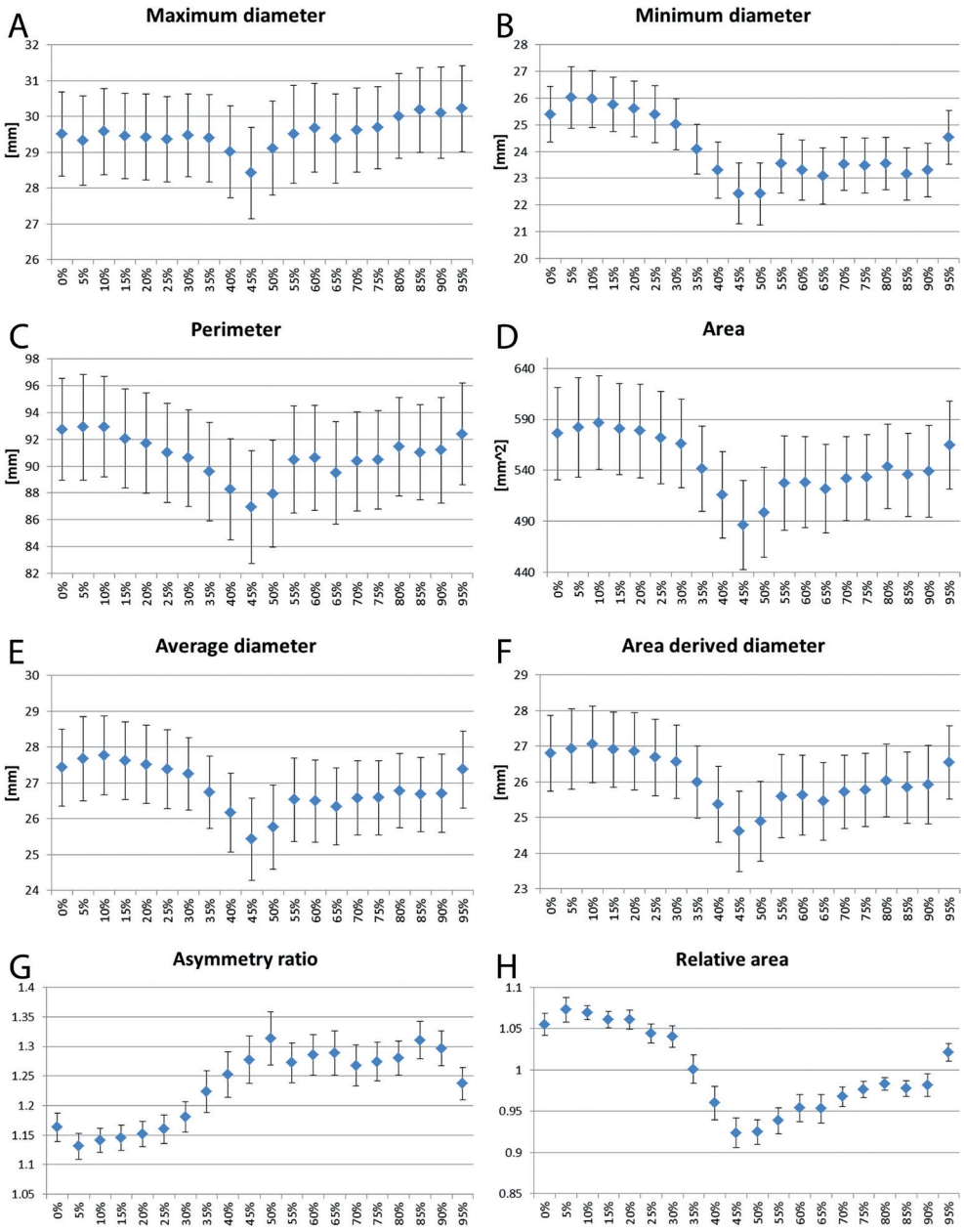

Figure 4. Mean annulus parameters per cardiac phase

Vertical bars indicate 95% confidence intervals (CI).

Variation of annulus parameters during the cardiac cycle per type of BAV

When analysed separately, all three types of BAV showed analogous dynamic changes (**Table 3** and **Figure 5**). All assessed parameters showed significant differences over time, with the exceptions of the maximum diameter for type 2 valves (p=0.15) and maximum diameter and perimeter for type 0 valves (p=0.2 and p=0.2 respectively) that did not show significant differences.

The AR was significantly different between BAV type 1 and 2 in early systole with valves type 1 showing a more elliptic annulus (p=0.024 at 10%; p=0.014 at 15%; p=0.023 at 20%; p= 0.016 at 25%). Patients with valves type 0 demonstrated a significantly more elliptic annulus than type 2 at phase 10% (p=0.047). The other parameters did not show significant differences between valve types at any of the time points.

Influence of heart rate on annulus dynamics

Scans were divided in 7 different categories based on heart rate (**Table 4**). All groups showed a smaller area between 40-60% of the cardiac cycle (**Figure 6**); however, the smallest values were reached earlier in the group with the slowest heart rate.

Intra and inter-observer variability

Intra and interobserver variability were good with all mean differences respectively ≤0.5±0.6mm and ≤1±1.2mm for maximum and minimum diameter and ≤8.1±25.9mm^2 and ≤18.2±17.9mm^2 for the area.

Table 3. Changes of the annulus parameters values during the cardiac cycle per valve type

	Max value*	Min value*	Relative Difference[%]†‡ (±SD of the difference)		p Value‡ Min vs Max
Maximum diameter [mm]					
Sievers type 0	30.4±3.8	28.6±4.2	2.3%	(±4,7%)	0.207
Sievers type 1	30±4.6	27.9±4.1	3.9%	(±5.2%)	0.001
Sievers type 2	32.3±2.9	29.8±3.7	2.7%	(±3.4%)	0.15
Minimum diameter [mm]					
Sievers type 0	25.8±4.1	20.6±3.9	19.5%	(±4.5%)	<0.001
Sievers type 1	25.5±3.8	22.2±3.8	11.6%	(±7.4%)	<0.001
Sievers type 2	29.6±2.2	23.5±3.3	19.4%	(±9.6%)	0.028
Average diameter [mm]					
Sievers type 0	27.8±4.2	24.6±3.7	7.3%	(±4.7%)	0.004
Sievers type 1	27.5±4.1	25±3.8	7%	(±3.4%)	<0.001
Sievers type 2	30.6±2.2	27.1±2.8	7.6%	(±4.8%)	0.028
Perimeter [mm]					
Sievers type 0	93.4±14.3	83.7±11.8	6%	(±6%)	0.027
Sievers type 1	91.8±14.7	85.8±13.5	5%	(±4.9%)	<0.001
Sievers type 2	102.5±8.1	93.7±11.9	3.5%	(±5.9%)	0.229
Area [mm^2]					
Sievers type 0	584.4±167.8	438.7±123.1	17.9%	(±6.5%)	0.001
Sievers type 1	574±172.7	475.4±140.9	13.2%	(±6.6%)	<0.001
Sievers type 2	690.9±117.4	542.8±122.5	14.2%	(±10.1%)	0.042
Diameter based on area [mm]					
Sievers type 0	27±23.4	23.4±3.3	9.5%	(±3.5%)	<0.001
Sievers type 1	26.7±4.0	24.3±3.7	6.9%	(±3.6%)	<0.001
Sievers type 2	29.6±2.6	26.1±3.0	7.5%	(±5.3%)	0.038
Relative area					
Sievers type 0	1.1±0.1	0.9±0.0	16.4%	(±6.0%)	<0.001
Sievers type 1	1.1±0.0	0.9±0.1	13.4%	(±6.5%)	<0.001
Sievers type 2	1.1±0.1	0.9±0.1	17.2%	(±7.5%)	0.004
Asymmetry ratio					
Sievers type 0	1.4±0.2	1.1±0.1	19%	(±8.6%)	0.012
Sievers type 1	1.3±0.1	1.2±0.1	12.1%	(±8.8%)	<0.001
Sievers type 2	1.3±0.2	1.1±0.0	17.6%	(±11.7%)	0.043

*Values calculated based on all data available for each phase; †relative difference compared to the maximum value; ‡ values calculated based on the number of cases available per comparison of the means; values for relative area and asymmetry ratio were calculated with Wilcoxon signed-ranked test.

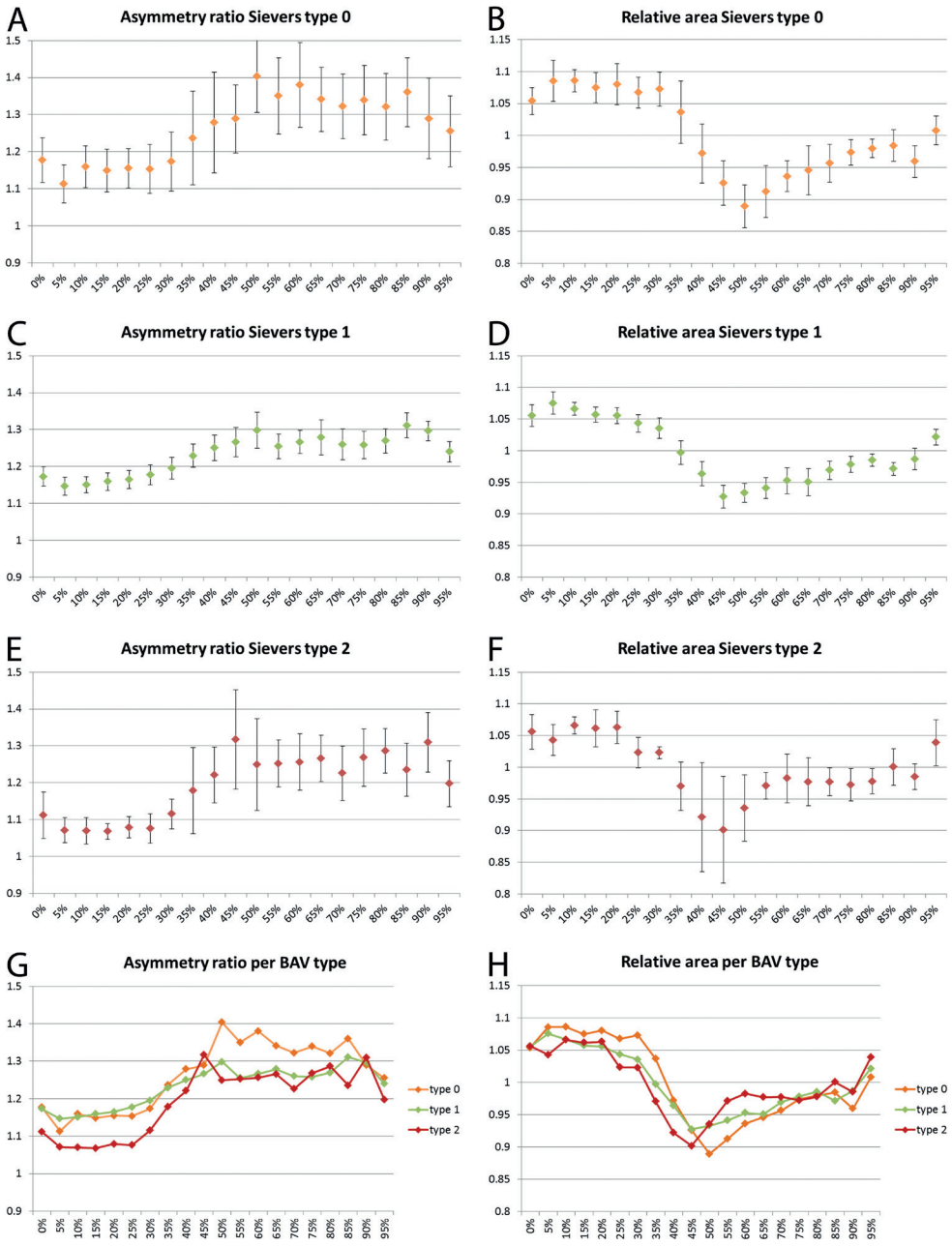

Figure 5. Mean AR and RA per phase and valve type

Vertical bars indicate 95% CI.

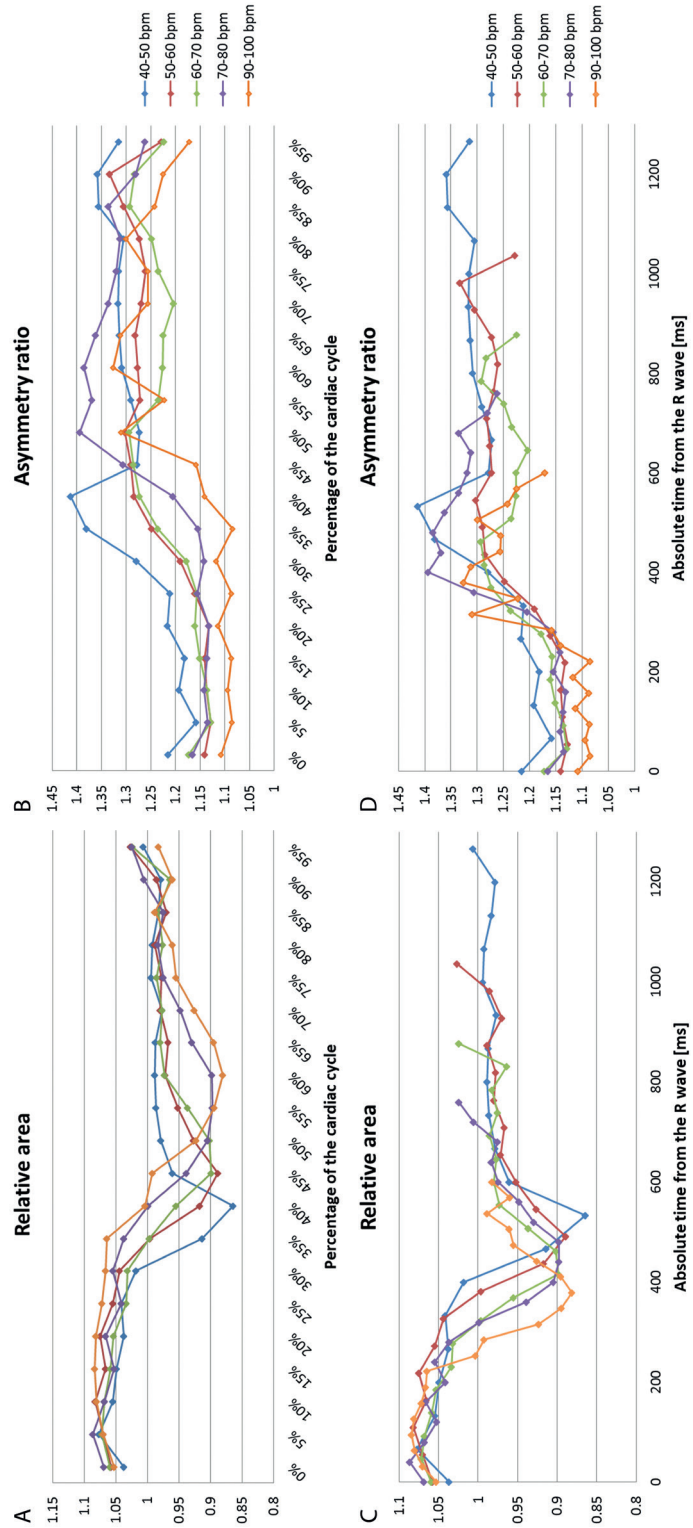

Figure 6

Mean AR and RA in groups with different heart rates during successive phases of the cardiac cycle expressed in terms of percentage (**A-B**) and absolute time (**C-D**).

Table 4. Classificaton of scans based on heart rate

Patients' heart rate	n
- 40-50	6
- 50-60	15
- 60-70	16
- 70-80	10
- 80-90*	4
- 90-100	4
- 100-110*	2

* Groups 80-90 bpm and 100-110 were not further analysed due to the absence of data for phase 55% and the low number of cases, respectively.

Discussion

In this study we described a standardized way to determine the annulus plane in patients with a bicuspid aortic valve and demonstrated that the BAV annulus undergoes significant changes in shape and size during the cardiac cycle. Overall, the annulus showed a larger area with an almost circular shape in systole and a smaller area with an elliptic shape in diastole. Each of the BAV types showed analogous morphological changes. However, type 1 valves had a more elliptic annulus in early systole. Furthermore, as the heart rate at the moment of the CT scan increased, the minimum area was reached at a later phase of the cardiac cycle but earlier in absolute time.

The term BAV includes a spectrum of morphological alterations of the aortic valve that have in common the resulting presence of only two functional cusps. BAV are commonly divided based on the classification system introduced by Sievers et al. [1]. This classification is based on the valve phenotype and more specifically on the presence and number of raphe. A raphe represents the line of fusion between two cusps that are often unequal in size. Due to the absence of the normal three cusps and corresponding three apposition surfaces, the opening orifice of the valve is often asymmetric. Furthermore, the aortic root is asymmetrically and characteristically enlarged in 58% of case [16].

The distortion of the valve opening in BAV patients has led to the exclusion of patients with this anomaly from most early studies assessing safety and results of TAVI, due to concerns about deformation and malposition of the implanted valve [3, 17, 18]. Although with limitations due to the inclusion of small populations, later investigations have shown that TAVI is in fact feasible also in the BAV population and, furthermore, has results comparable to those obtained in cohorts with TAV [4, 5, 19, 20].

Correct and precise pre-TAVI assessment of aortic root diameters is fundamental to choose the most appropriate valve size and avoid complications, particularly paravalvular regurgitation, that has been shown to occur more frequently in the BAV population [4, 21]. CT has been identified as the imaging modality of choice for this purpose. The most important entity to be assessed is the ring where the deployed valve will be anchored. These measurements will determine which valve size will be implanted among the limited number of available ones. This ring, commonly referred to as "annulus", contours the level with the smallest area along the junction between the LVOT and the aortic root but does not correspond to a well-defined anatomical structure [12, 22]. Recent guidelines (intended for patients with TAV, albeit not addressing valve anatomy variations) indicate that the annulus should be identified on MPR as the plane passing through the three hinge points of the cusps [11]. Although this same technique has been previously applied also to datasets of patients with BAV [5], we did not find this method feasible for all patients. First, in patients with BAV valve type 0 there are only two cusps and therefore, in most cases, only two hinge points (or in few cases two of the three are very close). Since there are infinite planes that pass through two points, more criteria for the identification of the correct annulus plane had to be introduced as detailed above in the Methods and **Figure 2**. Furthermore, in patients with BAV type 1 (and possibly type 2) one of three cusps is often malformed and/or underdeveloped resulting in a distortion of the normal anatomy of the aortic root. Therefore, the plane passing through the three hinge points might not be representative of the desired plane where to deploy the valve. In these patients, at first the hinge points of the two bigger cusps were used as landmarks and subsequently the so obtained plane was oriented following the same steps as in patients with valves type 0 (**Figure 1**). The application of this methodology, both in clinical and research settings, will likely improve the standardization of annulus measurements in BAV patients, and thereafter, provide accurate and appropriate sizing data as basis for future guidelines.

In patients with TAV it has been shown that the annulus has an elliptic shape that undergoes conformational changes during the cardiac cycle as well as significant variation in sizing parameters [8]. Knowledge of this phenomenon is fundamental in the pre-TAVI work-up to establish during which phase the annulus dimensions should be calculated. Although with some controversy attributable to the better quality and reproducibility of diastolic images [13], literature and guidelines suggest that measurements should be performed on images obtained in systole due to larger annular sizes in this phase [11, 23]. Our study demonstrated the occurrence of significant changes in sizing parameters during the cardiac cycle in all types of BAV. The RA, minimum diameter and area showed the most pronounced differences (13.8% and 13.7%), with all highest values in the phases between 0% to 10%, while the maximum diameter demonstrated the smallest difference (3.6%). The relative difference of 7.2% found for the area-derived diameter corresponded to an absolute difference of 1.9mm between systole and diastole. Considering that each

prosthetic valve size can be fitted in annuli presenting a range of diameters of 3mm at maximum (or 2mm depending on the type of valve employed), a 2mm difference could imply a different choice of valve size. For the patient with the highest relative difference in area-derived diameter (relative difference of 17%; minimum and maximum area-derived diameter of 24.5mm and 29.6mm respectively) measuring the annulus in a different phase could imply: employing a 29mm Medtronic CoreValve or not having an appropriate size for this type of valve; implanting a 26mm Edwards Sapien valve or risking paravalvular leakage with a possibly undersized 29mm valve of the same type.

Among the reasons that led to consider BAV patients as at high risk for TAVI procedures are some characteristics of the aortic annulus such as a more elliptic shape than in patients with TAV. This different conformation has been suggested as the cause for the higher rate of paravalvular regurgitation in BAV patients [17, 19, 24, 25]. With an AR >1 at all phases and for all BAV types, but significantly more in early systolic phase for valves type 1, our study demonstrated that the annulus of BAV patients has an elliptic shape. However, the overall and per valve type maximum average AR in our study (maximum AR: 1.3±0.2 overall; 1.4±0.2 for valves type 0; 1.3±0.1 for valves type 1; 1.3±0.2 for valves type 2) are comparable to those found in patients with TAV [7, 9, 23].

Hemodynamic characteristics might influence the mechanics of the annulus. Therefore, we investigated the influence of the patients' heart rate at the moment of the CT examination. CT images were reconstructed based on the percentage of the cardiac cycle and therefore the absolute time span between phases depended on the heart rate of the patient at the moment of the acquisition. Our results suggest that in patients with a higher heart rate changes in area of the aortic annulus occur at a shorter absolute time, which, however, corresponds to a later phase of the cardiac cycle. Therefore, to ensure that the largest sizing parameters are detected for all heart rates, measurements should be performed in early systolic phase and within 200ms from the R wave.

A limitation of the present study is the impossibility to compare planes and measurements obtained with the new method to a reference standard. However, for the annulus, even in TAV patients, there is no reference standard. In fact, measurements performed in operating rooms are subject to limitations such as non-physiological conditions and the use of an imprecise measurement tool and, furthermore, values of implanted valves size are influenced by other additional factors. Second, due to the relatively limited number of patients per type of BAV valve, ANOVA models for repeated measurements were not applicable and comparison between valve types had to be performed per time points. Furthermore, the mean age of the study population was relatively low with a limited number of severely stenotic aortic valves. Another limitation that has to be considered is the thickness of the reconstructions (1.5mm), which might have influenced the precision

of the measurements. Finally, the amount of calcium at the level of the annulus was not systematically and quantitatively scored. However, calcifications were considerable in one patient only.

Conclusions

We propose a new specific and systematic method for the definition of the annulus plane in patients with all types of BAV. The aortic annulus of patients with BAV undergoes dynamic changes during the cardiac cycle. In all three BAV types the annulus has an elliptical shape that undergoes conformational changes with a more flattened appearance in diastolic phase. Furthermore, the annulus presents significant dynamic variations in sizing parameters with the highest values in early systole. These changes occur earlier during the cardiac cycle for patients with a slower heart rate. Therefore, measurements for TAVI planning in patients with BAV should be performed in the early systolic phase to avoid underestimation of the annulus dimensions.

References

1. Sievers HH, Schmidtke C. A classification system for the bicuspid aortic valve from 304 surgical specimens. J Thorac Cardiovasc Surg. 2007;133(5):1226-33.
2. Ward C. Clinical significance of the bicuspid aortic valve. Heart. 2000;83(1):81-5.
3. Smith CR, Leon MB, Mack MJ, Miller DC, Moses JW, Svensson LG, Tuzcu EM, Webb JG, Fontana GP, Makkar RR, Williams M, Dewey T, Kapadia S, Babaliaros V, Thourani VH, Corso P, Pichard AD, Bavaria JE, Herrmann HC, Akin JJ, Anderson WN, Wang D, Pocock SJ; PARTNER Trial Investigators. Transcatheter versus surgical aortic-valve replacement in high-risk patients. N Engl J Med. 2011;364(23):2187-98.
4. Wijesinghe N, Ye J, Rodes-Cabau J, Cheung A, Velianou JL, Natarajan MK, Dumont E, Nietlispach F, Gurvitch R, Wood DA, Tay E, Webb JG. Transcatheter aortic valve implantation in patients with bicuspid aortic valve stenosis. JACC Cardiovasc Interv. 2010;3(11):1122-5.
5. Hayashida K, Bouvier E, Lefevre T, Chevalier B, Hovasse T, Romano M, Garot P, Watanabe Y, Farge A, Donzeau-Gouge P, Cormier B, Morice MC. Transcatheter aortic valve implantation for patients with severe bicuspid aortic valve stenosis. Circ Cardiovasc Interv. 2013;6(3):284-91.
6. Blanke P, Reinohl J, Schlensak C, Siepe M, Pache G, Euringer W, Geibel-Zehender A, Bode C, Langer M, Beyersdorf F, Zehender M. Prosthesis oversizing in balloon-expandable transcatheter aortic valve implantation is associated with contained rupture of the aortic root. Circ Cardiovasc Interv. 2012;5(4):540-8.
7. de Heer LM, Budde RP, van Prehn J, Mali WP, Bartels LW, Stella PR, Herwerden van LA, Kluin J, Vincken KL. Pulsatile distention of the nondiseased and stenotic aortic valve annulus: analysis with electrocardiogram-gated computed tomography. Ann Thorac Surg. 2012;93(2):516-22.
8. Sucha D, Tuncay V, Prakken NH, Leiner T, van Ooijen PM, Oudkerk M, Budde RP. Does the aortic annulus undergo conformational change throughout the cardiac cycle? A systematic review. Eur Heart J Cardiovasc Imaging. 2015;16(12):1307-17.
9. Hamdan A, Guetta V, Konen E, Goitein O, Segev A, Raanani E, Spiegelstein D, Hay I, Di Segni E, Eldar M, Schwammenthal E. Deformation dynamics and mechanical properties of the aortic annulus by 4-dimensional computed tomography: insights into the functional anatomy of the aortic valve complex and implications for transcatheter aortic valve therapy. J Am Coll Cardiol. 2012;59(2):119-27.
10. van den Hoven AT, Mc-Ghie JS, Chelu RG, Duijnhouwer AL, Baggen VJM, Coenen A, Vletter WB, Dijkshoorn ML, Bosch van den AE, Roos-Hesselink JW. Transthoracic 3D echocardiographic left heart chamber quantification in patients with bicuspid aortic valve disease. Int J Cardiovasc Imaging. 2017;33(12):1895-903.
11. Achenbach S, Delgado V, Hausleiter J, Schoenhagen P, Min JK, Leipsic JA. SCCT expert consensus document on computed tomography imaging before transcatheter aortic valve implantation (TAVI)/transcatheter aortic valve replacement (TAVR). J Cardiovasc Comput Tomogr. 2012;6(6):366-80.

12. Sievers HH, Hemmer W, Beyersdorf F, Moritz A, Moosdorf R, Lichtenberg A, Misfeld M, Charitos EI; Working Group for Aortic Valve Surgery of German Society of Thoracic and Cardiovascular Surgery. The everyday used nomenclature of the aortic root components: the tower of Babel? Eur J Cardiothorac Surg. 2012;41(3):478-82.
13. Kasel AM, Cassese S, Bleiziffer S, Amaki M, Hahn RT, Kastrati A, Sengupta PP. Standardized imaging for aortic annular sizing: implications for transcatheter valve selection. JACC Cardiovasc Imaging. 2013;6(2):249-62.
14. Queiros S, Dubois C, Morais P, Adriaenssens T, Fonseca JC, Vilaca JL, D'hooge J. Automatic 3D aortic annulus sizing by computed tomography in the planning of transcatheter aortic valve implantation. J Cardiovasc Comput Tomogr. 2017;11(1):25-32.
15. Watanabe Y, Morice MC, Bouvier E, Leong T, Hayashida K, Lefevre T, Hovasse T, Romano M, Chevalier B, Donzeau-Gouge P, Farge A, Cormier B, Garot P. Automated 3-dimensional aortic annular assessment by multidetector computed tomography in transcatheter aortic valve implantation. JACC Cardiovasc Interv. 2013;6(9):955-64.
16. Fazel SS, Mallidi HR, Lee RS, Sheehan MP, Liang D, Fleischman D, Herfkens R, Mitchell RS, Miller DC. The aortopathy of bicuspid aortic valve disease has distinctive patterns and usually involves the transverse aortic arch. J Thorac Cardiovasc Surg. 2008;135(4):901-7, 7 e1-2.
17. Zegdi R, Ciobotaru V, Noghin M, Sleilaty G, Lafont A, Latremouille C, Deloche A, Fabiani JN. Is it reasonable to treat all calcified stenotic aortic valves with a valved stent? Results from a human anatomic study in adults. J Am Coll Cardiol. 2008;51(5):579-84.
18. Joint Task Force on the Management of Valvular Heart Disease of the European Society of Cardiology (ESC); European Association for Cardio-Thoracic Surgery (EACTS), Vahanian A, Alfieri O, Andreotti F, Antunes MJ, Barón-Esquivias G, Baumgartner H, Borger MA, Carrel TP, De Bonis M, Evangelista A, Falk V, Iung B, Lancellotti P, Pierard L, Price S, Schäfers HJ, Schuler G, Stepinska J, Swedberg K, Takkenberg J, Von Oppell UO, Windecker S, Zamorano JL, Zembala M. Guidelines on the management of valvular heart disease (version 2012). Eur Heart J. 2012;33(19):2451-96.
19. Phan K, Wong S, Phan S, Ha H, Qian P, Yan TD. Transcatheter Aortic Valve Implantation (TAVI) in Patients With Bicuspid Aortic Valve Stenosis--Systematic Review and Meta-Analysis. Heart Lung Circ. 2015;24(7):649-59.
20. Mylotte D, Lefevre T, Søndergaard L, Watanabe Y, Modine T, Dvir D, Bosmans J, Tchetche D, Kornowski R, Sinning JM, Thériault-Lauzier P, O'Sullivan CJ, Barbanti M, Debry N, Buithieu J, Codner P, Dorfmeister M, Martucci G, Nickenig G, Wenaweser P, Tamburino C, Grube E, Webb JG, Windecker S, Lange R, Piazza N. Transcatheter aortic valve replacement in bicuspid aortic valve disease. J Am Coll Cardiol. 2014;64(22):2330-9.
21. Willson AB, Webb JG, Labounty TM, Achenbach S, Moss R, Wheeler M, Thompson C, Min JK, Gurvitch R, Norgaard BL, Hague CJ, Toggweiler S, Binder R, Freeman M, Poulter R, Poulsen S, Wood DA, Leipsic J. 3-dimensional aortic annular assessment by multidetector computed tomography predicts moderate or severe paravalvular regurgitation after transcatheter aortic valve replacement: a multicenter retrospective analysis. J Am Coll Cardiol. 2012;59(14):1287-94.
22. Anderson RH. Clinical anatomy of the aortic root. Heart. 2000;84(6):670-3.

23. Jurencak T, Turek J, Kietselaer BL, Mihl C, Kok M, van Ommen VG, van Garsse LA, Nijssen EC, Wildberger JE, Das M. MDCT evaluation of aortic root and aortic valve prior to TAVI. What is the optimal imaging time point in the cardiac cycle? Eur Radiol. 2015;25(7):1975-83.
24. Xie X, Shi X, Xun X, Rao L. Efficacy and Safety of Transcatheter Aortic Valve Implantation for Bicuspid Aortic Valves: A Systematic Review and Meta-Analysis. Ann Thorac Cardiovasc Surg. 2016;22(4):203-15.
25. Kawamori H, Yoon SH, Chakravarty T, Maeno Y, Kashif M, Israr S, Abramowitz Y, Mangat G, Miyasaka M, Rami T, Kazuno Y, Takahashi N, Jilaihawi H, Nakamura M, Cheng W, Friedman J, Berman D, Sharma R, Makkar RR. Computed tomography characteristics of the aortic valve and the geometry of SAPIEN 3 transcatheter heart valve in patients with bicuspid aortic valve disease. Eur Heart J Cardiovasc Imaging. 2018.

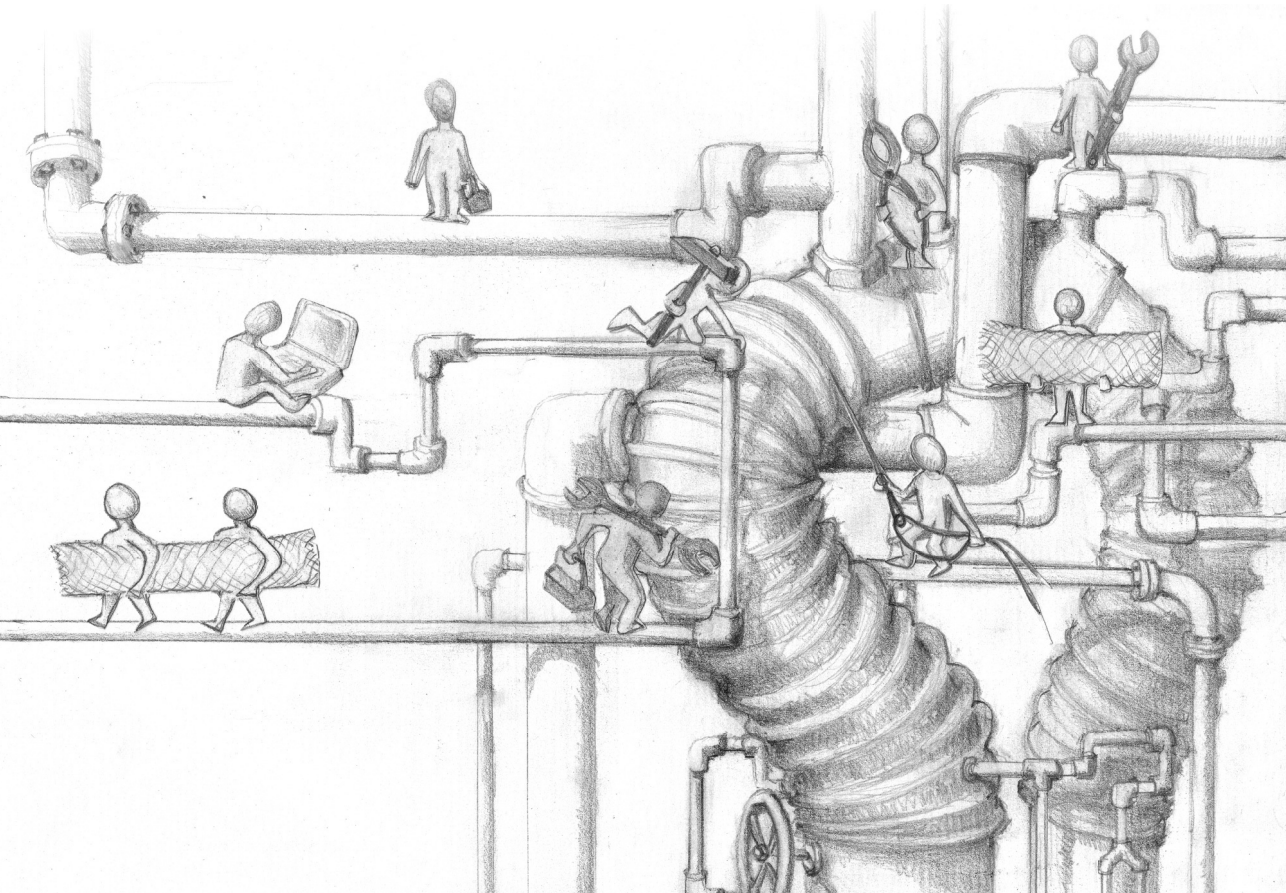

PART 2

CT assessment of the thoracic aorta after surgery and endovascular intervention

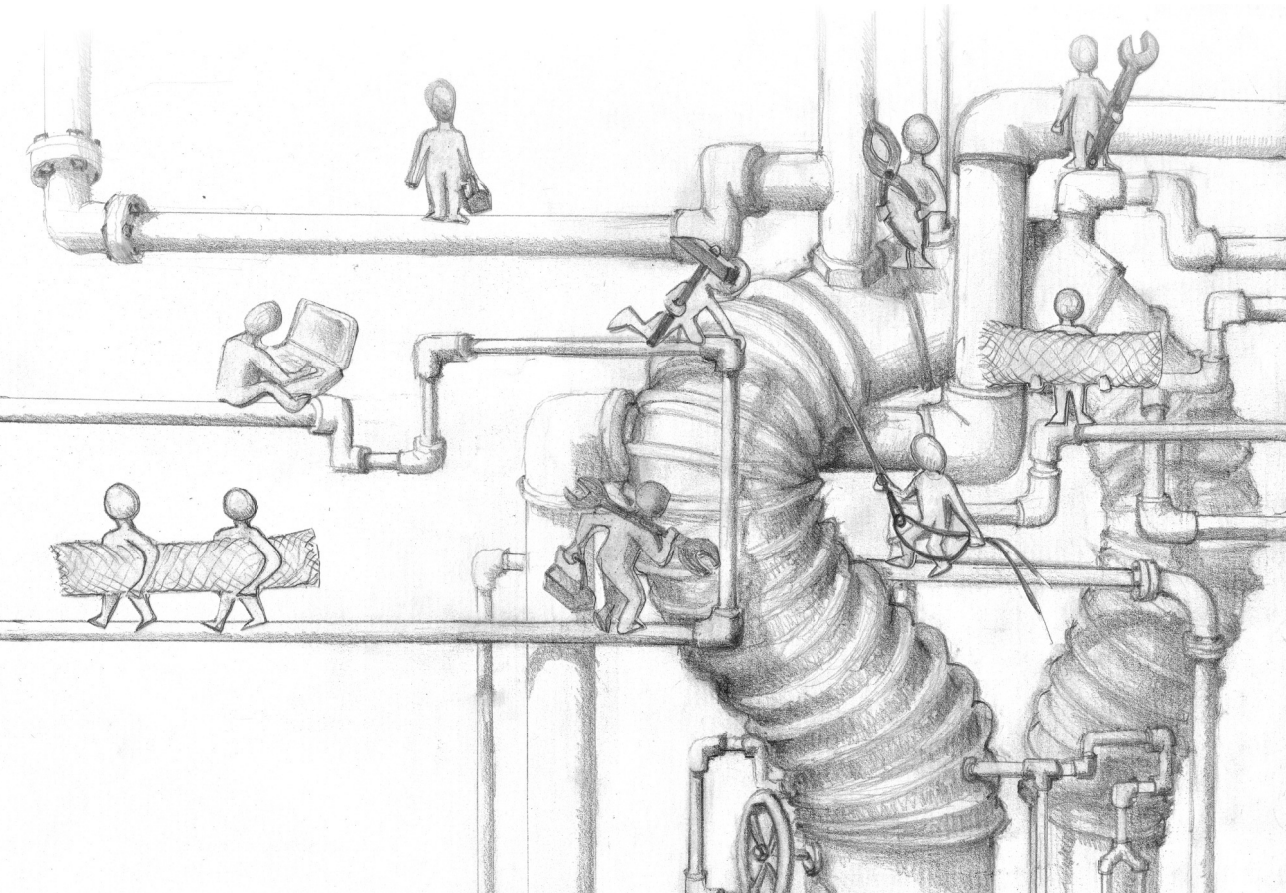

CHAPTER 7

CT Angiography for the depiction of complications after the Bentall procedure
Pictorial review

Sara Boccalini*, Laurens E Swart*, Jos A. Bekkers, Koen Nieman, Gabriel P Krestin, Ad JJC Bogers, Ricardo PJ Budde

Br J Radiol. 2018 Aug 13:20180226

Abstract

Following a Bentall procedure, which comprises a composite replacement of both the aortic valve and the ascending aorta, the imaging modality of choice to depict known or suspected complications is computed tomography angiography (CTA). An update and extension of the literature regarding complications after the Bentall procedure is provided. The wider availability of ECG-gating has allowed for a clearer depiction of the aortic valve and ascending aorta. This resulted not only in the identification of previously undetectable complications, but also in a more precise assessment of the pathophysiology and morphology of known ones, reducing the need for additional imaging modalities. Moreover, the possibility to combine positron emission tomography (PET) images with CTA offers new insights in case of suspected infection. Due to the complexity of the operation itself and concomitant or subsequent additional procedures, as well as the wide spectrum of underlying pathology, new scenarios with multiple complications can be expected.

The Bentall procedure

The most common pathologies that involve the ascending aorta, namely large aneurysms and type A dissections, require surgical treatment with aortic replacement mainly in an elective and emergency setting, respectively. This procedure may also involve simultaneous replacement of the aortic valve whenever the aforementioned pathology is accompanied by aortic stenosis or insufficiency. One of the options, representing the procedure of choice at our institution, is the implantation of a single composite graft in a one-step surgery (Bentall procedure) [1].

Since its introduction in 1968 different methods to perform this intervention have been practiced [1, 2]. A mechanical or biological aortic valve prosthesis can be employed with the same general indications and limitations as in isolated aortic valve replacements. The aortic valve prosthesis can be sutured to the aortic graft in the operating room by the surgeon or, more commonly, the two components can be manufactured and employed as a single unit. The native aortic wall can be left in place and wrapped around the prosthesis (inclusion technique) although it is generally excised and substituted by the graft (interposition technique, **Figure 1**). One of the most crucial aspects of the operation is the re-attachment of the coronary arteries. The original procedure described by Bentall involved directly suturing the aortic wall around the coronary ostia to the graft. This was complicated by bleeding and pseudoaneurysm formation caused by excessive wall tension and tearing of partial-thickness sutures. In 1981, with the introduction of the Cabrol procedure, a prosthetic conduit was anastomosed to the coronary ostia and side-to-side to the aortic graft. Intrinsic complications of the Cabrol procedure included early postoperative death in patients with aortic dissection, anastomotic leak, coronary graft insufficiency from kinking or intimal hyperplasia, acute coronary graft thrombosis, and endocarditis [3]. The modified Bentall procedure addressed these problems by mobilizing the coronary ostia with a button of native aortic wall, thus reducing wall tension and allowing an all-thickness suture to the aortic prosthesis (**Figure 1**).

The Bentall procedure can also be combined with other procedures extending to the aortic arch (such as a partial or complete aortic arch replacement, the Elephant trunk technique, etc.) depending on the extent of the aorta that is affected [4].

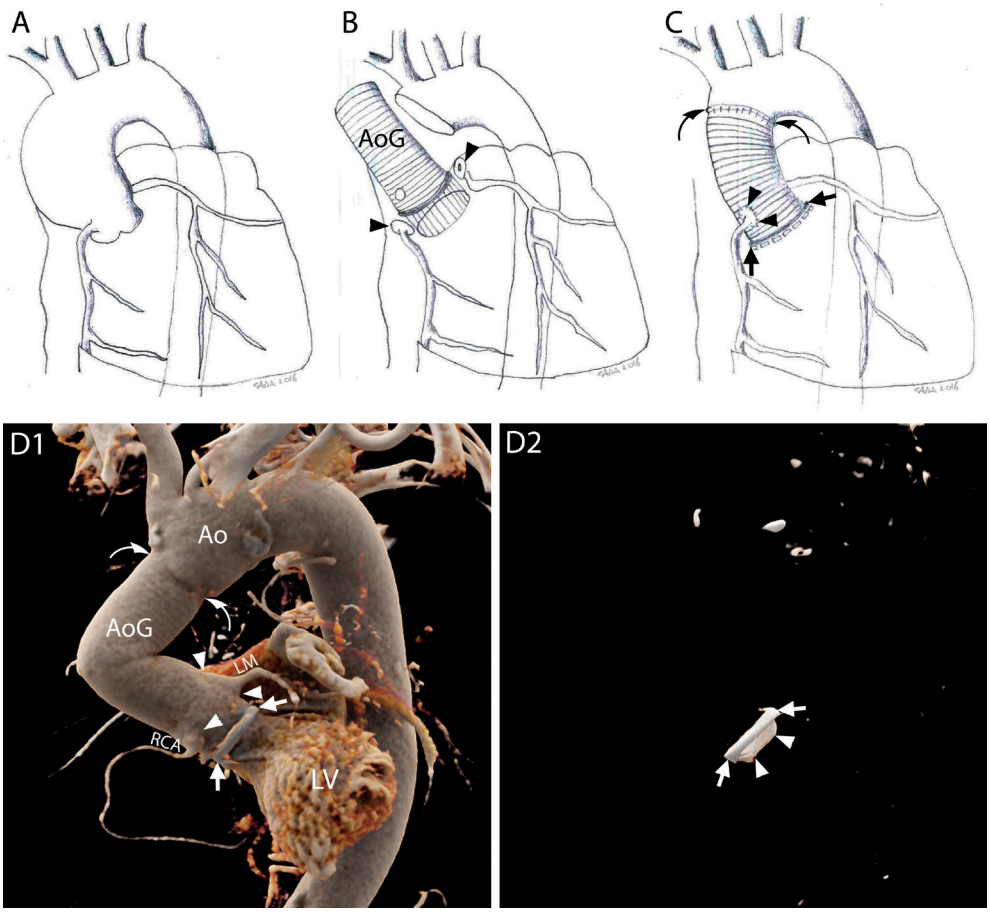

Figure 1. The Bentall procedure

A-C – Schematic representations of the most commonly practiced variation of the Bentall procedure. The native wall of the aneurysmatic (A) or dissected ascending aorta is excised together with the stenotic or insufficient aortic valve (interposition technique). The ostia of the coronary arteries are cut out with a button of the native aortic wall attached (button technique) (B, arrowheads). The aorta and the aortic valve are substituted by one or multiple grafts (B, AoG) and a prosthetic aortic valve which are sutured to the left ventricle outflow tract (LVOT) (C, arrows) and the native aorta (C, curved arrows). The buttons around the coronary ostia are reattached to the aortic graft (C, arrowheads).
D1-D2 - 3D reconstructions of CTA images of a patient who underwent a Bentall procedure with the implantation of a mechanical aortic valve, performed according to the technique described above, showing the exterior surface of the aortic prosthesis and native aorta (D1) and the prosthetic aortic valve within (D2), respectively. D1 – ring of the aortic valve (arrows); aortic grafts (AoG); anastomosis of the coronary arteries (arrowheads); distal suture line with the native aorta (curved arrows). D2 - metallic ring of the aortic valve (arrows); leaflet of the mechanical valve (arrowheads). *Ao* – native aorta, *LM* – left main, *LV* – left ventricle, *RCA* – right coronary artery.

CT scan: timing and protocol

After the Bentall procedure, imaging investigations are indicated not only if complications are suspected, but also for routine follow-up in asymptomatic patients. CT is generally the modality of choice [5-8]. However, the best timing for routine exams has not been ascertained and different schemes are suggested in guidelines [6, 7, 9]. The underlying pathology should also be taken into account to decide the best schedule. Whilst at least one CT scan should be performed within the first three post-operative months in all patients, in case dissection was the cause of the procedure, adding more controls, at 1 and 6 months, is suggested.[7] Thereafter, a control after the first year should be planned and, if no signs of complications are found, a yearly follow up can be foreseen.

When planning the scan the protocol should be adapted for each case, and tailored to the specific clinical question. Therefore, it is essential that the details of the surgical technique be provided (or searched if not provided) to optimize the acquisition as well as to aid in the successive interpretation.

If the scan is performed in the setting of routine follow-up, an aortic protocol with thin-slice reconstructions (≤1mm) can be employed. ECG-gating or triggering is always recommended. However, if no complications are suspected, prospective triggering and especially high-pitch prospectively triggered acquisitions, if available, should be preferred to limit the radiation dose.

Whenever complications involving the valve, either mechanical or infectious, are suspected, an acquisition with retrospective ECG-gating will allow assessment of the motility of the leaflets and the movement of any vegetations or thrombi. If the presence of hemorrhage (including intramural hematoma of the native aortic wall) or leakage is investigated, an unenhanced acquisition will help establishing the nature of any hyperdense areas and, therefore, distinguish surgical material from calcifications, blood and contrast. Reconstructions of both pre- and post-contrast injection acquisitions should be performed with the same thickness to ease comparison. In case coronary artery stenoses have to be ruled out, an appropriate protocol should be adopted.

Although in routine follow up the sole thoracic aorta/thorax can be investigated, in specific scenarios the scan should be extended to include also the abdomen. This is the case for suspected extension of the dissection and/or hematoma and patients presenting increasing aortic diameters on preceding controls. However, since aortic pathology might involve any segment of the vessel, the entire aorta should be included in the scan range and assessed at least once [6].

Normal findings on CT scans

The normal post-operative CT appearance of prosthetic aortic valves (**Figure 2**), aortic grafts (**Figure 3**), as well as other surgical materials (**Figure 4**) should be known beforehand to be able to distinguish complications and avoid misdiagnosis.

In particular, since surgical material is generally hyperdense and located at the level of the sutures, it could be confused for extravasated contrast media. The most reliable way to distinguish the two entities is by comparing enhanced and unenhanced images. While on enhanced images their appearance and density might be similar, on unenhanced images only the surgical material will be visible as a hyperdense structure (**Figure 4** and **Figure 5**).

The origin of the coronary arteries after the anastomosis commonly has a peculiar appearance that has been incorrectly referred to as a "pseudoaneurysm" (**Figure 6**) [10]. The aortic arch can be involved in the procedure, thus radiologists should be familiar also with procedures at this level (**Figure 7**). The native aorta should be assessed for the presence of residual or new complications (**Figure 7**), including dissections and intramural hematoma.
Multiplanar reconstructions should be employed to assess the valves in all their parts, on planes perpendicular and parallel to the long axis of the aorta. Three-dimensional reconstructions can also aid in the visualization of anomalies of the components of the valves (**Figure 2**).

Peri-aortic fluid

Postoperative changes can be expected in the tissues surrounding the aorta due to manipulation during the procedure and related healing processes, especially shortly after the operation. In particular, it has been shown that the presence of fluid around the aortic graft can be demonstrated in all patients undergoing a CT scan in the first three post-operative months. However, CT characteristics of the fluid can help establishing its aetiology and potential clinical consequences [11].

For instance, the presence of peri-aortic fluid in the form of stranding (fluid mingled with adipose tissue, without clear borders and completely surrounding the aortic graft) in the first three post-operative months can be considered a normal finding, even when extending up to 17 mm from the border of the graft (**Figure 8**) [11].

On the contrary, fluid with defined and clear borders, not necessarily completely encircling the aortic graft, is referred to as a fluid collection and can be divided into subtypes based

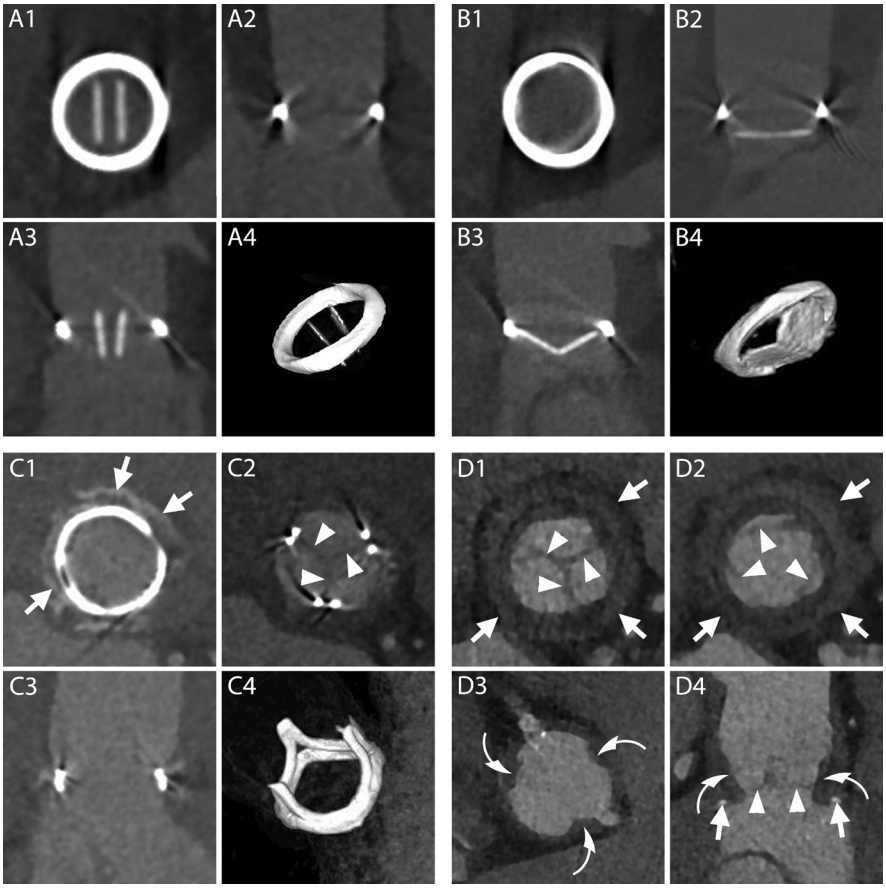

Figure 2. Normal aspect of prosthetic aortic valves

A1-B4 - CT aspect of the most commonly employed mechanical prosthetic valve (St. Jude, Abbot). The bi-leaflet valve is shown with open and closed leaflets respectively during systole (**A1-A4**) and diastole (**B1-B4**). **A1** and **B1** - multiplanar reconstructions (MPR) on planes perpendicular to the centerline of the aorta at the level of the outer ring of the valve. **A2** and **B2** - MPR parallel to the centerline of the aorta and parallel to the direction of the leaflets. **A3** and **B3** - MPR parallel to the centerline of the aorta and perpendicular to the direction of the leaflets. **A4** and **B4** - volume rendering (VR) of the valve.

C1-C4 - CT aspect of a stented biological valve during diastole. **C1** and **C2** - MPR on planes perpendicular to the centerline of the aorta respectively at the level of the most caudal (**C1**) and most cranial (**C2**) part of the metallic stent. In **C1** the pledgets used to reinforce the sutures on the suture ring are visible (**arrows**). The biological leaflets are attached to the frame and when closed have an appearance similar to a native tricuspid aortic valve (**C2, arrowheads**). **C3** - MPR parallel to the centerline of the aorta. **C4** - VR of the valve.

D1-D4 - CT aspect of a stentless biological valve. **D1** and **D2** - MPR on planes perpendicular to the centerline of the aorta at the level of the suture ring of the valve (**arrows**) showing the three closed (**D1**) and open (**D2**) leaflets (**arrowheads**). **D3** - More cranially, at the level of the coronary arteries ostia, the outer frame of the valve appears as small hypodense irregularities (**curved arrows**) of the aortic contour protruding in the lumen. **D4** - A MPR parallel to the centerline of the aorta shows the cusps of the leaflets (**arrowheads**), the outer frame of the valve (**curved arrows**) and the pledgets used to reinforce the sutures (**arrows**).

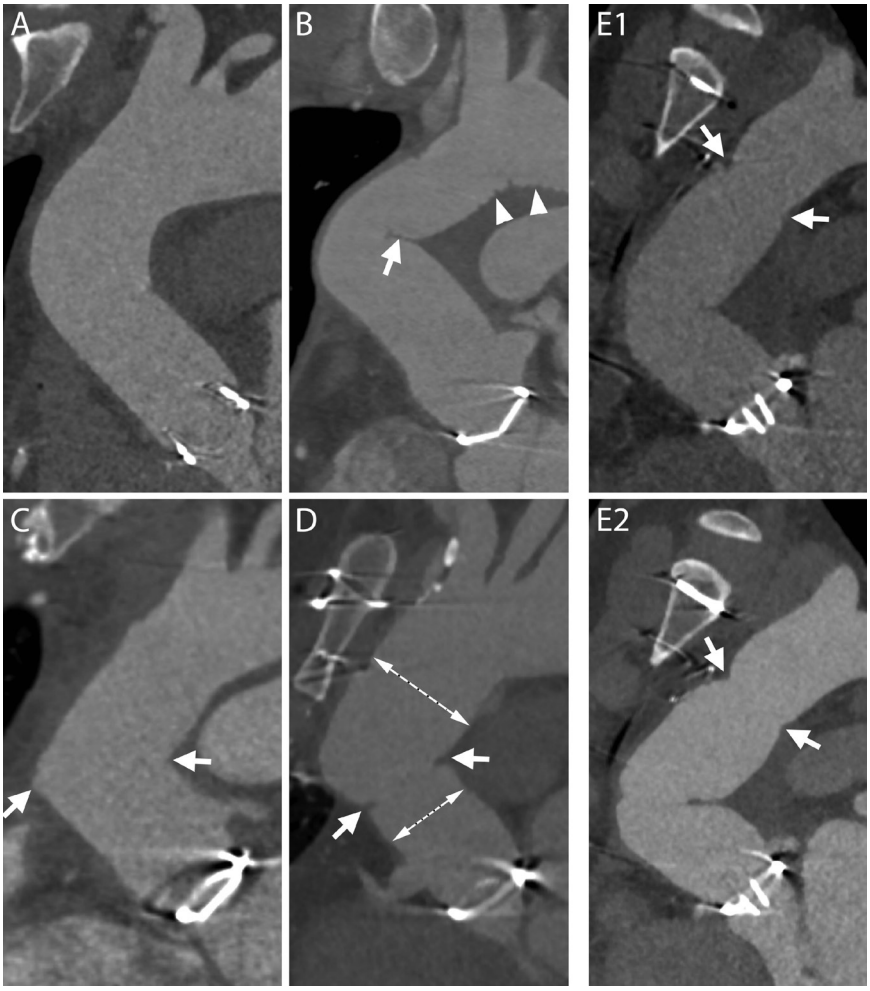

Figure 3. Normal aspect of aortic grafts

A - The aortic graft can present a smooth outer contour and appear similar to a native aorta.
B - Especially in case of a sharp angulation of the ascending aorta and in case a long graft has been employed, the fabric of the graft can present an inward fold projecting inside the aortic lumen (**arrow**). The small grooves of the outer surface of the graft can also be visible on CT scans (**arrowheads**).
C - When two grafts are employed, a sharp angle in the contour of the ascending aorta may develop at the level of the connection (**arrows**).
D - If needed for anatomical reasons, the two employed grafts can have different sizes (**two dashed lines**) and a slight inward fold is seen at the level of the suture (**arrows**).
E1-E2 - Two consecutive scans of the same patient, acquired within less than one year, show a change in angulation and appearance of the aortic grafts. The distal suture of the more caudal of the grafts with the native aorta is evident as it appears as a stricture in the aortic contour (**E1-E2**, **arrows**).

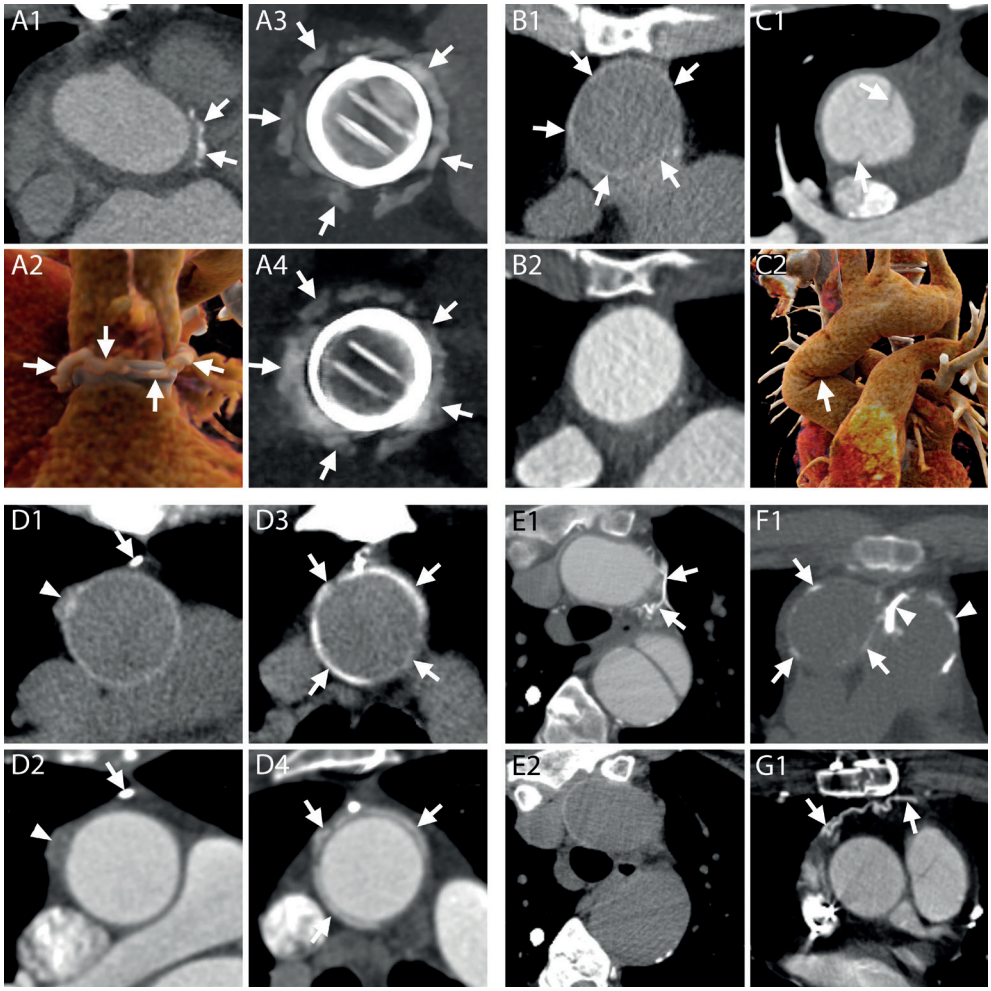

Figure 4. Surgical material and potential pitfalls

A1-A4 - CT appearance of pledgets. After a Bentall procedure or surgical aortic valve replacement, hyperdense material can be seen around the aortic root on axial images (**A1**, **arrows**). These hyperdense images represent pledgets that are employed by surgeons to reinforce the sutures on the suture ring of the valve and should not be mistaken for extravasated contrast. The material can be seen surrounding the junction of the LVOT and the aortic root (**A2, arrows**), at a short distance from the valvular ring (**A3, arrows**), although generally not all on the same plane (**A2**). An un-enhanced acquisition can be useful to assess the presence of the images also before contrast administration and confirm their nature (**A4 arrows**). **A1** – Axial image. **A2** - 3D reconstruction. **A3**-**A4** - MPR with maximum intensity projection reconstructions on planes perpendicular to the centerline of the aorta of enhanced and unenhanced acquisitions, respectively.
B1-B2 - CT appearance of the aortic graft. **B1 -** On unenhanced acquisitions, the aortic graft appears as a thin rim of hyperdense material (**arrows**). **B2 -** On contrast-enhanced acquisitions, the graft cannot be distinguished from the contrast in the aortic lumen. **B1-B2** - Axial images.
C1-**C2 -** At the level of the ascending aorta, one or two hypodense lines can be spotted in the aortic lumen (**C1**, **arrows**) of some post-Bentall scans. They should not be mistaken for new or residual

intimal flaps as they represent an inward fold of the graft that can be more easily identified on VR (**C2**, **arrow**) or MPR reconstructions (see panel B of **Figure 3**). **C1** - Axial image. **C2** - 3D reconstruction.
D1-D4 - Surgical material adjacent to the aortic graft. **D1-D2 -** Surgical material includes metallic clips with very high attenuation values (**D1** and **D2**, **arrows**) as well as other slightly hyperdense structures (**D1** and **D2**, **arrowheads**), usually placed at the cannulation sites, which are identifiable on unenhanced acquisitions (**D1**) but can hardly be distinguished from the adjacent periaortic tissue on enhanced acquisitions (**D2**). **D3**-**D4 –** PTFE can be employed to reinforce the distal suture line of the aortic graft and appears as hyperdense material surrounding the aorta (**D3** and **D4**, **arrows**), on both unenhanced (**D3**) and enhanced acquisitions (**D4**). **D1-D4** – MPR.
E1-E2 - It is not uncommon in these patients to have collateral vessels in the mediastinum that might fill with contrast (**E1**, **arrows**) and may therefore appear very hyperdense, making them easy to be mistaken for surgical material. Contrary to surgical material, the vessels are not visible on corresponding unenhanced slices (**E2**). **E1-E2, F1, G1** - Axial images.
F1 - Calcifications can appear on aortic grafts (**arrows**) implanted years before (in this case example the Bentall had been performed 12 years prior to the CT scan). Calcifications may also be seen at the level of the pulmonary valve (**arrowheads**) indicating a previous Ross procedure.
G1 - After the procedure the pericardium is generally left open and without sutures. However, in some circumstances, it can be closed with a patch of synthetic material (**arrows**).

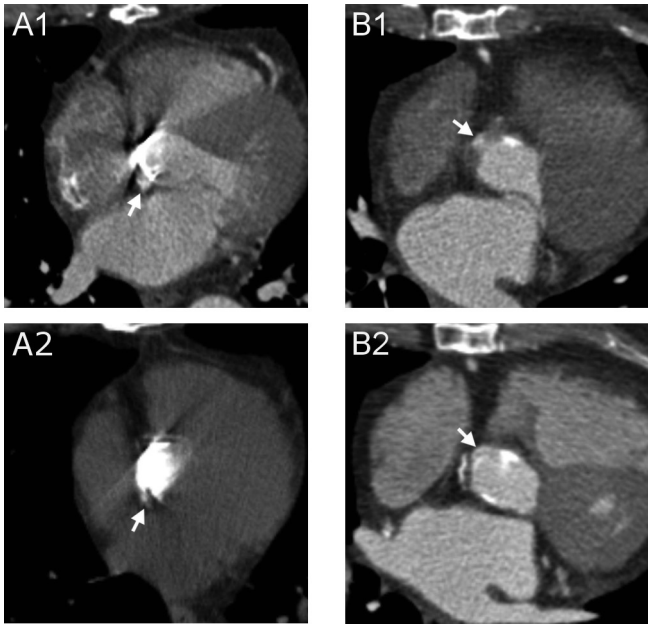

Figure 5. Differentiation between surgical and contrast material

A1-A2 - Surgical material adjacent to the prosthetic valve possibly mistaken for contrast medium. On enhanced acquisitions (**A1**), a hyperdense rounded structure situated in the close proximity of proximal (or distal) suture lines (**arrow**) could be interpreted as surgical material, particularly a pledget, or as extravasated contrast medium. However, on unenhanced acquisitions (**A2**) only surgical material is visible (**arrow**) and, therefore, hyperdense structures present in the same location on both acquisitions are attributed to exogenous matter employed during the Bentall procedure.
B1-B2 - Small pseudoaneurysm mistaken for surgical material. On a first postoperative scan (**B1**) an axial image of an enhanced acquisition showed a small hyperdense structure (**arrow**) close

to the aortic prosthesis that was not reported as it was mistaken for a pledget. In this case an unenhanced acquisition was not performed. The real eatiology of this structure was appreciated on a second enhanced exam (**B2**) where, due to changes in aortic orientation, it was clear that the structure (**arrow**) was in communication with the LVOT and should therefore be referred to a small pseudoaneurysm.

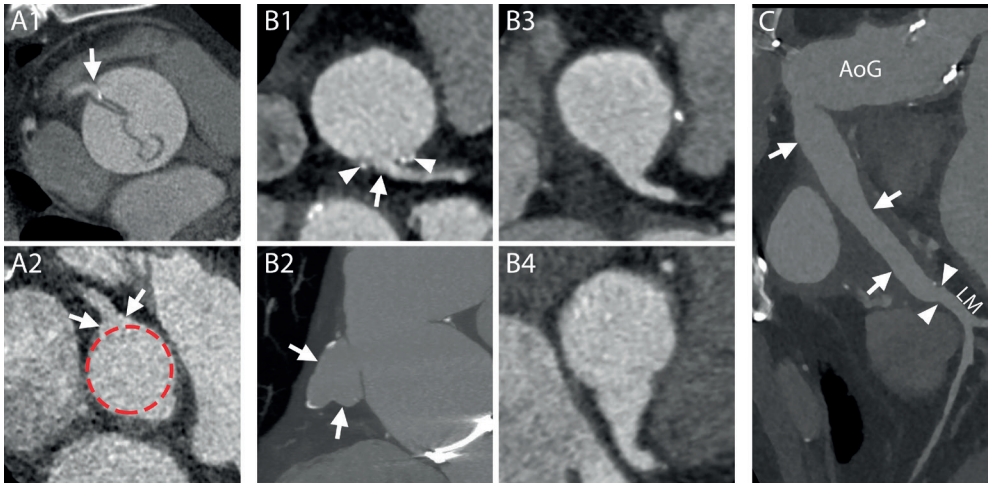

Figure 6. Normal aspect of coronary artery sutures and origin

A1-A2 - The most commonly practiced version of the Bentall procedure includes preservation of a "button" of native aortic wall around the coronary ostia that will be sutured to the aortic graft. Therefore, most commonly, even coronaries that before the operation had an abrupt origin from the aortic wall (**A1**, **arrow**) after the operation will show an enlarged emergence (**A2**, **arrows**) protruding from the circular profile of the graft (**A2**, **red line**) due to the additional tissue of the button of the native aorta. **A1-A2** - MPR perpendicular to the centerline of the aorta.
B1-B4 - B1 and **B2 -** Depending on the extension of the resected native aortic wall, the appearance of the new origin of the coronary artery can be very different, as shown in these two case examples: almost normal (**B1**, **arrow** at the origin of the left coronary artery) or very enlarged (**B2**, **arrows** at the origin of the right coronary artery). Surgical material can be seen at the level of the suture lines (**B1**, **arrowheads**). **B3** and **B4** - The shape of the origin can be different as well, and can have a "trumpet-like" (**B3**) or "flask-like" (**B4**) appearance. **B1, B3, B4** - MPR perpendicular to the centerline of the aorta. **B2** - MPR parallel to the centerline of the aorta.
C – A graft (**arrows**) can be interposed between the aortic graft (**AoG**) and the native coronary artery (**arrowheads**). In this case the procedure is referred to as "Cabrol procedure". Curved planar reformation (CPR).
AoG – aortic graft, *LM* – left main.

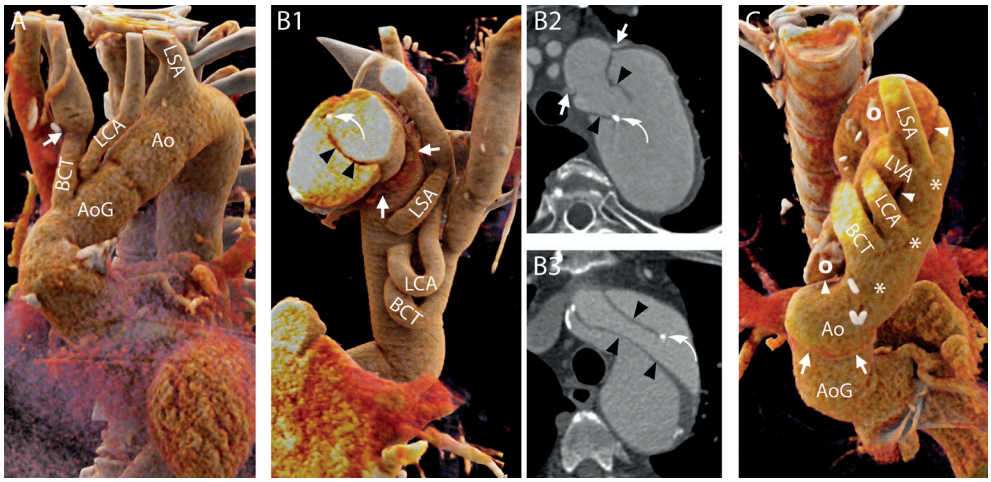

Figure 7. Normal aspect of the aortic arch and aortic branches

A – Hemi-arch replacement. In this patient, the aorta was replaced up to the mid-arch. Therefore, only the brachiocephalic trunk (**BCT**) and the left carotid artery (**LCA**) were "debranched" and re-attached to the aortic graft with the interposition of surgical grafts. In some cases, the level of the suture line along the aortic branches can be easily recognized due to the mismatch of caliber between the native vessel and the graft (**arrow**). On the contrary, the left subclavian artery (**LSA**) was left attached to the native aortic arch. 3D reconstruction.

B1-B2 and **B3** – Elephant trunk (**B1-B2**) and confounders (**B3**). In case the entire arch has to be replaced and the descending aorta is dilated to such an extent that further interventions are required, the "Elephant trunk" technique can be employed. During the first step of this procedure, the aortic arch is replaced and sutured to the native aorta, where the felt used to reinforce the suture can be seen on CT images (**B1** and **B2**, **arrows**), and the BCT, LCA and LSA are re-attached to the graft (**B1**). The most characteristic feature of the procedure is that the aortic graft has some additional fabric attached to the distal edge that is left floating freely in the lumen of the native aorta (thus the name "elephant trunk") and will guide and ease future interventions on the proximal descending aorta. The fabric appears on CT images as hypodense lines (**B1**-**B2**, **arrowheads**) that should not be mistaken for intimal flaps that might have an analogous aspect (**B3**, **arrowheads**). Although a metallic component is added to the distal end of the trunk to ease its visualization (**B1** and **B2**, **curved arrows**), intimal flaps can have similar looking calcifications (**B3**, **curved arrows**). **B1**- 3D reconstruction. **B2** and **B3** - axial images.

C – Residual dissection. Distal to the suture line (**arrows**) of the aortic graft the dissection can be left into place with its true lumen (**asterisks**) in continuity with the lumen of the graft. The aortic branches (including the independent origin of the left vertebral artery, **LVA**) all originated from the true lumen very close to the intimal flap (**arrowheads**) and the false lumen (**circles**). 3D reconstruction seen from above.

Ao – native aorta, *AoG – aortic graft, BCT – brachiocephalic trunk, LCA – left carotid artery, LSA – left subclavian artery, LVA – left vertebral artery.*

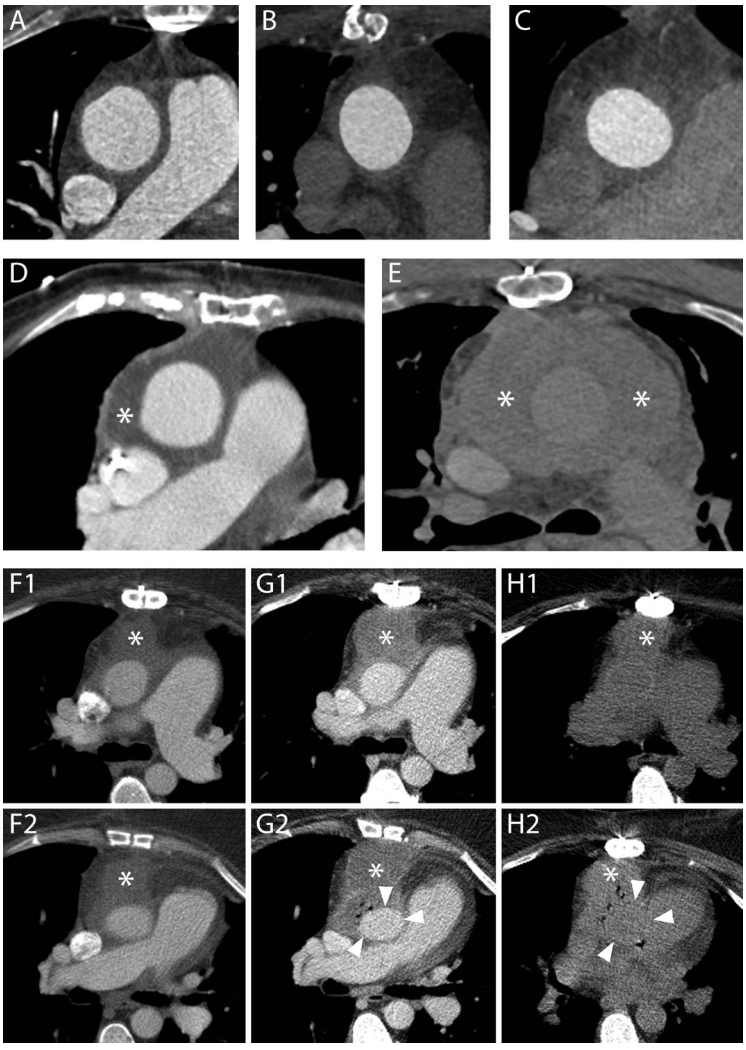

Figure 8. Peri-aortic fluid in the form of stranding and fluid collections

A-C – Three different cases showing increasing amounts of peri-aortic fluid in the form of stranding. The scans were performed 55 (**A**), 69 (**B**) and 59 (**C**) days after an uncomplicated operation, respectively. In all cases, the patients had undergone an uneventful procedure and did not have any complications within the first year following the operation.
D – A fluid collection with water-like content (**asterisk**) twelve days after a Bentall procedure in an 83-year-old woman. The patient was reoperated nine months later because of progressive dilation of the descending aorta.
E – The day after a Bentall operation for type A dissection extending to the right carotid artery, this 61-year-old man presented a reduction of hemoglobin levels that prompted to investigate the source of bleeding. A CT scan was performed which highlighted the presence of a hematoma completely surrounding the aorta (**asterisks**). The patient died two days later for neurological complications.
F1-H2 – A 53-year-old woman who had undergone a Bentall and a MAZE procedure four days before

started complaining of posterior chest pain at the level of Th7. A CT scan (**F1** and **F2**) performed for the suspicion of spondilodiscitis or mediastinitis demonstrated a fluid collection (**asterisks**) with water-like density surrounding the aortic graft. Three days later, the patient had high fever and a new CT scan was performed to locate the focus of infection. Axial images (**G1** and **G2**) showed an increase in diameter of the previously reported fluid collection (**asterisks**) that had, at that time, clear characteristics of an abscess with air bubbles inside and slight compression of the prosthesis (**arrowheads**). Appropriate antibiotic therapy was started. The day after an unenhanced CT scan (**H1** and **H2**) demonstrated an increase in the air content of the collection (**asterisks**) albeit with an overall reduction in size and a restoration of the normal aortic graft appearance (**arrowheads**). The following day, the patient was re-operated and the collection drained.

on the radiodensity (in HU) of its contents (water-like content, hematoma, contrast, contrast and hematoma together) (**Figure 8**). Although identifiable in the first months after the procedure, even in patients who underwent a successful operation without complications, fluid collections are more often associated with complicated procedures [11].

When infected, fluid collections may show CT characteristics of abscesses: wall enhancement, air inside the collection or fistula with other organs (**Figure 8**).

Complications

After Bentall procedures with mechanical valves, a pooled rate of early post-operative mortality of 5.6% and an event rate of reoperation of 1.01% per year have been reported [12]. Data on late mortality and complications are still lacking [12].

Valve

With an estimated cumulative incidence at 10 years of 26.6%, complications involving mechanical valves are among the most common [12]. Although traditionally investigated with transthoracic or trans-esophageal echocardiography, all complications at the level of the valve can be depicted with CT [13].

Mechanical causes of valve malfunctioning include the degeneration of the leaflets of biological valves and the presence of pannus/thrombus (**Figure 9**) [14]. Evaluation of these alterations is possible with ECG gated or triggered scans that reduce motion artifacts at the level of the valve and surrounding structures (**Figure 10**). Furthermore, ECG-gated acquisitions allow assessment of the dynamics of the valves and, for mechanical valves, the opening and closing angles of the leaflets, which have to be compared to normal values for that specific valve type [14].

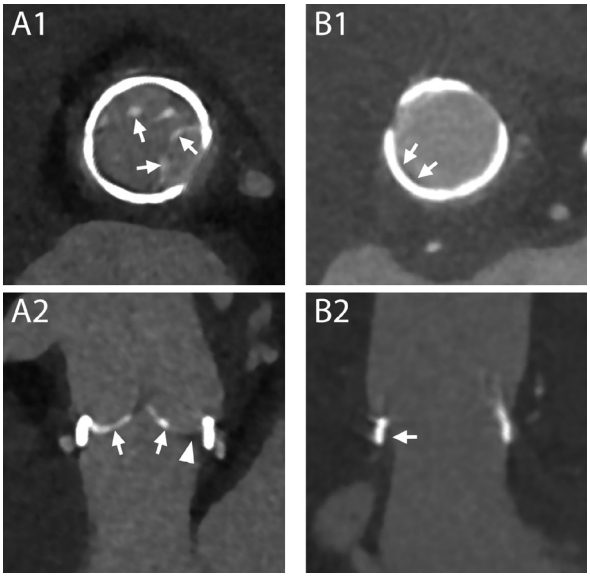

Figure 9. Mechanical alterations to aortic valve prosthesis function

A1-A2 – MPR reconstructions perpendicular (**A1**) and parallel (**A2**) to the centerline of the aorta demonstrating calcifications (**arrows**) and thickening (**arrowheads**) of the leaflets of a biological valve implanted 7 years before this scan in a 37-year-old man. The degeneration of the leaflets caused a severe, although asymptomatic, stenosis (4,5m/s at echo) and the valve was replaced a few months later.

B1-B2 – A follow-up CT scan in a 81-year-old woman revealed the presence of a thin rim of hypodense material (**arrows**) adjacent to the ring of this biological valve, which was implanted 4 months before, on both MPR reconstructions perpendicular (**B1**) and parallel (**B2**) to the centerline of the aorta. Although an infectious origin could not be ruled out with certainty based solely on CT characteristics, the laminated and smooth aspect of the material along the contour of the metallic ring indicated that it should more likely be ascribed to thrombus/pannus.

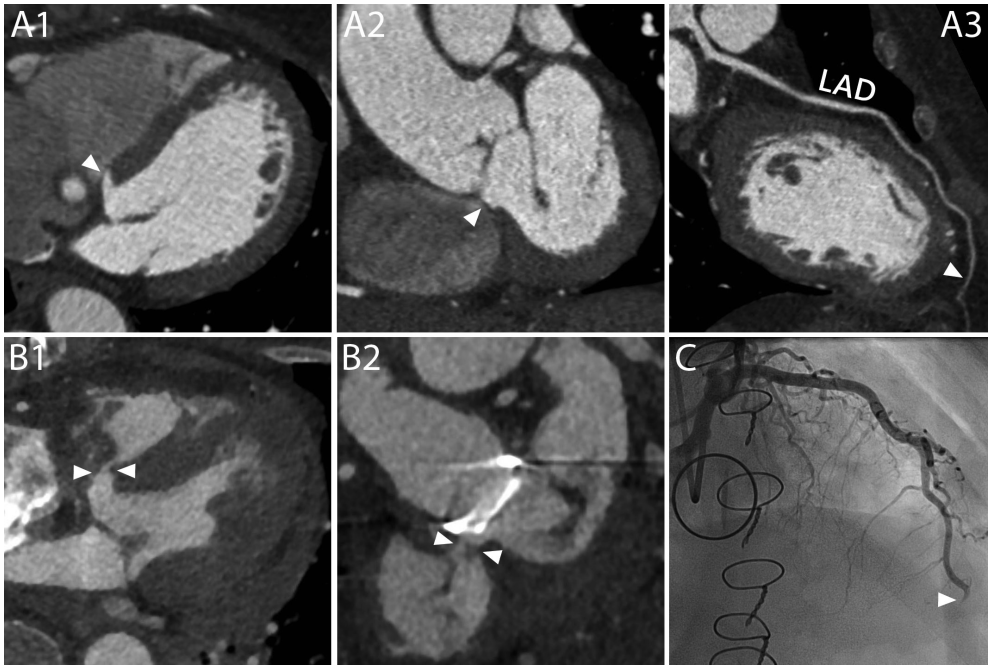

Figure 10. Small perforation of the membranous ventricular septum after resuscitation of a patient with a Bentall prosthesis due to an acute mid-LAD occlusion approximately 1 month after implantation

This 70-year-old female patient without prior history of coronary artery disease underwent a Bentall procedure for a dilated ascending aorta. At the last follow-up scan prior to the procedure, a distinct thin membranous part of the septum was clearly illustrated **(A1, A2, arrowheads)**. No signs of any concomitant coronary artery disease were found **(A3)**. One month after Bentall implantation, the patient experienced an acute ST elevated myocardial infarction (STEMI) with ventricular fibrillation, for which she was successfully resuscitated. An emergency CT scan didn't show any signs of aortic dissection, but did give the impression of a small perforation **(arrowheads)** of the membranous ventricular septum on the axial images **(B1)**, which became even more evident on the multi-planar reconstructions **(B2)**, possibly due to either the Bentall implantation or the resuscitation itself. Coronary angiography revealed a new mid-LAD occlusion **(C, arrowhead)** as the probable cause of the STEMI, but ensuing emergency PCI attempts failed. Although it is possible that a high Doppler signal over such a small perforation may have been overlooked, echocardiography did not show any signs of flow over the septum during follow-up, and the patient was discharged later on with good left ventricular function. *LAD* – left anterior descending artery.

Endocarditis at the level of the valve can cause the formation of vegetations attached to its structure (**Figure 11**) or mycotic pseudoaneurysms (**Figure 11** and **Figure 12**). While identification of voluminous pseudoaneurysms is relatively simple, millimetric ones could be easily missed or misinterpreted for surgical material. As mentioned above, the safest way to distinguish contrast media outside of the aortic lumen from surgical material is by comparing enhanced and unenhanced acquisitions (**Figure 5**). In case an unenhanced acquisition was not available, researching a communication between the vessel or left ventricular outflow tract and the suspected pseudoaneurysm by means of multiplanar reconstructions and comparing successive scans or acquisitions performed at different timing after contrast administration could be decisive (**Figure 5**).

The latter can be located cranially or caudally to the plane of the ring or involve both levels and cause paravalvular regurgitation.

The diagnosis of endocarditis, fundamental to avoid lethal consequences, remains difficult and is based on multiple criteria among which CT and [18]F-FDG PET are gaining an increasingly important role [15]. Images of [18]F-FDG PET can be fused with CTA images and provide information regarding the presence of active inflammatory processes, although results have to interpreted by an experienced multidisciplinary team to avoid pitfalls including those related to intake of carbohydrates before the examination, insufficient spatial resolution, cardiac motion, inflammation in recently implanted valves and prior use of surgical adhesives [15].

A rare complication after aortic valve replacement is the formation of a ventricular septal defect. Generally the perimembranous portion of the septum is involved. The aetiology of this perforation has been identified in iatrogenic disruption of the structure (**Figure 10**) and endocarditis [16, 17]. Treatment is required only for hemodynamically significant defects.

Coronary arteries

As mentioned, the dilated aspect of the coronary ostia is a normal finding after the operation and are not a complication [10]. The anastomosis of the coronary arteries is prone to leakages with pseudoaneurysms formation (**Figure 13** and **Figure 14**). Other more rare complications include stenosis and dissection of the ostia (**Figure 14**).

Aortic graft

The graft can be involved in (or surrounded by) infectious processes (**Figure 8**), hematomas (**Figure 7**), leakages from the sutures (including proximal and distal sutures and those between grafts) or combinations of the above (**Figure 15**).

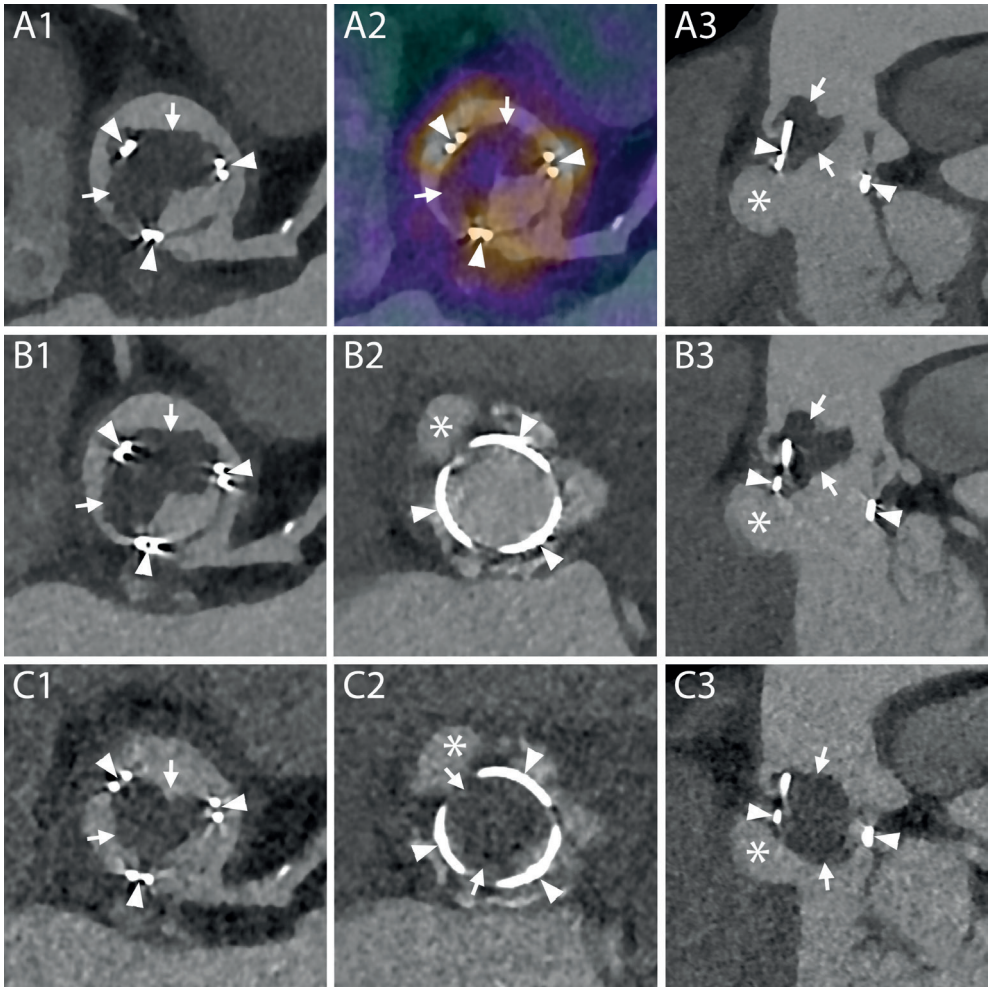

Figure 11. Endocarditis of a biological valve with a mass obstructing the aortic lumen of uncertain origin and a pseudoaneurysm in the LVOT

One year after having undergone a Bentall procedure for endocarditis, this 80-year-old man presented with fever and blood cultures positive for *S. Aureus* and *Candida parapsilosis*. A CT scan revealed the presence of a big hypodense mass (**A1**, **arrows**) attached to the structure of the valve (**A1**, **arrowheads**) and partially occluding the aortic lumen. A PET/CT, the images of which were fused with those of the CTA, demonstrated increased uptake of FDG at the level of the structure of the valve (**A2**, **arrowheads**) but not of the mass itself (**A2**, **arrows**). Therefore, doubts arose regarding the aetiology of the mass and whether it should be considered a vegetation (PET-negative because of incarceration of pathogen agents in the midst of fibrotic tissue and consequent lack of inflammatory response), a thrombus or a combination of the two. However, due to the positive PET exam and to the additional presence of a pseudoaneurysm (**A3**, **asterisk**) just below the valve (**A3**, **arrowheads**) and the mass (**A3**, **arrows**), which confirmed the occurrence of a destructive infectious process, the patient was treated with antibiotics and antifungals. Two weeks later a new CT scan was performed (**B1**-**C3**) with ECG-gating and reconstructions in both systole (**B1**-**B3**) and diastole (**C1**-**C3**). The new exam did not reveal any reduction in the size of the mass (**B1**, **B3**, **C1**-**C3**, **arrows**) which was still attached to the structure of the valve (**B1**, **B3**, **C1**-**C3**, **arrowheads**) and even

appeared slightly bigger. The pseudoaneurysm remained was unchanged in size (**B2-B3**, **C2-C3**, **asterisks**). Assessment of the dynamics of the mass during the cardiac cycle demonstrated partial obstruction of the aortic lumen during systole (**B1**-**B3**) with patent valve opening (**B2**, **arrows**) that was almost completely occluded during diastole with protrusion of the mass below the level of the metallic ring (**C2**-**C3**). The patient died 12 days later because of uncontrolled candidemia. **A1**-**A2**, **B1**, **C1** - MPR on planes perpendicular to the centerline of the aorta at the level of the left coronary artery. **B2**-**C2** - MPR on planes perpendicular to the centerline of the aorta at the level of the metallic ring of the valve. **A3**-**C3** - MPR on planes parallel to the centerline of the aorta.

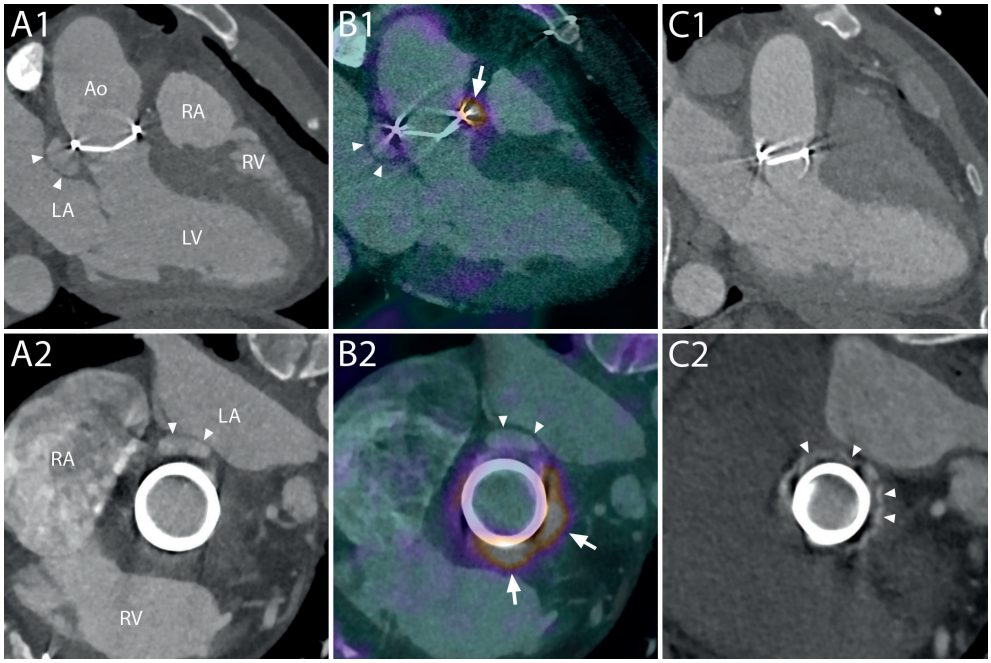

Figure 12. Endocarditis of a mechanical aortic valve prosthesis after Bentall procedure, with an aseptic perivalvular extension on fused ^{18}F-FDG PET–CT Angiography

A 47-year-old male patient who had undergone a Bentall-procedure for a dilated ascending aorta nine years before, was initially admitted for palpitations due to a new atrial flutter. Upon further questioning, it appeared he had been experiencing intermittent fevers over the previous weeks. Blood cultures were positive for a Gram-positive Streptococcus, and transesophageal echo revealed a small cavity close to the posterior annulus, which was found to be a perivalvular extension (i.e. pseudo-aneurysm) on subsequent CT angiography **(A1, A2, arrowheads)**. Interestingly, the ^{18}F-FDG PET/CT scan **(B1, B2, video 1)**, which is increasingly being used in patients suspected of prosthetic valve endocarditis and is now a new major diagnostic criterion according to the ESC Guidelines for infective endocarditis, revealed intense uptake of FDG around the entire annulus (after 12 days of intravenous antibiotics) **(arrows)**, except for the posterior part where the pseudo-aneurysm was located **(video 2)**. The patient was electively reoperated, the infected surgical material (including the perivalvular extension) removed, and a new composite valvular and aortic prosthesis was successfully implanted. Swab cultures of the valve and tissue of the pseudo-aneurysm showed no growth of any micro-organisms (after 22 days of intravenous antibiotics), and histopathology revealed only a slight chronic inflammation. Follow-up imaging **(C1, C2)** nicely showed the hyperdense felt pledgets around the new prosthetic valve, without any signs of endocarditis. *Ao* – aorta, *RA* – right atrium, *RV* – right ventricle, *LA* – left atrium, *LV* – left ventricle.

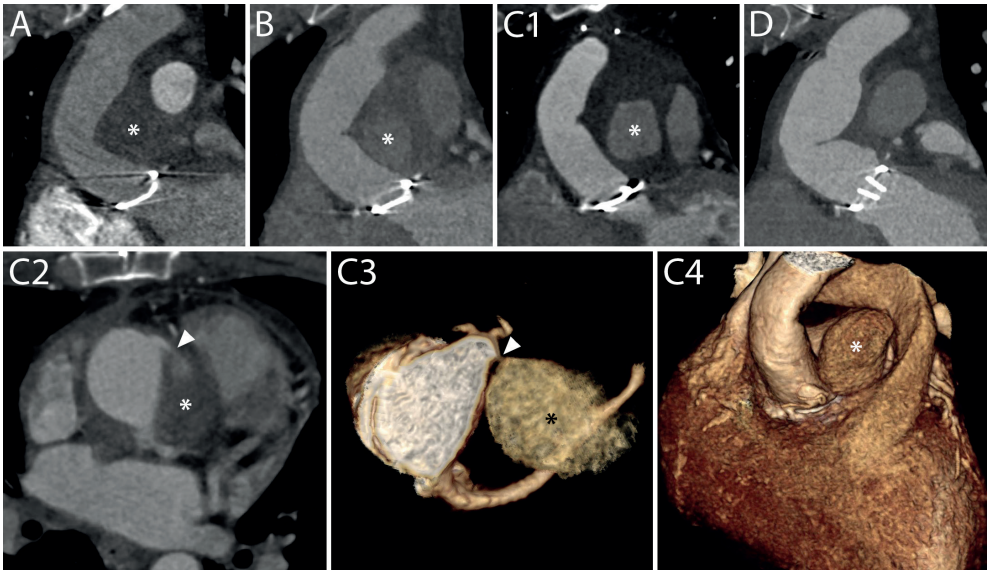

Figure 13. Gradually changing content of a pseudo-aneurysm after Bentall procedure due to contrast leakage from the right coronary anastomosis

A 30-year-old male patient who had undergone a Bentall procedure for acute Type-A aortic dissection three years before, was readmitted to the ER for acute chest pain. During routine yearly follow-up, a collection of fluid had been identified around the aortic root and ascending aorta, which, although its density had increased, had not changed in size **(A, B, asterisks)**. The routine clinical work-up at admission did not show any signs of acute myocardial infarction, but additional CT angiography **(C)** now showed a significant increase in size of the fluid collection, and clearly demonstrated the presence of contrast material inside **(C1, asterisk)**. A closer evaluation of the axial images **(C2)** revealed a "puff" of contrast emanating from the anastomosis of the right coronary button **(arrowhead)**, and the additional 3D volume rendering reconstructions highlighted this connection **(C3, C4, video 3, video 4)**. The pseudo-aneurysm was successfully removed during reoperation, as shown on a postoperative CT scan **(D)**, whereafter the leakage was macroscopically confirmed to originate from the anastomosis of the right coronary artery and could successfully be sealed.

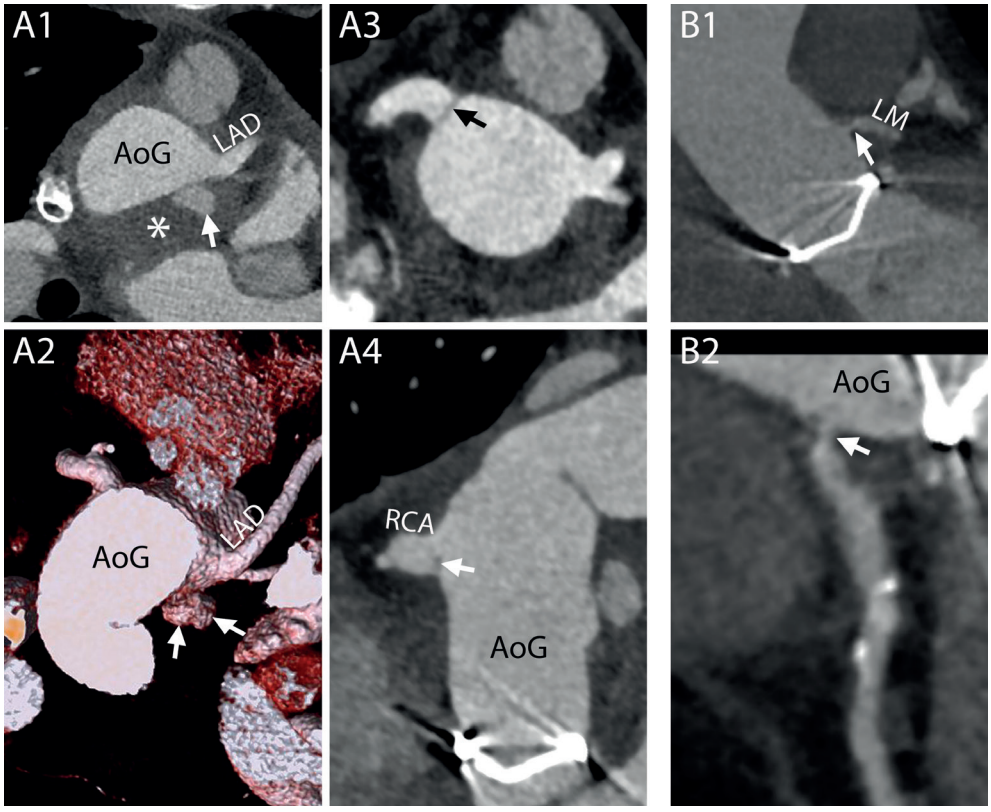

Figure 14. Complications at the site of coronary arteries anastomosis and ostia

A1-A4 – Different complications involving the two coronary arteries in the same patient. On a CT scan performed one month after a Bentall procedure, this 27-year-old man showed signs of complications at both coronary arteries. At the level of the suture line of the left main, a small collection of extravasated contrast material (**A1** and **A2**, **arrows**) surrounded by a hematoma (**A1**, **asterisk**) was identified. The right coronary artery, that had to be re-attached a second time to the aortic graft due to bleeding from the first suture, presented a hypodense line at the ostium (**A3** and **A4**, **arrows**) that could be attributed to a small intimal flap or to an inward fold of the graft. No invasive or surgical treatment was undertaken. **A1** - Axial mage. **A2** - VR. **A3** - MPR perpendicular to the centerline of the aorta. **A4** - MPR parallel to the centerline of the aorta.
B1-B2 – Stenosis of the coronary ostium. On a routine follow-up CT scan performed five months after the procedure, this 60-year-old man showed a stenosis of the left coronary artery (**B1** and **B2**, **arrows**). **B1** - MPR parallel to the centerline of the aorta. **B2** - CPR.
AoG – aortic graft, *LAD* – left anterior descending, *LM* – left main, *RCA* – right coronary artery.

CT is very sensitive for the detection of mediastinal collections and can provide some important elements to define their aetiology although with several limitations, especially in the differentiation of infectious processes. An overlap of CT characteristics between normal postoperative findings and endocarditis has to be expected. Clear signs of infection include the presence of a fistulous tract and the appearance or augmentation of wall enhancement and air within the collection. If a preceding scan is not available the latter are impossible to assess. However, as mentioned above, fluid encountered in patients who underwent uncomplicated procedures is usually in the form of stranding and completely surrounds the aorta. Therefore, any other appearance, namely the presence of a defined wall, focal extension around the aorta, wall enhancement and presence of air in the collection, although not pathognomonic by themselves especially in the very early postoperative period, should always warrant further investigation and follow up [11] While decisive in guiding the diagnosis if present, symptoms are often subtle and non-specific or can have a late onset when morphological damage is very advanced. Therefore, the absence of clinical complaints should not rule out the possibility of an ongoing infection. Although an [18]F-FDG PET-CT scan can provide additional information, the surgical adhesives used around the graft during surgery have been reported to be PET-positive and may result in misdiagnosis [15].

Fluid collections can dislocate and/or compress other adjacent structures. The risk is higher in case of collections with progressive increase of volume, such as hematomas, and multiple collections. The aortic graft and venous bypass grafts are particularly prone to this complication as they are completely encircled by the collection more frequently than other organs (**Figure 15**).

Native aorta

The native aorta and aortic branches should always be carefully assessed regarding the progression of the eventual residual dissection (**Figure 16**) and for the occurrence of any new complications such as a rupture, intramural hematoma or dissection. Aortic diameters should be measured on planes perpendicular to the long axis of the aorta and at predefined locations for all examinations [6].

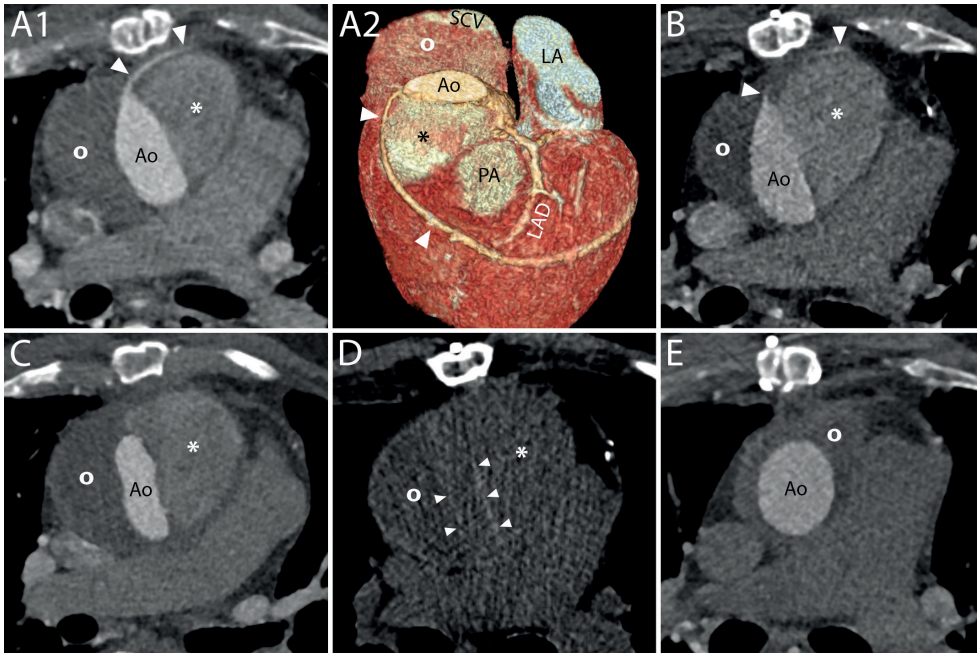

Figure 15. Loss of vein graft following combined Bentall and coronary artery bypass procedure due to progressive compression by two fluid collections

This 68-year-old male patient underwent a combined Bentall and coronary artery bypass procedure for a severely stenosed bicuspid aortic valve and concomitant three-vessel disease. Like most Bentall procedure performed at our institution, the interposition technique was used, implying that the native ascending aorta was excised and replaced by a vascular prosthesis (as opposed to the inclusion technique by which the aneurysm sac is closed around the vascular graft). Routine follow-up CT two months later **(A1, A2)** showed two fluid collections, one **(asterisk)** denser than the other **(circle)**, and both moderately compressed the aortic graft and encompassed but did not compress the vein graft **(arrowheads)**. Two follow-up scans were acquired four months **(B)** and 10 months later **(C)**, which did not show any distinguishable change in size of both fluid collections, but did reveal that the aortic prosthesis –and now also the vein graft **(arrowheads)**– had become compressed even further **(B, C)**, resulting in occlusion of the vein graft **(C)**. An additional non-enhanced scan **(D)** did not show any differences in density between the two fluid collections compressing the aortic graft **(arrowheads)**, indicating that the denser fluid collection **(asterisk)** had to have been partially filled with contrast on all previous contrast-enhanced scans. The patient was thereupon electively reoperated, the leaking right coronary artery button was resutured and the pseudo-aneurysm successfully removed, restoring normal aortic dimensions **(E)** and leaving only a small hematoma behind **(circle)**. *Ao* – aorta, *SCV* – superior caval vein, *LA* – left atrium, *PA* – pulmonary artery, *LAD* – left anterior descending artery.

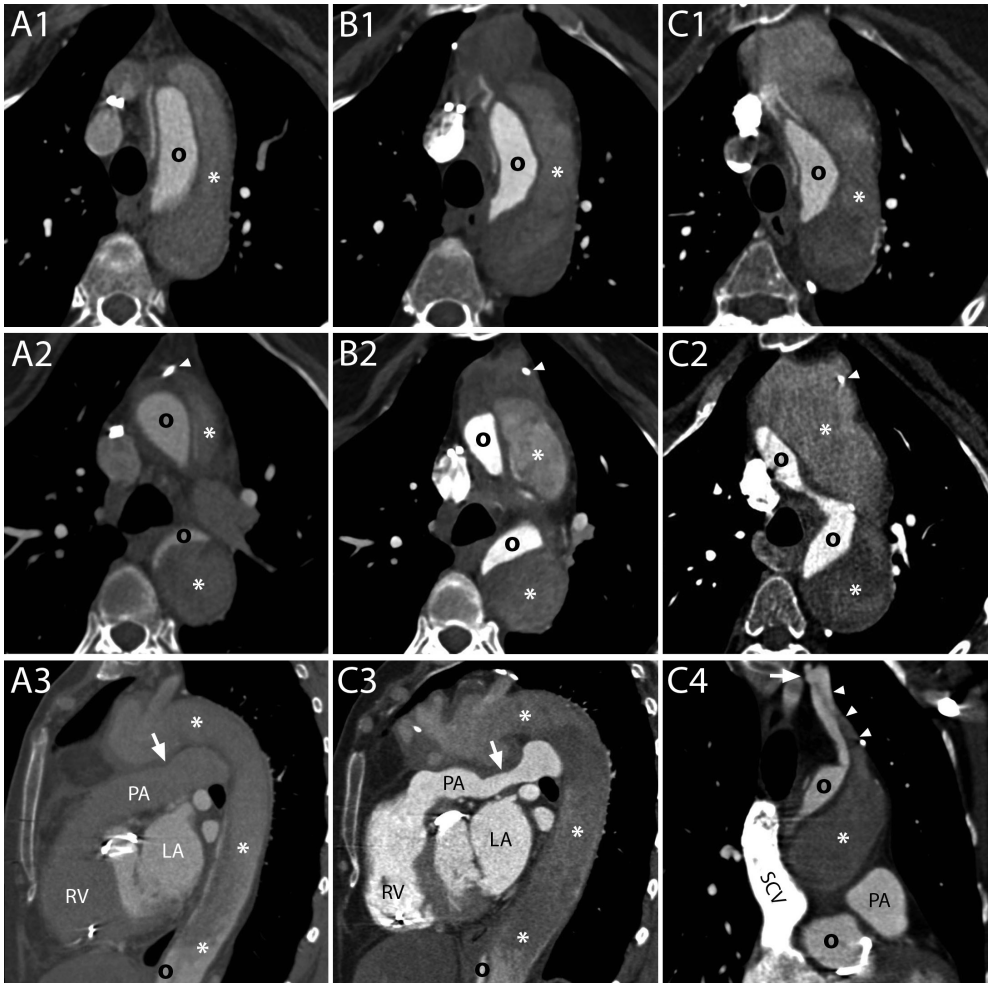

Figure 16. Natural history of a growing false lumen of a residual dissection after Bentall procedure for acute Type-A aortic dissection in a patient with Marfan's syndrome

This 63-year-old female patient with a family history of Marfan's syndrome underwent a Bentall procedure for acute Type-A aortic dissection at the age of 57 years. The first postoperative follow-up scan depicted a residual dissection of the aortic arch and descending aorta **(A)** with a large false lumen **(asterisk)** and a compressed true lumen **(circle)**. Over the ensuing 5 years, follow-up imaging showed a gradual enlargement of the persisting, partially thrombosed aneurysm sac directly distal to the aortic prosthesis, shown here at the level of the distal suture **(A1–C1)** and approximately 15mm below **(A2–C2, video 5)**, at the level of a metallic surgical clip **(arrowheads)**, clearly illustrating the anterolateral expansion of the outer aortic wall. After 5 years, the aneurysm sac had grown to approximately 6cm in diameter, no longer only compressing the true lumen but also the pulmonary artery **(A3, C3)**. One of the re-entry tears, through which the false lumen had been supplied with blood after surgical repair of the ascending aorta, was clearly depicted on the last scan **(C4)**, which distinctly showed a discontinuity of the intimal flap in the left subclavian artery at the level of the vertebral artery ostium **(arrow)**, where contrast was passing into the false lumen **(arrowheads)**. In the meantime, however, the patient had been diagnosed with a concomitant advanced stage malignancy, and was treated conservatively. *PA* – pulmonary artery, *RV* – right ventricle, *LA* – left atrium, *SCV* – superior caval vein.

Conclusions

After a Bentall procedure, CT is the imaging modality of choice for routine follow-up and to evaluate all complications. Whilst review of images with the surgeon is useful, it is fundamental for radiologists to be familiar with the surgical technique and materials employed to recognise the normal post-operative appearances and identify complications, thus avoiding misdiagnosis and unnecessary further examinations.

References

1. Bentall H, De Bono A. A technique for complete replacement of the ascending aorta. Thorax 1968;23.
2. Cherry C, DeBord S, Hickey C. The modified Bentall procedure for aortic root replacement. AORN 2006;84:52-70.
3. Kourliouros A, Soni M, Rasoli S, et al. Evolution and current applications of the Cabrol procedure and its modifications. Ann Thorac Surg 2011;91(5):1636-41.
4. Sundaram B, Quint LE, Patel HJ, Deeb GM. CT findings following thoracic aortic surgery. Radiographics 2007;27(6):1583-94.
5. Sundaram B, Quint LE, Patel S, Patel HJ, Deeb GM. CT appearance of thoracic aortic graft complications. AJR Am J Roentgenol 2007;188(5):1273-7.
6. Erbel R, Aboyans V, Boileau C, et al. 2014 ESC Guidelines on the diagnosis and treatment of aortic diseases: Document covering acute and chronic aortic diseases of the thoracic and abdominal aorta of the adult. The Task Force for the Diagnosis and Treatment of Aortic Diseases of the European Society of Cardiology (ESC). Eur Heart J 2014;35(41):2873-926.
7. Hiratzka LF, Bakris GL, Beckman JA, et al. 2010 ACCF/AHA/AATS/ACR/ASA/SCA/SCAI/SIR/STS/SVM guidelines for the diagnosis and management of patients with Thoracic Aortic Disease: a report of the American College of Cardiology Foundation/American Heart Association Task Force on Practice Guidelines, American Association for Thoracic Surgery, American College of Radiology, American Stroke Association, Society of Cardiovascular Anesthesiologists, Society for Cardiovascular Angiography and Interventions, Society of Interventional Radiology, Society of Thoracic Surgeons, and Society for Vascular Medicine. Circulation 2010;121(13):e266-369.
8. Quint LE, Francis IR, Williams DM, Monaghan HM, Deeb GM. Synthetic interposition grafts of the thoracic aorta: postoperative appearance on serial CT studies. Radiology 1999;211(2):317-24.
9. Svensson LG, Adams DH, Bonow RO, et al. Aortic valve and ascending aorta guidelines for management and quality measures. Ann Thorac Surg 2013;95(6 Suppl):S1-66.
10. Chwan Ng AC, Yiannikas J, Chiang Yong AS, Ridley L, Wilson MK, Kritharides L. Coronary ostial morphology after modified Bentall operation assessed with dual-source multidetector computed tomography. J Cardiovasc Comput Tomogr 2010;4(3):206-12.
11. Boccalini S, Swart LE, Bekkers JA, et al. Peri-aortic fluid after surgery on the ascending aorta: Worrisome indicator of complications or innocent postoperative finding? Eur J Radiol 2017;95:332-41.
12. Mookhoek A, Korteland NM, Arabkhani B, et al. Bentall Procedure: A Systematic Review and Meta-Analysis. Ann Thorac Surg 2016;101(5):1684-9.
13. Fagman E, Perrotta S, Bech-Hanssen O, et al. ECG-gated computed tomography: a new role for patients with suspected aortic prosthetic valve endocarditis. Eur Radiol 2012;22(11):2407-14.
14. Tanis W, Budde RP, van der Bilt IA, et al. Novel imaging strategies for the detection of prosthetic heart valve obstruction and endocarditis. Neth Heart J 2016;24(2):96-107.

15. Swart LE, Scholtens AM, Tanis W, et al. 18F-fluorodeoxyglucose positron emission/computed tomography and computed tomography angiography in prosthetic heart valve endocarditis: from guidelines to clinical practice. Eur Heart J 2018.
16. Ashmeik K, Pai RG. An unusual case of acquired ventricular septal defect as a complication of aortic valve endocarditis: echocardio- graphic delineation of multiple subvalvular complications in one patient. J Am Soc Echocardiogr 2000;13:693–695.
17. Holzer R, Latson L, Hijazi ZM. Device closure of iatrogenic membranous ventricular septal defects after prosthetic aortic valve replacement using the Amplatzer membranous ventricular septal defect occluder. Catheter Cardiovasc Interv. 2004;62:276–280.

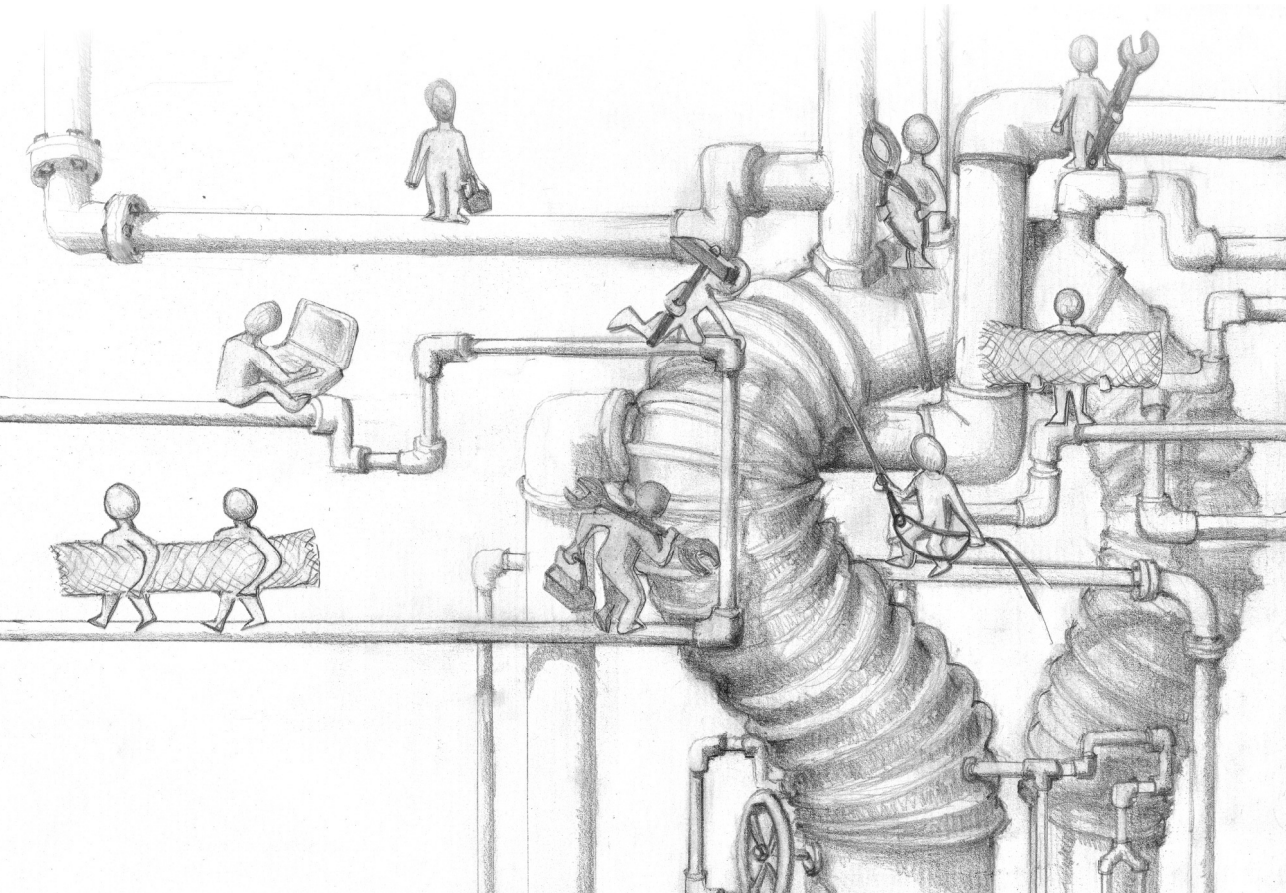

CHAPTER 8

Peri-aortic fluid after surgery on the ascending aorta: worrisome indicator of complications or innocent postoperative finding?

Sara Boccalini*, Laurens E Swart*, Jos A. Bekkers, Koen Nieman, Gabriel P Krestin, Ad JJC Bogers, Ricardo PJ Budde

Eur J Radiol. 2017 Oct;95:332-341

Abstract

Objective: The Bentall procedure is associated with several complications often accompanied by accumulation of fluid around the aortic graft. CT is the imaging modality of choice to detect these complications. Since these early complications are, however, not easily distinguished from physiological postoperative changes, our aim was to compare the appearance and amount of peri-aortic fluid on early CT scans following Bentall procedures with either an uncomplicated or a complicated course and follow-up.

Methods: Ninety-four scans performed within 3 months of a Bentall procedure were retrospectively included. Patients were divided into either the uncomplicated or the complicated group based on occurrence of Bentall-related complications or death up until 1-year after surgery. Diffuse fluid ("stranding") was distinguished from organized, more clearly delineated fluid collections such as haematomas, and was graded both subjectively and quantitatively.

Results: Forty-seven patients were assigned to each group. Stranding was found on most of the scans, both in the uncomplicated (7.7±3.9mm, range 0-17mm) and complicated (6.9±5.5mm, range 0-19mm) groups ($p=0.32$). There were, however, significantly more fluid collections (6 vs. 28; $p<0.001$), particularly haematomas (1 vs. 17; $p<0.001$), in the complicated group. When looking at isolated stranding, there was still no significant difference between the two groups (7.8±3.6mm vs. 9.2±3.7mm; $p=0.22$).

Conclusion: Isolated stranding of up to 17mm is a common finding on postoperative CT within three months of a Bentall procedure, regardless of the occurrence of complications during the procedure or within a 1-year follow-up. Fluid collections are more worrisome indicators of complications that may require closer monitoring.

Introduction

The so-called Bentall procedure consists of the replacement of the aortic valve and ascending aorta in a single operation[1]. The most common pathologies that require this kind of intervention are type A aortic dissections and large ascending aortic aneurysms with associated aortic valve stenosis or insufficiency.

This major intervention may lead to both peri- and post-procedural complications[2,3], of which some of the most fearsome and potentially fatal are infection of the aortic prosthesis and endocarditis. The imaging modality of choice to depict their occurrence is CT, which is also preferred for routine follow-up examinations.

Due to the extensive structural changes occurring during surgery, certain postoperative alterations can be expected, such as the presence of fluid and stranding in the adipose and soft tissue surrounding the prosthesis, especially in the earliest time period following the procedure. However, infections may show an analogous radiological appearance, resulting in diagnostic dilemmas. Moreover, in most cases the interpretation of the images cannot be guided by the patients' clinical information/presentation because post-operative CT scans are performed as routine follow-up in asymptomatic patients and, furthermore, complications such as endocarditis often present with no or generic symptoms. It is therefore of paramount importance for the radiologist to be familiar with the normal aspects and their physiological change as time progresses in order to be able to distinguish these from complications that need to be closely observed, treated with medical therapy or even a new intervention. Unfortunately, literature regarding normal postoperative CT features after Bentall procedures and their change over time is still limited.

To determine a normal reference, we have retrospectively assessed the appearance and amount of fluid surrounding the composite graft of the aortic valve and ascending aorta on CT scans performed within the first three months following both uncomplicated procedures and procedures with a complicated course or follow-up.

Material and Methods

Study population

In this single-center retrospective cohort study, for which a waiver was received from the local Medical Ethics Committee, patients were selected from a large database comprising 391 Bentall procedures performed in 388 patients in the period between August 2000 and February 2015. Through a search in their electronic files, 206 patients who had undergone at least one CT scan after the procedure were identified. In total, 417 postoperative scans were performed in these patients. Since most of the early complications of a Bentall procedure occur in the first three months[4–6] and this is when a reference of the spectrum of normal findings is most crucial, only patients who had undergone a CT scan during this period were selected for the purpose of this study. For each patient only the first scan performed within these three months was included in the analysis.

Complicated versus uncomplicated procedures

To determine the normal appearance and amount of peri-aortic fluid after a Bentall procedure, healthy patients with an uncomplicated follow-up had to be distinguished from patients who had experienced complications during or after the procedure. To accomplish this, all patient files were carefully analyzed and evaluated for strict criteria which had been postulated beforehand, in order to determine whether the procedure and follow-up had been uneventful: (a) the surgical report of the Bentall procedure itself mentioned no procedural complications, (b) the patient was discharged within 14 days of surgery, and was not reoperated upon (e.g. for bleeding or tamponade, infection, sternal dehiscence or other early complications) during this period, (c) the patient was neither readmitted for Bentall-related complications nor deceased within one year of the procedure, and (d) the CT-scan was not performed for suspicion of Bentall-related complications, but rather only as routine follow-up.

Patients who were reoperated upon were further divided based on whether the CT scan had been performed before or after the second procedure. A separate analysis was performed for the first subgroup but not for the second, due to the impossibility to ascribe the findings to either one of the operations. Unless stated otherwise, time was calculated in relation to the first operation.

CT scan assessment

All selected scans performed at our institution or an affiliated one, of which the images were readily available at our institution's PACS, were then retrieved and reassessed on a dedicated multimodality workstation (iSite Enterprise 4.1, Philips Healthcare, the Netherlands) by a blinded observer with over 4 years of experience in cardiovascular imaging. Firstly, several technical parameters of the scans were evaluated, including the

number of detectors of the scanner, the smallest reconstruction slice thickness with vascular or soft tissue kernel, and whether the scan had been gated electrocardiographically. Subsequently, the scans were systematically reviewed and scored with regard to technical image quality and the appearance and amount of fluid surrounding the ascending aorta using a predefined reference sheet. The observer had not been involved in the initial selection of scans and was blinded to the reported CT scan results, the request form and any other clinical data.

Overall scan quality was graded on a 5-point scale as 1. poor, 2. moderate, 3. reasonable, 4. good or 5. excellent, based mostly upon the presence of motion artefacts at the level of the ostium of the coronary arteries and ascending aorta, as well as on the extent of beam hardening and scatter artefacts due to any metallic components of the aortic valve prostheses. Key images exemplifying each quality grade are provided in figure 1.

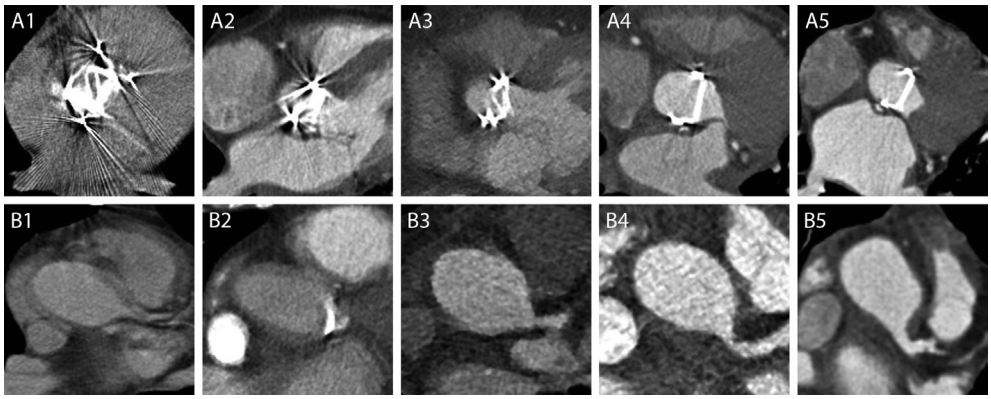

Figure 1

Rows **A** and **B**: Representative examples for the different CT quality grades, from poor (**A1**, **B1**) to excellent (**A5**, **B5**). The examples show axial images of different patients at the level of two of the most sensitive locations for grading purposes: the aortic valve prosthesis (**A1-5**) with the beam hardening and scattering artefacts, and left coronary artery ostium (**B1-5**) with motion artefacts.

Then, the periaortic fluid was categorized as stranding or a fluid collection based on its appearance. Stranding was defined as an encircling area of increased attenuation of the adipose tissue along the external edge of the aortic lumen, with ill-defined borders and an infiltrating appearance. Fluid collections were distinguished from stranding by their clearer, more regular delineation and their often-incomplete surrounding of the aortic circumference (figure 2).

Afterwards, we evaluated the amount of stranding, both subjectively and objectively. The overall quantity of the stranding extending in the adipose tissue surrounding the aortic prosthesis was subjectively graded with a 5-point scale as slight, mild, moderate or extensive. The scale was based both on the estimated volume of the stranding (determined

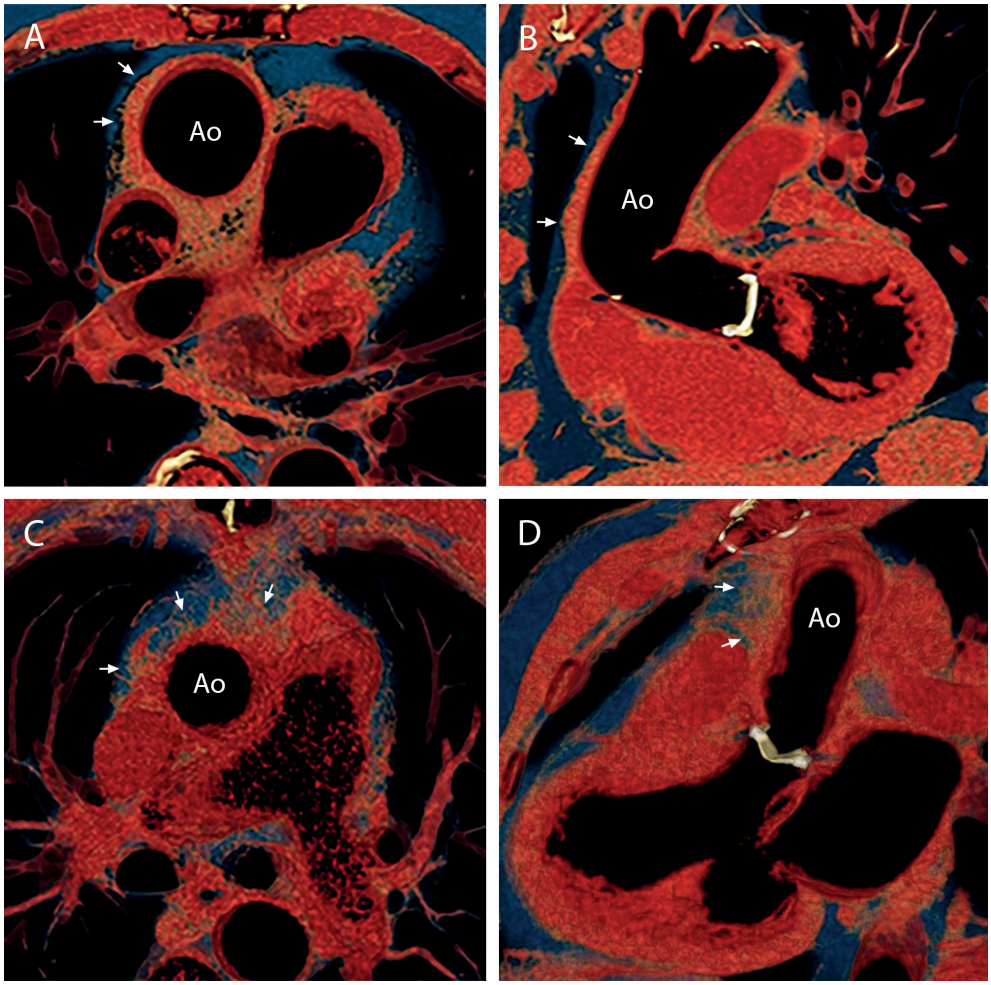

Figure 2

Distinguishing characteristics of fluid collections and stranding. Thin volume rendering technique (VRT) reconstructions on an axial (A) and a modified sagittal view (B) of a thin fluid collection localized along the anterolateral wall of the aorta (Ao) and characterized by sharply defined borders with the surrounding adipose and soft tissues (arrows). Thin volume rendering technique (VRT) reconstructions on an axial (C) and a modified sagittal view (D) of an example of stranding extending along all of the aortic circumference with ill-defined and irregular margins (arrows). **Figure 3** – Reference sheet for the different subjective grades of the amount of stranding. The panels show axial images of different patients at the level of the pulmonary trunk, demonstrating (**A1**) no stranding, (**A2**) slight, (**A3**) mild, (**A4**) moderate and (**A5**) extensive stranding.

by its farthest extension from the aorta at each level) and on the perceived proportion of fluid (vs adipose tissue) inside this volume. Figure 3 shows the reference sheet (compiled beforehand) based on which the scans were scored at the level of the pulmonary trunk. The thickness of the stranding was also objectively and quantitatively measured at the point of maximum extension from the inner border of the aortic wall on axial images as well as on multi-planar reconstructions (figure 4).

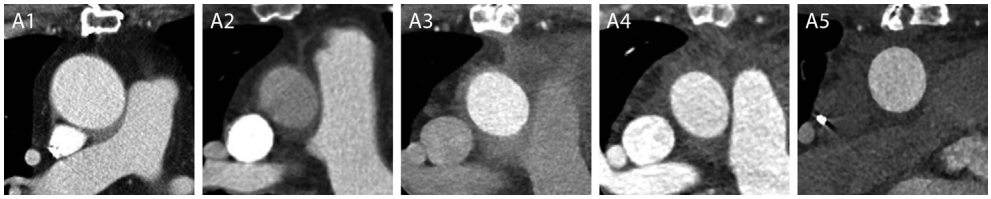

Figure 3

Reference sheet for the different subjective grades of the amount of stranding. The panels show axial images of different patients at the level of the pulmonary trunk, demonstrating (A1) no stranding, (**A2**) slight, (**A3**) mild, (**A4**) moderate and (**A5**) extensive stranding.

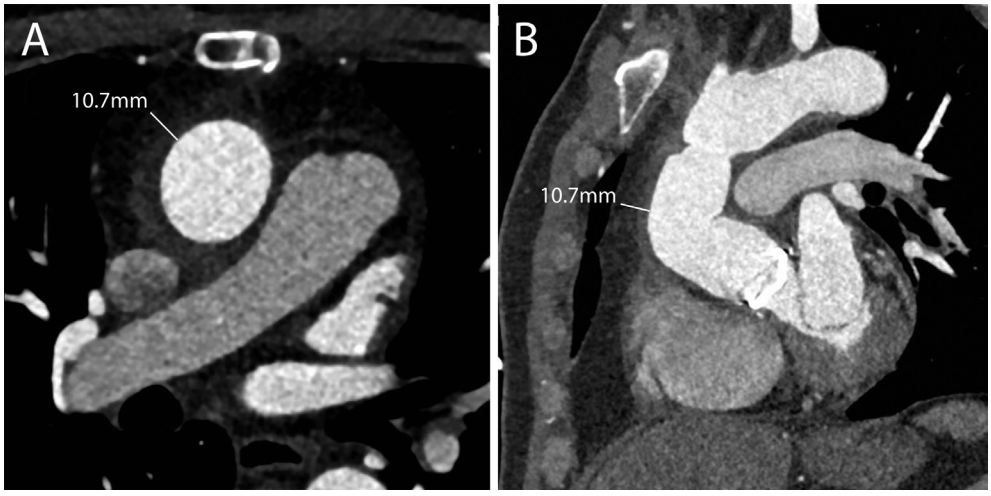

Figure 4

Quantitative assessment of peri-aortic stranding. Axial (A) and modified sagittal (B) views showing how measurements of stranding were performed at the point of its maximum extension from the inner border of the aortic wall.

The content of the fluid collections was derived from their attenuation and defined as fluid with a water-like density (0-35 HU), hemorrhagic (35-100 HU), contrast leakage (>100 HU) or contrast leakage with associated hemorrhagic content (figure 5). Wall enhancement of the fluid collections was separately scored, as well as whether there were air bubbles inside or other signs that resembled characteristics of an abscess, such as fistulous connections or extensions to adjacent anatomical structures. Fluid collections with a high density due to the presence of contrast were further categorized as suture aneurysms or pseudoaneurysms based on previously published criteria [2,7]. In case a fluid collection was surrounded by stranding (even if not entirely), they were both scored separately. Furthermore, because stranding surrounding a fluid collection is most likely a different entity, and because its shape and amount may have been influenced by the presence of that fluid collection, scans showing only stranding and no fluid collections (referred to as "isolated stranding") were also analyzed separately.

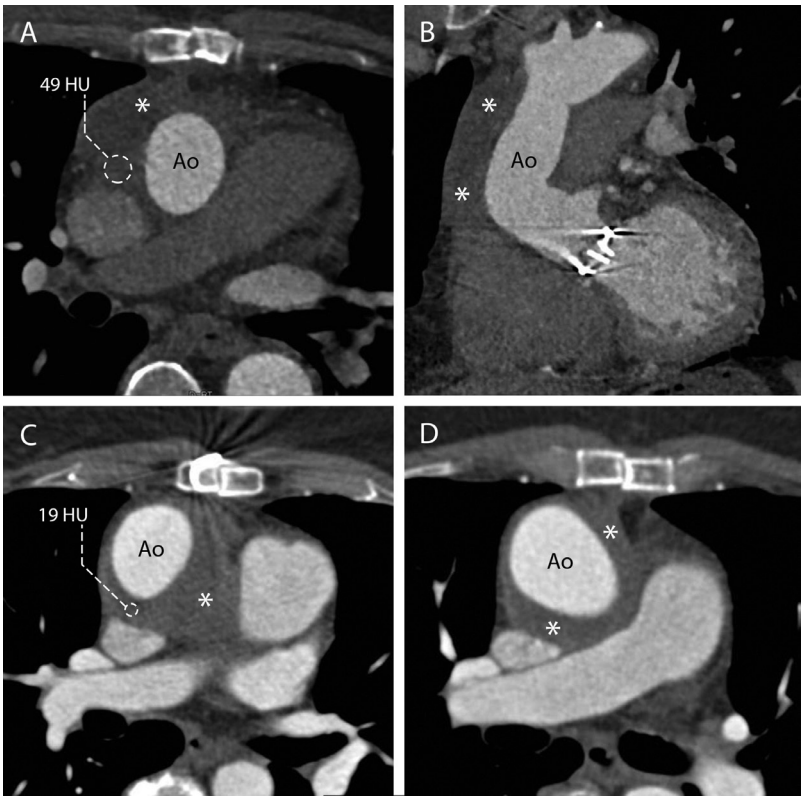

Figure 5

Differentiation of fluid collections. Axial (A) and modified coronal (B) views of a fluid collection (asterisks) with a high density content (49 HU lateral to the aorta) therefore classified as haematoma. Axial views at different levels (C, D) of a fluid collection (asterisks) with contents of a low water-like density (19 HU posterior to the aorta).

Particular attention was paid to the differentiation of stranding and fluid collections from other possible confounding findings such as residual thymus (especially in young patients), scars from previous surgeries and peri-aortic pericardial recesses filled with pericardial effusion. Furthermore, even in patients who did not undergo any surgical procedure involving the mediastinum, some stranding of the periaortic adipose tissue can be encountered. However, in these CT scans that were performed for unrelated reasons, stranding appears as thin lines and does not encircle the aorta. Exams with the just mentioned characteristics were considered to be without stranding for the purpose of this study.

The presence of other complications involving the prosthetic valve (vegetations and mycotic aneurysms) that could have possibly influenced the presence of fluid surrounding the aortic graft, was assessed as well.

Data collection and statistical analysis

All data retrieved from the surgical database and CT scan analyses were anonymized and registered into a secure online electronic database (MySQL, Oracle, Redwood Shores, CA, USA) that was tailor-made specifically for this study. For every scan inserted into the database, a web-based form was automatically created that comprised several fields for all the appropriate variables and findings.

For statistical analyses, SPSS version 22 (IBM Corp., Arbonk, NY, USA) was used. Besides descriptives, the independent t-test and Mann-Whitney U test were used to compare the complicated and uncomplicated patient groups regarding normally distributed and non-parametric variables and outcomes respectively. The Kolmogorov-Smirnov test was employed to test for normality of all involved continuous variables, including the amount of stranding in millimeters. To compare dichotomous variables such as the presence of fluid collections to the occurrence of complications, the Chi-Square test was employed. Finally, linear regression was used to analyze the course of stranding over time.

Results

Among the 206 patients with 417 postoperative scans in the database, 94 patients, who had been operated upon between March 2003 and February 2015, had received their first postoperative CT scan within three months of surgery (table 1).

Table 1. Patient population

	Uncomplicated(n=47)	Complicated(n=47)	Total(n=94)
Male	33(70%)	36(77%)	69(73%)
Age (mean, SD, range) in years	54.2±15.8(18-80)	55.5±14.9(22-83)	54.8±15.4(18-83)
Surgery indication			
- Aneurysm	34(72%)	24(51%)	58(62%)
- Dissection	3(6%)	11(23%)	14(15%)
- Other	10(21%)	12(26%)	22(23%)
Valve			
- Mechanical	41(87%)	45(96%)	86(91%)
- Biological	6(13%)	2(4%)	8(9%)
Postoperative hospitalization (mean, SD, range) in days	7.5±2.8 (4-19)	19.5±20.0 (5-110)	13.5±15.4 (4-110)

Patient classification

The scans of 47 patients were assigned to the complicated group for one or more of the following reasons (table 2): the post-surgical hospitalization period had been complicated by infection or extensive bleeding related to the procedure (n=29), a resternotomy for early bleeding/tamponade or infection (n=25) or even complete replacement of the Bentall graft (n=4) had been required due to Bentall-related complications; the patient had been readmitted because of Bentall-related complications (n=15), the patient had died (n=3) within 1 year of surgery, or the scan had been performed for clinical suspicion of Bentall-related complications (n=25). Among the patients who were reoperated, 5 underwent a CT scan before the second procedure (on average 38.25 days prior; in 4 cases within a time span of 6 days), which consisted of a replacement of the Bentall in three cases. The remaining 47 scans had all been acquired as routine clinical follow-up in patients who had experienced an uncomplicated procedure and uneventful 1-year follow-up.

Table 2. Occurrence of complications

Complication	Occurrence(n=94)*
- Complicated postoperative hospitalization	29(31%)
- Early re-sternotomy for bleeding or infection	25(27%)
- Reoperation on, or replacement of the Bentall graft	4(4%)
- Readmission within one year of surgery for Bentall-related complications	15(16%)
- Death within one year of surgery	3(3%)

*The occurrence of complications is reported relative to the total number of patients included. It is possible for one patient to have experienced multiple complications (e.g. complicated postoperative hospitalization and early re-sternotomy).

Time distribution and technical parameters

These examinations acquired in the uncomplicated group were mostly obtained in the second and third postoperative months (range 28-89 days, figure 6), as this is when routine follow-up is usually performed in our center. The scans in patients who experienced either a complicated procedure and/or follow-up were obtained at points in time more evenly spread throughout the entire 3-month postoperative period (range 1-90 days, figure 6), most notably because scans performed for suspicion of early Bentall-related complications (i.e. bleeding/tamponade and infection) were often acquired in the first weeks following the procedure.

Fifty-five (59%) scans were ECG-gated, and all scans were contrast-enhanced. Over the years, several scanners with different technical specifications were employed: 4 slice (1 scan, 1%), 16 slice (11 scans, 12%), 40 slice (1 scans, 1%), 64 slice (26 scans, 28%), 128 slice (44 scans, 47%) and 192 slice (11 scans, 12%). Average reconstruction slice thickness was 1.5±1.5mm (range 0.75-8mm).

Image quality

Overall image quality was reasonable to good, with an average quality of 3.2±1.0 (scale from 1 to 5). Five (5%) and 22 (23%) scans were graded as poor and moderate quality respectively, mostly due to scatter artefacts and motion of the ascending aorta. The remaining 67 scans were all of reasonable (22 scans, 23%), good (43 scans, 46%) or even excellent quality (2 scans, 2%). The quality score was higher in the uncomplicated group (3.5±0.78, median 4) than in the complicated (2.8±1, median 3; $p<0.001$), most likely due to a more frequent employment of the ECG-gating in the uncomplicated group (37 scans, 79%) than in the complicated group (18 scans, 38%; $p<0.001$).

Stranding

Stranding was, to some extent, present in all but two of the patients (96%) in the uncomplicated group (table 3). The subjectively graded amount of stranding in these patients ranged from none (2 scans, 4%) to moderate (6 scans, 13%), with most scans showing only slight (22 scans, 47%) or mild (17 scans, 36%) stranding around the aortic circumference. The maximum measured extent of stranding reaching out from the inner border of the aortic wall in these patients was 17mm, while on average there was 7.7mm ±3.9mm of stranding, with 43 scans (91%) showing more than 4mm and less than 15mm of stranding. On the two scans that did not show any stranding, a fluid collection was identified (see below).

Table 3. Comparison of findings on CT between patients with uncomplicated and complicated procedure/follow-up

	Uncomplicated(n=47)	Complicated(n=47)	
Stranding grade			p=0.23
- none	2(4%)	12(26%)	
- slight	22(47%)	15(32%)	
- mild	17(36%)	12(26%)	
- moderate	6(13%)	7(15%)	
- extensive	0(0%)	1(2%)	
Stranding (mean, SD, range) in mm	7.7±3.9 (0-17)	6.9±5.5 (0-19)	p=0.32
- Isolated stranding*	7.8±3.6 (2-17) [n=38]	9.2±3.7 (4-14) [n=17]	p=0.22
Fluid collections	6(13%)	28(60%)	p<0.001
- Hematoma	1(2%)	17(36%)	p<0.001
- Abscess	0(0%)	2(4%)	p=0.25
- Water-like density	5(11%)	9(19%)	p=0.19
Other			
- Suture-aneurysms	4(9%)	2(4%)	p=0.34
- Pseudo-aneurysms	0(0%)	2(4%)	p=0.25

*Excluding stranding around fluid collections and pseudo-/suture- aneurysms

In the complicated group on the other hand, no stranding was found in 12 patients (26%). However, in all of these 12 patients a fluid collection was identified. The results of the subjective assessment of the amount of stranding are the following: fifteen scans (32%) showed slight stranding, 12 scans (26%) mild, 7 scans (15%) moderate and 1 scan (2%) showed extensive stranding. No statistically significant difference could be found in the subjectively graded amount of stranding between patients with a complicated and an uncomplicated procedure (p=0.22). The maximum measured extent of stranding in these patients was 19mm, with an average of 6.9mm ±5.5mm of stranding, which was not significantly different from the uncomplicated group (p=0.32).

When excluding all scans with fluid collections (since these may have influenced the amount –and reliability of the measurements– of stranding), 38 scans (81%) in the complicated group and 17 scans (36%) in the uncomplicated group showed isolated stranding. The isolated stranding averaged 7.8mm ±3.6mm in the uncomplicated group, and 9.2mm ±3.7mm in the complicated group (p=0.22).

Overall, when considering the measurements performed on the scans of all the included patients (in-patient analysis was not possible as only the first scan of each patient was included), there was a non-significant downward trend in the amount of isolated stranding

over time, both in the complicated and uncomplicated group (uncomplicated: R^2 =0.02, p=0.39; complicated: R^2 =0.03, p=0.51) (figure 6).

In the five scans performed before a reoperation, stranding was not present in one case (20%), and had an average extension of 12±4,5 mm in the remaining four patients. Only in one case (20%) the stranding was isolated.

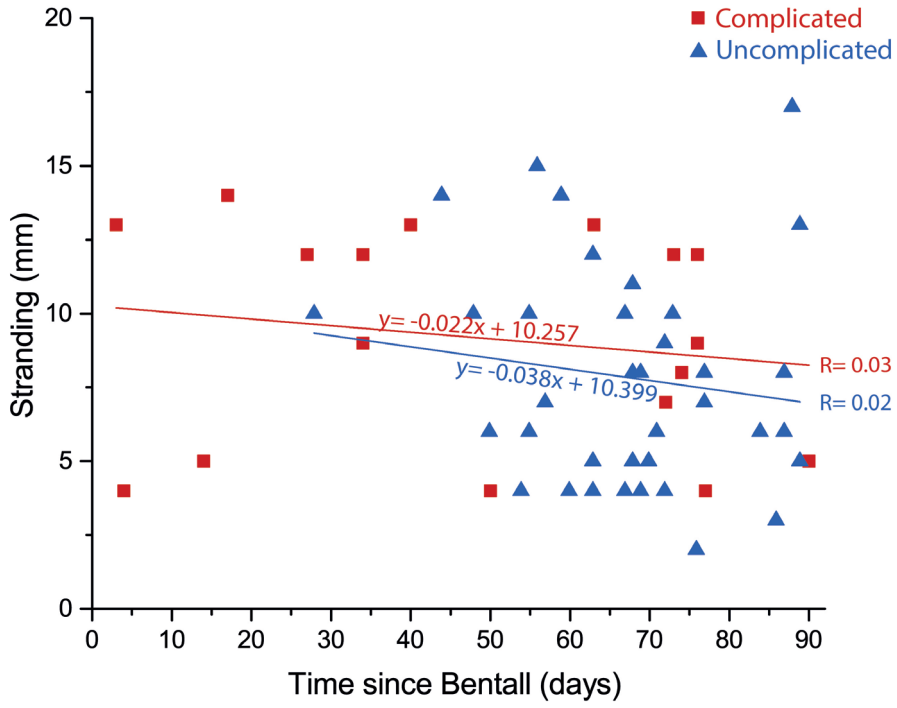

Figure 6

Distribution of time between scans and surgery (days) and measured stranding over time (mm) in uncomplicated (blue triangles, R^2= 0.02) and complicated (red squares, R^2= 0.03) patients. Neither trend was statistically significant.

Fluid collections

In total, 34 fluid collections were identified: 6 in the uncomplicated group (13%) and 28 in the complicated group (60%; p< 0.001). Most of these fluid collections (18) could be classified as haematomas, while 14 of them were classified as having contents with a water-like density and 2 collections showed characteristics of an abscess (table 3).

Almost all haematomas were identified in patients in the complicated group (1 vs. 17; p<0.001), whereas fluid collections with a water-like density were found in both groups (5 vs. 9; p=0.19). The one haematoma found in the uncomplicated group was identified on a scan that was acquired 66 days after the Bentall procedure and had a maximum diameter of approximately 26mm. The reporting radiologist considered it to be a normal residual hematoma at that time, and the patient did not experience any complications during the ensuing 1-year follow-up period, yet no follow-up scans were performed. No abscesses were found in the uncomplicated group (0 vs. 2; p= 0.25).

Some suture-aneurysms were found in both groups (4 vs. 2; p= 0.34), but only in the complicated group there were 2 pseudo-aneurysms (p= 0.25), one of which was reoperated upon shortly after the CT scan, whereas the other one was deemed to be a residual pseudo-aneurysm after extensive S. aureus endocarditis.

One of the abscesses involved the valvular plane and was therefore classified also as a mycotic aneurysm. With the limitations inherent to the image quality of the scans and the lack of ECG gating of part of the scans, no vegetations of the aortic valve were found.

Finally, in the group of reoperated patients with a scan performed before the second procedure one collection with water-like density and three hematomas were found. One patient had both a hematoma and a pseudoaneurysm.

More than half of the fluid collections were accompanied by slight to moderate stranding, but in 14 scans no distinct stranding was identified besides or surrounding the fluid collection. There were no scans with neither stranding nor a fluid collection: all 94 scans showed some form of fluid around the Bentall prosthesis.

Discussion

The principal finding of this study is that peri-aortic stranding is a normal postoperative phenomenon which occurs to some extent in nearly every patient following surgery on the ascending aorta, and does not necessarily warrant clinical vigilance in a patient without symptoms of bleeding or infection. We found that stranding extending up to 17mm from the aortic circumference is a common finding on CT imaging during the first three postoperative months in both healthy patients who did not experience any complications during a 1-year follow-up period and in patients with a complicated procedure or follow-up. No differences in the amount of isolated stranding were found between the patients who experienced complications and those who did not. On the contrary, fluid collections, while being a relatively common finding on routine CT follow-up after uncomplicated

procedures, were more frequently observed and showed more worrisome characteristics in the group of complicated procedures.

Peri- and post-procedural complications may occur after a Bentall procedure. The rate of early post-procedural complications varies greatly depending on the preoperative diagnosis and clinical setting[5,8], and can be divided in those related to thoracic surgery in general and those specific to the Bentall procedure. The latter include pseudo-aneurysms, suture aneurysms, leakages, valve regurgitation or obstruction, aortic graft infection and endocarditis. The clinical relevance of these complications may vary, ranging from self-limiting to life-threatening situations that require immediate pharmacological or surgical treatment as in the case of infection and endocarditis. Since clinical presentation and time of onset after surgery are also variable, the diagnosis of complications often relies on imaging findings. Therefore, most related guidelines suggest regular follow-up by means of imaging -even in the absence of symptoms-, although there is no general consensus regarding the most appropriate timing[5,9,10]. Preceded by transthoracic or transesophageal echocardiography, the method of choice to investigate post-Bentall patients is CT, which allows for a complete assessment of the aorta (along its entire tract, if necessary) as well as of the thorax.

However, due to the complexity of these procedures and the unique anatomical and functional features of the structures involved, morphological changes related to the physiological postoperative inflammatory response, haematoma reabsorption and an immunologic reaction to the aortic graft[11] without any pathological meaning can also be expected. The envisioned CT appearance of these post-procedural changes in the adipose and soft tissue surrounding the aorta may mimic that of worrisome complications such as infectious processes. This could result in either overestimation of the severity of the situation –caused in fact by a physiological process- and subsequent unnecessary investigations and therapy, or in misdiagnosis of potentially fatal complications.
These physiological changes due to the operation are expected to diminish over time; therefore, it is in the early postoperative period that the distinction with complications is expected to be more complex and a reference of normal findings is necessary. Thus, we focused our investigation on the first three postoperative months which, moreover, coincide with the time span when most early complications have been reported [4–6]. Accordingly, notwithstanding the absence of consensus on the optimal follow-up timing, different guidelines suggest that the first imaging exam should be acquired within the first three months [9,10].Although several investigators have reported the presence of stranding or collections of fluid around the aortic graft, to the best of our knowledge there is still no clear indication of what should be considered to be within acceptable limits. Sundaram et al.[11] regarded the presence of low-attenuation material with a thickness greater than 10mm adjacent to the graft as a complication, despite the fact that, in their

study, 10 out of the 20 patients with this finding were completely asymptomatic and demonstrated an otherwise uneventful follow-up. However, since three patients in this series had a proven graft infection and in five cases one was suspected, the presence of low attenuation material surrounding the aortic graft was later considered by others to have the potential to become a site of infection[12,13]. In Sundaram's study, low-attenuation material with a thickness of less than 10mm was considered normal, and these scans were not included in the study. On the other hand, Valente et al.[14] suggested an unsubstantiated upper limit of 15mm as a normal thickness of peri-aortic fluid. Quint et al.[15] reported on the presence of unspecified material adjacent to or surrounding the aorta in 74 out of 82 patients who had a CT scan in a time period of 6 months after aortic surgery. The maximum diameter of this material ranged from 4 to 80mm. Unfortunately, the authors did not specify whether any of these patients experienced any symptoms or complications. Fagman et al.[16] investigated the accuracy of aortic wall thickness as a sign of endocarditis in patients who underwent aortic valve replacement. All dense structures adjacent to the posterior side of the aortic lumen at the level of the left atrium, where measurements were performed, were considered to be constituents of the aortic wall. Their findings showed that, in the first three months after the operation, a cut-off value of 5mm has a sensitivity of 57% and a specificity of 67% for endocarditis.

Our study was designed to distinguish the scans of patients with relevant complications related to the procedure from those performed in patients with an uneventful follow-up, and to compare the appearance and amount of fluid surrounding the aortic graft between these two groups of patients. Therefore, for the first time, the correlation between the CT characteristics of periaortic fluid in the first three postoperative months and complicated Bentall procedures was systematically investigated based on predefined parameters. In addition, in our study, the scans were not excluded nor assigned to either one of the two groups based on the CT findings.

Criteria for the definition of a complicated procedure did not include symptoms and/or clinical presentation for two main reasons. First, in these patients the absence of a clear correlation between symptoms and complications (and even gravity of complications) is a matter of fact acknowledged by guidelines that, therefore, suggest to perform routine follow-up with imaging techniques in this population [10]. Routinely imaging post-operative patients implies that a large number of scans are performed in asymptomatic patients with no clinical suspicion of complications. Second, endocarditis and leakages can be asymptomatic (especially in the early phases) or manifest with generic symptoms while determining massive structural damages that need to be promptly treated. Hence, the diagnosis of endocarditis is based on the combination of multiple criteria [17]. Therefore, since many CT scans are performed as routine follow-up and the absence of symptoms does not guarantee that the patient is free from complications at the time of

the exam, we investigated the correlation between CT findings and complications and not with symptoms.

On top of all the scans that were assigned to the complicated group because the patient experienced a complicated procedure or 1-year follow-up, we additionally assigned any scan that was not performed as routine follow-up to the complicated group (i.e. any scan that was performed for suspicion of Bentall-related complications). In our case series, only 25 patients had a suspicion of Bentall-related complications at the moment of the CT examination. Furthermore, scans performed after reoperations (including second Bentall procedures) were also assigned to the complicated group (even if this reoperation had been uneventful) due to the impossibility to ascertain the date of appearance of any findings. For the same reason and due to the variety of the reoperations with subsequent different degrees of manipulation of the periaortic tissues and aortic graft, the exams performed after a second operation were not analyzed separately. The absence of statistically significant difference in the amount of stranding (based on both the subjective and objective scoring) between the uncomplicated and the complicated group, notwithstanding the fact that the latter included patients that were operated upon twice, seems to reinforce our conclusion that stranding is a normal postoperative finding. Patients who experienced a prolonged hospitalization and who died within the first post-operative year were assigned to the complicated group regardless of the specific cause. Apart from this, other events unrelated to the Bentall procedure were not taken into account due to the unlikelihood of their influence on the presence and amount of fluid surrounding the aortic graft. This way, we ensured that the remaining scans would represent a group of patients with a truly uncomplicated procedure, uneventful follow-up and low pre-test risk.

Theoretically, as guidelines and current clinical practice suggest to perform at least one follow-up imaging exam (mainly CT) within the first three months in all operated patients [9–11,15], even after uneventful, uncomplicated procedures and even in the absence of symptoms, the vast majority of the low-risk population should have undergone a CT scan in this period. Moreover, since in our study all operations and monitoring were performed at the same institution, the availability of the exam was the same for all patients. Real figures of the present study differ from these expectations. Out of the 388 patients who underwent at least one Bentall procedure, only 206 had a post-operative CT scan, of which 94 were obtained in the first three months. However, half of the patients we included represent the low risk, as well as the uncomplicated, cohort. We therefore believe that our results are representative and allow us to draw conclusions on what can be considered as a normal finding in this population.

Our results suggest that the presence of fluid surrounding the aortic graft is a very common finding in post-Bentall patients. Compared to the papers mentioned above, that reported the presence of material around the aorta in most post-operative patients as well, in the current study a systematic differentiation and classification of the fluid based on its CT characteristics (appearance and amount) was introduced. Thereafter, for the first time, different imaging features were separately correlated to complications allowing identification of the most worrisome CT characteristics and distinguish them from normal findings. In most patients, this fluid could be classified as stranding (fluid infiltrating the soft and adipose tissue surrounding the aorta), while in 34 patients at least part of the peri-aortic fluid was considered to be a fluid collection. This distinction, while evident in most cases (figure 2), was sometimes very subtle, especially when there was an abundance of fluid completely surrounding the aorta. In the few cases in which a high level of confidence in differentiation could not be achieved, the fluid was classified as stranding. On the contrary, no doubt arose regarding the distinction of the stranding from the thin hyperdense lines that can be found in the periaortic adipose tissue of patients who were not operated upon the ascending aorta. More importantly, isolated stranding was analyzed separately from stranding associated with other findings (i.e. stranding around fluid collections, pseudo-aneurysms etc.), since these are most likely two very different entities.

Fourteen of these fluid collections had contents showing attenuation values similar to that of water: 5 in the uncomplicated group and 9 in the complicated group. While fluid collections with hyperdense contents can be ascribed to the presence of blood and/or contrast, the etiology of the collections with water-like density is still under debate. The occurrence of peri-graft seromas with sterile fluid contents has been described for abdominal aortic grafts following open repair[18,19]. Although many hypotheses have been postulated, their cause remains unclear but is likely to involve a failure of normal graft healing and incorporation and/or transudation of fluid through graft pores. While the collections in our series showed some compatible features on CT, the reported diagnoses of peri-graft seromas in these studies were reached later on after surgery. For instance, Kadakol et al.[18] employed a cut off time of three months after surgery as a criterion in their definition of a seroma.

Some possibly confounding factors have to be taken into account concerning the definition of the extent of the stranding. Measurements were acquired mainly on the axial plane with the aid of reconstructions on coronal and sagittal planes, but double oblique reconstructions to obtain a plane perpendicular to the aortic axis were not routinely performed. We found that this did not substantially influence measurements because stranding is rarely a perfectly circular entity and the most prominent extension of the fluid is usually located along the anterior border of the aorta at the level of the pulmonary

trunk, where the aorta has a course nearly perpendicular to the transverse plane. However, in some of these patients the physiological conformation of the ascending aorta and of the aortic arch is altered with a sharp anterior curvature that can reach as far as few millimeters from the sternum, resulting in the reduction of the normal amount of adipose tissue anterior to the aorta and an underestimation of the stranding at this level. All these reasons prompted us to additionally introduce a subjective grading of the overall quantity of the stranding. The subjective scale was based on the volume of the stranding as well as on the perceived proportion of the fluid in respect to the adipose tissue it was mingled with. However, an objective measure of the HU density of stranding was not feasible due to its irregular borders and different compositions proceeding from the aortic wall. Fluid collections were not measured because they had such an irregular shape that linear measurements would not be representative of the real dimensions.

One of the limitations of the present study is the relatively small number of patients with an uncomplicated procedure who underwent a CT scan in the analyzed period. Another limitation which has to be considered, is the inconsistency of the time points at which the CT scans were acquired. The scans were widely spread throughout the second and third post-operative months in the uncomplicated group, while most scans in the complicated group were performed within the first month. Unexpectedly, we did not find any statistically significant reduction in the amount of stranding over time in either of the two groups; however, the short period we analyzed, the heterogeneous distribution of exams throughout this period, the choice to include only the first scan of each patient and the fact that some patients underwent two operations before the CT are all variables that might have influenced this result, that therefore has to be interpreted with caution. Furthermore, over the years, several different CT scanners, protocols and acquisition methods were employed, which may have influenced our findings to some extent. Finally, in order to assess normal findings, we separated CT scans that had been performed for indications other than a routine check and assigned them to the complicated group. All scans were re-assessed by an operator blinded to the patient's categorization and to the clinical report. To prevent a selection bias, the CT findings themselves, of both the clinical report and the independent re-assessment, were deliberately not used to distinguish normal from abnormal follow-up. However, due to the retrospective nature of this study, some degree of selection bias could not be avoided since CT findings were likely to have influenced the patients' management. This also implies that some of the findings such as the more extensive fluid collections or haematomas in otherwise uncomplicated patients -although not associated with any complications within a one-year follow-up- may not be representative of a normal healing process. Merely the fact that the patient did not experience any symptoms or adverse clinical outcome, does not mean that the findings on CT can be considered normal.

Conclusions

The presence of fluid around the aortic graft during the first three postoperative months can be found on CT in all patients following a Bentall procedure. This fluid can be classified as stranding or as a fluid collection based on its characteristics on CT. The extent of isolated stranding doesn't differ between patients who experienced a complicated or an uneventful procedure and follow-up, and can thus be considered a normal finding. Even when extending up to 17mm from the inner border of the aortic wall, the presence of isolated stranding does not necessitate any management other than the usual follow-up. Fluid collections on the other hand, are more common in patients who experienced complications either during the procedure or in the course of follow-up, and may require closer monitoring.

References

1. H. Bentall, A. De Bono, A technique for complete replacement of the ascending aorta, Thorax. 23 (4) (1968) 338–339.
2. L.C. Chu, P.T. Johnson, D.E. Cameron, E.K. Fishman, MDCT Evaluation of aortic root surgical complications, Am. J. Roentgenol. 201 (4) (2013) 736–744.
3. J.D. Christensen, D.M. Seaman, L. Washington, Imaging of Complications of Thoracic and Cardiovascular Surgery, Radiol. Clin. North Am. 52 (5) (2014) 929–959.
4. Y. Hirasawa, S. Aomi, S. Saito, S. Kihara, H. Tomioka, H. Kurosawa, Long-term results of modified Bentall procedure using flanged composite aortic prosthesis and separately interposed coronary graft technique, Interact. Cardiovasc. Thorac. Surg. 5 (5) (2006) 574–7.
5. L.G. Svensson, D.H. Adams, R.O. Bonow, N.T. Kouchoukos, D.C. Miller, P.T. O'Gara, D.M. Shahian, H. V Schaff, C.W. Akins, J. Bavaria, E.H. Blackstone, T.E. David, N.D. Desai, T.M. Dewey, R.S. D'Agostino, T.G. Gleason, K.B. Harrington, S. Kodali, S. Kapadia, M.B. Leon, B. Lima, B.W. Lytle, M.J. Mack, T.B. Reece, G.R. Reiss, E. Roselli, C.R. Smith, V.H. Thourani, E.M. Tuzcu, J. Webb, M.R. Williams, Aortic valve and ascending aorta guidelines for management and quality measures: executive summary, Ann. Thorac. Surg. 95 (4) (2013) 1491–505.
6. C.W. Akins, D.C. Miller, M.I. Turina, N.T. Kouchoukos, E.H. Blackstone, G.L. Grunkemeier, J.J.M. Takkenberg, T.E. David, E.G. Butchart, D.H. Adams, D.M. Shahian, S. Hagl, J.E. Mayer, B.W. Lytle, Guidelines for reporting mortality and morbidity after cardiac valve interventions, J. Thorac. Cardiovasc. Surg. 135 (4) (2008) 732–738.
7. B. Sundaram, L.E. Quint, H.J. Patel, G.M. Deeb, CT findings following thoracic aortic surgery., Radiographics. 27 (6) (2007) 1583–1594.
8. K.J. Zehr, T.A. Orszulak, C.J. Mullany, A. Matloobi, R.C. Daly, J.A. Dearani, T.M. Sundt, F.J. Puga, G.K. Danielson, H. V. Schaff, Surgery for aneurysms of the aortic root: A 30-year experience, Circulation. 110 (11) (2004) 1364–1371.
9. L.F. Hiratzka, G.L. Bakris, J.A. Beckman, R.M. Bersin, V.F. Carr, D.E. Casey, K.A. Eagle, L.K. Hermann, E.M. Isselbacher, E.A. Kazerooni, N.T. Kouchoukos, B.W. Lytle, D.M. Milewicz, D.L. Reich, S. Sen, J.A. Shinn, L.G. Svensson, D.M. Williams, 2010 ACCF/AHA/AATS/ACR/ASA/SCA/SCAI/SIR/STS/SVM Guidelines for the Diagnosis and Management of Patients With Thoracic Aortic Disease, Circulation. 121 (13) (2010) e266–e369.
10. R. Erbel, V. Aboyans, C. Boileau, E. Bossone, R.D. Bartolomeo, H. Eggebrecht, A. Evangelista, V. Falk, H. Frank, O. Gaemperli, M. Grabenwoger, A. Haverich, B. Iung, A.J. Manolis, F. Meijboom, C.A. Nienaber, M. Roffi, H. Rousseau, U. Sechtem, P.A. Sirnes, R.S. V. Allmen, C.J.M. Vrints, J.L. Zamorano, S. Achenbach, H. Baumgartner, J.J. Bax, H. Bueno, V. Dean, C. Deaton, C. Erol, R. Fagard, R. Ferrari, D. Hasdai, A. Hoes, P. Kirchhof, J. Knuuti, P. Kolh, P. Lancellotti, A. Linhart, P. Nihoyannopoulos, M.F. Piepoli, P. Ponikowski, P.A. Sirnes, J.L. Tamargo, M. Tendera, A. Torbicki, W. Wijns, S. Windecker, P. Nihoyannopoulos, M. Tendera, M. Czerny, J. Deanfield, C.D. Mario, M. Pepi, M.J.S. Taboada, M.R. V. Sambeek, C. Vlachopoulos, J.L. Zamorano, M. Grimm, O. Musayev, A. Pasquet, Z. Ku ljugi, M. Cikes, G.P. Georghiou, J. Stasek, H. Molgaard, S. Kovask, V. Kyto, G. Jondeau,

Z. Bakhutashvili, Y. von Kodolitsch, C. Tsioufis, A. Temesvari, R. Rubinshtein, F. Antonini-Canterin, O. Lunegova, P. Stradins, E. Chammas, R. Jonkaitiene, A. Cassar, K. Bjornstad, K. Widenka, M. Sousa Uva, D. Lighezan, J. Perunicic, J. Madaric, I. Vilacosta, M. Back, A. Mahdhaoui, R. Demirbag, I. Kravchenko, 2014 ESC Guidelines on the diagnosis and treatment of aortic diseases, Eur. Heart J. 35 (41) (2014) 2873–2926.

11. B. Sundaram, L.E. Quint, S. Patel, H.J. Patel, G.M. Deeb, CT appearance of thoracic aortic graft complications, Am. J. Roentgenol. 188 (5) (2007) 1273–1277.
12. J.K. Hoang, S. Martinez, L.M. Hurwitz, Imaging of the Postoperative Thoracic Aorta: The Spectrum of Normal and Abnormal Findings, Semin. Roentgenol. 44 (1) (2009) 52–62.
13. B. Sundaram, L.E. Quint, H.J. Patel, G.M. Deeb, CT findings following thoracic aortic surgery., Radiographics. 27 (6) (2007) 1583–1594.
14. T. Valente, G. Rossi, G. Rea, A. Pinto, L. Romano, J. Davies, M. Scaglione, Multidetector CT Findings of Complications of Surgical and Endovascular Treatment of Aortic Aneurysms, Radiol. Clin. North Am. 52 (5) (2014) 961–989.
15. L.E. Quint, I.R. Francis, D.M. Williams, H.M. Monaghan, G.M. Deeb, Synthetic interposition grafts of the thoracic aorta: postoperative appearance on serial CT studies., Radiology. 211 (2) (1999) 317–324.
16. E. Fagman, O. Bech-Hanssen, A. Flinck, C. Lamm, G. Svensson, Increased aortic wall thickness on CT as a sign of prosthetic valve endocarditis., Acta Radiol. 0 (0) (2016) 1–7.
17. G. Habib, P. Lancellotti, M.J. Antunes, M.G. Bongiorni, J.P. Casalta, F. Del Zotti, R. Dulgheru, G. El Khoury, P.A. Erbaa, B. Iung, J.M. Mirob, B.J. Mulder, E. Plonska-Gosciniak, S. Price, J. Roos-Hesselink, U. Snygg-Martin, F. Thuny, P.T. Mas, I. Vilacosta, J.L. Zamorano, C. Erol, P. Nihoyannopoulos, V. Aboyans, S. Agewall, G. Athanassopoulos, S. Aytekin, W. Benzer, H. Bueno, L. Broekhuizen, S. Carerj, B. Cosyns, J. De Backer, M. De Bonis, K. Dimopoulos, E. Donal, H. Drexel, F.A. Flachskampf, R. Hall, S. Halvorsen, B. Hoenb, P. Kirchhof, M. Lainscak, A.F. Leite-Moreira, G.Y.H. Lip, C. a. Mestresc, M.F. Piepoli, P.P. Punjabi, C. Rapezzi, R. Rosenhek, K. Siebens, J. Tamargo, D.M. Walker, 2015 ESC Guidelines for the management of infective endocarditis, 2015.
18. A.K. Kadakol, T.J. Nypaver, J.C. Lin, M.R. Weaver, J.L. Karam, D.J. Reddy, G.K. Haddad, A.D. Shepard, Frequency, risk factors, and management of perigraft seroma after open abdominal aortic aneurysm repair, J. Vasc. Surg. 54 (3) (2011) 637–643.
19. S.S. Ahn, H.I. Machleder, R. Gupta, W.S. Moore, Perigraft seroma: clinical, histologic, and serologic correlates., Am. J. Surg. 154 (2) (1987) 173–178.

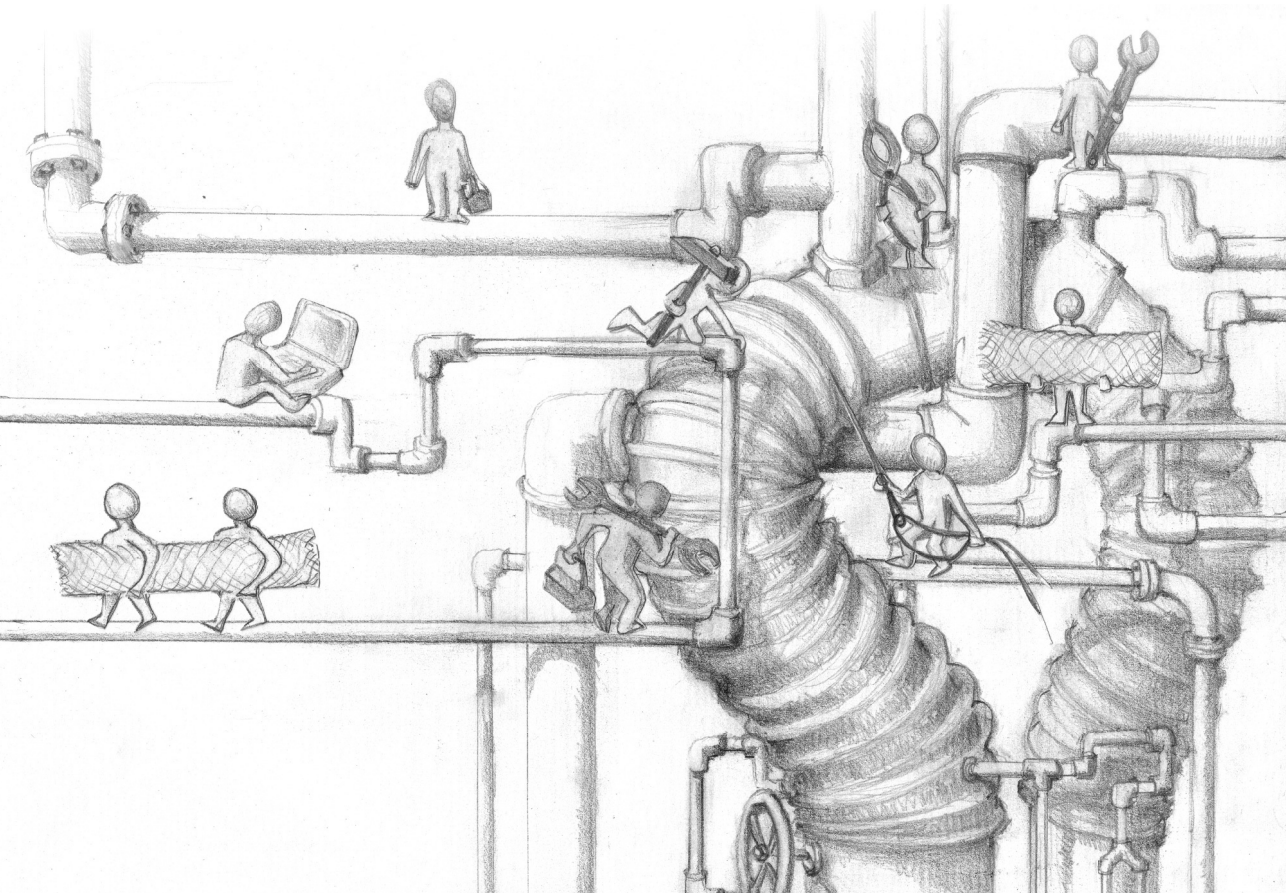

CHAPTER 9

Complications after Stent Placement for Aortic Coarctation: a Pictorial Essay of CT Angiography

Sara Boccalini*, Annemarie M. den Harder*, Maarten Witsenburg, Hans P.J.M. Breur, Gabriel P. Krestin, Ingrid M. van Beynum, Nicola Stagnaro, Maurizio Marasini, Pim A. de Jong, Tim Leiner, Ricardo P.J. Budde

J Thorac Imaging. 2017 Nov;32(6):W69-W80

Abstract

Stent placement is commonly used to treat aortic coarctation. Although invasive angiography remains the gold standard, follow-up is often performed using CT, which allows rapid, non-invasive assessment of the aorta and surrounding tissues. The goal of this pictorial essay is to provide a guide to the interpretation of these examinations. Normal and abnormal CT appearance of different stent types is shown along with reconstructions which can help assess stent integrity and the stent position in relation to the aortic wall and branches. Furthermore, imaging findings of complications including aortic wall injuries, restenosis and intimal hyperplasia are depicted.

Introduction

Coarctation of the aorta accounts for 5-8% of all congenital heart defects, with a prevalence of isolated forms of ~ 3/100,000 live births (1). Aortic coarctation consists of either a discrete narrowing of the aorta, or a long hypoplastic segment in the context of a generalized arteriopathy.

The typical location of the stenosis is in the juxtaductal position, immediately distal of the left-subclavian artery. This is in accordance with one of the theories regarding the pathogenesis of coarctation which suggests that the narrowing arises due to the presence of ectopic ductal tissue in the aorta (2). Usually the descending aorta immediately distal to the narrowed segment is dilated, which is also known as post-stenotic dilatation. Coarctation can occur as an isolated form or can be found in association with other cardiovascular anomalies such as bicuspid aortic valves and ventricular septal defects.

The treatment options for coarctation of the aorta include surgery, balloon dilation and stent implantation. The latter has gained wide acceptance from the 90s onwards and is now the treatment of choice in older children and adults (3). In adolescents and adults stent placement has a lower rate of acute complications than surgical treatment with a similar to only slightly higher probability of re-intervention (4–6). Stent treatment in young children is investigated in specific groups of patients only, namely patients undergoing isolated procedures for coarctation treatment and patients with a native coarctation that weight 10 Kg or more (3,7). In other studies patients with complete atresia and hypoplasia of the transverse and/or distal arch or patients under one year of age were excluded (8,9). These studies report that stent placement is more likely to require planned reintervention compared to surgical treatment in order to adjust the stent diameter for somatic growth. However, stent placement and surgical treatment have an equal rate of unplanned interventions. Also the outcomes, as assessed by hemodynamic measurements and imaging, are similar. Although sheath dimensions and concerns about redilatation procedures have limited stent treatment in neonates and infants, several studies demonstrated results comparable to those in the older population (3,8,9).

Complications after stent implantation are relatively rare but can occur both in the early and late postoperative period. Therefore, patients need to undergo lifelong follow-up. Computed tomography (CT) is the preferred imaging modality in many centers because it is readily available, rapid, non-invasive and has an excellent correlation with invasive angiography for the detection of complications, including in-stent restenosis (10–12). However, the material of the stent can cause severe artefacts on CT acquisitions which affect image quality and diagnostic accuracy. Since coarctation can be associated with other anatomic anomalies as well as previous interventional or surgical procedures that

might have altered the native anatomy, this anatomical knowledge is fundamental to distinguish complications from normal post-procedural findings.

Stent types

Different stent types can be employed to treat coarctation.
The most commonly implanted type of stent, and the only one with Food and Drug Administration (FDA) and CE mark approval for this use, is the Cheatham Platinum (CP) stent (NuMed Inc.) (13). Other stent types are used off-label and mainly in children. They include Palmaz (Johnson and Johnson), Genesis XD (Cordis Corp.), Atrium Advanta V12 (Atrium), IntraStent (EV3 Inc.), Formula (Cook Medical) and AndraStent (Andramed GmbH). In small children coronary stents have been employed as well due to the small diameter of the aorta.

Stents can vary both in material and architecture. There are three commonly used designs, namely closed-cell, open-cell and a hybrid design **(Fig. 1; A, B, C)**. A closed-cell design has numerous fixed points and is therefore less flexible and conformable compared to stents with an open-cell design (14). Open-cell designs are preferred for treatment of transverse aortic arch narrowing because they adapt better to the arch shape. Furthermore, separate balloon angioplasty through the cell into the aortic branches can be performed when using an open-cell design (6,15). Another architectural difference is the use of single wires welded together (for instance in the case of the CP stent) versus a single tube that is slotted without junctions between components **(Fig. 1; D, E, F)**. Welds represent weak points in the structure of the stent; thus, in the newer CP stents gold soldering was added to reinforce the welds (16).

Stents can be bare or covered. The most commonly used material for the cover is polytetrafluoroethylene (PTFE), which makes the stent impermeable. Conventionally, covered stents were solely employed to treat aortic wall complications. However, nowadays covered stents are implanted as the primary treatment of coarctation in patients at risk of complications. Risk factors for lesions to the aortic wall include narrow coarctation, tortuous aorta, genetic aortic pathologies and aneurysms/pseudoaneurysms derived from previous interventions (15,17,18).

The characteristics of each type of stent are summarized in **Table 1**.
During body growth, the aorta increases in diameter and a planned redilatation of the stent is often necessary. This procedure has proven to be safe and effective for non-covered stents (4,13,19). On the contrary, there is limited data about safety of redilatation of covered stents (20).

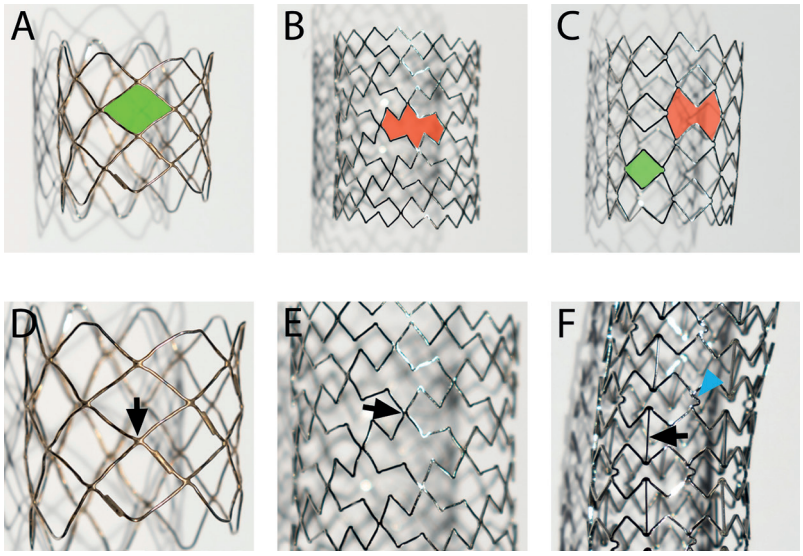

Figure 1. Stents design

Closed-, open-cell and hybrid stent design illustrated in **A**, **B** and **C**.
A) Stent with closed-cell design. All internal inflection points of the structural components are connected, thereby creating small closed cells **(green surface)**.
B) Stent with open-cell design. Some of the internal inflection points of the structural components are not connected. The absence of connections allows more longitudinal flexibility of the cells **(red surface)**.
C) Stent with hybrid design. Closed- and open-cells **(green and red surface respectively)** are combined.
Connections between structural components illustrated in **D**, **E**, **F**.
D) Welded joints. Structural components of the stent can be welded together at the inflection points **(arrow)**. In the CP stents these joints are over-brazed with gold.
E) Stiff connection **(arrow)** in a slotted-tube stent.
F) Non-flex and flex-connectors. Non-flex connectors **(arrow)** increase the stiffness of the structure. Flex-connectors **(arrowhead)** can have different shapes (U, V, S, N) and can deform during bending increasing the flexibility of the stent.
Connectors can bridge different parts of the stents: valley-to-valley **(arrow)**, peak-to-peak **(arrowhead)**, peak-to-valley.

Table 1. Characteristics of different types of stent

Stent type	Manufacturer	Material	Design	Cover	Specific advantages	Specific disadvantages
CP	NuMed Inc.	Platinum-Iridium and joints over brazed with gold	Closed-cell	• Possible • Outer cover of PTFE	• Only stent with FDA and CE approval for this use • Good radial strength • Rounded edges • Good radio-opacity	• Large delivery sheath for covered stents
Atrium Advanta V12	Atrium	316L stainless steel	Open-cell	• Yes • Outer and inner cover of PTFE		
IntraStent	EV3 Inc.	Stainless steel	Open-cell		• Minimal foreshortening • Good flexibility	
AndraStent	Andramed GmbH	Cobalt Chromium	Hybrid (open- and closed-cell)			
Formula	Cook Medical	316L stainless steel	Open-cell			
Palmaz 8	Cordis Corp (Johnson & Johnson)	Stainless steel	Closed-cell		Good radial strength	• Sharp edges • Stiff
Palmaz XL	Cordis Corp (Johnson & Johnson)	Stainless steel	Closed-cell		• One piece laser cut slotted tube (no welds) • Good radial strength	• Sharp edges • Stiff
Genesis XD	Cordis Corp	Stainless steel	Closed-cell		• One piece laser cut slotted tube (no welds) • Broader expansion range • Good radial strength • Good conformability	

Post-procedural CT scan

CT scan protocol

The timing of imaging follow up varies between institutions. Moreover, guidelines from the European Society of Cardiology propose to adapt follow-up times depending on the baseline pathology (1).

An aortic contrast-enhanced CT scan protocol should be employed. An additional unenhanced CT acquisition might be helpful, especially when there is clinical suspicion of complications. Also in patients who previously underwent surgical procedures, an unenhanced acquisition can be useful as it improves the visualization of the presence and location of surgical material, calcifications, periaortic and intramural hematoma of the native aorta and (sub)acute hemorrhage. Since coarctation, like other aortic pathologies, is an organ pathology, the entire aorta should be imaged at least once in each patient. Contrast should be administered from a vein on the right arm to avoid artifacts extending over the aorta due to the presence of concentrated contrast material in the left anonymous vein or in a persistent left superior vena cava. Thin reconstruction slices (1 mm or less) should be obtained for all acquisitions. A sharp kernel, similar to coronary stent imaging, improves the visualization of the stent and surrounding tissues by reducing blooming artifacts (21).

Because of the often young age of the aortic coarctation patients and the necessity of repeated examinations, radiation dose reduction strategies should be undertaken. Lower tube voltage, reduced scan length, and the application of automatic exposure control or automatic tube current modulation are options available on all scanners and should be tailored for each patient (22,23). Moreover, modern scanners from all vendors have integrated iterative reconstruction algorithms that enable dose reduction up to 81% for aortic stent imaging (24). In case ECG-gating/triggering is deemed necessary, prospective triggering should be used if this is compatible with the heart rate of the patient (25). If retrospective gating is employed, prospective dose modulation should be applied to reduce the radiation dose. With dual-source CT scanners, prospectively gated high-pitch acquisitions combine the high quality of gated acquisition with a low radiation dose (26).

Normal CT findings after stent placement

Each type of stent has a specific appearance on CT images **(Fig. 2)**. This is dependent on the material of the stent as well as the structure. Knowing beforehand which type of stent was deployed and what its characteristics are, can help CT assessment. Multiplanar reconstructions are useful to assess both the lumen and the surrounding tissues, while volume rendering techniques can improve the visualization of the stent metallic structure.

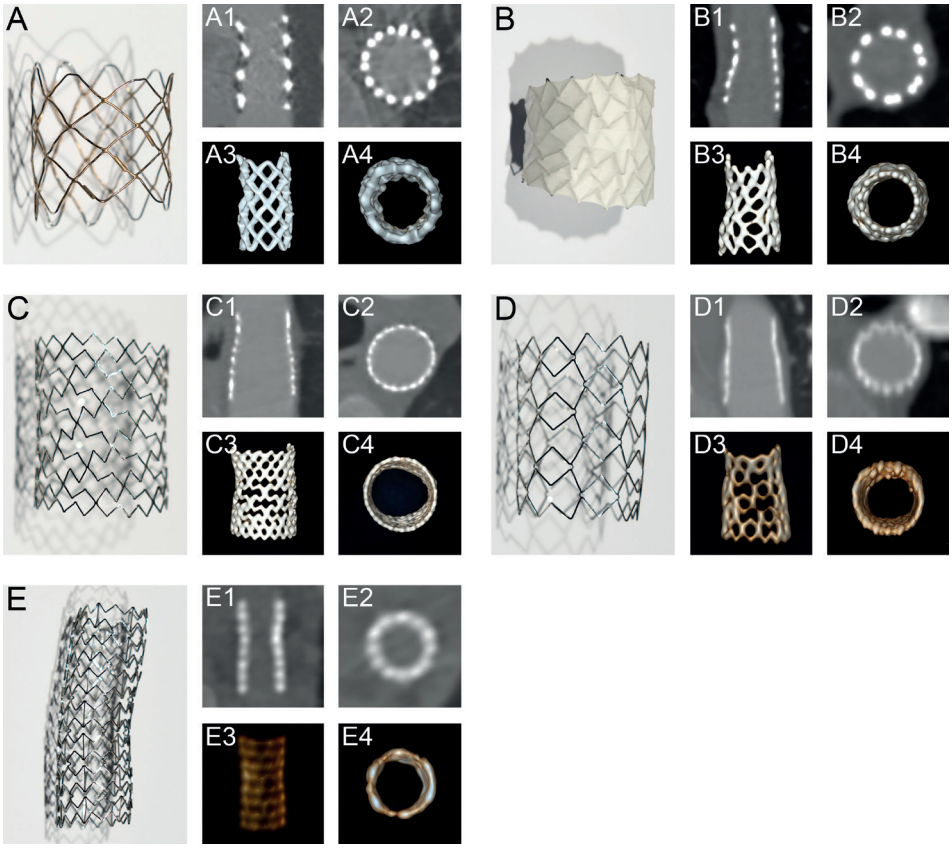

Figure 2. Normal appearance of different stent types

The most commonly employed stent types **(A, B, C, D, E).** Appearance of each type of stent on multiplanar **(A1, A2, B1, B2, C1, C2, D1, D2, E1, E2)** and volume rendering (VR) **(A3, A4, B3, B4, C3, C4, D3, D4, E3, E4)** reconstructions. Multiplanar reconstructions were performed on planes parallel **(A1, B1, C1, D1, E1)** and perpendicular **(A2, B2, C2, D2, E2)** to the longitudinal axis of the stent; VR reconstructions were oriented as the corresponding multiplanar reconstructions.

A) The Cheatham Platinum (CP) stent (NuMED Inc.) is composed of a Platinum/Iridium wire that is arranged in a "zig" pattern, laser welded at each joint, obtaining a closed-cell design, and over brazed with 24K gold. The covered CP stent is comprised of the bare CP stent covered with an expandable sleeve of ePTFE, which is not visible on contrast-enhanced CT scans. The CP stent is the one most commonly employed in the adult and adolescent population treated for coarctation of the aorta.

B) The Atrium Advanta V12 (Atrium Medical) stent is composed of stainless steel struts, organized in an open-cell design and completely covered with PTFE both inside and outside.

C) The IntraStent Mega LD (EV3 Inc.) stent is obtained from a stainless steel tube cut into an open-cell lattice design.

D) The AndraStent (Andramed GmbH) stent is composed of Cobalt/Chromium steel struts, organized in an hybrid (open- and closed-cell) design.

E) The Formula (Cook Medical) stent is composed of stainless steel struts organized in an open-cell design.

Multiplanar reconstructions can be used to obtain planes perpendicular to the long axis of the stent, which are useful to assess the presence of material inside the lumen of the stent, such as intimal hyperplasia or thrombus. Furthermore, stent diameters should be measured on planes perpendicular to the long axis of the stent. In addition, aortic diameters, including aneurysms and post-stenotic dilatations, should be assessed on cross-sections perpendicular to the centerline of the vessel (27). Multiplanar reconstructions can also generate planes parallel to the long axis of the stent, which are useful for the assessment of the outside contour of the stent and to distinguish the presence of extravasated contrast from artefacts. Finally, maximum intensity projection (MIP) reconstructions can highlight disruptions of the stent structure as well as its relationship with the aortic wall and branches.

The position of the stent should also be assessed **(Fig. 3; A1-B2)**. Previous exams (CT and invasive angiography) should always be compared to evaluate a possible change in position or morphology of the stent. Stents are commonly deployed with the central portion over the affected segment of the aorta which is generally located in the juxtaductal position, immediately after the left subclavian artery **(Fig. 3; A1-A3)**. In some cases the stent is not completely attached to the aortic wall: the extremities of the stent are suspended in the lumen **(Fig. 3; B1, B2)**. This can be ascribed to a residual degree of narrowing that can be left on purpose during the interventional procedure. Another possible cause is a dilation of the aorta adjacent to the coarctation in combination with the decision not to flare the extremities of the stent (11,15). However, it has been advocated that the presence of free space between the proximal borders of a covered stent and the aortic wall can create a pouch where the high speed flow of the descending aorta could displace the stent or even cause its collapse, resulting in obstruction, or thrombus formation (20). This is due to the impermeability of the covered stent that prevents blood from flowing through the cells back into the aortic lumen.

Another step of the CT evaluation is the assessment of the relationship between the stent and the aortic branches **(Fig. 3; C1-F2)**. Close proximity of the aortic branches (especially the left subclavian artery) to the stent is common. This can result in different situations depending on the type of stent. With bare metal stents aortic branches can be completely or partially overstented without clinically relevant consequences, while with covered stents complete occlusion of the branches is expected **(Fig. 3; C1, C2; D1, D2)** (19). In this case a surgical graft from the carotid to the left subclavian artery (LSA) will avoid complications such as left-arm ischemia, claudication, or possible vertebrobasilar infarct. Occlusion of aortic branches has to be distinguished from their absence, due to previous operations such as the "subclavian flap aortoplasty". With this technique the wall of the LSA is employed as tissue for an aortic patch to surgically correct the coarctation **(Fig. 3; E1, E2)**.

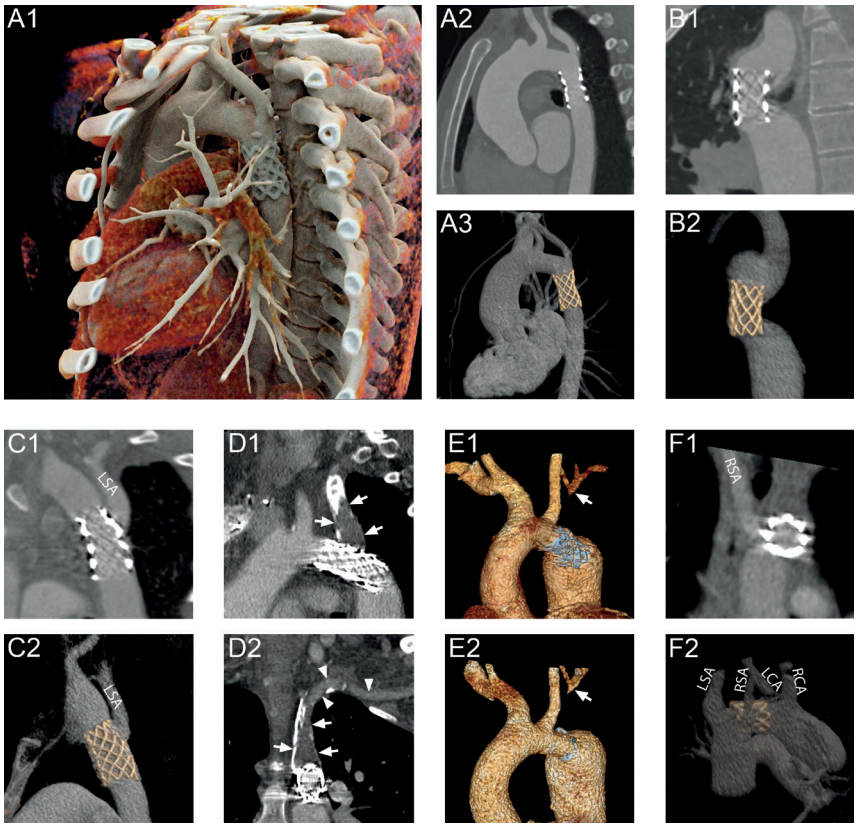

Figure 3. Normal variations in stents position

A) Most common position and spatial relationships of a CP stent. **A1:** 3D rendering; **A2**: multiplanar reconstruction parallel to the longitudinal axis of the stent; **A3**: VR reconstruction.
B) Extremities of the stent not in contact with the aortic wall. This can be expected, and considered to be within normal limits, in case of an initial mismatch between aortic diameters at the point of coarctation and nearby segments and/or the stent overriding an aortic branch ostium. **B1**: multiplanar reconstruction parallel to the longitudinal axis of the stent; **B2**: VR reconstruction.
C) Overstenting of side branches with non-covered stents. The left subclavian artery **(LSA)** remained patent due to the permeability of the non-covered CP stent employed. **C1**: multiplanar reconstruction parallel to the longitudinal axis of the stent; **C2**: VR reconstruction.
D) Overstenting of side branches with covered stents. After the deployment of a covered CP stent the LSA is thrombosed **(D1, D2, arrows)** and refilled distally **(D2, arrowheads)** through collaterals. **D1** and **D2**: multiplanar reconstruction parallel and perpendicular to the longitudinal axis of the stent respectively.
E) Subclavian flap aortoplasty. Absence of the proximal tract of the LSA with distal refilling **(E1, arrow)** in a patient with a CP stent at the level of the distal arch. However, a CT scan performed before the stent placement, demonstrated the same anatomic anomaly **(E2, arrow)** due to the previous surgical treatment with the "subclavian flap aortoplasty" technique. During the procedure the wall tissue of the artery was employed as an aortic patch. **E1** and **E2**: VR reconstructions.
F) Anomalies in number and position of the aortic branches. Right subclavian artery **(RSA)** emerging from a non-covered CP stent after the separate origin of the right **(RCA)** and left **(LCA)** carotid arteries and before the ostium of the left subclavian artery **(LSA)**. **F1**: multiplanar reconstruction perpendicular to the longitudinal axis of the stent; **F2**: VR reconstruction.

Aortic coarctation can be associated with normal anatomic variations in the number and/or order of the branches arising from the aorta. The most common are the distal displacement of the LSA and the origin of the right subclavian artery distal to the other head and neck branches **(Fig. 3; F1, F2)**(5).

Complications

Complications after stent positioning are relatively rare and can occur either in the immediate, early or intermediate period after the procedure while data on long term complications are still lacking (13,28). Most of these complications can be depicted with CT (10).

Lesions of the aortic wall. These uncommon complications include aneurysms, dissections, pseudoaneurysms, intramural hematoma, and aortic wall rupture (7,13,19,28). They can occur either immediately after the procedure or at later follow up. Risk factors include small initial coarctation diameters, with larger ratios of balloon to minimal aortic diameter, and stent placement preceded by balloon angioplasty (7,29). The use of covered stents can reduce the incidence of these complications with outcomes comparable to bare metal stents (17,30). Aortic wall rupture with contrast extravasation outside the aorta and aortic dissection type A are potentially lethal complications that require prompt recognition and treatment **(Fig. 4; A1-A7)** (28). On the contrary intramural hematoma and pseudoaneurysms rarely need treatment, as they might remain stable or spontaneously reabsorb without further intervention, but require follow-up **(Fig. 5; A1-A2)** (7). These complications, especially when small, might be very hard to detect due to the metallic artefacts surrounding the stent **(Fig. 5; B1-B2)**. If available, previous examinations should always be compared to avoid errors **(Fig. 6; A1-C2)**. Aneurysms should not be misdiagnosed for the native post-stenotic dilatation.

Disruption of the structure of the stent. The structure of the stent can be damaged in several ways including fracture, collapse and loosening of welds **(Fig. 7; A1-D4)**. Although frequently asymptomatic, stent fracture can be associated with embolization of stent fragments, vascular reobstruction, and injury to the aortic wall (13). Therefore, the patients' management depends on the specific setting, ranging from immediate treatment in case of stent collapse and rupture of the aorta to watchful waiting with imaging follow-up.
Disruption of the stent structure can be suspected also on plain films; nevertheless, CT images provide additional information such as changes in orientation of the stent, the presence of associated aortic wall lesions as well as the involvement of the surrounding tissues.

Restenosis. Restenosis is one of the most frequent complications with a reported incidence of 3-11% and results in an increased pressure gradient across the stent (15).

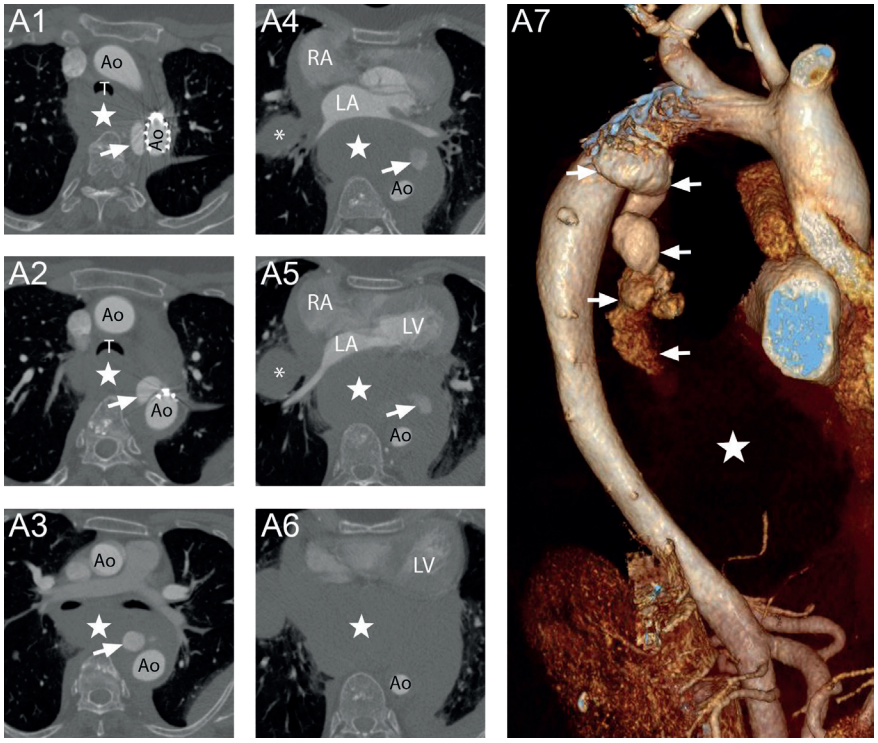

Figure 4. Rupture of the aortic wall

A CT scan performed during the same day of a successful deployment of a CP-covered stent demonstrated a massive and active contrast extravasation **(arrows)** with surrounding hematoma **(stars)** originating in the immediate proximity of the stent, extending to the level of the diaphragm and displacing anteriorly both the trachea **(T)** and the heart (**Ao**: aorta; **LA**: left atrium; **LV**: left ventricle; **RA**: right atrium). The patient died the same day.

A1) The origin of the extravasation was identified based on the presence of a very hyperdense collection of contrast material **(arrow)** medial to the distal part of the stent on a plane just caudal to the aortic arch. Around the contrast collection a hematoma **(star)** extended between the vertebral column and the trachea **(T)**, that was dislocated anteriorly and compressed.

A2) More caudally the collection of contrast rotated more towards the anterior side of the aorta **(arrow)**. The posterior wall of the trachea **(T)** was bent resulting in a half-moon shape with a reduced calibre.

A3) At the level of the pulmonary trunk, the extravasated contrast was less hyperdense **(arrow)**. The hematoma **(star)** almost completely surrounded the aorta and partly compressed the bronchi and pulmonary arteries.

A4) Progressing more caudally the contrast appeared even less hyperdense **(arrow)**. At this level the hematoma completely encircled and compressed the aorta **(Ao)** and the pulmonary veins. Furthermore, there was pleural effusion in the great fissure of the right lung **(asterisk)**.

A5) The heart **(LA**: left atrium; **LV**: left ventricle; **RA**: right atrium**)** was pressed anteriorly against the sternum because of the hematoma **(star)**.

A6) Directly above the diaphragm the hematoma **(star)** was most extensive. The aorta **(Ao)** was completely surrounded and had a small diameter but its normal circular shape was restored at this level.

A1-A6: axial images; **A7**: VR reconstruction.

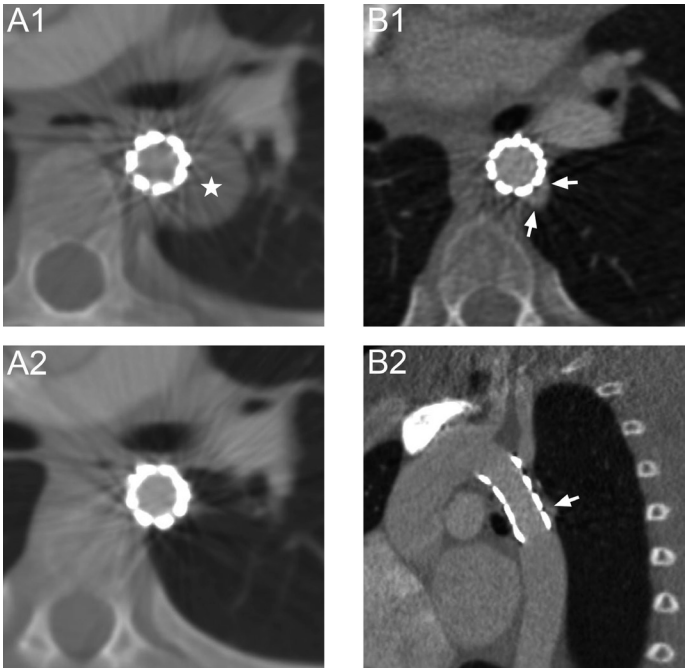

Figure 5. Pseudoaneurysms

Case 1 (A1-A2) – Spontaneous reabsorption of a big pseudoaneurysm. A CT scan performed 14 days after the implantation of a covered CP stent **(A1)** in a 9 year-old boy showed the presence of a collection of extravasated contrast adjacent to the lateral outer wall of the stent **(asterisk)**, compatible with a big pseudoaneurysm. Without any treatment the pseudoaneurysm completely reabsorbed and was not visible on a CT scan performed three months later **(A2)**. **A1** and **A2**: multiplanar reconstructions perpendicular to the longitudinal axis of the stent.
Case 2 (B1-B2) – Small pseudoaneurysm. Four months after the deployment of a CP stent inside a previously placed Atrium Advanta stent, a CT scan revealed the presence of a small pouch of contrast outside the aortic wall **(arrows)** at the distal third of the stents. The finding was referred to as a small pseudoaeurysm. **B1**: multiplanar reconstruction perpendicular to the longitudinal axis of the stent; **B2**: multiplanar reconstruction parallel to the longitudinal axis of the stent.

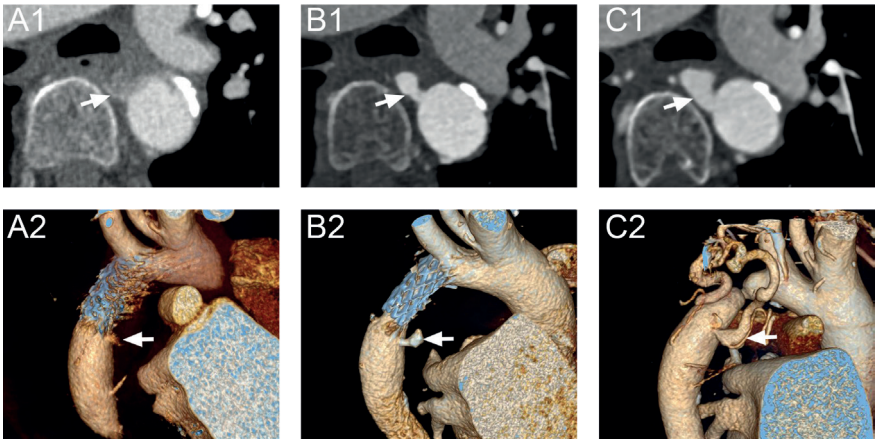

Figure 6. Disruption of the aortic wall

A routine postinterventional scan, acquired the day of the stent implantation (CP stent), showed the presence of a small rim of contrast, with irregular borders, outside the aortic wall in contact with the distal edge of the stent **(A1, A2, arrows)**. Two years later a small outpouching of contrast, with clearly defined borders, resembling a pseudoaneurysm, was found in the same spot **(B1, B2, arrows)**. However, looking back at pre-interventional scans the origin of a dilated collateral was identified at the same location **(C1, C2, arrows)** and, therefore, the finding was attributed to a process of reduced flow/thrombosis of the vessel due to the procedure, and subsequent hemodynamic changes, with partial refilling later on. **A1, B1** and **C1**: multiplanar reconstructions perpendicular to the longitudinal axis of the aorta; **A2, B2** and **C2**: VR reconstructions.

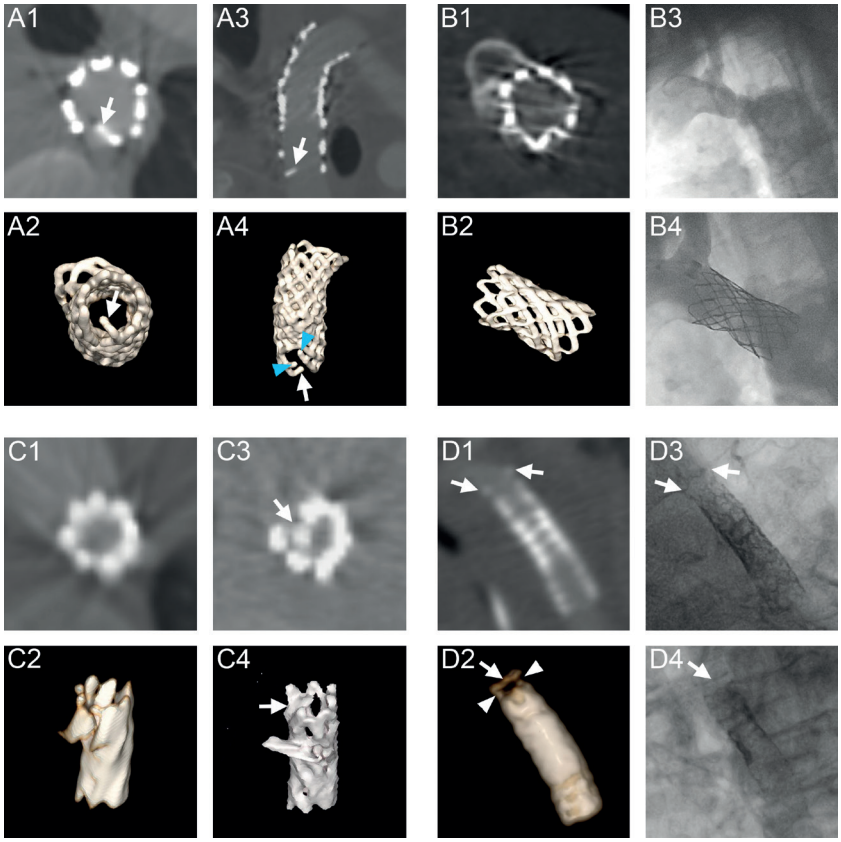

Figure 7. Structural integrity of the stents

A) Loosening of welds. Strut with a loose end **(A1-A4, arrows)** protruding inside the aortic lumen at the distal end of the more caudal one of two overlapping CP stents. Two other loose ends of the wire **(A4, arrowheads)**, with consequent disruption of the normal closed-cells design, could be appreciated. **A1** and **A3**: multiplanar reconstructions perpendicular and parallel to the longitudinal axis of the stent respectively; **A2** and **A4**: VR reconstructions.
B) Incomplete dilatation of the stent. Incomplete dilation of the middle third of a CP stent **(B1, B2)**. In case of very severe aortic coarctation and/or of a large difference in diameter between the coarctation and the adjacent aorta **(B3)**, this can represent the expected, and desired, post-procedural appearance of the stent **(B4)**. **B1**: multiplanar reconstruction perpendicular to the longitudinal axis of the stent; **B2**: VR reconstruction.
C) Stent collapse. Two CT scans of the same patient demonstrating a normal covered CP stent **(C1, C2)**, although with a small caliber, and, ten months later, the collapse of its proximal end **(C3, C4, arrows)** with further reduction of the caliber of the stent lumen. **C1** and **C3**: multiplanar reconstructions perpendicular to the longitudinal axis of the stent; **C2** and **C4**: VR reconstruction.
D) Stent fracture. Fracture of the most cranial of three overlapping coronary stents (Integrity (MedTronic), Aneugraft Dx (Amnis Therapeutix) and Graftmaster JoStent (Abbott)), that were chosen due to the small caliber of the aorta in this one-year old baby, with detachment of the most proximal wire **(D1, D2, arrows).** Only at two locations **(D2, arrowheads)** it was possible to appreciate the normal fusion points with the adjacent wire. The finding was confirmed by a later angiographic procedure **(D3, D4, arrows). D1**: multiplanar reconstruction parallel to the longitudinal axis of the stent; **D2**: VR reconstruction.

The most common causes of restenosis are recoil, disruption of the stent structure and intimal hyperplasia (20). The aim of treatment in these patients is the cure or control of hypertension and preservation of ventricular function. However, there are no strict and broadly accepted criteria for reintervention (7).

Restenosis can be ascribed to progressive recoil of the stent itself, generally involving its proximal and middle third **(Fig. 8; A1-C1; E1-F1)**. This situation has to be differentiated from an incomplete dilation of the stent at the time of deployment due to the small diameter at the level of the coarctation. Radiographic relief of stenosis on follow up CTs has been defined as a final diameter greater than 75% of the diameter of the diaphragmatic aorta (10).

Also a disruption of the structure of the stent causing a reduction of its caliber (collapse, rupture with dislocation of its portions etc.) can cause restenosis.

Intimal hyperplasia can be incidentally found in children undergoing staged dilation and identified as the cause of restenosis in up to half of the cases (9,28). CT has shown excellent correlation with digital angiography for the detection of in-stent restenosis (12). CT findings are the same as in other body districts: a layer of hypodense material attached to the wall of the stent in continuity or not with the native aortic wall **(Fig. 9; A1-D3; E1-G2)**.

Stent migration. Stent migration is the most common technical complication which can occur during the procedure, when it can be solved with immediate repositioning or additional stent placement. More rarely, it can be detected later at follow-up (29). The stent can migrate both proximally and distally **(Fig. 10; A-D)**.

Multiple stents

Multiple stents can be implanted in series (with or without overlapping portions) or inside a previously implanted stent. In the first case, they can be placed during a single procedure and are usually employed to treat a long narrowed segment for which one stent is not enough or to dilate two separate lesions. In the second case, the additional stent is implanted inside the first one during a later intervention to treat complications derived from the first procedure **(Fig. 8; C2-D2; F2-G2).** In this circumstance the second stent can be of the same or different type while a covered stent might be necessary in case of associated lesions of the aortic wall.

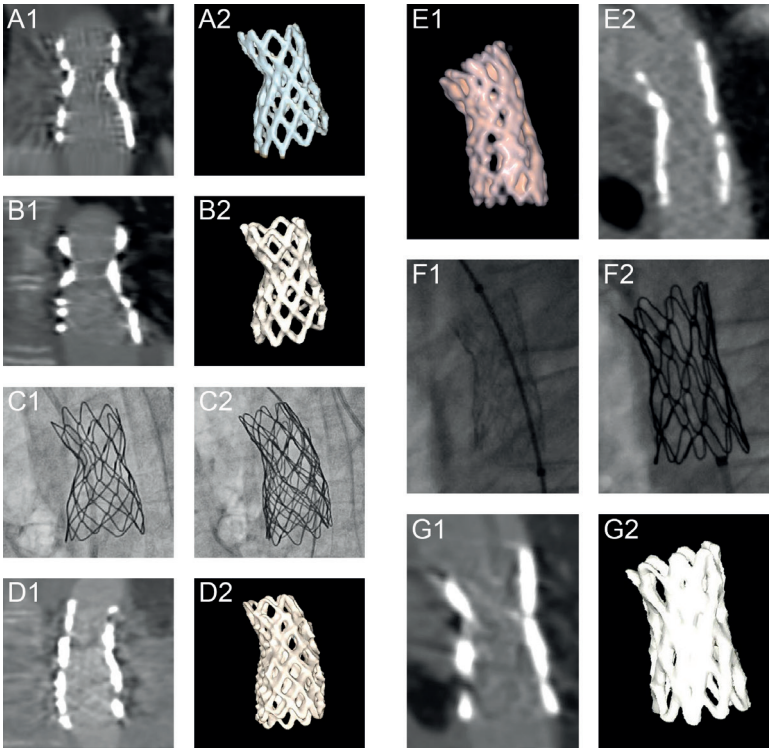

Figure 8. Recoarctation treated with stent in stent

Case 1 (A1-D2) - Restenosis of a CP stent treated with an additional CP stent. A few days after the implantation of a CP stent, a CT scan showed the reduced diameter of the middle third of the stent compared to its proximal and especially distal thirds **(A1, A2)**. A CT performed eleven years later demonstrated further reduction of the diameter of the middle segment **(B1, B2**). At angiography **(C1)** the stricture corresponded to a significant gradient and, therefore, another CP stent was deployed almost completely overlapping the first one **(C2)**. A CT performed a few hours after the procedure **(D1, D2)** showed the well dilated structure of both stents and no complications. **A1, B1** and **D1**: multiplanar reconstructions parallel to the longitudinal axis of the stent; **A2, B2** and **D2**: VR reconstructions.

Case 2 (E1-G2) - Restenosis of an Atrium Advanta stent treated with a CP stent. A CT scan of an Atrium Advanta V12 stent, placed in the descending aorta at the level of the origin of the left subclavian artery **(LSA)** 1.5 months before, showed a narrowing at mid-length **(E1, E2)**. The finding was confirmed by angiography **(F1)**. During balloon dilation a fracture of the stent occurred and thereafter an uncovered CP stent was placed inside. Due to the complete overlap of the two stents, only the structure of the CP stent can be recognized at both the post-procedural angiogram **(F2)** and CT **(G1, G2)** due to its more pronounced radio-opacity. **E1** and **G2**: VR reconstructions; **E2** and **G1**: multiplanar reconstructions parallel to the longitudinal axis of the stent.

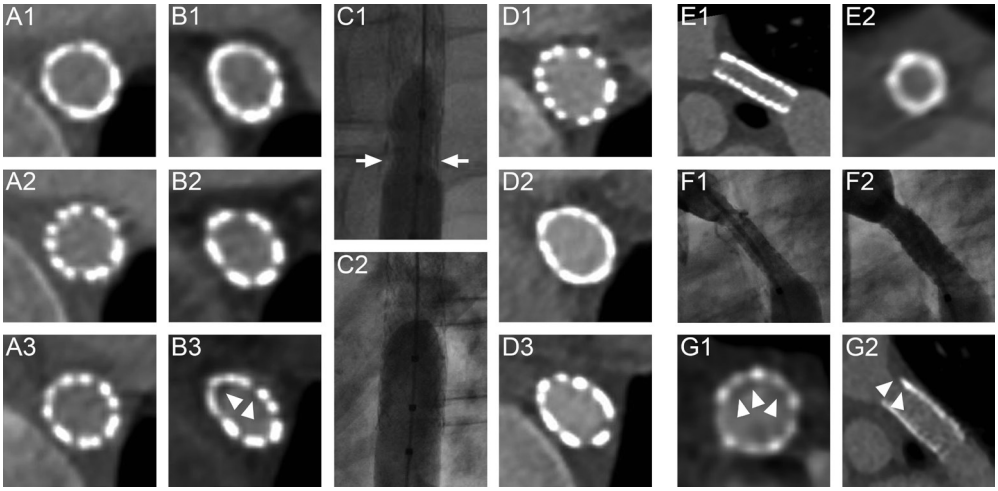

Figure 9. Intimal hyperplasia

Case 1 (A1-D3) - Distal intimal hyperplasia treated with balloon redilatation. The restenosis of a previously surgically treated coarctation of the thoracic descending aorta in a 16-year old man was corrected by stent (Atrium Advanta V12) placement. The day after the procedure a CT scan **(A1-A3)** showed the correct dilatation of the stent and did not demonstrate any complications. Three months later a newly performed CT revealed a deformation of the stent **(B1-B3)** gradually more pronounced moving towards the distal end **(B3)**. At the same level also a rim of hypodense material adjacent to the inner border of the structure of the stent **(B3, arrowheads)**, compatible with intimal hyperplasia, could be appreciated. Angiography confirmed the finding **(C1, arrows)** and a balloon redilatation was performed, which resulted in good patency of the stent **(C2)**. Three years later at a new CT examination **(D1-D3)** the distal portion of the stent did not show any signs of restenosis **(D3)**. **A1-A3, B1-B3** and **D1-D3**: multiplanar reconstructions perpendicular to the longitudinal axis of the stent at the proximal **(A1, B1** and **D1)**, mid **(A2, B2** and **D2)** and distal **(A3, B3** and **D3)** third of the stent.

Case 2 (E1-G2) - Proximal intimal hyperplasia after balloon redilatation. Recoarctation of a surgically treated coarctation in a five months old girl was treated with a Formula stent. Two years later a CT demonstrated a homogeneously small calibre of the stent **(E1, E2)**. A successful balloon dilation was performed to restore the normal dimensions **(F1, F2)**. Thereafter, a new CT suggested the presence of intimal in-growth, appearing as a rim of hypodense material extending from the aortic wall immediately cranial to the stent inside the proximal inlet of the stent **(G1, G2, arrowheads)**. **E1** and **G2**: multiplanar reconstructions parallel to the longitudinal axis of the stent; **E2** and **G1**: multiplanar reconstructions perpendicular to the longitudinal axis of the stent.

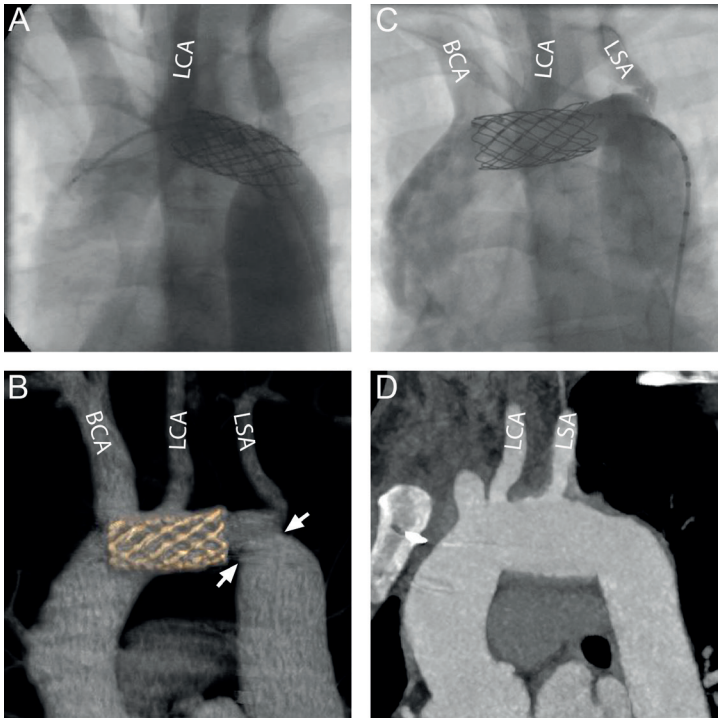

Figure 10. Proximal stent migration

A control angiogram after implantation of a CP stent (A) showed the location of its proximal extremity at the level of the left carotid artery (LCA). One year later a CT scan (B) demonstrated the proximal migration of the stent to the origin of the brachiocephalic artery (BCA) as well as the small diameter of the aorta (B, arrows) in the portion distal to the stent and to the left subclavian artery (LSA), that was interpreted as residual coarctation. Both findings were later confirmed by angiography (C). Surgical treatment included removal of the stent, reconstruction of the aortic arch with a graft and reimplantation of the left subclavian artery as shown by a post-surgical CT scan (D). B: VR reconstruction; D: multiplanar reconstruction parallel to the longitudinal axis of the aortic arch

Conclusion

CT is of great importance in the postoperative care of patients with stent treated coarctation. The knowledge of normal and pathological postoperative findings at CT allows prompt recognition of complications, which is crucial for correct patient management.

References

1. Baumgartner H, Bonhoeffer P, De Groot NMS, De Haan F, Deanfield JE, Galie N, et al. ESC Guidelines for the management of grown-up congenital heart disease (new version 2010). Eur Heart J. 2010;31(23):2915–57.
2. Yen Ho S, Anderson RH. Coarctation, tubular hypoplasia, and the ductus arteriosus Histological study of 35 specimens'. Br Hear. 1979;41(May 1978):268–74.
3. Moore JW, Vincent RN, Beekman RH, Benson L, Bergersen L, Holzer R, et al. Procedural results and safety of common interventional procedures in congenital heart disease: Initial report from the national cardiovascular data registry. J Am Coll Cardiol. 2014;64(23):2439–51.
4. Krasemann T, Bano M, Rosenthal E, Qureshi S a. Results of stent implantation for native and recurrent coarctation of the aorta-follow-up of up to 13 years. Catheter Cardiovasc Interv. 2011;45(4):405–12.
5. Vergales JE, Gangemi JJ, Rhueban KS, Lim DS. Coarctation of the aorta - the current state of surgical and transcatheter therapies. Curr Cardiol Rev. 2013;9(3):211–9.
6. Forbes TJ, Gowda ST. Intravascular stent therapy for coarctation of the aorta. Methodist Debakey Cardiovasc J. 2014;10(2):82–7.
7. Forbes TJ, Kim DW, Du W, Turner DR, Holzer R, Amin Z, et al. Comparison of surgical, stent, and balloon angioplasty treatment of native coarctation of the aorta: An observational study by the CCISC (Congenital cardiovascular interventional study consortium). J Am Coll Cardiol. 2011;58(25):2664–74.
8. Mohan UR, Danon S, Levi D, Connolly D, Moore JW. Stent Implantation for Coarctation of the Aorta in Children <30 kg. JACC Cardiovasc Interv. Elsevier Inc.; 2009;2(9):877–83.
9. Thanopoulos BD, Giannakoulas G, Giannopoulos A, Galdo F, Tsaoussis GS. Initial and six-year results of stent implantation for aortic coarctation in children. Am J Cardiol. Elsevier Inc.; 2012;109(10):1499–503.
10. Chakrabarti S, Kenny D, Morgan G, Curtis SL, Hamilton MCK, Wilde P, et al. Balloon expandable stent implantation for native and recurrent coarctation of the aorta-prospective computed tomography assessment of stent integrity, aneurysm formation and stenosis relief. Heart. 2010;96(15):1212–6.
11. Chessa M, Carrozza M, Butera G, Piazza L, Negura DG, Bussadori C, et al. Results and mid-long-term follow-up of stent implantation for native and recurrent coarctation of the aorta. Eur Heart J. 2005;26(24):2728–32.
12. Eichhorn JG, Long FR, Hill SL, O'Donovan J, Chisolm JL, Fernandez SA, et al. Assessment of in-stent stenosis in small children with congenital heart disease using multi-detector computed tomography: A validation study. Catheter Cardiovasc Interv. 2006;68(1):11–20.
13. Meadows J, Minahan M, McElhinney DB, McEnaney K, Ringel R. Intermediate outcomes in the prospective, multicenter coarctation of the aorta stent trial (COAST). Circulation. 2015;131(19):1656–64.

14. Stoeckel D, Bonsignore C, Duda S. A survey of stent designs. Minim Invasive Ther Allied Technol. 2002;11(4):137–47.
15. Godart F. Intravascular stenting for the treatment of coarctation of the aorta in adolescent and adult patients. Arch Cardiovasc Dis. 2011;104(12):627–35.
16. Tzifa A, Ewert P, Brzezinska-Rajszys G, Peters B, Zubrzycka M, Rosenthal E, et al. Covered cheatham-platinum stents for aortic coarctation: Early and intermediate-term results. J Am Coll Cardiol. 2006;47(7):1457–63.
17. Taggart NW, Minahan M, Cabalka AK, Cetta F, Usmani K, Ringel RE. Immediate Outcomes of Covered Stent Placement for Treatment or Prevention of Aortic Wall Injury Associated with Coarctation of the Aorta (COAST II). JACC Cardiovasc Interv. 2016;9(5):484–93.
18. Butera G, Manica JLL, Marini D, Piazza L, Chessa M, Filho RIR, et al. From Bare to Covered: 15-year single center experience and follow-up in trans-catheter stent implantation for aortic coarctation. Catheter Cardiovasc Interv. 2014;83(6):953–63.
19. Qureshi AM, McElhinney DB, Lock JE, Landzberg MJ, Lang P, Marshall AC. Acute and intermediate outcomes, and evaluation of injury to the aortic wall, as based on 15 years experience of implanting stents to treat aortic coarctation. Cardiol Young. 2007 Jun 26;17(03):307.
20. Chamié F, Chamié D, Simões LC do N, Silva RM. Uso de stents recobertos no tratamento da coarctação da aorta. Rev Bras Cardiol Invasiva. 2015 Apr;23(2):139–44.
21. Pugliese F, Cademartiri F, van Mieghem C, Meijboom WB, Malagutti P, Mollet NRA, et al. Multidetector CT for Visualization of Coronary Stents. Radiographics. 2006;26(3):887–904.
22. Kalra MK, Sodickson AD, Mayo-Smith WW. CT Radiation: Key Concepts for Gentle and Wise Use. RadioGraphics. 2015;35(6):1706–21.
23. Nievelstein R a J, van Dam IM, van der Molen AJ. Multidetector CT in children: current concepts and dose reduction strategies. Pediatr Radiol. 2011;40(8):1324–44.
24. Willemink MJ, Leiner T, De Jong P a., De Heer LM, Nievelstein R a J, Schilham AMR, et al. Iterative reconstruction techniques for computed tomography part 2: Initial results in dose reduction and image quality. Eur Radiol. 2013;23(6):1632–42.
25. Litmanovich DE, Tack DM, Shahrzad M, Bankier A a. Dose Reduction in Cardiothoracic CT: Review of Currently Available Methods. RadioGraphics. 2014;34(3):1469–89.
26. Xu J, Zhao H, Wang X, Bai Y, Liu L, Liu Y, et al. Accuracy, image quality, and radiation dose of prospectively ecg-triggered high-pitch dual-source ct angiography in infants and children with complex coarctation of the Aorta. Acad Radiol. Elsevier Ltd; 2014;21(10):1248–54.
27. Erbel R, Aboyans V, Boileau C, Bossone E, Bartolomeo RD, Eggebrecht H, et al. 2014 ESC Guidelines on the diagnosis and treatment of aortic diseases: Document covering acute and chronic aortic diseases of the thoracic and abdominal aorta of the adult. The Task Force for the Diagnosis and Treatment of Aortic Diseases of the European . Eur Heart J. 2014;35(41):2873–926.
28. Holzer R, Qureshi S, Ghasemi A, Vincent J, Sievert H, Gruenstein D, et al. Stenting of aortic coarctation: Acute, intermediate, and long-term results of a prospective multi-institutional

registry-Congenital cardiovascular interventional study consortium (CCISC). Catheter Cardiovasc Interv. 2010;76(4):553–63.

29. Forbes TJ, Garekar S, Amin Z, Zahn EM, Nykanen D, Moore P, et al. Procedural results and acute complications in stenting native and recurrent coarctation of the aorta in patients over 4 years of age: A multi-institutional study. Catheter Cardiovasc Interv. 2007;70(2):276–85.
30. Butera G, Gaio G, Carminati M. Redilation of e-PTFE covered CP stents. Catheter Cardiovasc Interv. 2008;72(2):273–7.

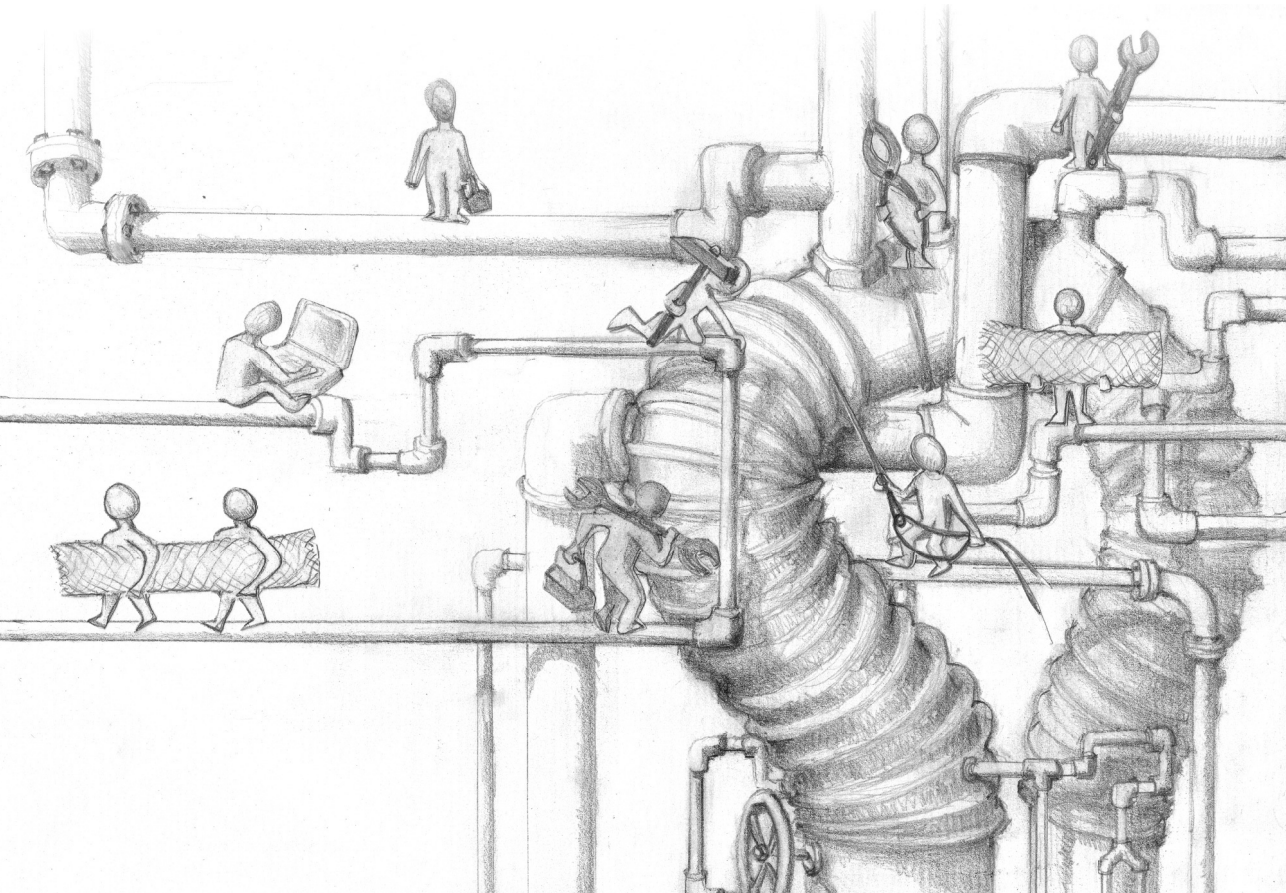

CHAPTER 10

Computed tomography image quality of aortic stents in patients with aortic coarctation: a multicentre evaluation

Sara Boccalini*, Annemarie M. den Harder*, Maarten Witsenburg, Hans P.J.M. Breur, Gabriel P. Krestin, Ingrid M. van Beynum, Nicola Stagnaro, Maurizio Marasini, Pim A. de Jong, Tim Leiner, Ricardo P.J. Budde

Eur Radiol Exp. 2018 Dec; 2: 17

Abstract

Background: Stents are commonly used to treat aortic coarctation. The objective of this study was to evaluate the post-implantation computed tomography (CT) image quality of different stent types used to treat aortic coarctation.

Methods: Adult and paediatric patients with stent-treated aortic coarctation who underwent contrast-enhanced CT were retrospectively included from three tertiary care centres. CT scans were subjectively scored for image quality using a 4-point scale (1=unacceptable; 2=poor; 3=good; 4=excellent). Furthermore, the amount of stent-induced blooming artefacts was measured as the percentage of the difference between outer and inner stent diameters over the outer stent diameter.

Results: A total of 35 children and 34 adults implanted with 71 stents of 6 different types were included. The most commonly used stent type was the Cheatham Platinum stent (52 stents, 73%). Subjective image quality of the Cheatham Platinum stents was moderate with a score of 2.0 ± 0.8 (mean ± standard deviation) in children and 2.3 ± 0.6 in adults. Image quality in patients with Formula stents was 2.3±1.2. Cheatham Platinum stents induced 34-48% blooming, Formula stents 44-55%. Image quality in patients with the less commonly used Atrium Advanta V12, IntraStent, AndraStent and Palmaz stents were scored 3 (good) to 4 (excellent) with less blooming. Electrocardiographic gating and tube voltage (kVp) did not affect image quality.

Conclusions: There is a substantial variation in CT image quality and blooming artefacts for different stent types used to treat aortic coarctation.

Background

Aortic stents are commonly used to treat aortic coarctation in both children and adults [1]. Contrast-enhanced computed tomography (CT) is often performed shortly after implantation to assess if complications have occurred during placement (e.g. dissection) and to evaluate the stent position. CT can also be used during follow-up to detect long-term complications such as in-stent stenosis, intimal hyperplasia, stent displacement and aneurysm formation [2]. According to European guidelines [3], imaging of the aorta should be performed after intervention to document post-implantation anatomy and detect possible complications, with the ideal imaging interval for follow-up depending on the exact baseline pathology. American guidelines [4] recommend follow-up with CT or magnetic resonance imaging (MRI) at intervals of five years or less after stent placement. Although both MRI and CT can be used [5], CT is often the modality of choice since in-stent assessment with MRI can be hampered by artefacts [6].

Several stent types are commercially available and used [7]. Stents were traditionally made of stainless steel, but nowadays different stent materials like cobalt-chromium and platinum-iridium are used as well. It is known that the stent material has a large influence on image quality and stent lumen assessment with CT in coronary stents [8]. However, studies investigating the effect of different stent types on CT image quality for coarctation stents are lacking. Therefore, in this multicentre study the image quality as well as the presence and extent of blooming artefacts generated by different types of aortic stents on CT images were evaluated in patients treated for aortic coarctation.

Methods

This study was performed at three tertiary centres of two different countries. At each centre, the study was approved by the local institutional review board (protocol number 16/243/C, MEC-2016-281 and 290REG2016 respectively). A waiver for the requirement for informed consent was granted at all institutions because the study only involved analysis of previously acquired data.

Patients

Patients with aortic coarctation who underwent a catheterization procedure between 2003 and 2016 were included using the local catheterization registries. Patients in whom an aortic stent was placed as well as patients who underwent re-dilatation of a previously implanted aortic stent were selected. Subsequently, the Picture Archiving and Communication System (PACS) was searched to select patients who underwent contrast-enhanced CT angiography after implantation. In case multiple follow-up scans were available for a patient, only the first scan after implantation was analysed. Exclusion criteria were an unknown stent type and multiple overlapping stents. For each patient, sex, date of stent implantation, weight and height at implantation, and stent type were recorded. Coded data were used for analysis.

A study flowchart is provided in Fig. 1. In total 96 patients were eligible in three different centres. Eleven patients were excluded because the stent type was unknown and 16 patients were excluded because multiple overlapping stents were present. Therefore, 69 patients were included of whom 35 were 18 years or younger at the time of stent implantation (paediatric patients).

CT protocols

For all acquisitions, the following parameters were recorded: date; whether or not electrocardiographic gating or triggering was used; heart rate; tube current (mAs); tube voltage (kVp); volumetric CT dose index; dose length product; CT system; and reconstruction slice thickness. The CT protocols adopted at each centre are summarized in Table 1. Characteristics of the CT acquisitions in the paediatric and adult populations are displayed in Table 2.

Table 1. CT protocols per centre

Centre (number of CT exams)		**Centre 1 (n=36)**	**Centre 2 (n=26)**	**Centre 3 (n=7)**
Type of scanner (number of slices)	Siemens Somatom Force (2x192)	6 (17%)	-	-
	Siemens Somatom Drive (2x128)	2 (6%)	-	-
	Siemens Somatom Definition Flash (2x128)	16 (44%)	-	-
	Siemens Somatom Definition AS+ (2x64)	8 (22%)	-	-
	Siemens Sensation 64 (64)	2 (6%)	-	6 (86%)
	Siemens Sensation 16 (16)	2 (6%)	-	-
	Philips Brilliance iCT (2x128)	-	25 (96%)	1 (14%)
	Philips Brilliance 16 (16)	-	1 (4%)	-
	Total	36 (100%)	26 (100%)	7 (100%)
ECG gating		18 (50%)	21 (%)	-
Heart rate (bpm)		79 ± 29	76 ± 21	-
mAs		198 ± 126	176 ± 66	80 ± 33
kVp	*70*	3 (8%)	-	-
	80	3 (8%)	8 (%)	1 (14%)
	90	3 (8%)	1 (%)	-
	100	9 (25%)	11 (%)	5 (71%)
	120	17 (47%)	6 (%)	1(14%)
	140	1 (3%)	-	-
	Total	36 (100%)	26 (100%)	7 (100%)
Volume CT Dose Index (mGy)		5.5 ± 5.2	8 ± 5	3.8 ± 3
Dose length product (mGy x cm)		190 ± 178	255 ± 277	132 ± 96
Slice thickness	0.8	8 (22%)	-	5 (71%)
	0.9	-	12 (50%)	1 (14%)
	1	26 (72%)	2 (77%)	1 (14%)
	1.5	-	12	-
	2	2 (6%)	-	-
	Total	36 (100%)	26 (100%)	7 (100%)
Kernel	B20f	7	-	-
	B26f	3	-	-
	B31f	4	-	-
	B40f	-	-	5
	B46f	1	-	-
	Bv40d	6	-	-
	I26f	16	-	-
	A	-	8	
	B	-	6	1
	C	-	1	-
	CB	-	2	-
	XCA	-	4	-
	XCC	-	5	-
	Total	36 (100%)	26 (100%)	7 (100%)

bpm beats per minute, *CT* computed tomography, *ECG* Electrocardiogram.
Data are frequencies and percentages or means ± standard deviations.

Table 2. CT characteristics in paediatric and adult cases

	Pediatric cases (n=35)	Adult cases (n=34)
Time between implantation and CT		
< 1 month	12 (32%)	28 (82%)
1 month – 1 year	15 (41%)	3 (9%)
> 1 year	10 (27%)	3 (9%)
ECG gating	19 (54%)	20 (59%)
Heart rate (bpm)	82 ± 28	73 ± 21
mAs	135 ± 75	219 ± 114
kVp		
70	3 (9%)	0 (0%)
80	10 (29%)	2 (6%)
90	2 (6%)	2 (6%)
100	15 (43%)	10 (29%)
120	5 (14%)	19 (56%)
140	0 (0%)	1 (3%)
Volume CT Dose Index (mGy)	4.9 ± 3.8	7.7 ± 6.0
Dose length product (mGy x cm)	128 ± 128	292 ± 266
Slice thickness ≤ 1mm	28 (80%)	27(79%)
Type of scanner		
16-slice	1 (3%)	2 (6%)
64-slice	5 (14%)	3 (9%)
>64 slice	29 (83%)	29 (85%)

bpm beats per minute, *CT* computed tomography, *ECG* Electrocardiogram.
Data are frequencies and percentages or means ± standard deviations.

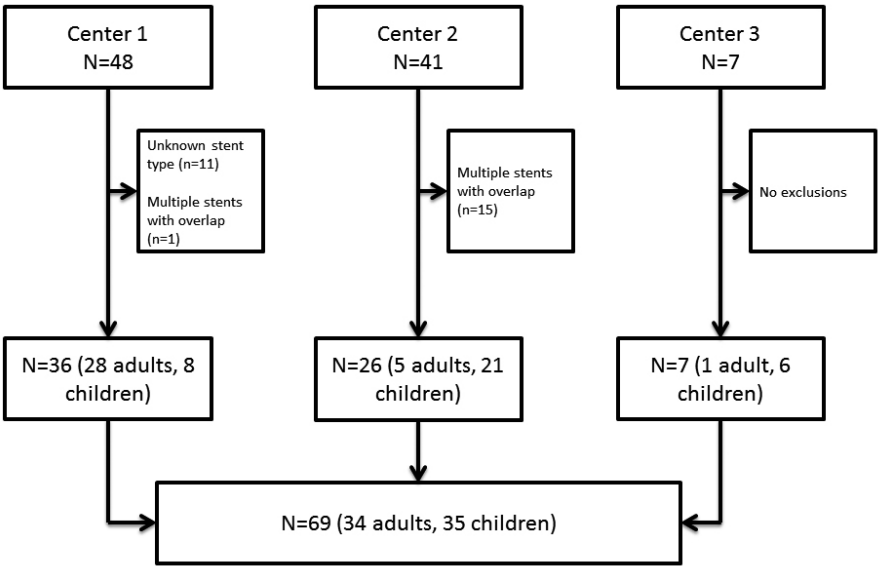

Figure 1

Flowchart of study inclusion

Image quality assessment

Both overall subjective image quality of the lumen and the aortic wall at stent level were scored by one radiologist (SB) with 5 years of CT experience. The aortic wall was scored at three levels (proximal, central and distal third of the stent). Overall subjective image quality of the aortic lumen at the stent level was scored as: 1) unacceptable, non-diagnostic image quality; 2) poor, limited diagnostic value; 3) good, diagnostic image quality; and 4) excellent, optimal diagnostic image quality. Subjective image quality of the aortic wall at stent level was assessed as: 1) unacceptable, non-diagnostic image quality of the aortic wall, aortic wall not assessable due to severe artefacts or excessive noise; 2) poor, image quality of the aortic wall with limited diagnostic value, aortic wall is assessable but partially obscured due to moderate artefacts or noise; 3) good, diagnostic image quality of the aortic wall, possible to diagnose/exclude aortic wall abnormalities with minor artefacts or noise; and 4) excellent, excellent image quality of the aortic wall, possible to diagnose/exclude aortic wall abnormalities without artefacts or noise. Furthermore, it was evaluated if the stent was adjacent to the aortic wall. If there was a distance of ≥5 mm between the proximal and/or distal part of the stent and the aortic wall, this was judged as not adjacent.

A random sample of one third of the cases (n=23) was scored twice by the same observer with an interval of at least two months in between to assess intra-observer variability. The observer was blinded to the previous scores. The same sample was scored by a second observer (RB), a radiologist with 10 years of experience in cardiovascular imaging, to assess inter-observer variability. The second observer was blinded to the results of the first observer.

Objective image quality was evaluated by one observer with 3 years of CT experience (AH) using a bone setting (window width 1600, window level 300). A region of interest (ROI) was placed in the aorta at the level of the pulmonary trunk using thin slice reconstructions with a dedicated angiographic kernel. The ROI was drawn as large as possible without including the vessel wall. In the same slice a ROI was placed in the muscle tissue. Noise was defined as the standard deviation (SD) in Hounsfield Units (HU) of the ROI. Signal to noise ratio was defined as the ratio between the mean HU and the SD of the same ROI. Contrast to noise ratio was calculated using the following equation [8-10]:

$$CNR = \frac{HU_{contrast\ aorta} - HU_{muscle}}{\sqrt{\frac{1}{2}(SD_{constrast\ aorta}{}^2 + SD_{muscle}{}^2)}}$$

The area-derived stent diameter was measured at three levels at the proximal, central, and distal third of the stent using a bone setting (window width 1600, window level 300). Multiplanar reformations were used to obtain a cross-sectional plane of the stent where measurements were performed. Both the inner and the outer stent diameters were derived. Stents struts can appear thicker than they are in reality due to metal related artefacts such as blooming, scatter and partial volume averaging which may lead to the spurious appearance of obstruction of the stent lumen on CT images. For simplification we will refer to this type of artefact as blooming, which was calculated by the following formula [5]:

$$blooming = \frac{\text{Measured outer stent diameter} - \text{Measured inner stent diameter}}{\text{Measured outer stent diameter}} \text{ x100\%}$$

Furthermore, the influence of stent diameter on image quality was assessed. For this purpose, the mean of the outer and inner diameter was used, averaged over three measurements (proximal, central, distal). It was assessed if the subjective image quality and the aortic wall image quality was significantly different between electrocardiogram (ECG) gated and non-ECG-gated acquisitions and if the image quality differed for different tube voltage or mAs levels.

Objective image analysis was performed using PACS viewers. Subjective image analysis and diameter measurements were performed locally using the PACS system at one institution and centrally with the same multimodality workstation with multiplanar reconstructions for the other two centres.

Assessment of complications

Each scan was assessed regarding the presence of any anomalies/complications in regard to the stent structure and position, the aortic wall, and aortic branches. The official reports were also retrospectively evaluated. Thereafter, patients' files were retrieved to assess if the changes were already mentioned in the description of the procedure and if the patient underwent further examination that confirmed the CT findings. Furthermore medical records were checked to verify if any change in patient management directly related to the CT findings had been undertaken.

Statistical analysis

SPSS version 21.0 for Windows (IBM, Armonk, New York, USA) and RStudio version 1.0.153 (RStudio, Inc., Boston, Massachusetts, USA) were used for statistical analysis. Values are displayed as mean ± SD unless stated otherwise. Differences in scores between stent types were assessed with the Mann-Whitney U test. The influence of ECG gating, kilovoltage and mAs on image quality was tested using the χ^2-test, Fischer's exact test, and Kruskall-Wallis test. The correlation between blooming artefacts and kVp and mAs was investigated with the Spearman correlation coefficient. A p-value below 0.05 was considered statistically significant. To assess the intra-observer agreement and reliability, the percentage of agreement and the quadratic weighted κ were calculated. For the remaining data descriptive analysis was used.

Results

Patient characteristics

Baseline patient characteristics are provided in *Table 3*. All adults had the Cheatham Platinum stent (NuMed Inc., Hopkinton, New York, USA) implanted, while different stent types were used in the paediatric patients namely Cheatham Platinum (n=18), Atrium Advanta V12 (n=5, Atrium, Maquet Holding B.V. & Co. KG, Rastatt, Germany), IntraStent (n=4, EV3 Inc., Plymouth, Minnesota, United States), Formula (n=3, Cook Medical, Bloomington, Indiana, United States), AndraStent (n=4, Andramed GmbH, Reutlingen, Germany) and Palmaz (n=3, Johnson & Johnson, New Brunswick, New Jersay, USA). The characteristics of the different stents are provided in *Table 4*. An example of CT images of the different stents is provided in *Fig. 2*. Two paediatric patients had two stents which were not overlapping. The mean stent diameter was 15 ± 4 mm.

Table 3. Patient characteristics

		Paediatric cases (n=35, 37 stents)	Adult cases (n=34)
Males		20 (57%)	17 (50%)
Age (years)		10 ± 5	42 ± 16
Length (cm)		136 ± 37	173 ± 11
Weight (kg)		37 ± 20	84 ± 20
Type of stent			
	Cheatham Platinum	18 (49%)	34 (100%)
	Atrium Advanta V12	5 (14%)	0 (0%)
	IntraStent	4 (11%)	0 (0%)
	AndraStent	4 (11%)	0 (0%)
	Formula	3 (8%)	0 (0%)
	Palmaz	3 (8%)	0 (0%)
Multiple stents			
	2 stents	2 (6%)	0 (0%)

Data are frequencies and percentages or means ± standard deviations.

Table 4. Stent characteristics

Stent type	Manufacturer	Material	Design
Cheatham Platinum	NuMed Inc.	platinum-iridium and joints over brazed with gold	Closed-cell
Atrium Advanta V12	Atrium	316L stainless steel	Open-cell
IntraStent	EV3 Inc.	stainless steel	Open-cell
AndraStent	Andramed GmbH	cobalt chromium	Hybrid (open- and closed-cell)
Formula	Cook Medical	316L stainless steel	Open-cell
Palmaz	Johnson & Johnson	stainless steel	Closed-cell

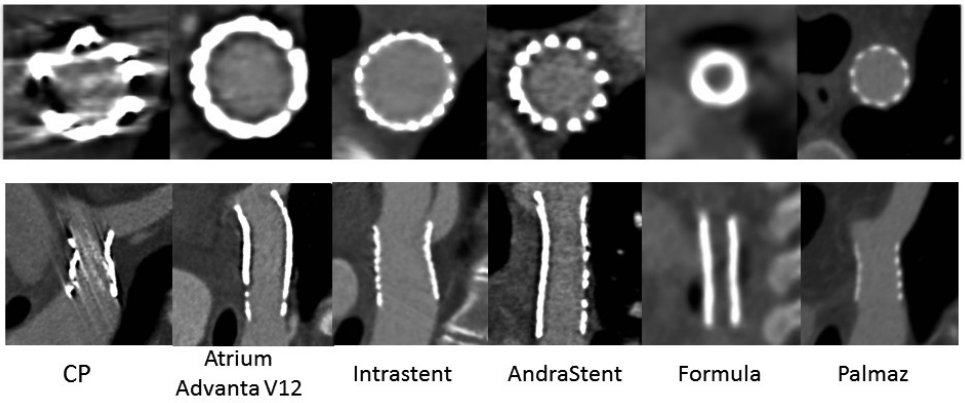

Figure 2

Overview of the different stent types. All images were acquired using a bone setting (window width 1600, window level 300), which was also used for image quality assessment. *CP*, Cheatham Platinum.

CT characteristics

ECG-gating was used in 54% of paediatric and 59% of adult patients. The heart rate was higher in paediatric patients:82 ± 28 beats per minute (bpm) compared to 73 ± 21 bpm in adults. The mAs and kVp were lower in the paediatric population, resulting in a lower radiation dose. The majority of acquisitions (83% paediatrics, 85% adults) were performed on ≥64 slice scanners.

Image quality

Subjective and objective image quality results are provided in *Table 5*. Objective image quality was comparable between paediatrics and adults. The Cheatham Platinum and Formula stents had an overall subjective image quality of the lumen between 2 (poor) and 3 (good). Formula stents also had a relatively small stent diameter of 6 ± 1 mm. Other stents scored good (score 3) to excellent (score 4) namely 3.4 (Atrium Advanta V12), 3.5 (IntraStent), 3.8 (AndraStent) and 4.0 (Palmaz). The results for the aortic wall image quality were similar, with poor scores for the Cheatham Platinum stent while the other stents scored good to excellent. When comparing Cheatham Platinum stents against each of the other stent types, the differences in subjective scores were statistically significant at all levels and for all stents (Advanta Atrium V12: lumen $p=0.003$, proximal aortic wall $p=0.001$, central aortic wall $p<0.001$, distal aortic wall $p=0.05$; Formula: proximal aortic wall $p=0.006$, central aortic wall $p=0.002$, distal aortic wall $p=0.019$; Intrastent: lumen $p=0.001$, proximal aortic wall $p<0.001$, central aortic wall $p<0.001$, distal aortic wall $p<0.001$; Palmaz: lumen $p<0.001$, proximal aortic wall $p<0.001$, central aortic wall $p<0.001$, distal aortic wall $p=0.001$; Andrastent: lumen $p<0.001$, proximal aortic wall $p=0.001$, central

Table 5. Objective and subjective image quality per stent type

	Average stent diameter (mm)	Noise Aorta (HU)	Noise Muscle (HU)	Signal to noise ratio Aorta	Signal to noise ratio Muscle	Contrast to noise	Overall subjective image quality	Image quality aorta proximal score	Image quality aorta central score	Image quality aorta distal score
Paediatrics										
Cheatham Platinum (n=18)	14 ± 3	30 ± 13	24 ± 10	13 ± 7	3 ± 2	12 ± 6	2.0 ± 0.8	2.3 ± 0.7	2.0 ± 0.7	2.4 ± 0.8
Atrium Advanta V12 (n=5)	11 ± 3	28 ± 16	23 ± 8	13 ± 2	3 ± 1	11 ± 3	3.4 ± 0.9	3.6 ± 0.5	3.6 ± 0.5	3.6 ± 0.5
IntraStent (n=4)	12 ± 4	44 ± 21	26 ± 9	12 ± 7	3 ± 1	13 ± 6	3.5 ± 0.6	4.0 ± 0.0	4.0 ± 0.0	4.0 ± 0.0
AndraStent (n=4)	17 ± 3	32 ± 17	32 ± 23	15 ± 6	3 ± 1	14 ± 7	3.8 ± 0.5	3.8 ± 0.5	3.8 ± 0.5	3.8 ± 0.5
Formula (n=3)	6 ± 1	30 ± 17	15 ± 5	10 ± 2	6 ± 1	9 ± 1	2.3 ±1.2	3.7 ± 0.6	3.7 ± 0.6	3.7 ± 0.6
Palmaz (n=3)	15 ± 1	29 ± 16	28 ± 13	17 ± 11	3 ± 1	14 ± 8	4.0 ± 0.0	4.0 ± 0.0	4.0 ± 0.0	4.0 ± 0.0
Adults										
Cheatham Platinum (n=34)	17 ± 3	27 ± 11	24 ± 8	14 ± 7	3 ± 1	12 ± 6	2.3 ± 0.6	2.3 ± 0.8	1.9 ± 0.8	2.6 ± 0.7

Data are means ± standard deviations. *HU* Hounsfield unit

aortic wall p<0.001, distal aortic wall p=0.003) with the exception of the image quality score of the lumen for the Formula stent (p=0.564). An example of the different scores for the aortic wall image quality is provided in *Fig. 3*. In *Fig. 4* a case example of a patient with both a Cheatham Platinum stent and an AndraStent illustrates the differences in image quality between the stents. Seventeen percent (12/71) of the stents were not completely adjacent to the aortic wall.

The subjective image quality and the aortic wall image quality were not significantly different between ECG-gated and non-ECG-gated acquisitions. Also the tube voltage and mAs did not significantly alter the subjective image quality of the overall lumen (p=0.703 and p=0.425, respectively) and of the aortic wall at the proximal (p=0.412 and p=0.263, respectively) and distal third (p=0.568 and p=0.225, respectively). A weak influence on the image quality of the aortic wall at the level of the central third of the stent was found for the kVp (p=0.038) but not for the mAs (p=0.227).

The percentages of blooming per stent type are provided in *Table 6*. Blooming was highest for the Formula stent 55% (at the centre of the stent). Also the Cheatham Platinum stents were associated with considerable blooming, namely 48% in paediatrics and 42% in adults. In the remaining stents, there was from 22% to 37% blooming. In most stent types, blooming was higher at the centre of the stent compared to the outlets. A weak negative correlation was found between mAs and blooming artefacts at all levels of the stents (proximal, ρ=-0.345, p=0.003; central, ρ=-0.299, p=0.012; distal, ρ=-0.258, p=0.031). No influence of kVp on blooming artefacts was found (proximal, p=0.085; central, p=0.285; distal, p=0.122).

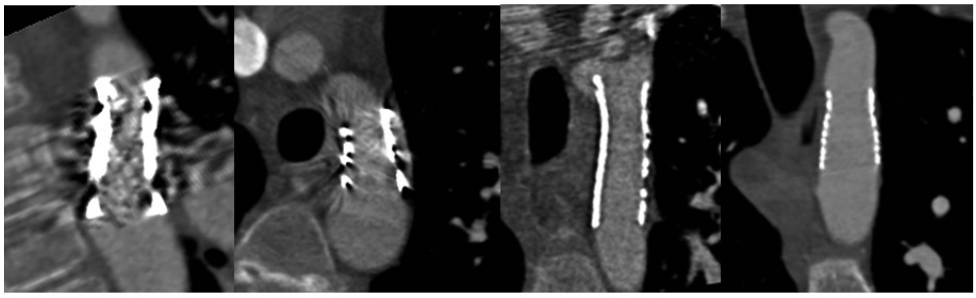

Figure 3

Examples of the scores from 1 to 4 for the aortic wall image quality. All images were acquired using a bone setting (window width 1600, window level 300), which was also used for image quality assessment.

Figure 4

Differences in image quality between stents. Example illustrating the different image quality of two stents implanted in the same patient and, therefore, imaged with the same CT technical parameters (A). The more cranial stent (B1-B4) was an AndraStent that showed excellent quality of the lumen (B1) and of the aortic wall at stent level at the proximal (B2), mid (B3) and distal (B4) thirds of the stent. The more caudal stent was a Cheatham Platinum stent that showed lower image quality for both the lumen (C1) and the aortic wall at the three examined levels (C2, C3, C4).

Table 6. Amount of blooming per stent type

	Percentage blooming proximal (%)	Percentage blooming central (%)	Percentage blooming distal (%)
Paediatrics			
Cheatham Platinum (n=18)	42 ± 7	48 ± 10	35 ± 15
Atrium Advanta V12 (n=5)	34 ± 13	37 ± 11	32 ± 7
IntraStent (n=4)	29 ± 7	36 ± 12	31 ± 11
AndraStent (n=4)	24 ± 1	23 ± 5	22 ± 6
Formula (n=3)	47 ± 5	55 ± 5	44 ± 13
Palmaz (n=3)	24 ± 4	22 ± 5	30 ± 19
Adults			
Cheatham Platinum (n=34)	35 ± 4	41 ± 10	34 ± 5

Data are means ± standard deviations.

The influence of the stent diameter on the image quality was only assessed for the Cheatham Platinum stents, since only a limited number of stents were included for the other stent types. The results are provided in *Table 7*. A bigger stent diameter was associated with a higher subjective image quality and image quality of the aortic wall as well as less blooming.

Table 7. Influence of stent diameter on the subjective image quality, image quality of the aorta and the amount of blooming for the Cheatham Platinum stent
Stents implanted in adults (n=34) and paediatrics (n=18) were combined

	Subjective image quality	Image quality aorta proximal score	Image quality aorta central score	Image quality aorta distal score	Percentage blooming proximal	Percentage blooming central	Percentage blooming distal
< 13 mm (n=9)	1.8 ± 0.7	1.7 ± 0.4	1.7 ± 0.5	1.9 ± 0.3	45.8 ± 5.8	51.1 ± 10.0	40.5 ± 4.3
13 – 15 mm (n=11)	1.9 ± 0.7	2.2 ± 0.8	1.6 ± 0.7	2.5 ± 0.7	40.0 ± 4.6	50.7 ± 12.6	39.3 ± 6.3
15 – 17 mm (n=15)	2.1 ± 0.5	2.1 ± 0.6	1.9 ± 0.7	2.6 ± 0.7	36.7 ± 3.7	41.3 ± 5.0	32.2 ± 1.5
17 – 20 mm (n=10)	2.6 ± 0.5	2.6 ± 0.5	2.3 ± 0.7	2.6 ± 0.8	34.2 ± 2.8	38.4 ± 5.0	32.7 ± 2.7
>20 mm (n=7)	2.7 ± 0.5	3.0 ± 1.0	2.4 ± 1.1	3.1 ± 0.7	29.7 ± 2.0	33.9 ± 4.2	27.5 ± 2.3

Data are means ± standard deviations.

Intra- and inter-observer reliability and agreement

Intra-observer agreement for subjective image quality was 96%. Agreement for the image quality of the aortic wall at stent level was 96%, 87% and 79% for the proximal, central and distal part of the stent, respectively. The intra-observer reliability was excellent with a weighted κ of 0.955 for the overall subjective image quality and 0.973, 0.928 and 0.848 for the image quality of the aortic wall for the proximal, central, and distal part of the stent respectively.

Inter-observer agreement for the subjective image quality of the lumen was 67%. Agreement for the image quality of the aortic wall at the proximal, central and distal part of the stent was 63%, 63% and 42%, respectively. The inter-observer reliability was good with a weighted κ of 0.695 for the overall subjective image quality and 0.755 and 0.763 for the image quality of the aortic wall for the proximal and central part of the stent, respectively. The inter-observer reliability for the image quality of the aortic wall at the level of the distal part of the stent was moderate with a weighted κ of 0.529. In no cases the difference between the scores of the two observers was of more than one point.

Detection of anomalies/complications

In total, 1 active bleeding, 1 pseudoaneurysm, 11 branches arising from the stent, 1 occluded branch, 2 cases of suspected intimal hyperplasia, 8 cases with focal stricture of the stent, and 2 cases with both a stricture and a branch emerging from the stent were found.

In 2 cases the presence of a portion of the stent with a smaller diameter noticed on the CT scan had not been previously mentioned in the report of the stent implantation procedure. In 1 of these cases, as a consequence of the CT finding, the patient underwent an angiographic procedure that confirmed the restenosis, as well as its hemodynamic significance, and allowed subsequent re-dilatation. The procedural reports of the cases in which the active bleeding and the pseudoaneurysm were found on the follow-up CT scans, indicated a regular and uneventful intervention. Following the CT scan, the first patient with massive haemorrhage was operated upon but died the same day. For the second patient a conservative management was undertaken after the CT scan and a later exam showed complete reabsorption of the pseudoaneurysm. The two cases with suspicion of intimal hyperplasia were not further investigated. In the other cases, the CT findings did not result in a modification of the patient management.

Discussion

Coarctation of the aorta represents 5-10% of the cases of congenital heart disease [11]. In former times the only treatment option was surgery, however, since the 1980s transcatheter treatment with balloon angioplasty and, since the 1990s, stent implantation have evolved [11]. Data from the United States National Cardiovascular Data Registry of 671 transcatheter procedures in patients with aortic coarctation show that balloon angioplasty is the most common treatment (50.5%), followed by stent treatment (37.9%) or a combination of both (11.6%) [12]. Until March 2016, there were no United States Food and Drug Administration approved stents for use in the aorta and therefore stents were used off-label for this indication [13]. In 2016 the Cheatham Platinum stent obtained Food and Drug Administration approval, while the stent already had a CE mark for use on the European market[14]. A prospective multicentre trial in 105 patients showed that the Cheatham Platinum stent is safe and effective [13]. Data on the safety and effectiveness of off label stents are absent or limited to small retrospective studies [11; 15-17]. The choice to implant a specific type of stent relies on clinical and anatomical characteristics of the patients such as age, diameter of the aorta and of the stricture, previous operations/ interventions, site of the lesion and anatomy of adjacent aorta and aortic branches [18].

There is consensus that follow-up imaging should be performed after stent implantation; however, the modality and the time interval are less clear [3; 4]. Early on, follow-up is necessary to rule out aortic rupture and delayed bleeding. Later on, other complications like delayed aneurysm formation, restenosis or fracture of the stent might occur. A consortium study with data from 34 centres in 302 patients showed that CT is the most often used imaging modality for follow-up [11]. Three months after implantation 63% of patients had underwent a follow-up CT, while cardiac catheterization (10%) and MRI (12%) were less commonly used. In 16% of patients no follow-up imaging was performed [11].

Although CT is commonly used for follow-up of stents implanted for aortic coarctation, data on the image quality of different stent types on CT are lacking. In this multicentre evaluation of the CT image quality in patients with aortic coarctation implanted with aortic stents, we showed that the most commonly used stent type (Cheatham Platinum) is associated with moderate but still diagnostic image quality on CT, while less commonly used stent types were associated with superior image quality. In addition, ECG gating and tube voltage did not demonstrate any effect on image quality.

The Cheatham Platinum stent consists of platinum-iridium and joints over brazed with gold. The other stent types were made of 316L stainless steel (Atrium Advanta V12 and Formula), stainless steel (IntraStent and Palmaz) and cobalt chromium (AndraStent). Our results regarding the Cheatham Platinum, i.e. the association with a worse but still

diagnostic image quality, are in agreement with the in-vitro study by Köhler et al.[19] who evaluated 22 different types of peripheral artery stents with CT angiography. A poorer image quality was reported for the platinum-iridium and tantalum stents due to blooming artefacts. They attributed this to the higher atomic number of platinum (78) and tantalum (73) compared to cobalt (27), steel (26), and chromium (24) [19]. Other factors which might have an effect on image quality besides the stent material are the stent diameter, strut design and acquisition parameters. In the current study we assessed the influence of stent diameter on the image quality for the Cheatham Platinum stent, and smaller stent diameters were associated with poorer image quality and a larger amount of blooming. This might also explain the results of the Formula stent, which was associated with moderate diagnostic image quality and substantial blooming. However, patients receiving the Formula stent were on average 3-year old, therefore the smaller stent diameters used in those young children might explain the moderate image quality. The subjective image quality of Cheatham Platinum stents with a diameter below 15 mm was poor, however the number of patients in this subgroup analysis was small. Although the image quality of Cheatham Platinum was poor for stents with a small diameter, CT might still be the preferred imaging modality for follow-up in small children because it is relatively non-invasive and adjacent organs can be assessed as well. Although the number of patients with different stent types was too small for analysis, the objective image quality of the scan did not seem to have an impact on the subjective image quality of the stent.

We found a weak negative correlation between mAs and percentage of blooming. Conversely, no effect of ECG-gating and tube voltage on image quality was demonstrated, with the exception of a weak association between tube voltage and image quality of the aortic wall at the middle third of the stent. This might seem in contradiction with previous studies which reported a reduction in terms of metal artefacts by employing reconstructions with higher energy levels obtained from dual energy scans [20-22]. However, in our study the limited number of scans per kVp category and, especially, the additional differences in other scanning parameters are likely to have influenced the results. Moreover, our subjective scoring system was focused on the diagnostic value of the image quality which does not exactly correspond to the amount of artefacts [20]. Therefore, further studies with more standardized imaging protocols are necessary to establish if dual-energy scans and monochromatic reconstructions can improve the image quality of aortic stents.

This is the first large patient study that systematically compared the CT image quality of different stent types used for the treatment of aortic coarctation. It provides insights into differences between stent types and the associated amount of blooming. However, this study has limitations. First, the retrospective design implied that different CT systems and different protocols were used. As a consequence, it was not possible to study the influence

of parameters like contrast medium, kernel and reconstruction technique due to the large heterogeneity of the collected data. However, this resembles the real-world situation in which differences between hospitals are common. Second, the number of patients receiving a stent other than the Cheatham Platinum was limited. Therefore, we could only assess the influence of the stent diameter for the Cheatham Platinum stents, since data for the other stent types was insufficient due to small numbers. Third, the true diameter to which the stent was inflated during angiography was often unknown. Therefore, it was not possible to investigate if the stent diameter measured on CT images differed from the true stent diameter. Finally, although the subjective score for image quality was designed to assess if the image quality was diagnostic, in this study we did not investigate the CT diagnostic accuracy in the absence of a reference test such as angiography performed at the same time. However, the occlusion of aortic branches and their origin from the stent as well the presence of strictures of the stent frame were detected on CT images. Furthermore, the two most relevant complications occurred in this study population (active bleeding and pseudoaneurysm) were identified on CT examinations.

In conclusion, this study provides insights into the image quality and blooming artefacts of different stent types used to treat coarctation of the aorta on CT images. Both radiologists and clinicians should be aware of these differences when prescribing imaging exams, writing reports, and interpreting the results. Radiologists should provide detailed information of the image quality of the CT scans in addition to the findings.

References

1. Eichhorn JG, Long FR, Hill SL et al (2006) Assessment of in-stent stenosis in small children with congenital heart disease using multi-detector computed tomography: a validation study. Catheter Cardiovasc Interv 68:11-20
2. Eichhorn JG, Long FR, Jourdan C et al (2008) Usefulness of multidetector CT imaging to assess vascular stents in children with congenital heart disease: an in vivo and in vitro study. Catheter Cardiovasc Interv 72:544-551
3. Baumgartner H, Bonhoeffer P, De Groot NM et al (2010) ESC Guidelines for the management of grown-up congenital heart disease (new version 2010). Eur Heart J 31:2915-2957
4. Warnes CA, Williams RG, Bashore TM et al (2008) ACC/AHA 2008 Guidelines for the Management of Adults with Congenital Heart Disease: a report of the American College of Cardiology/ American Heart Association Task Force on Practice Guidelines (writing committee to develop guidelines on the management of adults with congenital heart disease). Circulation 118:e714-833
5. den Harder AM, Sucha D, van Hamersvelt RW et al (2017) Imaging of pediatric great vessel stents: Computed tomography or magnetic resonance imaging? PLoS One 12:e0171138
6. Jurcut R DA, Lorber A (2011) Coarctation of the aorta in adults: what is the best treatment? Case report and literature review. J Med Life 4:189-195.
7. Maintz D SH, Raupach R et al (2003) Balloon expandable stents for coarctation of the aorta: review of current status and technical considerations. Eur Radiol 5:25–41
8. Maintz D, Seifarth H, Raupach R et al (2006) 64-slice multidetector coronary CT angiography: in vitro evaluation of 68 different stents. Eur Radiol 16:818-826
9. den Harder AM, Willemink MJ, Bleys RL et al (2014) Dose reduction for coronary calcium scoring with hybrid and model-based iterative reconstruction: an ex vivo study. Int J Cardiovasc Imaging 30:1125-1133
10. Szucs-Farkas Z, Strautz T, Patak MA, Kurmann L, Vock P, Schindera ST (2009) Is body weight the most appropriate criterion to select patients eligible for low-dose pulmonary CT angiography? Analysis of objective and subjective image quality at 80 kVp in 100 patients. Eur Radiol 19:1914-1922
11. Holzer R, Qureshi S, Ghasemi A et al (2010) Stenting of aortic coarctation: acute, intermediate, and long-term results of a prospective multi-institutional registry--Congenital Cardiovascular Interventional Study Consortium (CCISC). Catheter Cardiovasc Interv 76:553-563
12. Moore JW, Vincent RN, Beekman RH, 3rd et al (2014) Procedural results and safety of common interventional procedures in congenital heart disease: initial report from the National Cardiovascular Data Registry. J Am Coll Cardiol 64:2439-2451
13. Meadows J, Minahan M, McElhinney DB, McEnaney K, Ringel R, Coast I (2015) Intermediate Outcomes in the Prospective, Multicenter Coarctation of the Aorta Stent Trial (COAST). Circulation 131:1656-1664

14. Zuckerman B (2016) FDA approval Cheatham Platinum stent. https://www.accessdata.fda.gov/cdrh_docs/pdf15/P150028a.pdf. Accessed 20 April 2018.
15. Venczelova Z, Tittel P, Masura J (2013) First experience with AndraStent XL implantation in children and adolescents with congenital heart diseases. Catheter Cardiovasc Interv 81:103-110
16. Bondanza S, Calevo MG, Marasini M (2016) Early and Long-Term Results of Stent Implantation for Aortic Coarctation in Pediatric Patients Compared to Adolescents: A Single Center Experience. Cardiol Res Pract 2016:4818307
17. Hak Lee Ang TCWL (2014) Coarctation of the aorta: nonsurgical treatment using stent implantation. Singapore Med J 55:302-304
18. Boccalini S, den Harder AM, Witsenburg M et al (2017) Complications After Stent Placement for Aortic Coarctation: A Pictorial Essay of Computed Tomographic Angiography. J Thorac Imaging 32:W69-W80
19. Kohler M, Burg MC, Bunck AC, Heindel W, Seifarth H, Maintz D (2011) Dual-Source CT Angiography of Peripheral Arterial Stents: In Vitro Evaluation of 22 Different Stent Types. Radiol Res Pract 2011:103873
20. Meinel FG, Bischoff B, Zhang Q, Bamberg F, Reiser MF, Johnson TR (2012) Metal artifact reduction by dual-energy computed tomography using energetic extrapolation: a systematically optimized protocol. Invest Radiol 47:406-414
21. Secchi F, De Cecco CN, Spearman JV et al (2015) Monoenergetic extrapolation of cardiac dual energy CT for artifact reduction. Acta Radiol 56:413-418
22. Bamberg F, Dierks A, Nikolaou K, Reiser MF, Becker CR, Johnson TR (2011) Metal artifact reduction by dual energy computed tomography using monoenergetic extrapolation. Eur Radiol 21:1424-1429

PART 3

Epilogue

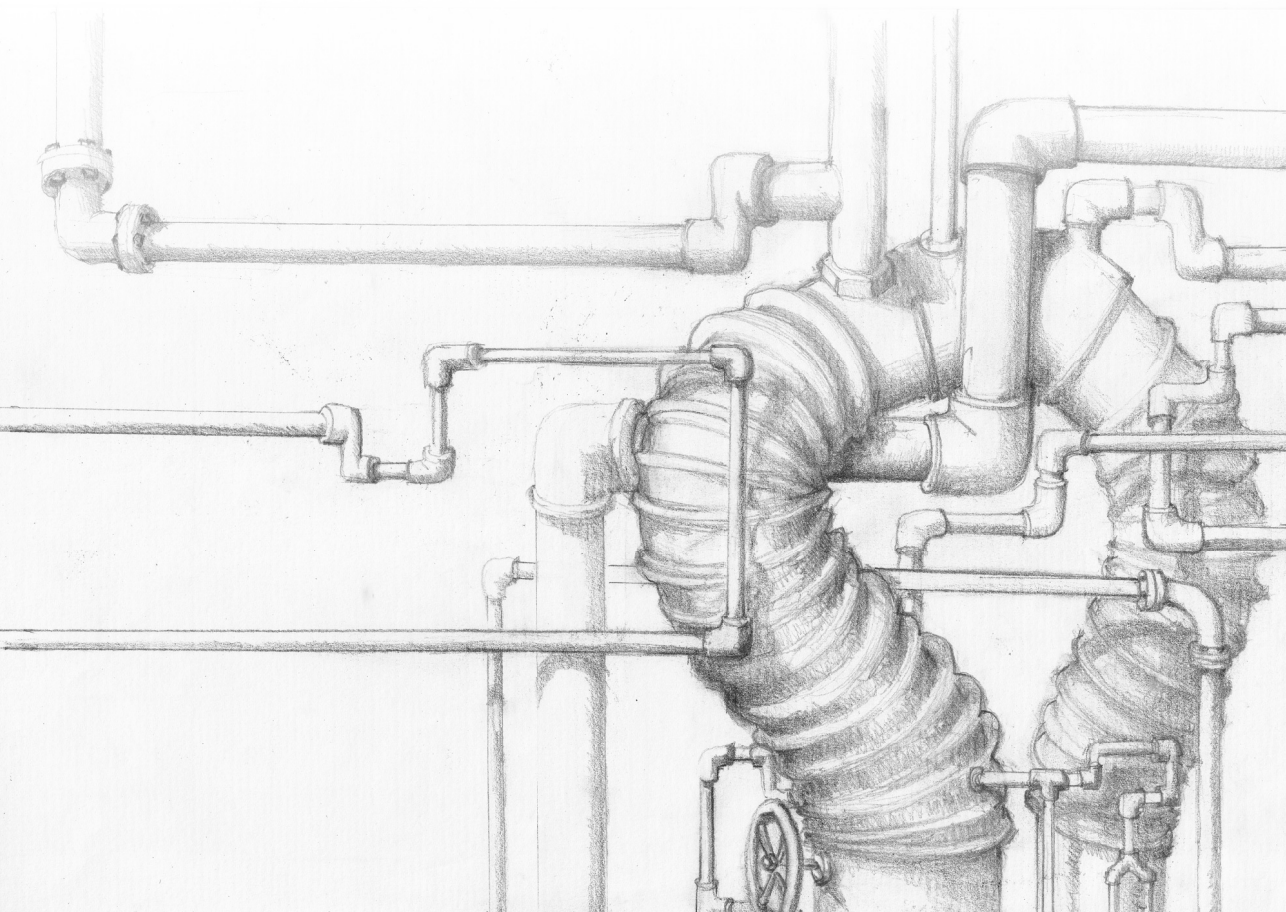

CHAPTER 11

Discussion and general conclusions

Discussion

CT imaging plays a major role in all phases of the care of patients with aortic pathology. Although this role is acknowledged by guidelines, many aspects of these examinations still have to be systematically investigated to define the best technical modalities and how to best interpret some findings and integrate them in the patients' management.

CT assessment of aortic diameters

Thoracic aorta

Although measurement of aortic diameters is a fundamental aspect in the assessment of the vast majority of imaging examinations of the aorta, the best method to assess them on CT scans has not been established yet. The first difficulty is the lack of a reference standard to which compare results obtained on CT images. Many of these patients will not be operated in a short timeframe after the exam. Even when patients are operated, intraoperative measurements cannot be considered a reference standard due to the non-physiological conditions in which they are performed (e.g. cardioplegia) and the inaccurate instruments employed (manual calipers). Therefore, the accuracy of measurement methods based on imaging techniques can be assessed only by comparison with another imaging method or technique. However, as highlighted in our review in Chapter 2, due to the broad variability of methods available to measure aortic diameters on CT images, there are only a few studies providing results that can be compared. The process to obtain aortic measurements consists of multiple successive steps, each presenting different options that might influence the final output. When comparing two different measurements methods, changing also other parameters will influence the results to an extent that cannot be calculated and discerned from the one intended for analysis.

As a consequence, good data are often lacking and some of the indications provided by guidelines seem to rely more on common sense than on evidence. For instance, measurements performed on axial planes intuitively result in the assessment of the diameter of a section of the aorta as visualized at various angles. However, we did not find evidence demonstrating that measurements of minimum diameters performed on axial planes are less accurate than measurements on cross-sections perpendicular to the longitudinal axis of the aorta[23, 24]. Therefore, further studies are needed to assess the accuracy of this method that allows faster measurements, especially when comparing multiple scans, and is likely to be easier to employ also for radiologists who are not specialised in cardiovascular imaging.

Yet, guidelines recommend identifying planes perpendicular to the centreline[2]. This suggestion has important effects on clinical routine. Workstations where to perform double

oblique measurements have to be easily available in the department, radiologists have to be experienced in multiplanar reconstructions and be familiar with aortic anatomy[25]. Even when these prerequisites are met, manually identifying multiple planes per each exam is time consuming and particularly so when comparing several scans of the same patient. Due to a lack in standardization of aortic measurements between operators and centres and even in the same centre, when assessing diameters on follow up scans, it is generally necessary to repeat all measurements on at least two examinations to reduce variability.

Several software frameworks have been proposed to automate, standardize and speed up measurements of the aorta, leading to an even broader variability of measurement methods. Semi-automatic software requires human interaction during one or more steps. Although improvements in technology have led to completely automated tools, operators still have to be familiar with the framework function in order to check results (and eventually edit them). At the moment there is no consensus on how to best integrate these tools in clinical practise, albeit already commonly used, and about what should be the minimum user interaction to ensure precise measurements. Furthermore, there are no commercially available solutions that allow comparing multiple scans of the thoracic aorta of the same patient. Although a framework allowing automatically calculating volumes of the abdominal aorta of two different scans has been described, no such solution has been proposed for the thoracic aorta[26]. Therefore, even when relying on automatic software, radiologists have to employ the software multiple times to assess one scan at the time and manually calculate the difference between aortic diameters. In chapter 3, we presented the first software able to automatically calculate aortic diameters on two consecutive exams and to calculate their difference. The software can segment the aorta of both the baseline and follow-up scan and align them in order to detect differences in aortic dimensions over time. Measurements are performed, in accordance with guidelines, on planes perpendicular to the longitudinal axis of the vessel at several locations that have to be identified by an operator only on the baseline scan. To ease the visualization of changes between scans, several tools have been implemented in the software, such as superimposition of the 3D contours of the two aortae and side-by-side visualization of cross-section as well as stretched MPR of the lumina. Automatic measurements were compared with diameters manually obtained with the double oblique technique. Results showed mean differences ≤1 mm at all locations. These values are in line with previously reported results of comparisons between software and manual assessment of the thoracic aorta as well as intra- and inter-observer values[27–31]. Furthermore, automatic measurements obtained based on the definition of the landmarks by two operators showed small differences of ≤1mm. Indicating a good reproducibility with low variability, these results are particularly important in the absence of a reference standard and subsequent impossibility to calculate the precision of any method. Although the

assessment of aortic diameter progression over time is a rather common clinical request in cardiovascular radiology, the topic is still debated. Guidelines of the American Heart Association in 2010 stated that an increase in diameter of more than 2.5mm/year of a dilated aorta should prompt invasive treatment[3]. However, in the guidelines of 2014 of the European Society of Cardiology it was noted that the variability of these measurements is still so relevant that only a difference of >5mm should be considered significant[2]. In this context an automatic software providing results similar to manual measurements and demonstrating an inter-observer variability as the one we presented is a very promising tool.

In clinical practise it is not uncommon to have to compare aortic diameters calculated on CT images with diameters obtained with different modalities[6]. Therefore, we assessed agreement between CT, echocardiography and MRI. Measurements were obtained with the three imaging modalities and with different techniques for the same modality in the same patients on the same day. We focused our attention on measurements of the ascending aorta as this part of the aorta presents additional confounding factors for diameter assessment such as the variable and often steep angulation, the non-tubular shape of the sinus of Valsalva and the more pronounced influence of heart beats and blood flow. Our findings confirm the existence of considerable intermodality differences with maximum differences up to 18mm for measurements at the sinus of Valsalva. On the contrary, the inter- and intraobserver variability for measurements performed with the same techniques was good. These findings strongly support the recommendation to follow up patients with the same method and technique. Leading-edge to leading-edge 2DE and inner-edge to inner-edge CT and MRI measurements were found to have the smallest differences. As expected systolic diameters were larger than diastolic ones for all methods and for most locations. Furthermore, CT based cusp-to-cusp and cusp-to-commissure measurements at the sinus of Valsalva seem to be interchangeable as no significant difference was found.

Overall our findings confirm the variability of aortic diameter values when calculated with different techniques thereby underlying the importance of employing always the same method and technique to compare measurements of the same patient. Moreover, we confirmed the possibilities of automatic software that could speed up radiologists work and have variability values similar to inter and intraobserver values.

Aortic annulus

Interest in the so-called "aortic annulus" has been increasing subsequently to the introduction and more and more common employment of TAVI procedures. Due to the angiography-guided nature of the procedure, the so-called "landing zone" of the valve has to be assessed with imaging modalities prior to the intervention. Since valves are produced

in a limited number of sizes that are appropriate for valves differing only a few millimetres in diameter, precise assessment of annular dimensions is essential for the choice of the correct prosthesis. Over- or under-sizing can both lead to lethal complications such as rupture of the LVOT or paravalvular regurgitation, complications that can be reduced with appropriate sizing[12].

Valves are deployed (or sutured) at the level with the smallest diameter between the left ventricular outflow tract and the aortic sinus. This level, which does not correspond to any defined anatomical structure, has been named "virtual basal ring" and "annulus" [10, 32]. On echo images measurements were (and are) performed at the level of the lowest visible part of the cusps. However, with the role of CT becoming predominant for the pre-procedural evaluation a new standardized definition of this entity, encompassing the 3D nature of both the structure to measure and the imaging modality, was necessary. Thus, the annulus plane has been defined as the one passing through the lowest points (hinge points) of the three cusps[13].

Therefore, manual identification of the annulus requires even more specific anatomic knowledge and ease of use of multiplanar reconstructions than for the rest of the aorta. Furthermore, a complete pre-TAVI assessment should include additional measures of the aortic root and provide indication of the best angle for deployment of the valve[33]. Due to the multistep process necessary to identify the annulus and to all the additional parameters required for a complete pre-interventional assessment, post-processing time for this examination is an important factor. Standardized automated definition of the annulus plane and dimensions might help improve measurement precision and reproducibility as well as reporting time. However, new software had to be created to address the specific anatomy of this location, such as the identification of the three hinge points[5, 34–36]. We proposed a new fully automatic framework based on the same principle. With mean differences of annulus diameter of 0.2 ± 1.0 mm and 1.0 ± 1.2 mm between the automatic method and observer 1 and 2 respectively our results were not only comparable to interobserver variability (1.2 ± 0.6mm) but also similar to findings of other studies assessing the performance of automatic software. One advantage of our framework was the reduced processing time, which is a very relevant aspect of pre-TAVI evaluations in clinical practise. Furthermore, our framework is capable to automatically calculate the optimal projection curve and the best projection angle that can be employed to minimize contrast and radiation exposure during the procedure.

Another effect derived from the possibility to visualize cross-sections of the region on CT images, was that the annulus has been proven to have an elliptical shape [16]. Furthermore, during the cardiac cycle the annulus undergoes conformational changes, becoming more flattened in diastole, to such an extent that most parameters present

significant differences between systole and diastole[16]. Therefore, the phase when to perform measurements is essential to provide accurate values for correct valve sizing. However no such data exist for the annulus of patients with BAV.

Since the presence of a BAV has been traditionally considered a contraindication to TAVI, studies regarding the anatomy and physiology of the annulus have been restricted to patients with TAV[37, 38]. In more recent years, the procedure has been proved to be safe also for patients with BAV[39–42]. Furthermore, results similar to those obtained in TAV patients lead to an increase in the number of procedures. However, a higher incidence of post-procedural paravalvular regurgitation in BAV patients has been reported by some authors[12, 39]. As this finding might seem to confirm past doubts that indicated the allegedly more elliptical shape of BAV annuli as a contraindication to TAVI, more data regarding the morphology of the BAV annulus was needed[37, 41, 43]. Therefore we decided to investigate conformational changes of the BAV annulus during the cardiac cycle and assess if any difference between BAV types could be demonstrated.

The first step was to establish a standardized method for the definition of the annulus plane in BAV patients. In fact, we found that the established and commonly employed technique based on the identification of the plane passing through the three hinge points was feasible only for some of these patients depending on the valve type and symmetry of the cusps. The term BAV encompasses a broad spectrum of malformations of the aortic valve that result in a deformed orifice determined by only two juxtaposed leaflets and represents the most common congenital heart disease [44]. The most commonly employed classification is the one by Sievers[44], which is based on the number and position of lines of fusion between the cusps (referred to as "raphae"). In valves type 0 there are no raphe and only two leaflets; in type 1 there is one raphe and thus two of the three cusps are fused together; in type 2 there are two raphae with the three leaflets fused to each other at two locations. Therefore, in valves type 0 there are only two cusps and two hinge points. Moreover, in valves type 1 and 2 the cusps are sometimes so asymmetric that the plane passing through the three hinge points determines an acute angle respect to the centerline. Although it is known and accepted that the annulus plane might not be exactly perpendicular to the centreline[13], in these BAV patients the angulation is so steep that it might not represent the desired plane where to deploy the valve. Therefore, measuring the annulus on this plane would lead to an overestimation of all parameters with subsequent oversizing of the valve. Our new method for a standardized identification of the annulus in all BAV patients was based on a combination of previously published definitions of this plane. Unfortunately it was not possible to compare measures obtained with our method to a reference standard. In fact, although the implanted valve size has been employed as a comparison for pre-interventional assessment based on imaging, its definition relies on several other factors that include, but are not limited to, annular

parameters. In addition, we could not relate our values with those obtained with the established method for TAV patients as in subjects with BAV it is either impossible to apply or is deemed to result in incorrect measurements.

Thereafter, we assessed the anatomy and physiology of the annulus throughout the cardiac cycle. Overall BAV patients showed a slightly elliptic annulus that became more flattened in early diastole and resumed a more circular shape in late diastole. All sizing parameters (with the exception of the maximum diameter) were significantly larger in early systole. When examined separately, the three valve types showed the same pattern of modifications. We demonstrated that BAV annuli change shape during the cardiac cycle similarly to TAV ones. Moreover, the asymmetry index was >1.1 in all phases with the highest value of 1.3 demonstrating an elliptic form. Data reported in the literature regarding the asymmetry index of TAV annuli are comparable to ours. Therefore, our findings are against the hypothesis of a more elliptical shape of BAV annuli. In addition, sizing parameters were significantly higher in early systole, thus dictating the appropriate phase when to perform measurements. Overall, based on our results, there seem to be no decisive differences between BAV and TAV patients in annular anatomy and physiology, which could constitute an a priori contraindication to TAVI procedures in the first group.

CT assessment of the thoracic aorta after surgery and endovascular intervention

CT has gained the role of imaging modality of choice after surgical and endovascular procedures of the aorta[3, 6, 21]. The number of these examinations is likely to increase in the future due to the higher burden of aortic pathologies and better prognosis after operations[45, 46]. Not only the number of scanned patients is likely to increase but also, thanks to technological improvements, the spectrum of potentially assessable findings/complications is broadening.

Two clinical scenarios can be identified: routine follow-up and suspicion of complications.

In the first setting the patient undergoes the examination in the absence of symptoms and altered lab-test. As a consequence, any diagnosis of complication has to rely on imaging or on a combination of multiple criteria where imaging has a fundamental role[47]. As in any other diagnostic modality, pathology is usually identified as a condition different from normality. However, after operations baseline anatomy is usually modified either as a consequence of the operation itself or as a reaction of the organism to the changes related to the intervention. Therefore, the radiologist has to be familiar with the technical

details of the procedure as well as its possible variations, and the resulting appearance on imaging examinations.

In case a complication is suspected, clinical data will help guide and tailor the examination protocol. In fact, especially if the aortic valve needs to be investigated, the choice of the scanning parameters and technique is fundamental to obtain diagnostic images. Nevertheless, since symptoms of postoperative complications can be generic and/or multiple complications can occur, also in this scenario it is necessary the radiologist being knowledgeable of the procedural details and their CT appearance.

Therefore, our aim was twofold. On one hand, we described by means of pictorial reviews what radiologists should know beforehand when approaching CT examinations performed after a specific aortic intervention or procedure as well as the imaging characteristics of all possible complications. On the other hand, we tried to broaden current knowledge regarding imaging features that are still troublesome.

We focused our attention mainly on the Bentall procedure and on stent implantation for aortic coarctation treatment.

Consisting of the replacement of the aortic valve and ascending aorta in a single operation, the Bentall procedure is a particularly invasive intervention[18]. Although the presence of periaortic fluid, especially in the early postoperative period, is a common finding that had already been described, its clinical meaning was still unclear[48–51]. Due to the extensive manipulation of the mediastinal adipose tissue occurring during the procedure, the presence of periaortic hematoma and/or inflammation can be expected. However, the expected CT appearance of endocarditis, a potentially lethal and often asymptomatic complication, is similar. Our aim was to describe the range of normal postoperative findings and differentiate it from complications. At first we classified periaortic fluid based on its characteristics. The most important distinction was between stranding, indicating fluid extending in the adipose tissue with an infiltrating appearance and completely surrounding the aorta, and fluid collections, which presented a clearly distinguishable border and a focal involvement of the aortic circumference. Our results showed that stranding is a normal finding in the first three postoperative months after the Bentall procedure and is found also in nearly all patients that underwent an uneventful surgery and did not present any complication in the following year. On the contrary, fluid collections are more frequent in patients who had either a complicated procedure or follow-up. Therefore, while stranding does not raise any concern and can be considered normal, fluid collections require more caution and prompt further inquires. These results can be immediately translated into clinical practise and can help reduce misdiagnosis and unnecessary additional examinations and controls.

Stent implantation to treat aortic coarctation has been used increasingly in the last years in children while being already the established treatment of choice for adults and adolescents[20, 52–54]. These patients will require lifelong imaging surveillance. However, the metallic structure of the stent determines the presence of artefacts on all imaging modalities, including CT, which might hamper the diagnostic value of the examination. Moreover, although only one stent type has both FDA and CEE approval for this use, other types can be utilized[55, 56]. These stents differ in structure and materials and possibly yield various artefacts at imaging. Our aim was to evaluate the image quality of CT scans of different types of stents. Our results showed that the type of stent most commonly employed in our series (the Cheatham Platinum) yields the most extensive artefacts and the worst image quality of the lumen and of the aortic wall as assessed with both subjective and objective scales. Nevertheless, the average subjective score indicated a diagnostic image quality also for this type of stent. We found a negative correlation between stent diameters and quality scores indicating more artefacted images for stents with smaller calibre. In addition, we evaluated the effect of CT technical parameters on image quality showing that ECG gating and kV do not influence image quality. Further prospective studies are needed to establish the accuracy of CT scans for the detection and quantification of intimal hyperplasia, the assessment of which is the most likely to be affected by metallic artefacts in our opinion, compared to invasive angiography and hemodynamic measurements. As most vendors have metallic artefact reduction tools, it would be interesting to evaluate their added value for this kind of examination.

Conclusion and future perspectives

Although CT is a very commonly employed imaging technique for the management of aortic valve and aortic pathology, there are many unsolved questions regarding its optimal employment in clinical practise. Our aim was to systematically review the available literature regarding aortic diameter measurements based on CT images as well as to propose new techniques, including automatic and manual solutions. Moreover, we updated the literature regarding specific findings after the Bentall procedure and implantation of stents for the treatment of aortic coarctation. Finally, we investigated the boundaries between normal and pathological findings after both interventions.

Our works as well as previous studies highlight the importance of standardization in aortic pathology imaging assessment. As the number of these examinations is increasing while the time available for reporting has been decreasing, software frameworks are the most likely key to the future. Undoubtedly artificial intelligence will play a major role in this scenario. Foreseen and desired developments include faster calculation of aortic diameters with automatic derivation of differences between successive scans at any point along the aorta. As it is probable that the software will be able to evaluate all scans of a single patient with less variability than what is possible today, more precise thresholds for diameters increase requiring surgical or interventional therapy should be investigated and indicated. Regarding post-surgery CT scans, for the evaluation of which software are still far from clinical practice, standardization is also necessary and could be ameliorated by performing the exams at fixed time points for all patients even if asymptomatic. Although generalization about the best CT protocol is not possible due to the enormous differences in CT scanner hardware and software, some general recommendations include: acquisitions and reconstructions of CT images should be performed with a thickness ≤1mm; ECG synchronization is necessary for the assessment of the ascending aorta; a non-contrast enhanced acquisition is necessary if acute aortic syndrome is suspected and should be considered for post-interventional imaging. Further considerations about CT protocols for specific clinical scenarios are included in Chapter 7 and 9. This would lead to a more precise assessment of what are the normal findings in these patients in large populations. In addition having a baseline postoperative scan for comparison would ease the recognition of successive complications in clinical practise. Furthermore, the introduction of other modalities, such as PET-CT, and CT techniques, such as spectral imaging, might help improve diagnosis by adding information about glucose uptake and material composition and by reducing metal artefacts.

Bibliography

1. Lal BK, Cerveira JJ, Seidman C, Haser PB, Kubicka R, Jamil Z, Padberg FT, Hobson RW, Pappas PJ (2004) Observer variability of iliac artery measurements in endovascular repair of abdominal aortic aneurysms. Ann Vasc Surg 18:644–652
2. Erbel R, Aboyans V, Boileau C, et al (2014) 2014 ESC Guidelines on the diagnosis and treatment of aortic diseases: Document covering acute and chronic aortic diseases of the thoracic and abdominal aorta of the adult. The Task Force for the Diagnosis and Treatment of Aortic Diseases of the European . Eur Heart J 35:2873–2926
3. Hiratzka LF, Bakris GL, Beckman J a., et al (2010) 2010 ACCF/AHA/AATS/ACR/ASA/SCA/SCAI/SIR/STS/SVM Guidelines for the Diagnosis and Management of Patients With Thoracic Aortic Disease: A Report of the American College of Cardiology Foundation/American Heart Association Task Force on Practice Guidelines, A. Circulation 121:e266–e369
4. Sprouse LR, Meier GH, Parent FN, Demasi RJ, Stokes GK, Lesar CJ, Marcinczyk MJ, Mendoza B (2004) Is three-dimensional computed tomography reconstruction justified before endovascular aortic aneurysm repair? J Vasc Surg 40:443–447
5. Delgado V, Ng ACT, Schuijf JD, et al (2011) Automated Assessment of the Aortic Root Dimensions With Multidetector Row Computed Tomography. Ann Thorac Surg 91:716–723
6. Goldstein SA, Evangelista A, Abbara S, et al (2015) Multimodality Imaging of Diseases of the Thoracic Aorta in Adults: From the American Society of Echocardiography and the European Association of Cardiovascular Imaging. J Am Soc Echocardiogr 28:119–182
7. Kirbas C, Quek F (2004) A review of vessel extraction techniques and algorithms. ACM Comput Surv 36:81–121
8. Fazel SS, Mallidi HR, Lee RS, Sheehan MP, Liang D, Fleischman D, Herfkens R, Mitchell RS, Miller DC (2008) The aortopathy of bicuspid aortic valve disease has distinctive patterns and usually involves the transverse aortic arch. J Thorac Cardiovasc Surg. doi: 10.1016/j.jtcvs.2008.01.022
9. Erbel R, Aboyans V, Boileau C, et al (2014) 2014 ESC Guidelines on the diagnosis and treatment of aortic diseases. Eur Heart J 35:2873–2926
10. Piazza N, de Jaegere P, Schultz C, Becker AE, Serruys PW, Anderson RH (2008) Anatomy of the aortic valvar complex and its implications for transcatheter implantation of the aortic valve. Circ Cardiovasc Interv 1:74–81
11. Blanke P, Reinöhl J, Schlensak C, et al (2012) Prosthesis oversizing in balloon-expandable transcatheter aortic valve implantation is associated with contained rupture of the aortic root. Circ Cardiovasc Interv 5:540–548
12. Willson AB, Webb JG, Labounty TM, et al (2012) 3-dimensional aortic annular assessment by multidetector computed tomography predicts moderate or severe paravalvular regurgitation after transcatheter aortic valve replacement: A multicenter retrospective analysis. J Am Coll Cardiol 59:1287–1294
13. Achenbach S, Delgado V, Hausleiter J, Schoenhagen P, Min JK, Leipsic J a. (2012) SCCT expert consensus document on computed tomography imaging before transcatheter aortic valve

implantation (TAVI)/transcatheter aortic valve replacement (TAVR). J Cardiovasc Comput Tomogr 6:366–380

14. Queirós S, Dubois C, Morais P, Adriaenssens T, Fonseca JC, Vilaça JL, D'hooge J (2016) Automatic 3D aortic annulus sizing by computed tomography in the planning of transcatheter aortic valve implantation. J Cardiovasc Comput Tomogr. doi: 10.1016/j.jcct.2016.12.004
15. Samim M, Stella PR, Agostoni P, et al (2013) Automated 3D analysis of pre-procedural MDCT to predict annulus plane angulation and C-arm positioning: Benefit on procedural outcome in patients referred for TAVR. JACC Cardiovasc Imaging 6:238–248
16. Suchá D, Tuncay V, Prakken NHJ, Leiner T, Van Ooijen PM a., Oudkerk M, Budde RPJ (2015) Does the aortic annulus undergo conformational change throughout the cardiac cycle? A systematic review. Eur Heart J Cardiovasc Imaging 16:1307–1317
17. Jurencak T, Turek J, Kietselaer BLJH, Mihl C, Kok M, van Ommen VGV a, van Garsse L a FM, Nijssen EC, Wildberger JE, Das M (2015) MDCT evaluation of aortic root and aortic valve prior to TAVI. What is the optimal imaging time point in the cardiac cycle? Eur Radiol 25:1975–1983
18. Bentall H, De Bono A (1968) A technique for complete replacement of the ascending aorta. Thorax 23:338–339
19. Forbes TJ, Kim DW, Du W, et al (2011) Comparison of surgical, stent, and balloon angioplasty treatment of native coarctation of the aorta: An observational study by the CCISC (Congenital cardiovascular interventional study consortium). J Am Coll Cardiol 58:2664–2674
20. Moore JW, Vincent RN, Beekman RH, et al (2014) Procedural results and safety of common interventional procedures in congenital heart disease: Initial report from the national cardiovascular data registry. J Am Coll Cardiol 64:2439–2451
21. Svensson LG, Adams DH, Bonow RO, et al (2013) Aortic valve and ascending aorta guidelines for management and quality measures: executive summary. Ann Thorac Surg 95:1491–505
22. Hiratzka LF, Bakris GL, Beckman JA, et al (2010) 2010 ACCF/AHA/AATS/ACR/ASA/SCA/SCAI/SIR/STS/SVM Guidelines for the Diagnosis and Management of Patients With Thoracic Aortic Disease. Circulation 121:e266–e369
23. Rengier F, Weber TF, Partovi S, Müller-Eschner M, Böckler D, Kauczor H-U, von Tengg-Kobligk H (2011) Reliability of Semiautomatic Centerline Analysis versus Manual Aortic Measurement Techniques for TEVAR among Non-experts. Eur J Vasc Endovasc Surg 42:324–331
24. Müller-Eschner M, Rengier F, Partovi S, Weber TF, Kopp-Schneider a., Geisbüsch P, Kauczor HU, Von Tengg-Kobligk H (2013) Accuracy and variability of semiautomatic centerline analysis versus manual aortic measurement techniques for TEVAR. Eur J Vasc Endovasc Surg 45:241–247
25. Diehm N, Kickuth R, Gahl B, Do D-D, Schmidli J, Rattunde H, Baumgartner I, Dick F (2007) Intraobserver and interobserver variability of 64-row computed tomography abdominal aortic aneurysm neck measurements. J Vasc Surg 45:263–268
26. Kauffmann C, Tang A, Therasse É, Giroux MF, Elkouri S, Melanson P, Melanson B, Oliva VL, Soulez G (2012) Measurements and detection of abdominal aortic aneurysm growth: Accuracy and reproducibility of a segmentation software. Eur J Radiol 81:1688–1694

27. Lu T-LC, Rizzo E, Marques-Vidal PM, Segesser LK Von, Dehmeshki J, Qanadli SD (2010) Variability of ascending aorta diameter measurements as assessed with electrocardiography-gated multidetector computerized tomography and computer assisted diagnosis software. Interact Cardiovasc Thorac Surg 10:217–221
28. Entezari P, Kino A, Honarmand AR, Galizia MS, Yang Y, Collins J, Yaghmai V, Carr JC (2013) Analysis of the thoracic aorta using a semi-automated post processing tool. Eur J Radiol 82:1558–1564
29. Biesdorf A, Rohr K, Feng D, von Tengg-Kobligk H, Rengier F, Böckler D, Kauczor HU, Wörz S (2012) Segmentation and quantification of the aortic arch using joint 3D model-based segmentation and elastic image registration. Med Image Anal 16:1187–1201
30. Kauffmann C, Tang A, Dugas A, Therasse É, Oliva V, Soulez G (2011) Clinical validation of a software for quantitative follow-up of abdominal aortic aneurysm maximal diameter and growth by CT angiography. Eur J Radiol 77:502–508
31. Quint LE, Liu PS, Booher AM, Watcharotone K, Myles JD (2013) Proximal thoracic aortic diameter measurements at CT: repeatability and reproducibility according to measurement method. Int J Cardiovasc Imaging 29:479–488
32. Anderson RH (2000) Clinical anatomy of the aortic root. Heart 84:670–673
33. Gurvitch R, Wood D a., Leipsic J, Tay E, Johnson M, Ye J, Nietlispach F, Wijesinghe N, Cheung A, Webb JG (2010) Multislice computed tomography for prediction of optimal angiographic deployment projections during transcatheter aortic valve implantation. JACC Cardiovasc Interv 3:1157–1165
34. Lou J, Obuchowski N a., Krishnaswamy A, et al (2015) Manual, semiautomated, and fully automated measurement of the aortic annulus for planning of transcatheter aortic valve replacement (TAVR/TAVI): Analysis of interchangeability. J Cardiovasc Comput Tomogr 9:42–49
35. Ionasec RI, Voigt I, Georgescu B, Wang Y, Houle H, Vega-Higuera F, Navab N, Comaniciu D (2010) Patient-specific modeling and quantification of the aortic and mitral valves from 4-D cardiac CT and TEE. IEEE Trans Med Imaging 29:1636–1651
36. Elattar M, Wiegerinck E, van Kesteren F, Dubois L, Planken N, Vanbavel E, Baan J, Marquering H (2016) Automatic aortic root landmark detection in CTA images for preprocedural planning of transcatheter aortic valve implantation. Int J Cardiovasc Imaging 32:501–511
37. Zegdi R, Ciobotaru V, Noghin M, Sleilaty G, Lafont A, Latrémouille C, Deloche A, Fabiani JN (2008) Is It Reasonable to Treat All Calcified Stenotic Aortic Valves With a Valved Stent?. Results From a Human Anatomic Study in Adults. J Am Coll Cardiol 51:579–584
38. Smith CR, Leon MB, Mack MJ, et al (2011) Transcatheter versus Surgical Aortic-Valve Replacement in High-Risk Patients. N Engl J Med 364:2187–2198
39. Wijesinghe N, Ye J, Rodés-Cabau J, et al (2010) Transcatheter aortic valve implantation in patients with bicuspid aortic valve stenosis. JACC Cardiovasc Interv 3:1122–1125
40. Hayashida K, Bouvier E, Lefèvre T, et al (2013) Transcatheter aortic valve implantation for patients with severe bicuspid aortic valve stenosis. Circ Cardiovasc Interv 6:284–291

41. Phan K, Wong S, Phan S, Ha H, Qian P, Yan TD (2015) Transcatheter Aortic Valve Implantation (TAVI) in Patients With Bicuspid Aortic Valve Stenosis - Systematic Review and Meta-Analysis. Hear Lung Circ 24:649–659
42. Mylotte D, Lefevre T, Søndergaard L, et al (2014) Transcatheter aortic valve replacement in bicuspid aortic valve disease. J Am Coll Cardiol 64:2330–2339
43. Xie X, Shi X, Xun X, Rao L (2016) Efficacy and safety of transcatheter aortic valve implantation for bicuspid aortic valves: A systematic review and meta-analysis. Ann Thorac Cardiovasc Surg 22:203–215
44. Sievers HH, Schmidtke C (2007) A classification system for the bicuspid aortic valve from 304 surgical specimens. J Thorac Cardiovasc Surg 133:1226–1233
45. Clouse WD, Hallett JW, Schaff H V., Gayari MM, Ilstrup DM, Melton LJ (1998) Improved prognosis of thoracic aortic aneurysms. A population-based study. J Am Med Assoc 280:1926–1929
46. Sampson UK a., Norman PE, Fowkes FGR, et al (2014) Global and regional burden of aortic dissection and aneurysms: Mortality trends in 21 world regions, 1990 to 2010. Glob Heart 9:171–180
47. Habib G, Lancellotti P, Antunes MJ, et al (2015) 2015 ESC Guidelines for the management of infective endocarditis. Eur Heart J. doi: 10.1093/eurheartj/ehv319
48. Hoang JK, Martinez S, Hurwitz LM (2009) Imaging of the Postoperative Thoracic Aorta: The Spectrum of Normal and Abnormal Findings. Semin Roentgenol 44:52–62
49. Fagman E, Bech-Hanssen O, Flinck A, Lamm C, Svensson G (2016) Increased aortic wall thickness on CT as a sign of prosthetic valve endocarditis. Acta Radiol 0:1–7
50. Sundaram B, Quint LE, Patel HJ, Deeb GM (2007) CT findings following thoracic aortic surgery. Radiographics 27:1583–1594
51. Sundaram B, Quint LE, Patel S, Patel HJ, Deeb GM (2007) CT appearance of thoracic aortic graft complications. Am J Roentgenol 188:1273–1277
52. Krasemann T, Bano M, Rosenthal E, Qureshi S a. (2011) Results of stent implantation for native and recurrent coarctation of the aorta-follow-up of up to 13 years. Catheter Cardiovasc Interv 45:405–412
53. Vergales JE, Gangemi JJ, Rhueban KS, Lim DS (2013) Coarctation of the aorta - the current state of surgical and transcatheter therapies. Curr Cardiol Rev 9:211–9
54. Forbes TJ, Gowda ST (2014) Intravascular stent therapy for coarctation of the aorta. Methodist Debakey Cardiovasc J 10:82–87
55. Zuckerman B (2016) FDA approval Cheatham Platinum stent.
56. Meadows J, Minahan M, McElhinney DB, McEnaney K, Ringel R (2015) Intermediate outcomes in the prospective, multicenter coarctation of the aorta stent trial (COAST). Circulation 131:1656–1664

Nederlandse samenvatting

Computer tomografie (CT) heeft een centrale rol gekregen bij de beoordeling van vrijwel alle aandoeningen van de aorta en kan essentiële gegevens opleveren tijdens alle fases van klinische besluitvorming. Sommige aspecten van het gebruik van CT bij deze aandoeningen blijven echter onduidelijk of slecht afgebakend. In Hoofdstuk 1 geven we een kort overzicht van enkele van deze aspecten die wij in dit proefschrift hebben onderzocht, met als doel om de huidige stand van zaken en kennis samen te vatten en hierop voort te bouwen.

In **Hoofdstuk 2** beschouwen we alle beschikbare literatuur betreffende onderlinge vergelijkingen tussen alle verschillende CT technieken die gebruikt kunnen worden om de diameter van de aorta te beoordelen. Ons onderzoek heeft laten zien dat de grote verscheidenheid in meetmethoden heeft geresulteerd in armzalige vergelijkende literatuur. Derhalve lijken veel van de aanbevelingen in hedendaagse richtlijnen meer gebaseerd op gezond verstand dan harde data. Bovendien was de variatie in meetmethoden groot en waren de inter- en intra-observer overeenstemming bij axiale metingen slecht. Geautomatiseerde software leverde de best reproduceerbare waarden, vooral bij onervaren beoordelaars. Meer onderzoek is dus nodig, niet alleen om de beste meetmethode te bepalen, maar ook om betrouwbaardere afkapwaarden voor een pathologisch verwijdde aortadiameter te kunnen vaststellen.

In **Hoofdstuk 3** presenteren we nieuwe software waarmee semi-automatisch verschillen in aortadiameter tussen opeenvolgende CT-scans van dezelfde patiënt kunnen worden berekend. Het enige wat de bediener van de CT-scan moest doen was het identificeren van het gewenste herkenningspunt op de eerste scan. De betrouwbaarheid van dit programma voor de beoordeling van de eerste en daarop volgende diameters was, wanneer we deze vergeleken met handmatige metingen, gelijk aan die van eerder gepubliceerde software. Verschillende beeldvormingstechnieken werden geïmplementeerd om de detectie van veranderingen in diameter gemakkelijker en beter te detecteren. De tijd die nodig was voor het berekenen hiervan was half zo lang als de tijd die nodig was om dit handmatig te doen. Onze bevindingen laten zien dat deze software een betrouwbaar en zeer handig hulpmiddel zou kunnen zijn in de klinische praktijk waarin het meten van veranderingen van aortadiameter nog steeds een tijdrovende en veel expertise vereisende taak is.

In **Hoofdstuk 4** hebben we de variatie bij metingen van de aorta ascendens tussen CT, magnetische resonantie imaging (MRI) en tweedimensionale echografie (2DE) onderzocht. Onze resultaten hebben laten zien dat de variabiliteit in diameter tussen de verschillende beeldvormingsmodaliteiten hoog is, namelijk tot wel 18mm. De inter- en intra-observer variabiliteit was daarentegen laag binnen de individuele technieken.

Daarom is standaardisatie noodzakelijk voor een juiste beoordeling van aortadiameters, vooral wanneer opeenvolgende scans binnen dezelfde patiënt worden vergeleken.

In **Hoofdstuk 5** presenteren we nieuwe automatische software voor het definiëren van het vlak waarin de annulus van de aorta en het berekenen van diens dimensies. Dit programma is gebaseerd op de herkenning van de ophangpunten van de drie klepbladen. Geautomatiseerde bepalingen lieten slechts verschillen in de orde grootte van 1mm zien wanneer deze vergeleken werden met handmatige metingen, en kwamen goed overeen met eerder gepubliceerde resultaten van andere programma's terwijl deze in kortere tijd werden berekend. Bovendien kan de optimale projectiecurve voor de angulatie van de tafel tijdens bepaalde TAVI procedures automatisch worden berekend. Deze software zou in de dagelijkse praktijk gebruikt kunnen worden om betrouwbare en snelle pre-procedurele annulusmetingen te verrichten en de stralings- en contrastdosis beperkt te houden.

In **Hoofdstuk 6** presenteren we een nieuwe gestandaardiseerde methode voor de bepaling van het annulusvlak bij patiënten met een bicuspide aortaklep (BAV), waarbij de anatomische verschillen tussen kleptypes in acht worden genomen. Op basis van deze methode hebben we de veranderingen die de annulus ondergaat tijdens de cardiale cyclus onderzocht. We hebben aangetoond dat bij alle verschillende typen bicuspide kleppen de vorm van de annulus in belangrijke mate verandert tijdens de cardiale cyclus door het krijgen van een groter oppervlakte en een rondere vorm. Bij BAV patiënten zouden daarom, bij de planning voor een transcatheter aortaklep vervanging, de annulusdiameters gemeten moeten worden in de diastole.

In **Hoofdstuk 7** beschrijven we de karakteristieken van normale bevindingen, complicaties en verstorende factoren op CT-scans welke verricht waren na een Bentall procedure. Een gedetailleerde beschrijving van hoe een gestandaardiseerde acquisitie verricht kan worden afhankelijk van de klinische setting wordt gegeven. De mogelijke associatie van een Bentall operatie met andere procedures wordt uiteengezet, en speciale aandacht ging uit naar de beschrijving van complicaties op het niveau van de klep, waaronder endocarditis.

In **Hoofdstuk 8** hebben we de karakteristieken van peri-aortaal vocht op CT-scans welke binnen 3 maanden na een Bentall operatie zijn verricht onderzocht. We vonden dat de aanwezigheid van peri-aortaal vocht in de vorm van induratie onomstotelijk aanwezig is, zelfs bij patiënten die een ongecompliceerde procedure hadden ondergaan zonder enige complicatie binnen 1 jaar follow-up. Derhalve kan worden geconcludeerd dat induratie een normale reactie is van het weefsel op de manipulaties tijdens een dergelijke operatie.

Vochtcollecties daarentegen vereisen verdere diagnostiek en follow-up, aangezien deze vaker samen lijken te gaan met het optreden van complicaties.

In **Hoofdstuk 9** hebben we de karakteristieken van normale bevindingen, complicaties en mogelijke verstorende factoren op CT-scans welke verricht waren na implantatie van een stent ter behandeling van een aortacoarctatie onderzocht. De uiterlijke eigenschappen van de meest gebruikte typen stents hebben we weergegeven in verschillende vlakken en 3D-reconstructies. Evenzo hebben we verstoringen van de structuur van de stent, recoarctatie, aortarupturen en alle andere veel en minder voorkomende complicaties beschreven.

In **Hoofdstuk 10** hebben we de beeldkwaliteit van CT-scans van verschillende typen stents welke gebruikt worden voor aortacoarctaties beoordeeld. We vonden een significant verschil in subjectieve en objectieve beeldkwaliteit tussen verschillende stent typen, waarbij de meest gebruikte stent de slechtste waarden liet zien. De beeldkwaliteit verbeterde naarmate de diameter van de stent toenam. ECG-gating en kVp leken geen significante invloed te hebben.

In **Hoofdstuk 11** zetten we onze bevindingen uiteen in relatie tot het steeds verder toenemende gebruik van CT voor de beoordeling van aortapathologie, en sluiten we af met mogelijke toekomstperspectieven.

List of publications

Papers

Virtual versus true non-contrast dual-energy CT imaging for the diagnosis of aortic intramural hematoma.
Si-Mohamed S, Dupuis N, Tatard-Leitman V, Rotzinger D, **Boccalini S**, Dion M, Vlassenbroek A, Coulon P, Yagil Y, Shapira N, Douek P, Boussel L.
Eur Radiol. 2019 Jul 1. doi: 10.1007/s00330-019-06322-5. [Epub ahead of print]

A novel software tool for semi-automatic quantification of thoracic aorta dilatation on baseline and follow-up computed tomography angiography.
Gao X*, **Boccalini S***, Kitslaar PH, Budde RPJ, Tu S, Lelieveldt BPF, Dijkstra J, Reiber JHC.
Int J Cardiovasc Imaging. 2019 Apr;35(4):711-723.

Intermodality variation of aortic dimensions: How, where and when to measure the ascending aorta.
Bons LR, Duijnhouwer AL, **Boccalini S**, Van Den Hoven AT, Van Der Vlugt MJ, Chelu RG, McGhie JS, Kardys I, Van Den Bosch AE, Siebelink HMJ, Nieman K, Alexander Hirsch A, Broberg CS, Budde RPJ, Roos-Hesselink JW.
Int J Cardiol. 2019 Feb 1;276:230-235

CT angiography for depiction of complications after the Bentall procedure.
Boccalini S*, Swart LE*, Bekkers JA, Nieman K, Krestin GP, Bogers AJJC, Budde RPJ.
Br J Radiol 2018; 91: 20180226.

Computed tomography image quality of aortic stents in patients with aortic coarctation: a multicentre evaluation.
Boccalini S*, den Harder AM*, Witsenburg M, Breur JPMJ, G.P. Krestin GP, van Beynum IM, Stagnaro N, Marasini M, de Jong PA, T. Leiner T, Budde RPJ.
European Radiology Experimental. 2018; 2:17

Peri-aortic fluid after surgery of the ascending aorta: range of normal findings on early postoperative CT.
Boccalini S*, Swart LE*, Bekkers JA, Nieman K, Krestin GP, Bogers AJJC, Budde RPJ.
Eur J Radiol. 2017 Oct;95:332-341.

CT Angiography for the depiction of complications after stent implantation for treatment of aortic coarctation.
Boccalini S*, den Harder AM*, Witsenburg M, Breur JPMJ, G.P. Krestin GP, van Beynum IM, Stagnaro N, Marasini M, de Jong PA, T. Leiner T, Budde RPJ.
J Thorac Imaging. 2017 Nov;32(6):W69-W80.

Quantification of aortic annulus in computed tomography angiography: development and validation of a novel fully automatic methodology.
Gao X, **Boccalini S**, Kitslaar PH, Budde RPJ, Tu S, de Graaf MA, Ondrus T, Penicka M, Scholte AJ, Lelieveldt BP, Dijkstra J, Reiber JH.
Eur J Radiol. 2017 Aug;93:1-8.

Cloud-processed 4D CMR flow imaging for pulmonary flowquantification.
Chelu RG, Wanambiro KW, Hsiao A, Swart LE, Voogd T, van den Hoven AT, van Kranenburg M, Coenen A, **Boccalini S**, Wielopolski PA, Vogel MW, Gabriel P. Krestin GP, Vasanawala SS, Budde RPJ, Roos-Hesselink JW, Nieman K.
Eur J Radiol. 2016 Oct;85(10):1849-56.

Comparison of coronary flow reserve estimated by dynamic radionuclide SPECT and multidetector x-ray CT.
Marini C, Seitun S, Zawaideh C, Bauckneht M, Castiglione Morelli M, Ameri P, Ferrarazzo G, Budaj I, Balbi M, Fiz F**, Boccalini S**, Galletto Pregliasco A, Buschiazzo A, Saracco A, Bagnara MC, Bruzzi P, Brunelli C, Ferro C, Bezante GP, Brunelli C, Sambuceti GM.
J Nucl Cardiol. 2017 Oct;24(5):1712-1721. Epub 2016 May 5.

Stress Computed Tomography Myocardial Perfusion Imaging: A New Topic in Cardiology.
Seitun S, Castiglione Morelli M, Budaj I, **Boccalini S**, Galletto Pregliasco A, Valbusa A, Cademartiri F, Ferro C.
Rev Esp Cardiol (Engl Ed). 2016 Feb;69(2):188-200. Epub 2016 Jan 14.

Anomalous single coronary artery (R-type) in the elderly: Description of benign and isolated variant.
Zingarelli A, Seitun S, **Boccalini S**, Budaj I, Zawaideh C, Valbusa A, Balbi M, Bezante GP, Brunelli C.
Int J Cardiol. 2015 Mar 1;182:10-2. Epub 2014 Dec 27.

Managing a "hole" during acute myocardial infarction: the role of CT and MRI.
Valbusa A, Zawaideh C, **Boccalini S**, Galletto A, Castiglione Morelli M, Deferrari L, Rosa GM, Seitun S.
Int J Cardiol. 2014 May 15;173(3):e53-5. Epub 2014 Mar 21.

Ultrasound-guided interventional procedures around the shoulder.
Tagliafico A, Russo G, **Boccalini S**, Michaud J, Klauser A, Serafini G, Martinoli C.
Radiol Med. 2014 May;119(5):318-26. Epub 2013 Dec 3. Review.

Contributions to conferences receiving prizes

Computed tomography image quality of aortic coarctation stents.
Boccalini S, den Harder AM, Witsenburg M, Breur JPJM, Krestin GP, Stagnaro N, de Jong PA, Leiner T, Budde RPJ. Submitted to ESCR 2017. Accepted as oral presentation.
Winner of the "YAP Programme" grant.

Automatic quantification and visualization of thoracic aorta diameters on successive CTA scans.
Boccalini S, Gao X, Kitslaar P, Budde RPJ, Reiber H. Submitted to ESCR 2017. Accepted as oral presentation. *Winner of the "YAP Programme" grant*.

CT imaging after the Bentall procedure: an updated and comprehensive guide.
Boccalini S, Swart LE, Bekkers JA, Nieman K, Krestin GP, Bogers AJJC, Budde RPJ. Submitted to RSNA 2016. Accepted as poster with ECM presentation.
Winner of a Certificate of Merit from RSNA.

Peri-aortic fluid after surgery of the ascending aorta: range of normal findings on early postoperative CT. **Boccalini S**, Swart LE, Bekkers JA, Nieman K, Krestin GP, Bogers AJJC, Budde RPJ. Submitted to ECR 2016. Accepted as poster with oral presentation.
Winner of a "Invest in the Youth" grant.

Seitun S, **Boccalini S**, Castiglione Morelli M, Zawaideh C, Cademartiri F, Ferro C. Ruolo emergente della cardio-TC nella valutazione della perfusione miocardica. Poster. SIRM 2014. 22-25 Mai 2014. Firenze, Italie.
Winner of the second prize for the best poster.

Portfolio of awarded ECTS points

Research skills:	Year	**ECTS**
Integrity Course	2017	**0.3**
The basic introduction course on SPSS	2017	**1**
In-depth courses:		
Aneurysmal disease, COEUR Erasmus MC	2018	**0.5**
Heart failure research, COEUR Erasmus MC	2018	**1.5**
Cardiovascular imaging and diagnostics (part 1), COEUR Erasmus MC	2017	**0.75**
Congenital heart disease, COEUR Erasmus MC	2015	**1.5**
Arrhythmia research methodology, COEUR Erasmus MC	2015	**1.5**
Spectral CT Academy	2017	**1**
CT course EMC (level 1)	2015	**1**
CT course EMC (level 2)	2015	**1.5**
Symposia and congresses:		
ECR (European Congress of Radiology) 2018	2018	**1.5**
ESCR (European Society of Cardiovascular Radiology) 2017	2017	**0.9**
ECR (European Congress of Radiology) 2017	2017	**1.5**
RSNA (Radiological Society of North America) 2016	2016	**1.8**
SIRM (Societá Italiana di Radiologia Medica) 2016	2016	**1.2**
ECR (European Congress of Radiology) 2016	2016	**1.5**
Milan Cardiac Imaging 2016	2016	**0.6**
Presentations and posters:		
ECR 2018 (oral presentation)	2018	**0.3**
ESCR 2017 (2 oral presentations)	2017	**0.6**
ECR 2017 (poster with oral presentation)	2017	**0.3**
RSNA 2016 (poster with oral presentation and poster)	2016	**0.6**
ECR 2016 (poster with oral presentation)	2016	**0.3**
Teaching activities:		
CT course EMC	2018	**0.3**
CT course EMC	2017	**0.3**
CT course EMC	2016	**0.3**
Other activities:		
Postprocessing, reconstructions and interpretation of images	2018	**14**
MRI and clinical meetings	2015-2018	**5**
Peer review for articles for scientific journals	2017-2018	**0.3**
Total ECTS		**38.7**

About the author

Sara Boccalini was born in Genova, Italy in 1985. She graduated from the Liceo-Ginnasio A. D'Oria cum laude in 2004. She graduated cum laude and medal of the University from the Medical School of the University of Genova in 2010 and completed her residency in Radiology at the University of Genova in 2016.

Due to her strong interest in Cardiovascular Radiology she spent the last year of her residency as clinical and research fellow at the Radiology Department of the Erasmus Medical Center in Rotterdam. After the end of her residency she returned to the Erasmus Medical Center for a one-year Fellowship in Cardiovascular Imaging of the European School of Radiology (ESOR). In addition, she was enrolled as a PhD student at the same institution with research projects focused on CT imaging of the aorta before and after surgery or interventions under the supervison of Dr. R. Budde, Prof. G. Krestin and Prof. Roos-Hesselink which resulted in this thesis.

Since May 2018, she is working as Radiologist at the University Hospital of Lyon in France with specialization in Cardiovascular as well as Thoracic Imaging. She is currently involved in several research projects including the development of Spectral Imaging, in particular regarding myocardial perfusion.

Dankwoord

Although this thesis was ideated and developed at EMC, I consider it as a part of a broader chapter of my life. Not only this journey was inspired by people and events linked to my past in my hometown Genova, but it was intermingled to my path to become Radiologist and specialize in cardiovascular imaging. All of this wouldn't have been possible without the many wonderful persons, from different countries and backgrounds, I had the chance to meet and to whom I would like to say thank you.

Geachte Professor Krestin, thank you for making it possible for this project to become reality. Thank you for giving me the possibility to grow in an environment where research is put in the foreground and researchers are encouraged and supported. I remember that late Friday evening when I emailed you for the first time and your answer about ten minutes after. From that moment onwards I couldn't but admire your kind intelligence and determination. Thank you for all the times you listened to my projects and for all your bright, clear and practical comments and suggestions.

Geachte Jolien, thank you for being part of this project. Thank you for all your teachings in congenital cardiac diseases, one of the most fascinating and difficult topics of the field. Thank you for all the meetings you did in English so that I and the other foreigner fellows could follow.

Beste Ricardo, my co-promotor and guide throughout this journey, thank you. I'm not sure this project would have seen the light without you. From that somehow weird Italian sky-resort to EMC skype call to our last French hospital to the Netherlands phone call a lot of things changed for both. However, all throughout this journey it is your enthusiasm and calm resolution that kept me motivated and on track. Thank you for teaching me how to write a scientific paper. Thank you for your encouraging words and constant support while I was learning that not all projects will end as we would have hoped. Thank you for reminding me that science not always has to do with Pindaric flights but can be (and many times should be) a down-to-hearth matter. Thank you for the many clinical cases we have reported together. Since our first emails I don't remember any questions, email or phone call of mine going unanswered even when it meant working late in evenings, weekends and holidays which is quite amazing and a good lesson. Last but definitely not least, thank you for always asking me if I liked my life in the Netherlands at all our meetings. A few times the answer was not so straightforward but I have appreciated this question every single time. I hope in the future we will have new projects together, meet at congresses to share scientific progresses but also a nice drink and a good meal. Regarding your solicitations that I could be more succinct, well, it looks like I'm still working on it.

Geachte Prof. Wentzel, Prof. Bogers and Prof. Reiber, thank you for accepting to be part of the kleine commissie. Dear Prof. Bogers and Reiber, thank you for our works together. It was always most interesting to know your more clinical and more technical vision of our projects.

Geachte Prof. Derchi, Prof. Leiner, Prof. van der Lugt and Prof. Zijlstra thank you for accepting to be part of the grote commissie. Dear Prof. Derchi, a special thank you for bringing a bit of Europe to Genova and bringing a bit of Genova to the top of European Radiology. Dear Prof. Leiner, thank you for our past projects and I'm looking forward to the future ones.

To my paranymphs Laurens and Michela.
Dear Michela, thank you for coming all the way from Verona and to be on my side for this occasion. And not only. Your support during and after your six months in Rotterdam was and is exceptional. Although I cannot imagine two more different persons from a lot of points of view, all your suggestions and ideas have became a fundamental part of my life in the last years. Remembering all the occasions spent together and all the reasons I should thank you for goes well beyond the purposes of these pages. For this reason and in honour of your love for conciseness, I will summarize: thank you!!

Dear Laurens, thank you for your presence by my side today at the end of this journey of which we shared so many moments together!! I remember you smiling when I met you the first time and your immediate willingness to help me set up my desk. All throughout the years spent at EMC with their ups and downs these two elements did not change and I always knew I could count on your counselling and help. I learned a lot from you and with you. You were the soul of our office social life, so many events being organized by you with your unmistakable energy and enthusiasm. Sinterklaas, tompuces, drop, stampot: these are only some of the Dutch traditions and foods that you let us discover and enjoy together. In bocca al lupo for your training as cardiologist and don't ever lose your kindness and smile.

To my colleagues of the room Ca207-a. That room that was a lot more than an office. It was a great pleasure to meet each one of you. Inside and outside lunches, cakes, dinners, parties etc were an essential part of this project as well as one of the most tasteful. I will never thank you enough for having spoken English so many times in my presence and for your help with all sorts of bureaucratic matters. Dear Marisa, I was very surprised to read your thesis because I have always looked at you as to the steady and hardworking one in the office. I was sure you would be there and that I could always count on your help (such as in my fights against the BIG), thanks! Congratulations for your book and your beautiful Myla and success for your training. Dear Raluca, it was inspiring to see your many plans for

work, sport, languages and life. Although at times things were not so easy you were always positive and optimistic. Your joy and love for your family last time I saw you was tangible and great to see. Hope you will finish your book soon. Dear Adriaan, as your life changed over the years your smile seemed to increase and get deeper. Congratulations for your beautiful family and hopefully your residency and book will bring you even further joy. Dear Fay, your arrival brought smiles, freshness and new enthusiasm to the office. Having lived abroad for a while I think you understood better than others some of the issues expats are deemed to face which was undoubtedly an important point of contact. Good luck with your thesis and your residency, don't let temporary drawbacks get into the way to your final goal. Dear Nikki, it was cool to find you in the office in the morning and to get the first coffee/the of the day together. We didn't get to run the bruggenloop but it was really nice to discuss with you running, other sports, vacations and all other matters. Keep up your hard work, I'm sure you will get your satisfactions! Dear Ivo, thanks for reminding me my flaws over cakes, "half hours" and lunches. Remember that we still have to go sky together (on a real mountain I mean). Dear Kevin, Juste, Wiebe, Ali thank you for the time spent together.

To my co-authors, thank you to all of you. Dear Anne-Marie, I think I have never seen anyone so efficient, productive and fast while staying positive and goodhearted with others. All the best for your future career. Dear Xinpei, thank you for showing me your work and your word. I had been using radiology software for a long time but until I met you they looked to me like a black and incomprehensible box. I'm not saying that now it is all clear but at least they look friendlier. Thanks for discovering for me the secrets of the Chinese New Year and for tasting with me some of your best delicacies. Being an expat you face a lot of difficult questions for which I hope you will find the best possible answers. Dear Lidia, it was nice to discuss with you aortic matters. Dear Pieter, thank you for all your work behind the scenes.

Thank you to Koen Nieman, Mohamed Attrach, Alexander Hirsch, Mohamed Ouhlous, Karel Wallecam and Annick Weustink for the CT ad MRI seen and discussed together. I wish they had been more. Thank you to Maarten Witsenburg for your kindness and the all the clinical cases you reviewed with me.

To the Italians met here and there in EMC. Dear Marco, Giorgia, Chiara and Giulia, it is difficult to translate in a few words what it means to find a friendly presence from your homecountry abroad. I think that thanking you for our 'pause caffé' can summarize a lot of it.

As this journey started a few years before I set foot in the Netherlands I would like to take a step backwards and thank some of the people that inspired me to become a radiologist,

to specialize in cardiovascular radiology and to pursue a future in research. Dear Giuseppe, I have literally seen my first CT scans with you. You have shown me the Radiologist I would like to become. Your knowledge and humanity as well as continuous aim at improvement have been and are a source of inspiration. Some of your quotes such as "You have to heal people and not images" are an essential part of my cultural baggage. I hope you have some other chair legs to make even with this third thesis. Dear Prof. Martinoli, our paths crossed for a relatively short time but you have deeply influenced what came after. Whenever I thought I had some basis in a particular field I would just look at you working and was immediately aware that I had actually just scratched the surface. The abstracts and papers from that period were the beginning of my fascination for research. Dear Sara, thank you for the many hours spent looking at coronary arteries and aorta that taught me the importance of looking restlessly at every pixel of examinations. It was you suggesting that I spend my year abroad at EMC, thank you. Dear Nicola, thank you very much for sharing your deep knowledge in cardiopaediatric radiology and your coarctation patients with me. Thank you very much to all the radiologists I met during my residency who taught me so much far away from the light of reflectors.

To my fellow colleagues specializzandi in Genova. Dear Marta, thank you for all the days spent together in all the hospitals we frequented. Thanks for all the scans we looked at together, the endless discussions, the laughs, the coffees and lunches. I couldn't have asked for a better colleague. Dear Irilda, Margherita and Athena, happy members of the "quartetto cetra", the first hearts were with you. The first kebabs to write abstracts into the night were with you. Thank you for transforming those long days in a passion. Dear Claudia, Erica and Beppe, we shared another history, plenty of muscles and long hours anyways. Dear Alice, Marco, Alberto, Michela, Romina, Angelo, it was a pleasure to share with you these years. I wish you all the best.

Thank you to all the TSRM, laborants and MER I worked with. Not only you are the ones who make my job possible but sometimes you were also the ones who guided it. Dear Marcel, a special thank to you for our discussions over CT technical issues. Your knowledge is amazing and often prompted me to study more.

Thank you to all the secretariaat and trial bureau (thanks Laurens) of the Radiology department from EMC for your support. Dear Annelise, special thanks to you. From day 0 you helped me out dealing with an endless list of diverse and often weird questions.

Dear Prof. Revel, Prof. Douek, Dr. Chirossel, Salim and Ludovic, Prof. Boussel, Delphine, Véronique and Delphine, thank you for your warm welcome in Lyon. Thank you for making it possible to continue my path in clinical work and research. I look forward to the next years of work with you.

Dear Giacomo, thank you!! Since Noemi's 30th birthday when we met the first time to your 30th birthday in your countryside house the path was long. You better than others know how these years have been difficult at times. Your risotti and all other delicacies have been essential to make it a great period. Your house was a secure place where I could take shelter from the rest of the world. Hadn't I met you the history would have definitely been different. You are one of those very rare people you meet in life with whom you can just be yourself and discuss anything and everything. Can't wait to see you in person and do that again!

Dear Liana, Mina, Andreea, beste inhabitants of the apartment of Coolhaven, you were the best flatmates I could have ever hoped for. Not always living together, especially with such small common spaces, is simple. Not only you made it easy but also a pleasure. Coming home, it was great to meet you in the kitchen, discuss our daily adventures (and try to laugh about them) and get ready for the next ones. I wish you all the best for your lives and projects and a lot of well-deserved happiness.

Dear Oana, Tess, Adrien, Diego, Erika, Alessandro, Nina, Mihai, Eva, Szilard, Larissa, Yasmine, Amy and Joost, thank you for the countless beautiful moments spent together. Great friends, food, drinks, music and games: ingredients for the cosiest and most power-regenerating events. Nevertheless, it was also more than this. Thanks for sharing bits of your work, expositions, Conversas and Manifest with me. It was all interestingly new to me and opened my eyes on a world I didn't know.

Dear Maaike, Monika, Esther T, Gwen, Leandra and Esther H, thank you for all the long conversations, short incisive sentences and for everything you have taught me. And, of course, thank you for some of best days and evenings in the Netherlands! Dear Monika, thank you for sharing your enthusiasm for marathons and for your unfaltering support to my far-fetched projects that helped me running through the winter.

Dear Elena, Mian, Noemi, Velia, Simone, Teresa, Marco, Giulia, Fulvio, Laura, Max, Giorgio, Tommaso, Anna, Pietro, dearest friends from home. Although due to my choices I cannot see you as often as I would like to, I know you are always there for me. Your presence in my life is priceless.

Cara mamma, caro papi, caro Dado, questa parte sarà in italiano. Non perché non sappiate l'inglese, tutt'altro, ma perché l'italiano è la lingua di casa. Quanto c'è di buono in questa tesi, e non solo, è grazie a voi e per voi. Siete voi che mi ispirate costantemente a fare di più e meglio.

Cari mamma e papi, grazie per avermi supportato e sopportato sempre e comunque, non solo quando appoggiavate le mie scelte (quasi mai) o almeno le comprendevate ma soprattutto quando non eravate affatto d'accordo. Grazie per il vostro amore.